warwick.ac.uk/lib-publications

Three Dimension Cellular Automata Modelling of Recrystallisation in Steel

by

Gabriel Abah Ekoja

A thesis submitted in partial fulfilment of the requirements for the
degree of
Doctor of Philosophy in Engineering

University of Warwick, Warwick Manufacturing Group

September 2021

Table of contents

Contents

Acknowledgements

I would like to acknowledge the University of Warwick, Engineering and Physical Sciences Research Council (EPSRC) and Tata Steel as my sponsors for this work.

I am especially grateful for the time, support and expertise provided by my supervisors Prof. Claire Davis, Dr Carl Slater and Dr Martin Strangwood.

I am indebted to Dr Kees Bos my industrial supervisor for his support and expertise especially in the programming aspect.

Also thanks and recognition to Fengzhai Tang for training on SEM and Nanoindentation.

Finally, I owe a special thanks to my family and friends whose support and encouragement enabled me to complete this project.

Declaration

This thesis is presented in accordance with the regulations for the degree of Doctorate of Philosophy. It has been written and complied by myself and has not been submitted anywhere else. The work in this thesis has been undertaken by me except where otherwise stated.
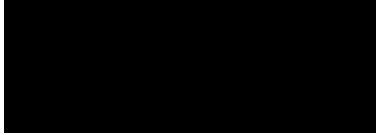
Signed: ██████████████   Date:24/09/2021

Abstract

A physical based 3D cellular automata (CA) model that includes the recrystallisation process has been developed for strip steels. The CA model allows the full starting austenite grain size distribution to be considered (rather than the frequently used empirical recrystallisation equations where average grain sizes are considered) and to predict the recrystallised grain size distribution and recrystallisation kinetics. A key objective of the work was to determine the cause for the temperature dependency from the previous CA model and a physically based approach to give correct recrystallised grain size predictions.

In order to be able to correctly predict both the recrystallisation kinetics and resultant grain size distribution and their appropriate dependence / independence on strain and temperature, consideration of the recrystallisation nucleation and growth to a critical nucleus size are essential and they are driven by the local stored energy conditions. This work has looked at the implementation of a boundary intensity factor to drive the recrystallisation nucleation event and subsequent growth to exceed the critical nucleus, the critical radius uses the dislocation density which is assumed to be the same at both the grain boundary and the grain interior and without the introduction of the boundary intensity factor the kinetics of recrystallisation agree poorly. The introduction of the boundary intensity factor (BIF) accurately reflects the experimentally observed inhomogeneous dislocation density in deformed samples, where higher dislocation density at the grain boundaries occurs, which results in changes in the nucleation and sub-grain growth to critical size. The width of the 'boundary' has been determined based on the experimental observations and the value of the boundary intensity factor for the stored energy was determined by fitting to literature experimental data for a Fe-30Ni-0.044 wt. % Nb steel, with a starting average grain size of 160 µm at a strain of 0.3, considering deformation at two temperatures (900°C and 950°C). A BIF of 2.2 was derived to match the recrystallised grain size distribution and the recrystallisation kinetics of Fe-30Ni-0.044 wt. % Nb experimental data. The recrystallised modal grain size (D50%) from the CA with a strain of 0.2 was 100 µm and 60 µm with a strain of 0.3 and both were in excellent agreement with the experimental recrystallised modal grain sizes. The recrystallisation starting time (R_s) and the recrystallisation time at 50% ($R_{50\%}$) are also in good agreement with the experimental results.

10

List of Figures

19

List of Tables

22

1 Introduction

The advent of steel led to the industrial revolution and as a result our modern society, with advanced infrastructures. As of today, the production of crude steel stands at over 1870 million tons per year worldwide (**Figure 1**) and 1500 million tons is hot rolled steel products (**Figure 2**). A large body of research stems from the high demand for a wide variety of steels, of which there are more than 3500 different grades of steel. These grades all have their roots based in a range of physical and chemical properties of steel and are used to produce a vast range of thicknesses and shapes. Twenty years ago, over seventy-five percent of the steel grades in use today did not exist. These grades of steel give it specific properties designed for particular applications and innovative steel continues to be developed. The expansion of applications for steel has instigated developments in the improvement of the mechanical properties of steel.

Steels used in engineering are required to have good mechanical properties, for example high strength and toughness. These properties are achieved from the microstructures that evolve during and after processing, of particular importance is a fine and uniform grain size. Therefore, it is desirable to know the effect the various processing parameters have on the microstructure development, in order to manage the key parameters that affect it and thereby manipulate the final mechanical properties.
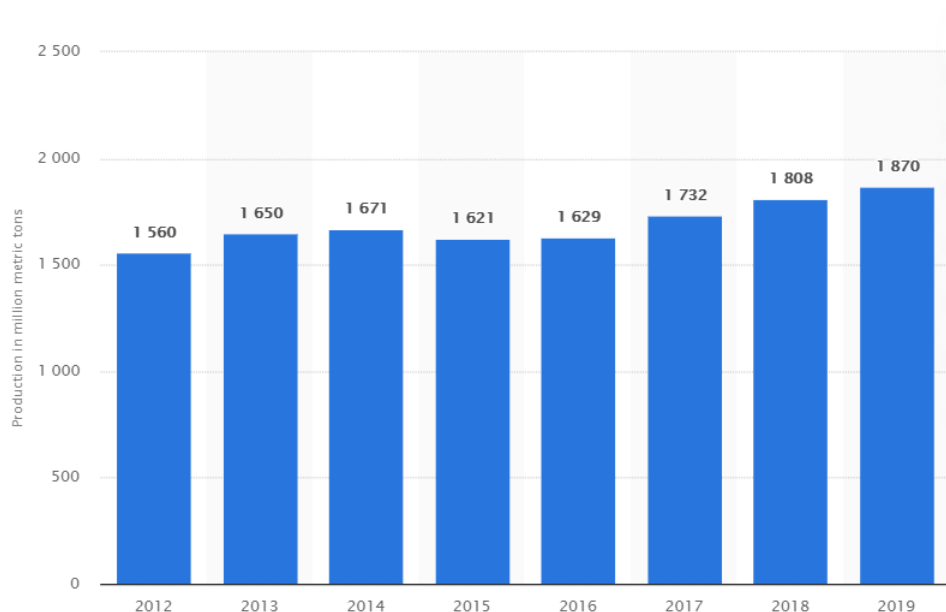
Figure 1 – Total production of crude steel between 2012 and 2019[1].
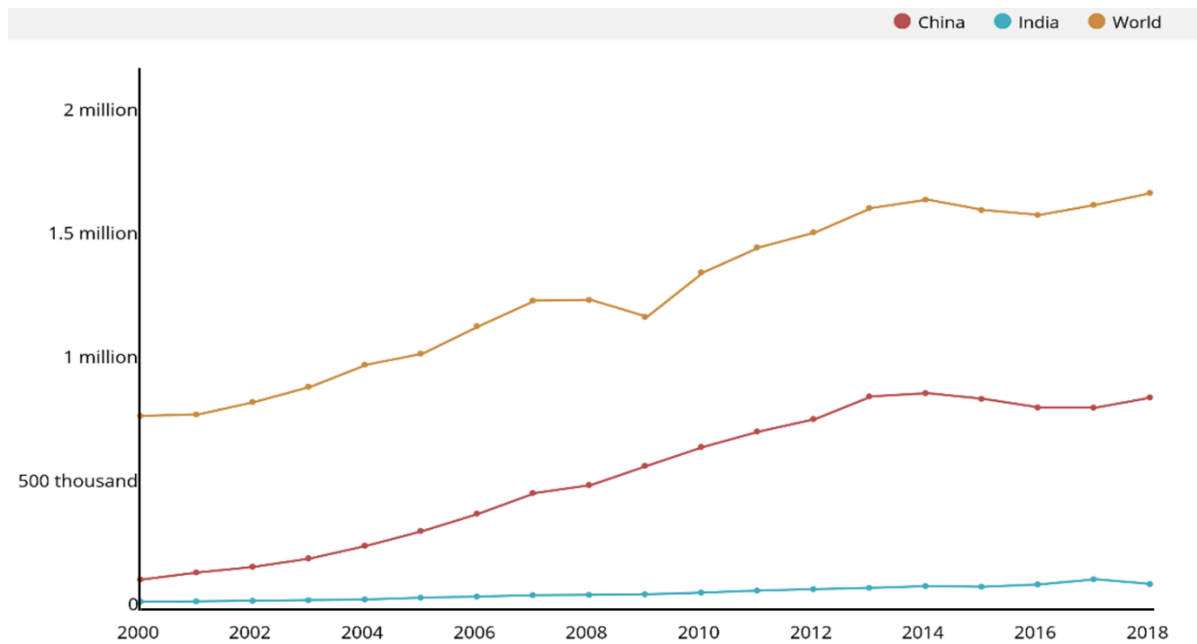
Figure 2 – Total production of hot rolled products(thousand tonnes) between 2000 and 2018[1].

1.1   Development of high strength low alloy (HSLA) steels

Structural changes during hot deformation have been shown to be vital in the determination of the final properties of steel. The intensification of studying these changes were a result of increasing demand for higher strength steels. By controlling the thermal and mechanical processes employed in making the steel, stronger and tougher steels can be produced. Demands for these steels gave rise to the development of high strength low alloy (HSLA) steels evolving from a low carbon steel base. HSLA steels have a yield strength above 275 MPa and include additions in the alloy designed to deliver specific desirable combinations of properties[2]. Such combinations of strength, toughness, weldability, formability and resistance to atmospheric corrosion are highly sought-after. Applications for HSLA steels include bridges, buildings, ships, pipelines and pressure-vessels. Moreover, they reduce weight and therefore the fuel consumption of automotive equipment.

1.2   Production process of hot rolled steel

There are different processing stages for microalloyed steels before a uniform and fine microstructure is derived (refined). These stages are casting, reheating and hot rolling, annealing before the final microstructure is obtained. Currently most plates or strip

25

steels with a uniform grain size distribution or fine final ferrite grain sizes typically 5-10μm for thermomechanical controlled rolling (TMCR) of HSLA are produced from forging or through hot deformation via TMCR. Steels with high yield strength (greater than 275MPa) and adequate toughness (like in pipelines) are examples of these. TMCR is mostly used to control the microstructure while still shaping the dimensions of the steels.

To produce line pipe steel, firstly the high strength low alloy (HSLA) steel begins as continuous cast slabs. These are re-heated at a temperature range between $1100°C$ and $1300°C$ (soaking temperature) for a particular length of time prior to rolling. The purpose of the reheating is to enable the formation of a uniform microstructure. Existing large (typically 100 – 300 nm) micro-alloy precipitates formed during the moderate cooling of the as-cast slab are dissolved, thus allowing the microalloying elements to be available in solid solution for subsequent fine scale precipitation (<10 nm) during or after rolling[3]. The rolling process that follows has two stages; the roughing stage, which is the first deformation phase, is done at high temperatures of between $1050°C$ to $1150°C$ with the purpose of refining as cast coarse grain through static recrystallisation. This is then followed by the second deformation phase (finish rolling) where the bar is held at a temperature between $1000°C$ to $900°C$. This ensures recrystallisation is complete during the roughing stage and there is no recrystallisation at the finishing stage (see **Figure 3)**. This process is done through a carefully planned rolling schedule, which controls the number of passes, reduction in percentage per pass, hold temperature and time, finishing rolling temperature and the cooling rate after rolling. This process is illustrated in **Figure 4**.
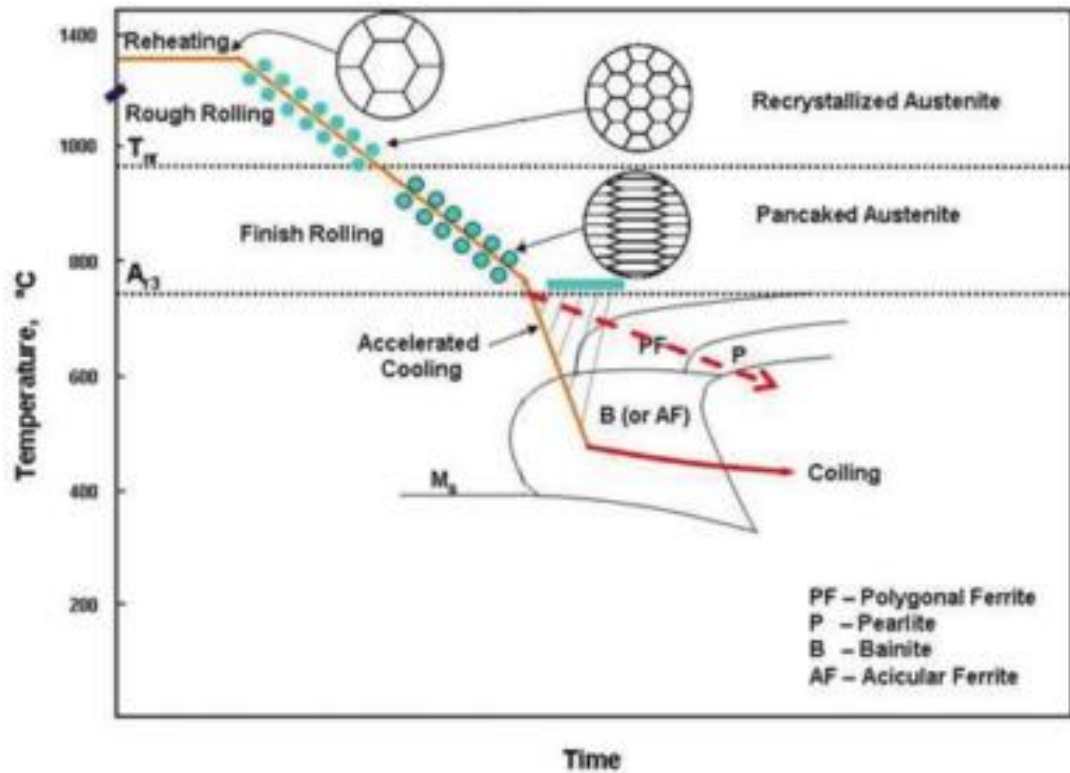
Figure 3 – The thermo-mechanical processing of steel, showing the roughing and finishing windows[4].
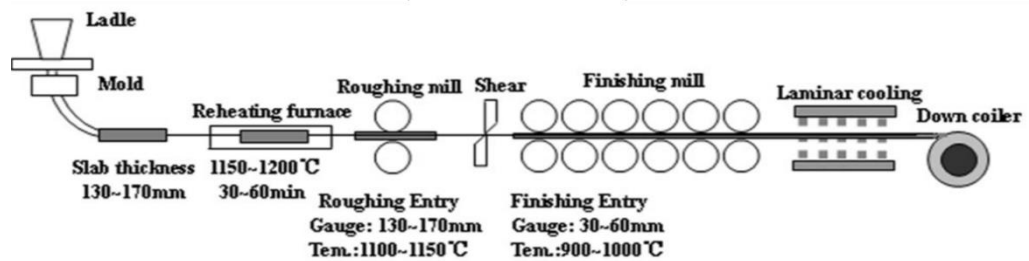
Figure 4 – Schematic diagram of the hot rolling process[5].

1.3 The thesis structure

The thesis is made of the following chapters:

Chapter 2 contains the literature review concerning the evolution of microstructure during hot rolling of steel. This contains a review of the structural changes and the key metallurgical processes of recovery and recrystallisation in thermomechanical processing of steel. A review of recovery and recrystallisation models is also found in this chapter.

Chapter 3 contains review of CA for modelling of recrystallisation with a starting grain size distribution, as implemented in the as-received cellular automata model for hot rolling of steel.

Chapter 4 contains the sensitivity analysis of the various parameters in the as-received cellular automata model.

Chapter 5 contains the aims and objectives, indicating the gaps in the cellular automata model and how to tackle it.

Chapter 6 discusses the new development and improvement in the model to address some of the gaps in the model.

Chapter 7 is the discussion/ validation of the improved model. This includes case studies for hot deformed samples at 900°C and 950°C of 160µm and 100µm at different strains.

Lastly, in Chapter 8 the conclusion and future work are given.

2 Literature review

Mechanical properties are controlled by the microstructural elements of steel like the composition, grain size, precipitation, phase volume and other structural factors like shape and thickness. Therefore, being able to determine the mechanical properties by understanding the relationship between the microstructure and the mechanical properties, is an objective of the steel industries. In order to improve properties, the steel is subject to various rolling processes involving deformation at high temperatures to refine the microstructure. Post rolling, transformation then further refines the structure. Normally the dependent parameters or variables during hot deformation like reheating temperature and rolling schedules will have a very large effect on ferrite transformation and precipitation kinetics. The final microstructure can only be indirectly correlated back to the high temperature structure, i.e. austenite, since the ferritic transformation changes the microstructure. The effects of thermomechanical processing conditions and cooling rate on the final microstructure of the steel can be calculated using predictive modelling. A lot of progress has been made over the decades towards the thermomechanical processing of microalloyed steel modelling during hot rolling. Central to this is to capture the process of recovery, recrystallisation and precipitation and the interdependency of these metallurgical processes[6-10] to capture the evolution of the microstructure. Moreover, this has led to semi-empirical models developed with great accuracy[11-15] to describe the relationships between recovery, recrystallisation and precipitation. The following sections describe theoretical advancements made towards the understanding of key processes involved in the hot rolling of steels.

2.1 Predicting recrystallised grain size

During thermomechanical controlled rolling (TMCR), the key metallurgical processes taking place are recovery, recrystallisation, precipitation and grain coarsening[16][17]. Therefore, it is paramount to predict accurate recrystallised grain size distributions and hence the recrystallisation kinetics. From this, prediction of the coarse grain distribution can be obtained, in order to design the best effective schedules to get a uniform fine grain distribution.

These key metallurgical processes in hot rolled steel can describe to some extent the tensile strength, based on the modal or average grain size but properties like toughness are dependent on the larger grain sizes in the grain size distribution. Therefore, any model to predict grain size needs to include the full grain size distribution[18][19] instead of just using the modal or average grain size, which are commonly used in most models[19].

There are several equations developed base on Sellars approaches in the literature for the prediction of recrystallised grain sizes see section 2.2. These equations show that the recrystallised grain sizes are dependent on the initial grain size and the applied strain[18]-[23]. The majority of these equations can predict the modal grain size but specifically for a particular strain, initial grain size and steel grade[20][21]. These equations can adequately predict the average grain size but not all these equations derived from empirical methods can model the recrystallised grain size distributions[19]. Kundu[18], [19][20] suggested using an individual grain size class distribution of Nb-containing HSLA (high strength low alloy) steel in the range of 240-280 µm and deformed only at 0.3 strain. This approach did not consider a range of initial grain sizes and different levels of strain. Furthermore, the impact of high strain values on the density of the nucleation sites, which may lead to variations in the recrystallised grain size distributions, was not taken into account. Therefore, there is the need for a more vigorous approach for modelling recrystallised grain size distributions using the initial grain size distributions.

2.1.1   3D Grain size modelling- the Voronoi approach

Numerical analysis of the microstructure is enabled by modelling the properties such as geometrical shape and grain size. The distribution of grain size and the geometrical shape of the grains are the relevant properties to model. For any further meaningful analysis to be done, a mathematically analytic description of a microstructure that is similar enough to the real structure of the material is needed. One way of approximating the microstructure in polycrystalline materials is with the Voronoi diagram (Voronoi tessellation)[24]. Voronoi diagram is a partitioning of a plane into regions based on distance to points in a specific subset of the plane. That set of points (seeds) is specified beforehand, and for each seed there is a corresponding region

consisting of all distances closer to that seed than to any other. These seed regions are called Voronoi cells[25].

There are three geometrical parameters for capturing microstructure morphology of a polycrystalline material and is used, based on its ability to describe the particle shape, the local and overall distribution patterns. They are the form factor (FF) which is used to characterise the shape. The second order intensity function, describes the statistics of spatial distributions. It characterises the expected number of points of interest to lie within a distance of an arbitrary located point [26][27]. **Figure 5** shows the two - dimensional microstructure generated using the conventional Voronoi and the Laguerre Voronoi (LV) which is a partition of the Euclidean plane into polygonal cells defined from a set of circles.

The Laguerre Voronoi diagram has a strong distribution of the sphere volume for a random close pack sphere.

The nearest neighbour distance (NND) which is defined as the minimum distance from a grain to its nearest neighbour. This method provides more useful information or patterns on the local distributions of the microstructure (**Figure 6**).
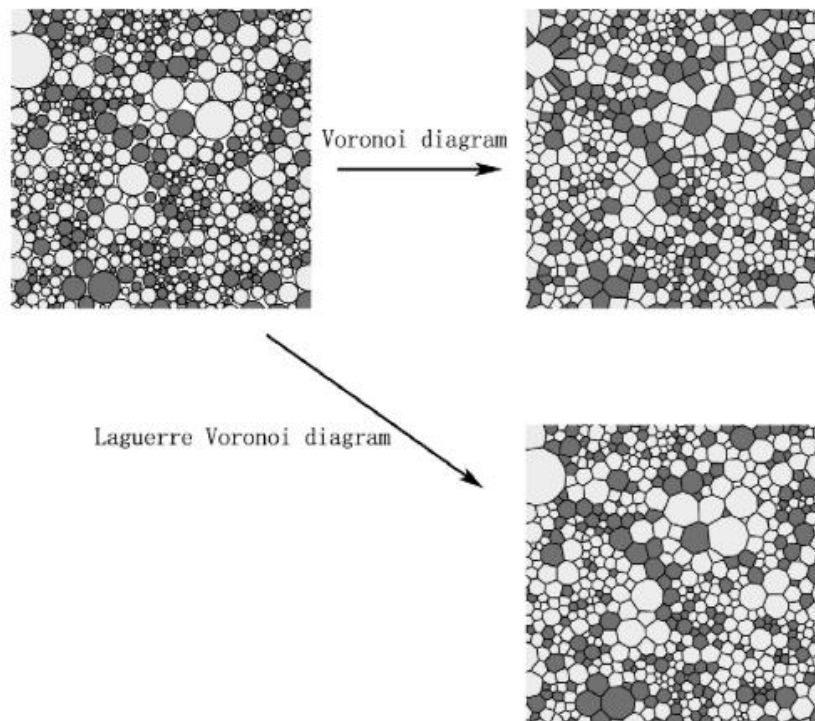
Figure 5 – Two-dimensional illustrations for constructing a conventional Voronoi diagram and a LV diagram with a same two-phase random cube packing (RCP)[26].
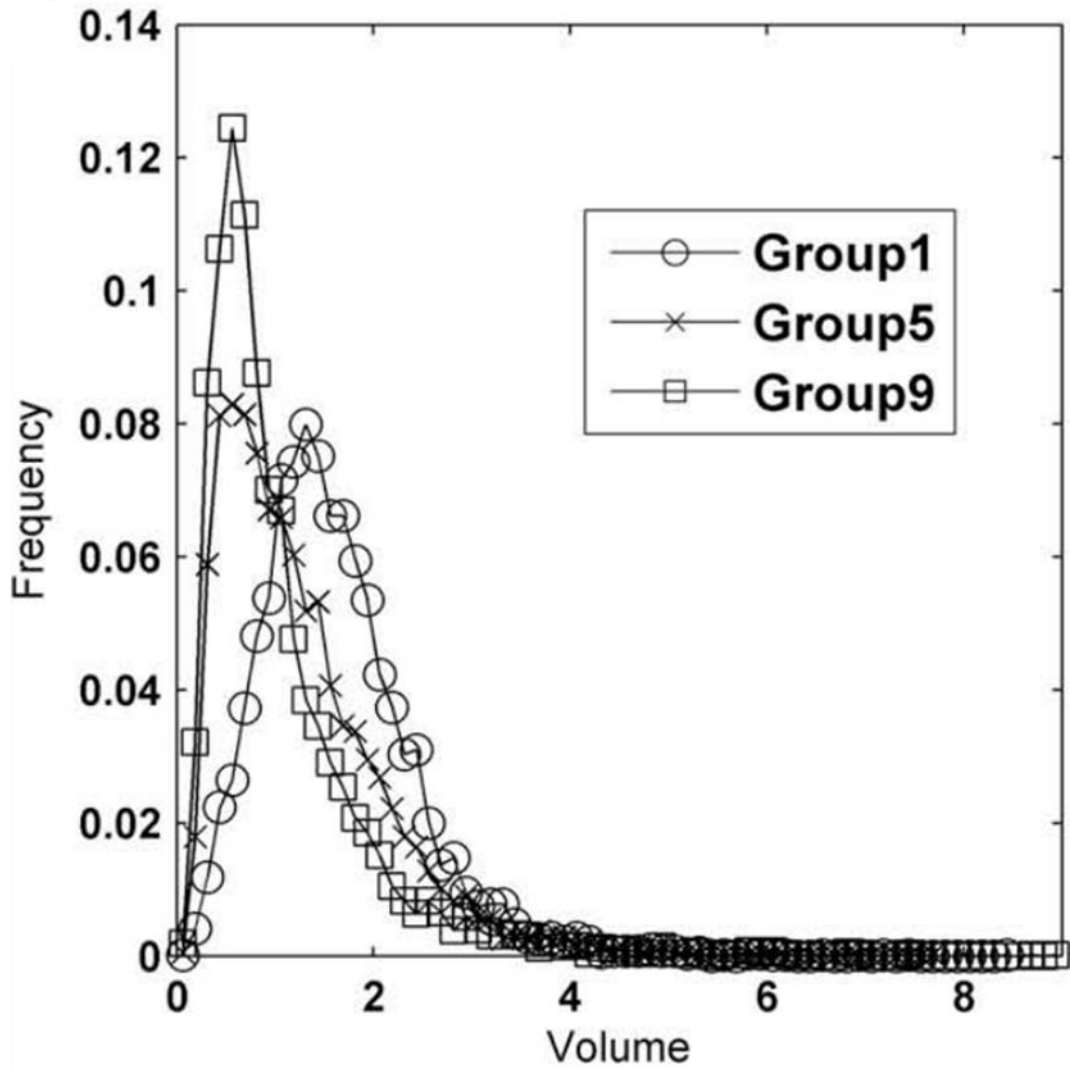
Figure 6-Total grain distribution for different groups using nearest neighbour distance (NND) [26].

In order to simulate the grain structure of a wide range of materials, the Laguerre Voronoi technique provides control over the size and shape of the cells. The Laguerre Voronoi is normally called the power diagram, the points are circles. The distance between a point and a circle on the sphere is called the Laguerre and is the geodesic length of the tangent line segment from the point to the circle. Falco *et al* verified the capability of this method by reproducing the microstructure of polycrystalline alumina with various ranges of grain sizes, deriving from different sintering procedures [28]. This approach provides the algorithm based on microstructure from an experimentally obtained set of 2D micrographs. It compares 2D sections of the numerical model

against 2D imaging of real polished surfaces to find a representative set of input values (**Figure 7**).
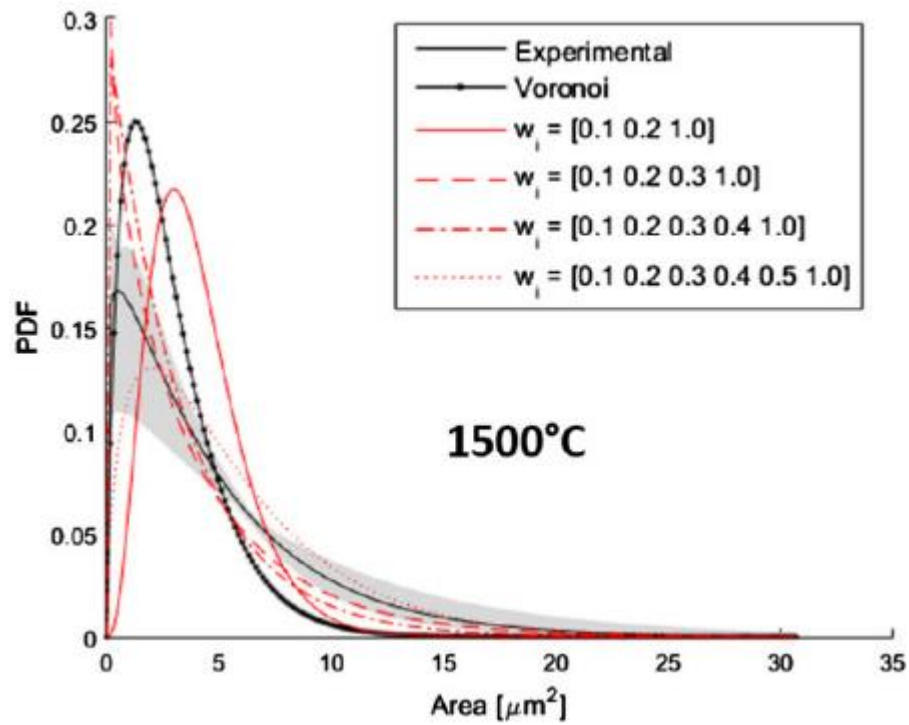
Figure 7 – Comparison of grain size distribution of experimental measure at 1500ºC and numerical models generate with classic Voronoi and Laguerre-Voronoi with different number of bins[28].

2.2 Hot deformation

During the rolling process, hot deformation occurs and this drives recovery, recrystallisation and, under the right conditions, grain growth. These processes give rise to key microstructural changes. Therefore, it is important to understand the parameters that govern the deformed state, so that changes in the microstructure can be understood. These parameters include strain, strain rate, deformation temperature, holding time and initial grain size[19][3].

As strain is applied during hot deformation, dislocations in the microstructure is introduced and an increase in strain causes an increase in the dislocation density (dislocations per unit volume), and this is the driving force for recrystallisation (discussed in 3.6.5).

The increase in dislocation density with plastic deformation in metals is given by the expression[29]:

$$\rho = k.10^{15} * \varepsilon$$ Equation 2.1

Where ρ is the dislocation density and k is the dislocation generation rate. Face centred cubic (FCC) structure has a greater generation rate than body centred cubic (BCC) structure because of the difference in the slip system[29]. In steels there are higher dislocations in finer microstructure compared to coarse grains, which have a more heterogenous dislocation density distribution[29][30].

2.2.1   Effect of applied strain

The driving force for recovery is dislocation density and increasing strain increases dislocation density. This means that increasing the strain increases rate of recovery and in microalloyed steels this affects the microstructure.

Strain also affects recrystallisation, the amount of strain determines the nuclei density (nuclei per volume) and the driving force for recrystallisation. As the strain is increased, the recrystallisation growth rate also increases. Strain is not homogenously distributed because of the inhomogeneous nature of deformation and hence the rate of recrystallisation growth will differ. In high stored energy region. The nuclei will grow quicker following a recrystallisation nucleation. The recrystallisation growth rate will reduce once these regions are consumed and so this will affect the recrystallisation kinetics[30].

After deformation, there are regions in the microstructure that have been highly deformed (such as the grain boundaries, deformation bands and triple points) and regions that have experienced low deformation, which means the stored energy varies locally after deformation so there is variation in the recrystallisation rate[31]. If the heavily deformed regions recrystallise first, there will be less stored energy causing a reduction in recrystallisation rate for the lightly deformed regions. It was observed that, in aluminium, highly deformed regions tend to recrystallise quicker than less deformed regions[31] and Humphrey observed this also in copper[32].

Recrystallisation (see 2.4 and 2.5) is nucleation-dominated, which means that recrystallised grain sizes depend on the strain and prior grain size. The average

recrystallised modal grain size decreases with increasing applied strain because the higher the strain the greater the rate of recrystallisation hence finer grain sizes (see **Figure 8**) [33][30][21].
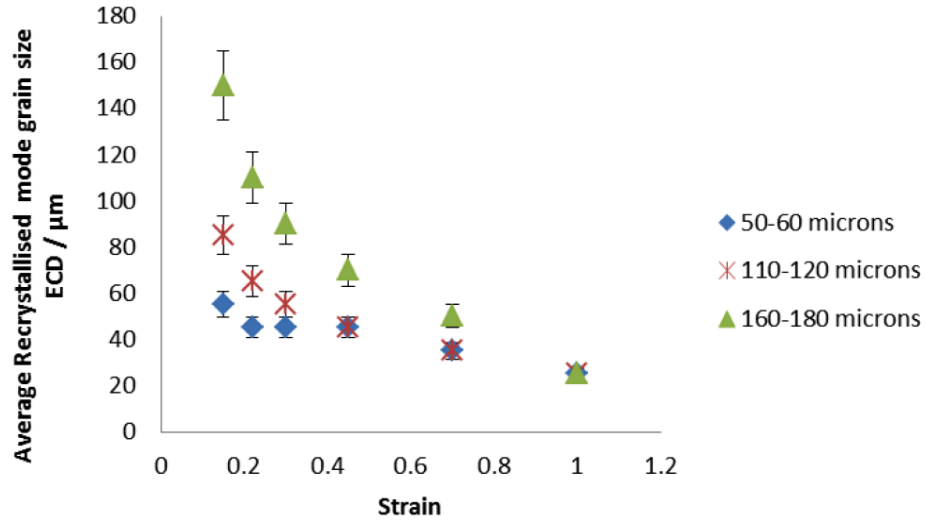
Figure 8 – Effect of strain on the average modal grain size after recrystallisation in C-Mn and Nb-treated steels with initial modal grain sizes of 50-60 µm,110-120 µm and 160-180 µm [21][27][31].

The recrystallised grain size *(D_{rex})* in C-Mn and Nb-treated steels has been found to be related to the initial grain size *(D_o)* and the applied strain *(ε)* by the following equations[21] :

For C-Mn steels

$$D_{rex} = D' D_o^{0.67} \varepsilon^{-1}$$ Equation 2.2

For Nb-bearing steels

$$D_{rex} = D' D_o^{0.67} \varepsilon^{-0.67}$$ Equation 2.3

D' is a fitting parameter and varies according to the material. There a also different values of *D'* for C-Mn steels and Nb-bearing steels quoted in the literature[21][34].

2.2.2 Stored energy estimation

In the process of deformation, microstructure changes according to the macroscopic strain applied. As the grain is deformed, the grain boundary area increases and the dislocation density increases. Also following deformation, the shape of the grain is elongated. Internal deformed structures including dislocations, cell blocks, microbands, shear bands and deformation bands appear within the grain, depending on the strain level[35].

Dislocation density will increase with increasing strain, if restoration does not take place during deformation, so the internal energy increases. The existence of distortion around the dislocation is its strain energy (E_0) and for one dislocation it can be expressed by[36]:

$$E_o = \frac{Gb^2}{4\pi} ln(\frac{R}{r}) = \alpha Gb^2 \qquad \text{Equation 2.4}$$

G is shear modulus

b is Burgers vector

α is 0.5 – 1 depending on the dislocation distribution.

R is the cut off radius of a dislocation

r is the core radius

The stored energy, E, for a material with a dislocation density of $\Delta\rho$ is expressed by:

$$E = \alpha Gb^2\Delta\rho \qquad \text{Equation 2.5}$$

$\Delta\rho$ is dislocation density.

The increase in flow stress during deformation is due to the increase in the dislocation density. Therefore, the dislocation density can be estimated by a Forest Hardening–type relation[37]:

$$\sigma = \sigma_o + M\alpha\mu b\sqrt{\Delta\rho} \qquad \text{Equation 2.6}$$

σ_0 is initial flow stress

M is the Taylor factor, 3.1 for isotropic FCC crystals

α is a constant taken to be 0.15.

b is the Burgers vector is 2.52 x 10^{-10} m

μ is the shear modulus at 900°C is 45 GPa[38]

ρ is the dislocation density in m^{-2}

The misorientation between sub-grains and the sub-grain diameter can express stored energy, if the deformation microstructure contains cell-like microstructure[13]. It is given by:

$$E = \frac{A\theta}{d}$$

Equation 2.7

A is a constant.

θ is the misorientation between adjacent sub-grains.

d is the diameter of the sub-grain.

This expression shows that increasing misorientation increases stored energy. A stored energy range of 0.6 – 7 Jmol^{-1} for FCC materials has been measured by different authors for a 0.3 strain[39]–[41]. However, instantaneous stored energy remains difficult to measure, as recovery, phase transformation and measurement of dislocation density all hinder the process and thus these measurements tend to be fitted to trends for specific alloys/conditions.

2.2.3 Effect of grain size distribution on stored energy

Local lattice curvatures mean that strain cannot be homogeneous across the material or within a grain and the grain texture gives rise to different deformation behaviour depending on the direction of straining relative to the grain[42]. Ashby states that for a polycrystalline material, the shape change from neighbouring grains during deformation must be accommodated by each individual grain. Therefore, extra geometrically necessary dislocations i.e dislocations needed to compensate for plastic bending in a crystalline material (GND) must form along the grain boundaries. This is shown in

Figure 9. The equation given by Ashby to estimate the GNDs is:

$$\rho^{G} \approx \frac{\bar{\varepsilon}}{4bD}$$

Equation 2.8

$\bar{\varepsilon}$ is the mean strain

b is the Burgers vector

D is the average grain size

Measuring the effect of austenite grain size on stored energy for HSLA steels is challenging because of the phase transformation during cooling. Most studies have been carried out using austenitic steel, copper and aluminium. Cizek and Palmiere reported that grain boundaries and triple points have a higher distortion compared to the grain interior for Fe-30Ni-0.044wt.%Nb and 304 stainless steel[44][45]. It has been reported that the stored energy level increases with decreasing grain size at low and medium strain levels (less than 0.5). This would correspond to the requirement for additional GNDs to accommodate the differential strain in neighbouring grains[46].
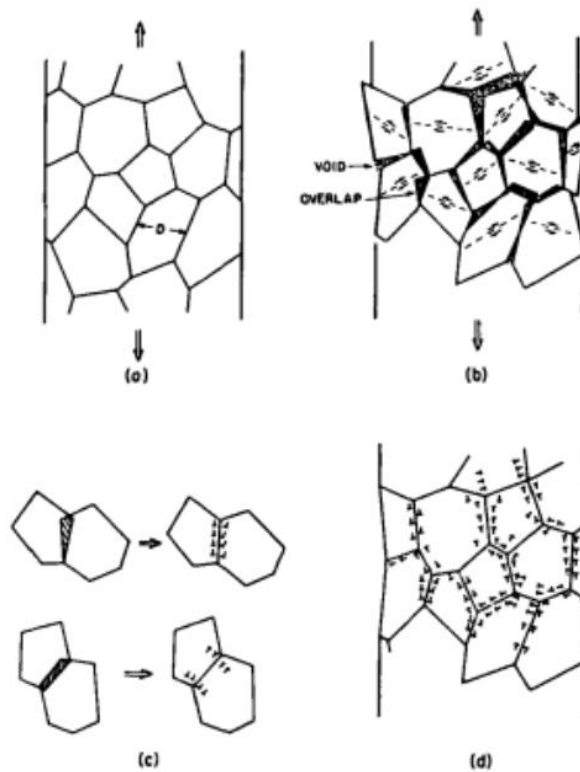
Figure 9 – Schematic diagram of the geometrically necessary dislocations along the grain boundaries[43]. (a) onset of deformation (b) overlap and voids occur if there is no local deformation (c) geometrically necessary dislocations are introduced to accommodate the local distortion along the grain boundary (d) extra GNDs are located along the boundaries[38].

Across the grain size range of 60 – 760 μm in copper, the stored energy variance reported was between 6 and 30%[47]–[49]. Williams published an increase of 0.59 MPa in stored energy for a grain size decrease of 300 to 30μm for copper. Baker presents an equation for the effect of grain size on stored energy[50] .

38

$$E = \alpha Gb^2 \left(\rho^s + \rho^G \right) = \frac{\alpha GbM \varepsilon}{D} \left(\frac{1}{\alpha_s + C} \right)$$ Equation 2.9

α, α_s and C are materials constants

G is shear modulus

M is the Taylor factor

ε is the applied strain

D is the average grain size

ρ^s is the statistically stored dislocation density

ρ^G is the geometrically necessary dislocation density

2.2.4 Key parameters affecting microstructure

The **Burgers vector**, named after Dutch physicist Jan Burgers, is a vector, normally denoted as **b**, which represents the magnitude and direction of the lattice distortion resulting from a dislocation in a crystal lattice[51]. The Burgers vector is done basically by drawing a rectangular counter clockwise circuit from a starting point to enclose the dislocation **Figure 10**. The Burgers vector will be the vector to complete the circuit, i.e., from the end to the start of the circuit [51].The direction of the vector depends on the plane of dislocation, which is usually on one of the closest-packed crystallographic planes.

The recrystallisation rate and final microstructure is affected by the initial grain size distribution **Figure 11**. The grain size affects the austenite grain boundary length per unit area, which determines the nuclei number density which increases with decreasing grain size. Since the grain boundaries are primarily the nucleation sites,hence a microstructure with a fine average grain size tends to have a more uniform spatial distribution of nuclei compared to a microstructure with a coarse grain size[52].

There have been numerous studies aluminium for aluminium and copper and this is well summed up by Humphreys[52] which shows that coarser grains are more inhomogenous such as deformation and shear bands forming , the number of nucleation sites is greater in fine grain material because recrystallisation nucleation

sites is facilitated by the grain boundaries and also in a deformed material for a strain (<0.5),the stored energy increases with decreasing grain size.

The initial grain size also affects the Avrami exponent as in the studies done with the JMAK model. It has been reported that with the same temperature and strain, fine grained copper (15µm), gave an n value of 2.7 whereas the coarse- grain copper (50µm) gave an n value of 1.7 [53]. Similarly Type 304 stainless steel, as the grain size increases from 140 – 530 µm at 0.5 strain, the Avrami exponent decreased from 2 to 1 **Figure 12** [53].
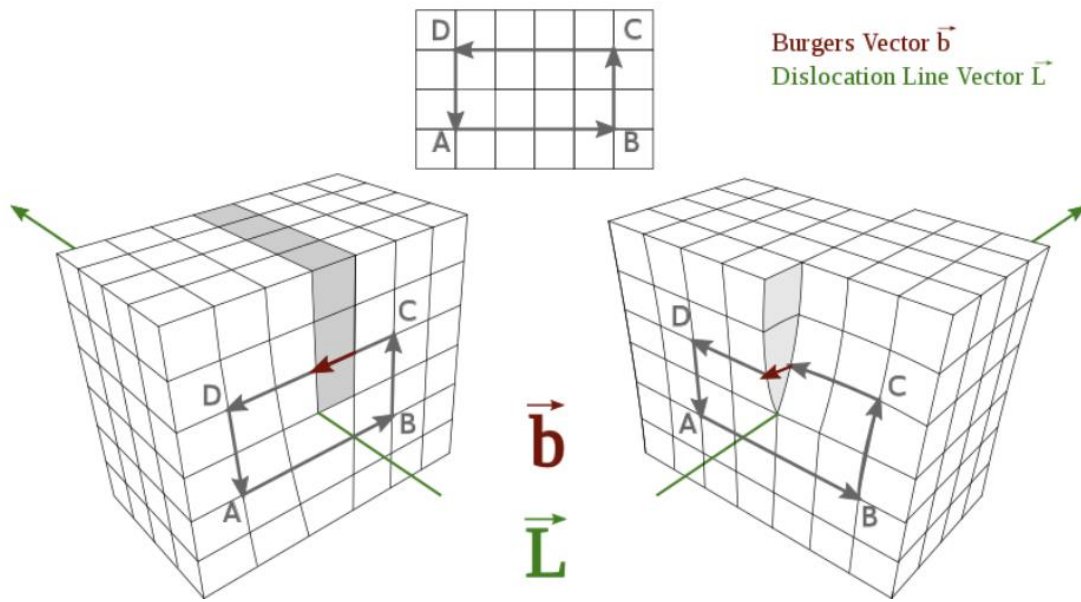
Figure 10 – Burgers vector in an edge dislocation (left) and in a screw dislocation (right). The edge dislocation can be imagined as the introduction of a half plane (gray boxes) that does not fit the crystal symmetry. The screw dislocation can be imagined as cut and shear operation along a half plane[51].
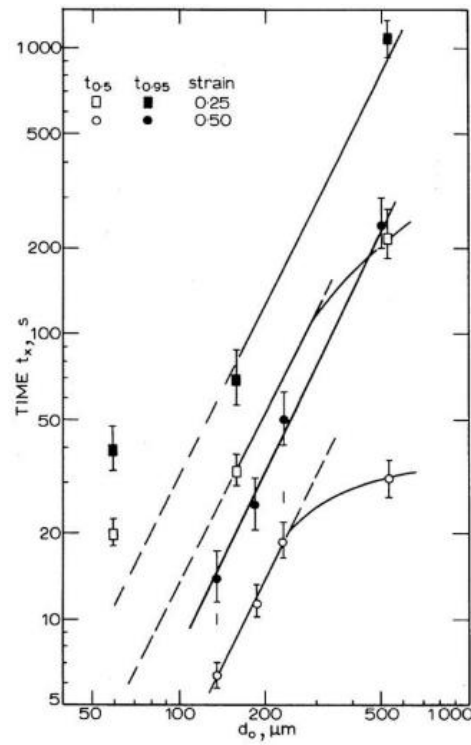
Figure 11 – Effect of average initial grain size on the 50% and 95% recrystallisation time [52]
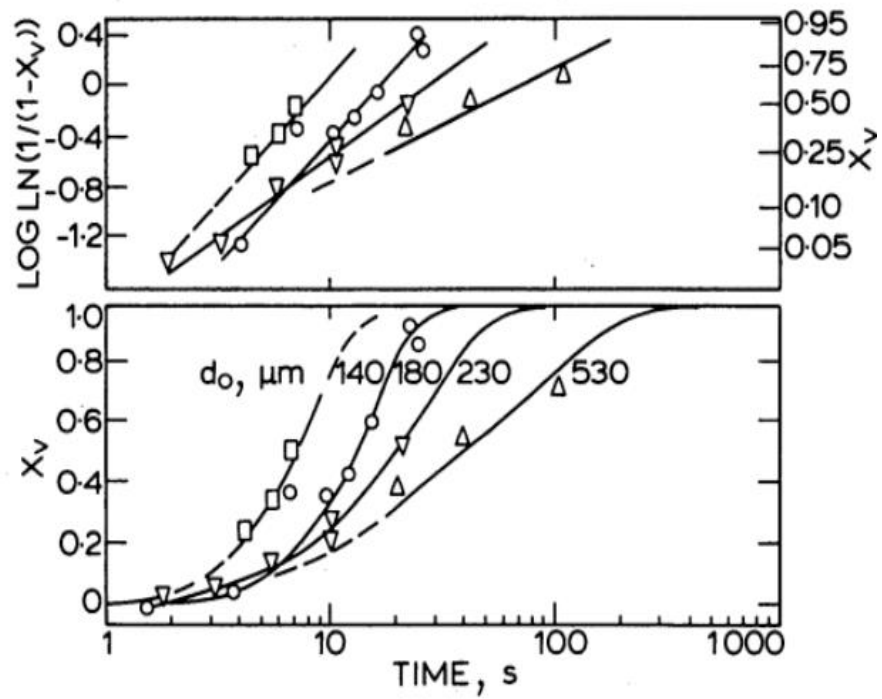
Figure 12 – Effect of grain size on static recrystallisation kinetics, samples deformed at 0.5 strain, 1050°C and 1 s-1[52].

41

The dislocation density affects the calculation of the recrystallisation nucleation and growth rate. The dislocation density is calculated from the stress increment. The dislocation density for coarser grain is lower since the stress increment gives rise to the dislocation density because coarser (softer) grains have higher strain but a lower stress increment **Figure 13.**
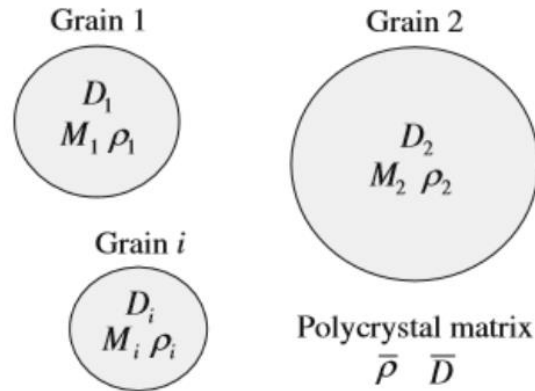
Figure 13 – Schematic diagram of grains with different dislocation density after dislocation after deformation as a result of different sizes, D_i and orientation/Taylor Factor, M_i [53].

2.3 Recovery

2.3.1 The mechanism of recovery

Recovery is the elimination and rearrangement of dislocations in order to reduce stored energy[42]. It happens during deformation (dynamic recovery) or after deformation (static recovery).

Gradual changes in the microstructure that result in restoration of material properties take place over a period prior to recrystallisation. It is the changes in the dislocation structure of the material during high temperature deformation that gives rise to the recovery stage. Most of the applied deformation energy during hot rolling of steel gets converted to heat and only a fraction of about 1-10% is used as stored energy[15].

Recovery can happen in any crystal containing a high concentration of point (i.e. lattice defects with zero dimensionality and do not have lattice structure in any dimension) or line defects (i.e lines along which whole rows of atoms are arranged anomalously) Depending on the point at which this phenomena occurs, it can be referred to as either

dynamic or static recovery[15]. Recovery is said to be the process by which deformed grains reduce their stored energy, through rearrangement and annihilation of dislocation in their crystal structure. Some or all of the sub process (namely the formation of cells, annihilation of dislocations inside the cells, formation of low-angle sub-grains and sub-grain growth) run depending on the stacking fault energy (SFE)[54]. The sub processes (see **Figure 14**) are achieved by a combination of dislocations glide, cross-slip (movement of screw dislocation from one plane to another) and climb (dislocation motion that allows edge dislocation to move out of its slip plane). As recovery is the gradual annihilation of dislocations in a given system, then this lowers the stored energy of the material. This will influence the recrystallisation kinetics (see section 2.4) and thus in turn the final grain size. It is therefore critical to understand this process to be able to predict the subsequent stages of recrystallisation. The recovery process reduces the driving force for recrystallisation.

(a) Dislocation tangles   (b) Cell formation   (c) Annihilation of dislocations within cells

(d) Subgrain formation   (e) Subgrain growth
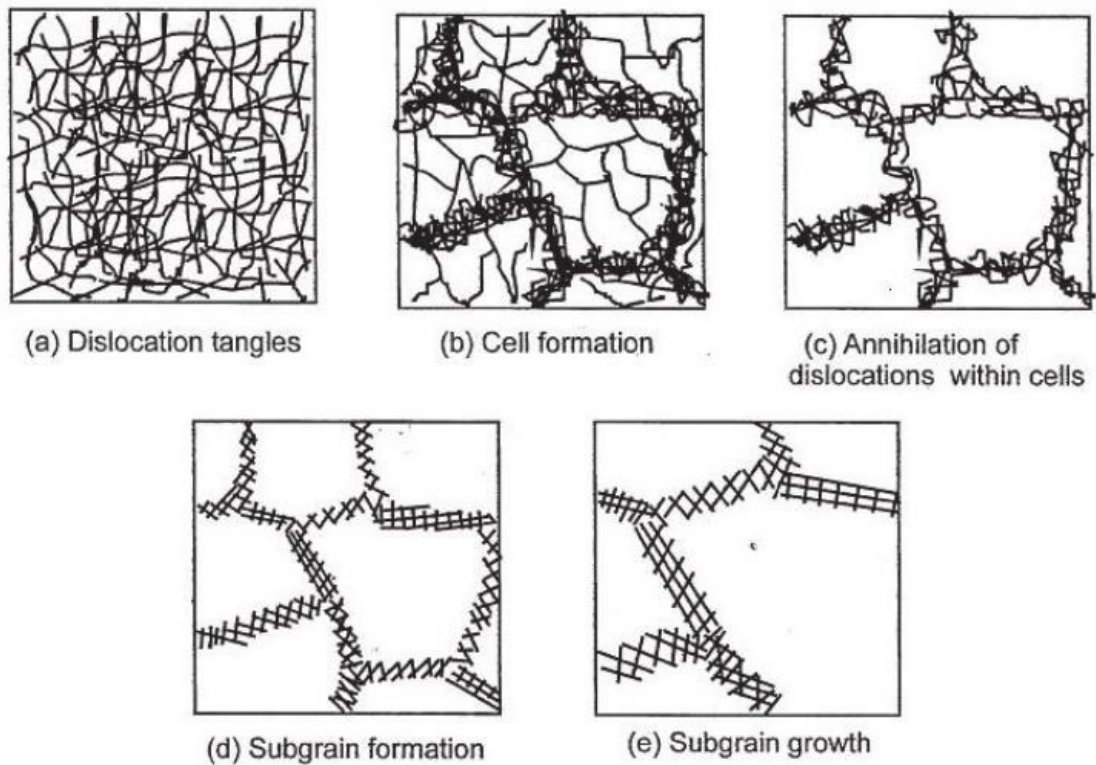
Figure 14 – The stages of recovery showing dislocation tangles, cell formations, annihilation of dislocations, formation of sub grains and growth of sub grains [22].

2.3.2 Measurement of recovery

Due to the small microstructural changes that occur, it is difficult to measure the extent of recovery directly, but recovery still plays a role in the overall kinetics of recrystallisation. The energy stored from the deformed state provides the driving force for both recovery and recrystallisation. This causes a competing effect between recovery and recrystallisation. As the recrystallisation phase follows recovery, the driving force for recrystallisation will be reduced. Any method that can measure the stored energy can invariably measure the recovery kinetics, since recovery is a measure of the reduction in stored energy of deformation. Counting of dislocations is very difficult because of the high value of dislocation density involved. The total stored energy of deformation is measured either directly, by calorimetry or X-ray diffraction, or indirectly by changes in the physical properties (like electrical resistivity and the mechanical properties such as yield stress, hardness and density). Recovery is usually measured using the changes in mechanical properties, even though the changes happen at a minor scale. The changes are subtle since physical properties are very sensitive to small phase transformations, which usually occur during annealing[15].

Macroscopic properties are usually affected by recovery, like the resistivity, density, flow stress and hardness. From an engineering point of view, the most popular way to determine recovery includes double hit tests and stress relaxation tests. These produce flow stress evolution values, which can be used directly by engineers for design and analysis. Flow stress evolution figures can easily be converted to dislocation density values using the Forest Hardening **Equation 2.10** and **Equation 2.11.**

$$\sigma = \sigma_y + M\alpha\mu b\sqrt{\rho} \qquad\qquad \text{Equation 2.10}$$

$$\sigma_D = \sigma - \sigma_y \qquad\qquad \text{Equation 2.11}$$

where σ is the flow stress, σ_y is the yield stress, σ_D is stress due to dislocation, μ is the shear modulus, b is Burgers vector, ρ is dislocation density, α is a constant of the order of 0.15 and M is the Taylor factor which is 3.1 for FCC material[4][55].

The effect of recrystallisation on dislocation density values obtained using the Forest Hardening calculation may be avoided by using recovery studies done under T_{NR}

(Temperature of No Recrystallisation) or recovery studies done for short times above that temperature[4].

For the double hit test, the sample is reheated, deformed to a fixed strain and then the stress is removed. This gives rise to the first flow stress curve, showing the yield stress. The sample is then held for a fixed time and deformed again, to measure its new yield stress. The shape of the second flow stress curve depends on the softening occurring during the inter-pass time. An example of flow stress curves is shown in **Figure 15**.

These flow stress curves from the double hit test are analysed by a chosen method, such as the offset method or mean flow stress method or by back extrapolation[56], [57]. These options are shown in **Figure 16**.
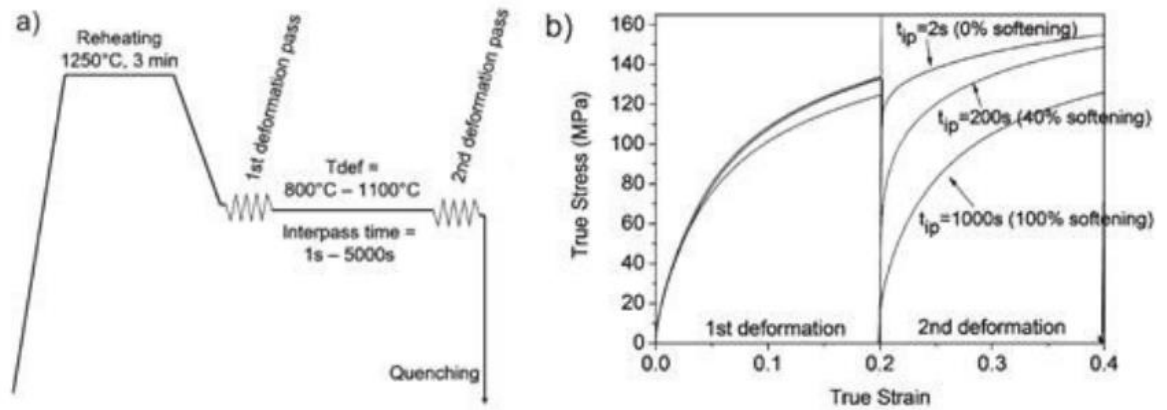
Figure 15 – (a) double deformation test and (b) stress-strain curves for calculating fraction for softening[56][57].

Unfortunately, each data point requires a new sample that has been given the same thermomechanical treatment. This makes the double hit method laborious, requiring many experiments to obtain the flow stress curves.

A single hit test (stress relaxation test) can be used as an alternative to measure the complete softening kinetics using one sample. The sample is reheated, deformed to a fixed strain and then the stress is removed. As the sample recovers, the stress is measured over time, giving rise to recovery kinetics.

45

The table in the figure contains the following content:

Offset Method (0.2 % and 2 %)

$$FS = \frac{\sigma_m - \sigma_{r,offset}}{\sigma_m - \sigma_{0,offset}}$$

σ_m = maximum stress of first deformation

$\sigma_{0,offset}$, $\sigma_{r,offset}$ = stresses at a plastic strain of 0.2 % or 2 % for the first and second deformation, respectively.

Back Extrapolation Method

$$FS = \frac{\sigma_m - \sigma_{r,be}}{\sigma_m - \sigma_{0,0.2\%offset}}$$

σ_m = maximum stress of first deformation

$\sigma_{0,0.2\%offset}$ = stress of first deformation at 0.2 % plastic strain

$\sigma_{r,be}$ = stress value at the intersection of the translated first curve with the unloading line.

5 % True Strain Method

$$FS = \frac{\sigma_{m,5\%TS} - \sigma_{r,5\%TS}}{\sigma_{m,5\%TS} - \sigma_{0,5\%TS}}$$

$\sigma_{m,5\%TS}$ = flow stress at 5 % true strain of a hypothetical second curve corresponding to zero softening.

$\sigma_{0,5\%TS}$, $\sigma_{r,5\%TS}$ = stress at 5 % true strain, first and second deformation, respectively.

Mean Flow Stress Method

$$FS = \frac{\bar{\sigma}_m - \bar{\sigma}_r}{\bar{\sigma}_m - \bar{\sigma}_0}$$

$\bar{\sigma}_0$, $\bar{\sigma}_r$ = area under the stress strain curve of the first and second deformation, respectively.

$\bar{\sigma}_m$ = area under a hypothetical second curve corresponding to zero softening.

Figure 16 – Common methods used in calculating softening from double hit test (Nb microalloyed steel, T_{def}=1000°C, t_{ip}=200s)[4][58].

2.3.3 Effect of solutes on recovery

The field matrix created by dislocations gives rise to potential sites for solute segregation, hence relieving stress. The influence of solutes in recovery is occurs through the changing stacking fault energy[59] and dislocation pinning, both within cells and sub-grain boundaries. Solutes also affect the mobility and concentration of the vacancies[60]. Sub-grain boundary migration commonly occurs by dislocation climb and its rate is controlled by solutes diffusion[61]. Dynamic and static recovery is inhibited by dislocation pinning caused by solutes and this will give rise to a higher stored energy than for a material that is solute free[62]. By varying the Nb content on two steels Zadeh *et al.* [63] showed that, for the same temperature, the steel with higher Nb content exhibited lower recovery kinetics. Yamamoto *et al.* [64] conducted exhaustive experimental studies on the impact of microalloying elements on recovery. He used different microalloyed steels and removed the effect of precipitates by decarburising it and appraising the softening kinetics using the double-deformation test for a wide range of temperatures **Figure 17**.
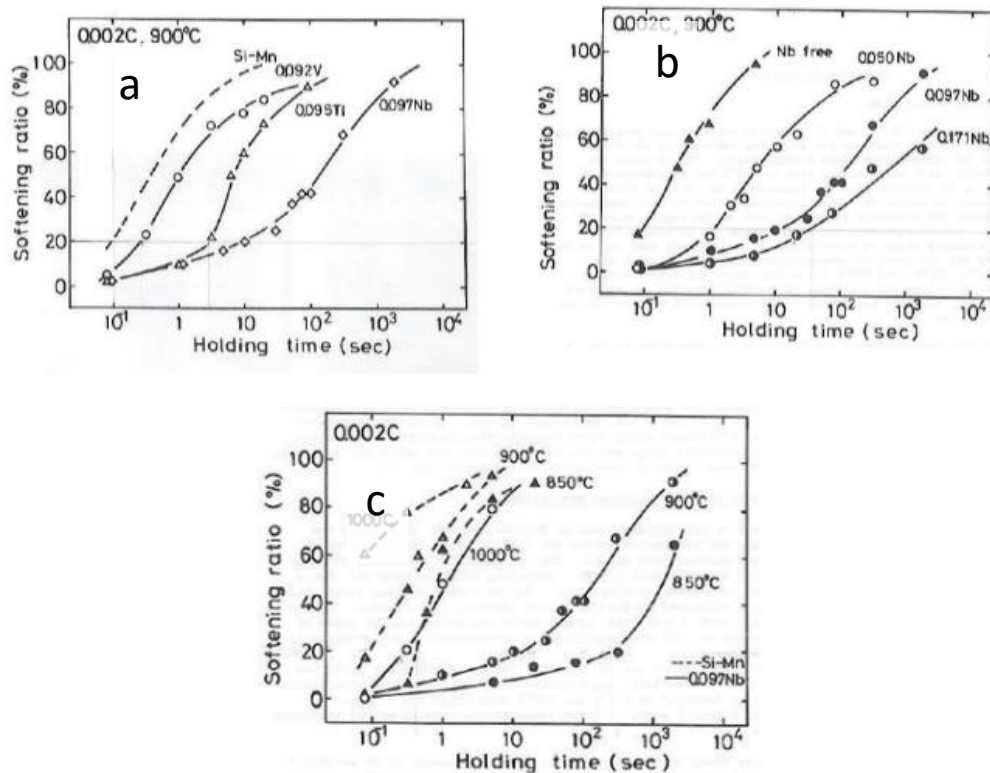
Figure 17 – (a) Effect of various solutes on softening kinetics. (b) Effect of solute content on softening kinetics. (c) Effect of temperature on softening kinetics[64].

47

The first 20% softening is solely due to recovery and hence can be interpreted in terms of effect on recovery[64]. The key findings from the work of Yamamoto *et al.* [64] in **Figure 17** are that:

There is significant retardation in the recovery kinetics by microalloying elements (Nb, Ti and V). The increase in retardation is of the order V<Ti<Nb and the consequence of this is definitely apparent in **Figure 177**(a). The 20% initial softening is clearly due to the recovery and this is also confirmed by the metallographic observations[64] and as a result the 20% softening time (t_{20}) can be used to compare the recovery kinetics conveniently. In **Figure 177**(b) the increase in Nb also leads to increase in t_{20} and hence the extent of the retardation is dependent on the solute content. Another important observation is how the concentration of solute changes recovery as a function of temperature. This is clearly seen in **Figure 177**(c) where the softening curve gradient changes with temperature. The sub-grain formation and growth is slowed down owing to the solute drag effect in the case of Nb at higher temperature. At low temperatures, a fine dispersion of niobium carbide precipitates are formed, which inhibits recovery [63]–[65].

McElroy[66] proposed that when solute elements interact with dislocations it changes the stacking fault energy (SFE). The SFE of austenite is also significantly affected by Nb and Ti [67]. An addition of 1% Nb to a 15-15 stainless steel was found to lower SFE by $20mJ/m^2$. Nevertheless, Nb is usually less than 0.1 wt.% in microalloyed steel and as such its effect on the SFE is not expected to be significant. Changes in the solutes cause the activation energy for recovery to be dependent on both the initial dislocation density and solute misfit[68][64].

2.3.4 Particles effect on recovery

Prior to recovery, there may be second phase particles present or they may precipitate during recovery. In both situations they have a dramatic effect on recovery kinetics. From **Figure 18** the initial 20% can be explained as being as a result of recovery. There is to a greater extent the deviation at lower temperature when comparing the dotted lines (precipitate free) with the solid ones (with precipitate) and this emphasizes a converse relationship between recovery and precipitation kinetics.
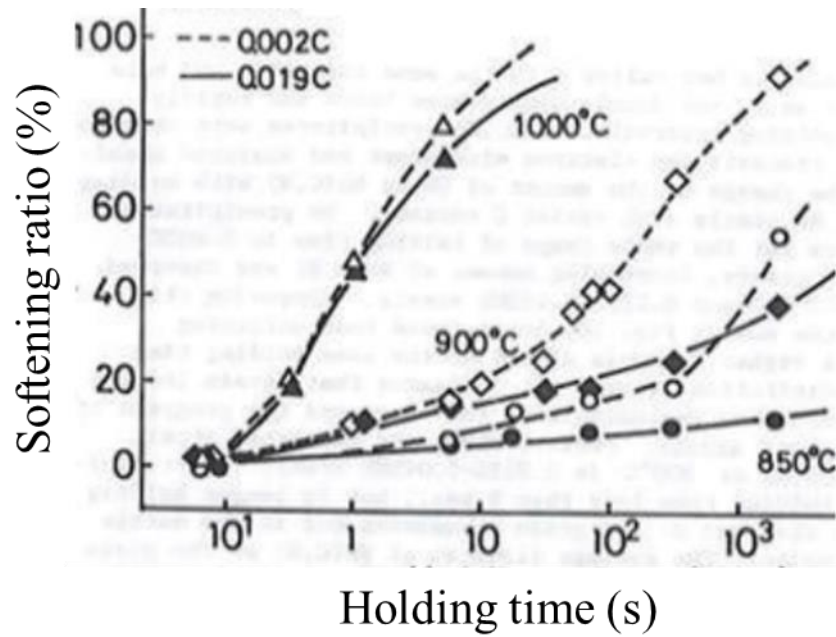
Figure 18 – Effect of particles on recovery kinetics dotted lines is precipitate free and the solid line with precipitate[64].

There are several ways in which second phase particles may affect recovery. Humphreys[60] specifies that amid the initial stage of recovery, when there is rearrangement of dislocations into low angle boundaries, the individual dislocations can be pinned by the second phase particles. Consequently, this prevents the rearrangement of dislocations, so retarding recovery. He also stated that if the inter-particle distance is small and comparable to the scale of the dislocation network, then the particles will inhibit recovery.

2.3.5 Recovery models

The large number of dislocations ($\sim10^{15}$ /m^2) and heterogeneous distribution of the dislocations makes modelling recovery complicated. In a heavily deformed steel a dense dislocation network is formed, which makes the direct microscopic observation of the mechanism difficult. This leads to indirectly modelling the strain energy distribution (and associated dislocations) and the different individual processes, namely cross-slip, glide and climb. This is done at both scales of inter-grain (50-500µm) and intra–grain (1-10µm)[4]. Of key importance to the engineer is the relationship between the sub-grain level and the multi-granular level which gives rise to the macroscopic mechanical properties. In literature the two most significant

49

isothermal relations for recovery modelling are the logarithmic kinetics and power law kinetics. At an intermediate annealing temperature ($T_m/2$) in microalloyed steels, the logarithmic kinetics is typically observed. The logarithmic kinetics is a function of the dislocation glide or solute drag as the rate controlling step. Generally, the decay of flow stress is governed by either logarithmic or power law kinetics[60], as expressed below:

$$\sigma_D = c_1 - c_2 \, ln(\, t\,)$$
Equation 2.12

$$\sigma_D = c_3 - c_4(\, t\,)^{-m}$$
Equation 2.13

where, C_1, C_2, C_3 and C_4 and m are constants and vary with material and processing conditions. The logarithmic decay equation is only valid at low annealing temperature of heavily strained FCC metals[69] and is a thermally activated cross-slip mechanism. The logarithmic kinetics could result from solute drag or glide control[70], [71]. The power law kinetics are usually seen in polycrystals[72], [73]. Nes [74] modelled recovery using two parameters, since recovery is made up of growth in the cellular structure and dislocation density decomposition inside the cellular structure, using:

$$\sigma(\, t\,) = \sigma_i + M\mu b \left[f_s \alpha_1 \sqrt{\rho(\, t\,)} + f_n \alpha_1' \frac{1}{\sqrt{\delta(\, t\,)}} \right]$$
Equation 2.14

where σ_i is frictional stress, δ is sub-grain size and α_1, α_1' are constants.

It is assumed in the model that the decay in the flow stress is attributed to the sub-grain boundary and the dislocation density inside the sub-grain. Recovery progress in high SFE materials is controlled by the sub-grains coarsening. A single parameter model based on sub-grain size was developed by Sellars *et al.* [75] and correlated to the strength in Al alloys and the decay in flow stress. The decay in flow stress is similar to the Hall-Petch relationship of decay in yield stress, owing to the increment in grain size. The problem is applying both these models to microalloyed austenite, since it has an intermediate SFE. To achieve this there is a need for a different model to capture both dislocation density decay in the cell structure and the increase in the cell/sub-grain size. The issues of misorientation, leading to the boundary mobility as the sub-grain grows, was not captured in the above models. Also other challenges that are

difficult to quantify are the changes in the volume fraction of the cell size and the grain boundary thickness. In small strains Verdier *et al.* [76] observed that yield stress decay is logarithmic regardless of the evolution of the cellular microstructure. Therefore, using a single internal variable (average dislocation density), the strength decay can simply be modelled and this is related via the Forest Hardening-type relationship shown in **Equation 2.10**. This model developed assumes that the internal stress relaxation is as a result of thermally activated dislocation rearrangement and annihilation. The plastic relaxation rate $\dot{\varepsilon}$ is related to change in internal stress σ_d by:

$$\frac{d\sigma_d}{dt} = -\dot{\varepsilon}E \qquad\qquad \text{Equation 2.15}$$

where E is Young's modulus. The relation between $\dot{\varepsilon}$ and dislocation density is given by Orowan's Law:

$$M\dot{\varepsilon}_p = \rho b \overline{V} \qquad\qquad \text{Equation 2.16}$$

where M is the Taylor factor, ρ is the dislocation density and $\overline{V}$ is the average dislocation velocity. The dislocation velocity is thermally activated and is governed by σ_d as per:

$$\overline{V} = b\nu_D\, exp\left(-\frac{U_a}{k_bT}\right) sinh\left(\frac{\sigma_d V_a}{k_bT}\right) \qquad\qquad \text{Equation 2.17}$$

where ν_D is the Debye frequency. And finally the flow stress evolution is given by equation below:

$$\frac{d\sigma_d}{dt} = -\frac{64\sigma_d^2}{9M^3\alpha^2 E}\, exp\left(-\frac{U_a}{k_bT}\right) sinh\left(\frac{\sigma_d V_a}{k_bT}\right) \qquad\qquad \text{Equation 2.18}$$

In this equation U_a is activation energy and V_a is activation volume. The activation energy values ranges from that of pipe diffusion (i.e vacancy-mediated diffusion along dislocations) to bulk diffusion. In this model the activation energy actually represents the mechanisms of cross-slip, climb or solute drag. As such the recovery kinetics is affected since recovery is dislocation rearrangement. The activation volume V_a is related to the spacing of the pinning centres and the activation volume corresponds to an activation length of V_a/b^2 and this is within the range of 20-40b. The activation

length is the average measurement of the distance between two pinning centres. The pinning centres may be the jogs on a screw dislocation as in the case of glide, or solute atoms in the case of solute drag. The activation spacing changes with a change in pre-strain levels as the cell walls tighten[77].

When the Verdier model is fitted with experimental recovery data, a trend can be observed for the activation volume as related to the Nb content and the relaxation temperature. This is in line with the understanding that as Nb concentration increases the distance between the pinning centres decreases, also raising the temperature for the same Nb concentration increases the mobility of Nb atoms and this results in reduction of the activation volume because the pinning centres become less effective.

2.4 Types of recrystallisation

Primary recrystallisation takes place by the nucleation and growth of new grains at the deformed and recovered matrix. There is an incubation period during which viable nuclei are formed at a number of preferred sites which are the deformed austenite grain boundaries and also the recrystallised-unrecrystallised interface[78]. The driving energy for recrystallisation is stored energy after recovery. Nucleation occurs by strain induced boundary migration due to the local strain energy gradients and these gradients are more pronounced at the lower deformations because of the local strain inhomogeneity[79]. Also, at the recrystallised-unrecrystallised interface, due to effect of pinning of the carbonitride particles, nucleation of new grains occurs instead of the growth of the already recrystallised grains[80]. In a heavily deformed austenite, the deformation bands formed are also sites for recrystallisation nucleation[81]–[84]. Though, many of these bands are deformed annealing twin boundaries[93][94] and do not act as nuclei[79]. These are probably as a result of the variations of the strain associated with the deformation bands[81][82][84]. Lastly, larger undissolved precipitates will also act as a site for recrystallisation[88]. Smaller particles may also act as nuclei, as the critical nucleus size decreases with increasing rolling strain[60].

Based on the conditions of deformations, there are four different mechanisms to transform the original set of equiaxed grains into a different set through thermomechanical processes[89][90], namely static recrystallisation, dynamic recrystallisation, metadynamic recrystallisation and continuous recrystallisation.

2.4.1 Static recrystallisation of austenite

The major restoration process is static recrystallisation, which takes place when the nucleation and growth takes place after deformation[91]. The driving force for static recrystallisation during the rolling process is the energy stored during deformation and to achieve this a minimum critical deformation is needed for static recrystallisation to occur[92]. The rate of static recrystallisation is increased by a high deformation temperature and the number of recrystalising nuclei. This depends on the grain boundary per unit volume(SV) of the austenite prior to deformation. As the degree of strain and temperature of deformation is increased and the initial grain size reduces, the rate of static recrystallisation increases[93],[94]. The recrystallised grain size is statistically independent of the deformation temperature and also is refined by a decrease in the starting grain size and an increase in the applied strain[21] [94], [95].

2.4.2 Dynamic recrystallisation

Dynamic recrystallisation is a consequence of both nucleation and growth which take place during the deformation process[96]. The favourable conditions for dynamic recrystallisation to take place are deformation at high temperatures, large reductions in strain rate and a low strain rate[97]. The conditions in the existing rolling mills are not generally compatible with these combinations. The use of dynamic recrystallisation is limited in relations to grain refinement because recrystallisation at high rolling temperature is not favourable to fine recrystallised grains. The extent of the dynamically recrystallised grain is only dependent on the temperature and strain rate of the rolling reduction, and it does not depend on the initial grain size or the draught [21] [94], [95]. The beginning of dynamic recrystallisation is characterised by the drop in flow stress during deformation.

The peak (ε_p) strain which is the strain at the maximum stress is used to monitor dynamic recrystallisation[98]–[100]. For a given chemistry, the peak strain increases with the rate of deformation and grain size but reduces with increasing temperature[101]. Nonetheless, there is a critical strain for dynamic recrystallisation and it is always less than the peak strain[98], typically <0.5 for hot rolling.

2.4.3 Metadynamic recrystallisation

Metadynamic recrystallisation takes place when the nucleation of the new grains happens during hot deformation but the growth takes place after the hot deformation[92]. Djaic *et al*. [92] observed a sudden change from strain dependent to strain independent at a strain ~ 0.8 ε_p and this is due to the presence of pre-existing recrystallisation nuclei in the deformed matrix when the strain is greater than the critical strain. The static recrystallisation under these conditions is referred to as metadynamic in order to distinguish it from the classical recrystallisation at lower strains, when the nuclei are formed after deformation. The recrystallisation start times in metadynamic cases are always less than the static one[102].

2.4.4 Continuous recrystallisation

Continuous recrystallisation is to some extent different from the others in the sense that it is not strictly a recrystallisation process but an advanced form of recovery in which there is no gross movement of high angle grain boundaries[103], [104]. It is understood that continuous recrystallisation is the process of forming grain microstructure with a low lattice defect density, in which migration of high angle grain boundaries (HAGBs) does not occur or is vigorously reduced. It is a homogeneous process that takes place under certain specific conditions in heavily deformed materials[105].

Of all the recrystallisation processes then, static is the most applicable to hot rolling of line pipe steel. Therefore the mechanisms for grain refinement need to be understood in more depth.

2.5 Recrystallisation kinetics

Static recrystallisation begins when deformed metals are heated at an elevated temperature that means it is a thermally activated process and also involves the migration of high angle grain boundaries with angle of misorientation usually greater than 10° to 15° [52], [72], [106], [107]. This migration is driven by the stored energy of deformation. The term recrystallisation in itself is a misnomer. It was believed that the loss of ductility after deformation is owing to the destruction of the crystalline structure, which is then restored. Therefore the term recrystallisation was used to

describe the process [108]. Recrystallisation has a pronounced effect on the overall mechanical properties of a material. Humphreys[52] defines it as a process wherein deformed grains are replaced by a new set of strain free grains. The average dislocation density reduces drastically due to the gradual decreases in the deformed grains and this causes the yield strength of the material to decrease and increases the ductility. First the un-deformed grains nucleate and grow to consume the whole structure of the deformed grains. The nucleation rate and the growth rate of each nucleus governs the overall recrystallisation kinetics. In the case of steels, recrystallisation after deformation is the only metallurgical process to refine grain size, shape and texture. Recrystallisation causes greater significant reduction in strength and increase in ductility when compared to recovery. Recrystallisation is very useful industrially because it softens the material in order to restore ductility and this gives room for additional processing[109].

The major factors affecting static recrystallisation are pre-strain, starting grain size, annealing temperature, solute content, precipitate volume fraction and size [110].

2.5.1 Nucleation of recrystallisation

Recovery is a continuous process whereas recrystallisation is discontinuous and has a distinct incubation period, after which nucleation occurs, followed by the growth of nuclei. Nucleation of recrystallisation does not occur in a classical thermodynamic sense. The nuclei are formed from the pre-existing cells/sub-grains as long as certain growth criteria has been achieved and not arising from a different phase[109]. The mechanisms for nucleation in the literature are: particle stimulated nucleation, nucleation due to sub-grain coarsening and strain induced boundary migration (SIBM) [52]. Researchers have concluded that in this current context of static recrystallisation (in low strain, high temperature microalloyed steels) that SIBM is the dominant mechanism[111], [112][113]. The sub structure developed after deformation coarsen as a result of recovery and SIBM takes into account the presence of pre-existing grain boundaries. The sub-grains bordering the boundaries bulge into the adjacent grains when it has coarsened enough to overcome the capillarity drag effects, as shown in **Figure 19**. This bulging becomes thermodynamically favourably once the sub-grains have coarsened substantially. Defects are eliminated as a result of the movement of the

boundary, so the stored energy is reduced, which is greater than the increase in total grain boundary surface due to bulging [114]–[116].
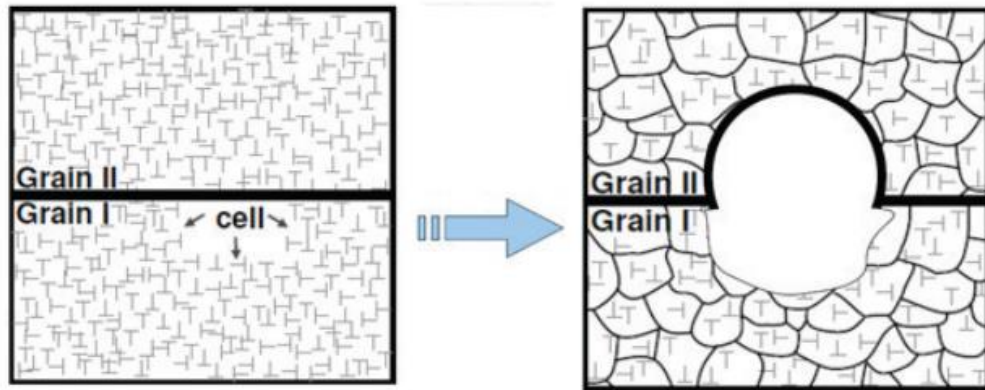
Figure 19 – Graphic of the sub-grain coarsening and boundary bulging associated with recrystallisation nucleation[112].

In SIBM, because there is no new creation of a high angle boundary, the orientation of the new grain is similar to the original grain from which it was deformed. Although the effect of strain rate was not investigated, Hurley and Humphreys reported that for total strains less than 0.7, SIBM is the dominant mechanism[111]. Also according to Humphreys, a stored energy gradient across the boundary triggers boundary migration in SIBM [17], [117] moving as a front (multiple sub-grain or as a boundary bulge adjacent to a single large sub-grain), see **Figure 20**.
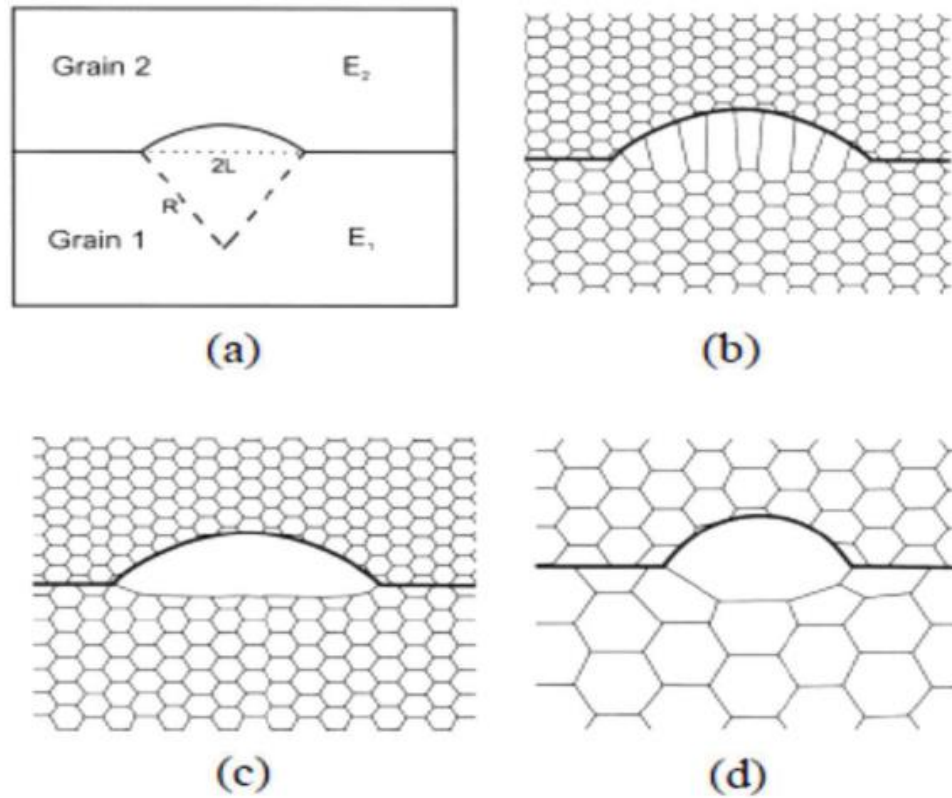
Figure 20 – (a) SIBM of a boundary separating a grain of low stored energy (E_1) from the higher energy one (E_2), (b) dragging of the dislocation structure behind the migrating boundary, (c) the migrating boundary is free from the dislocation structure (d) SIBM originating at a single large sub-grain [52].

For materials that have large stored energy differences and poorly developed dislocation cell structures, Bate *et al.* [118] and Hurley *et al.* [111] agree that SIBM occurs by well recovered sub-structures. Multiple SIBM will be preferred in materials that contain a significant number of secondary phase particles. After measuring growth rates of SIBM in aluminium, Hurley [111] states that an incubation time is required for nucleation to happen, proving that prior recovery is necessary for SIBM to occur and so placing emphasis on the effect of recovery on SIBM.

An incubation period for recrystallisation nucleation was published by Lauridsen *et al.* [119] based on X-ray diffraction. The work shows 80% of nucleation occurs before the material has recrystallised by 10% and the other 20% of nucleation occurs much later (assuming a critical nucleus size of 1µm). It can be seen in **Figure 21**, that nucleation does happen at later times, which could be attributed to heterogeneous

distribution of stored energy. Given this evidence, site saturation cannot be assumed in all cases.
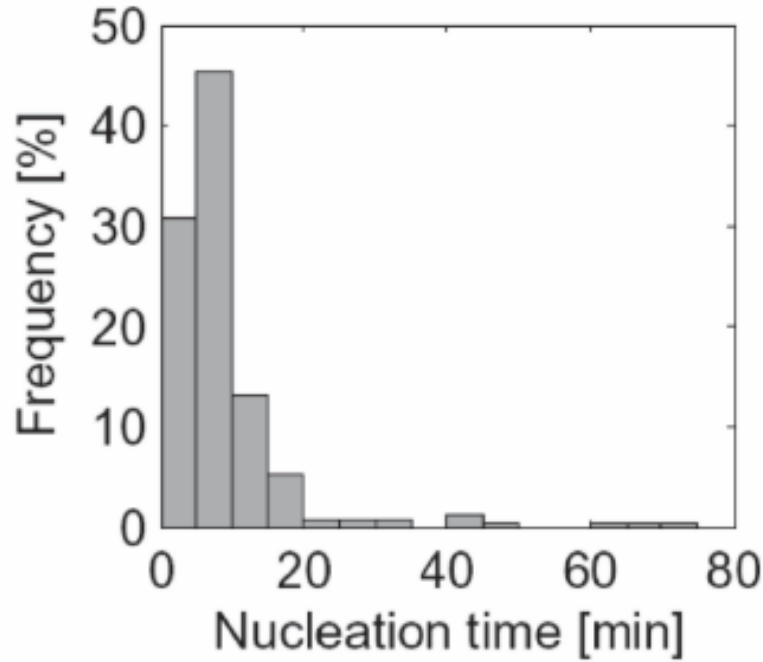
Figure 21 – Distribution of nucleation times determined from 244 recrystallisation curves by 3-d X-ray diffraction[119].

2.5.2 Growth kinetics

When nucleation has occurred, deformed substructure is consumed as the bulged high angle boundary moves across the deformed grains giving rise to clean, strain free microstructure. This migration of high angle boundaries is how recrystallisation proceeds and it is also common to grain coarsening, although the driving force for each of these processes is different. Grain coarsening is driven by the minimization of grain boundary surface energy whereas recrystallisation is driven by the dislocation density difference across the high angle boundary. From the theory of thermally activated growth, the relationship between boundary migration rate and driving force under non-equilibrium conditions is usually expressed as:

$$V = M_{GB}\left(P - P_z\right)$$
<div align="right">Equation 2.19</div>

where, V is the boundary velocity, M_{GB} is a proportionality constant (or grain boundary mobility), P is the driving pressure and P_z is the drag force due to second phase particle.

Mobility, in pure materials, refers to the energy spent to transfer an atom from a shrinking grain to the growing grain across the grain boundary. The following expression for the grain boundary mobility in pure single phase materials was derived by Turnbull [120] from first principles:

$$M_{pure} = \frac{\delta D_{GB} V_m}{b^2 RT}$$

Equation 2.20

In this equation δ is the grain boundary thickness, D_{GB} is the grain boundary self-diffusion coefficient, V_m is the molar volume, b is the Burger vector. The grain boundary diffusion has exponential dependence on temperature as shown below:

$$D_{GB} = D_0 \exp\left(-\frac{Q}{RT}\right)$$

Equation 2.21

Due to the exponential dependence of diffusion on temperature, the mobility can be expressed in an Arrhenius type relationship as follows:

$$M_{GB} = M_0 \exp\left(-\frac{Q}{RT}\right)$$

Equation 2.22

Where M_o is the intrinsic mobility .It can be seen in **Figure 22** that the process of recrystallisation has an incubation time, which is related to the time it takes for the sub-grain to overcome the capillary barrier. When nucleation starts, migration of high angle boundaries continues until they all meet. There is a heterogeneous distribution of recrystallised regions around the deformed grain and even at the early stages of recrystallisation, impingement of the growth of nuclei occurs [108].
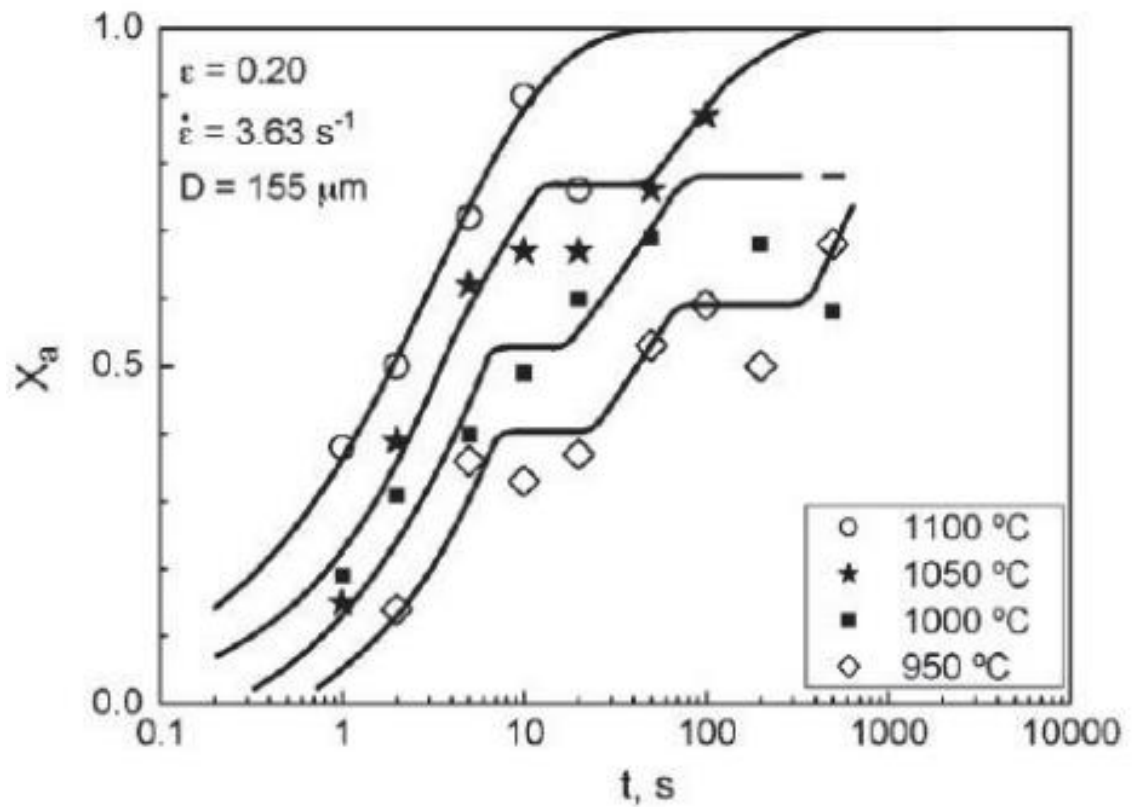
Figure 22 – A plot of recrystallized volume fraction as a function of time for a steel containing 0.13 V and 0.48 C[121].

2.5.3 Solute drag

Solute drag effect is the process by which solute elements reduce grain boundary mobility and various authors have looked into this effect in detail in a number of published papers[122]–[124]. The addition of small amounts of solutes decreases recrystallisation kinetics significantly[125]–[127].
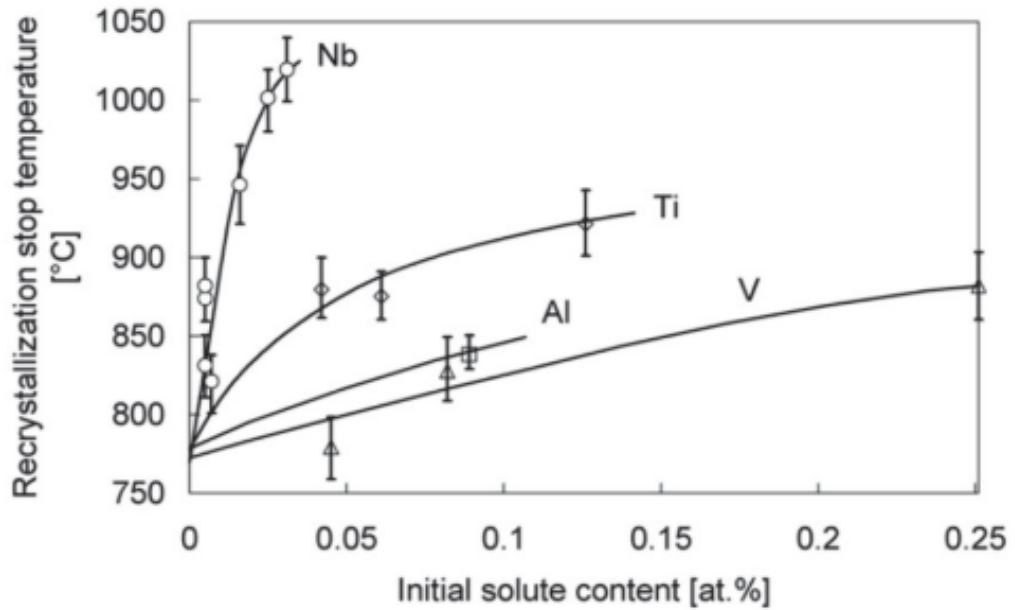
Figure 23 – Effect of the initial solute content on the recrystallisation stop temperature[126].

At higher temperatures in microalloyed steels, the microalloys remain in solution and by the effect of solute drag retard the kinetics of recrystallisation. At low temperatures the microalloys precipitate and this further pins recrystallisation. Yamamoto *et al.* [125] showed that niobium has the greatest solute drag effect as shown in **Figure 23**. To study the effect of solute drag and remove interference with the precipitates, decarburization/denitriding experiments were carried out.

Dynamic segregation of solutes on a moving boundary, which reduces their lattice misfit strain energy, is a way of visualizing solute drag. In a single phase material with a stationary boundary, the concentration profile of the solute in front of the boundary and behind, cancelled out any attractive or repulsive force on the boundary because they are absolutely equivalent. Although, more solute atoms are left behind when the boundary moves than are assimilated from the front (due to the slow movement relative to the moving boundary), thus forming a concentration profile that is asymmetric. As a result a drag force is experienced by the boundary halting its advance. Solute drag is very effective in decreasing the growth kinetics of recrystallisation and grain coarsening by reducing the boundary mobility, even in a small concentrations. Rearranging **Equation 2.19** for a precipitate free case yields:

$$P = \frac{V}{M_{GB}}$$

Equation 2.23

or,

$$P = f_iV$$

Equation 2.24

and

$$f_i = \frac{1}{M_{GB,i}}$$

Equation 2.25

f_i reciprocal is the mobility of the boundary $M_{GB,i}$ which is the intrinsic boundary mobility in the absence of any solute. f_i is the intrinsic friction of the material and relates to the energy needed to move an atom from one side of the boundary to the other side. Generalising the above equation to include the drag from other sources yields:

$$P = f_iV + P_{solute} + P_{zener}$$

Equation 2.26

Where P_{solute} represents the solute drag experienced by the boundary and P_{Zener} is the Zener drag due to second phase particles.

Independently P_{solute} can be calculated using Hillert's treatment of solute drag, in other words it can be expressed as Vf_{solute} where V is the boundary velocity and f_{solute} is solute drag force, which can be calculated using Cahn[128] and by Lucke and Stewart treatment[124] (CLS model) of solute drag[129].

The CLS and Hillert's model will give the same outcome irrespective of whether the migration of high angle boundaries in a single phase microstructure is as result of recrystallisation or grain coarsening. Nonetheless, if there are different phases across the boundary, like in the case of phase transformation, then the stability of the solute is different across the two sides of the boundary and the solute drag formulation changes. In this case only the Hillert's model is applicable. In this current work only the Cahn's model is being used, since the treatment of solute drag can easily be integrated into the growth equations discussed in the previous section. In Cahn's model, with respect to low velocity branch (see **Figure 24**), the solute drag is proportional to the solute concentration:

$$P_{solute} = \alpha C_0$$

Equation 2.27

62

Where, C_0 is the microalloying element concentration in solution. α is a constant and is a function of both solute-boundary binding energy and cross-boundary solute diffusion coefficient. It is given by:

$$\alpha_m = \frac{\beta N_v (k_b T)^2}{E_b D_x} \left(sinh\left(\frac{E_b}{k_b T}\right) - \frac{E_b}{k_b T} \right)$$

Equation 2.28

Where β is the grain boundary thickness, N_v is the number of atoms per unit volume, E_b is the solute-boundary binding energy and D_x is the trans-interface boundary diffusion.

Combining **Equation 2.24**, **Equation 2.26** and **Equation 2.27**, the overall boundary mobility ($M_{GB,eff}$) is given by:

$$\frac{1}{M_{GB,eff}} = \frac{1}{M_{GB,i}} + \alpha C_0$$

Equation 2.29

This approach is used by Zurob and Dunlop [112], [130] to model the solute drag effect on recrystallisation kinetics. In the absence of all possible attachment kinetics, the maximum value of intrinsic mobility used was given by Turnbull mobility [110], [120].
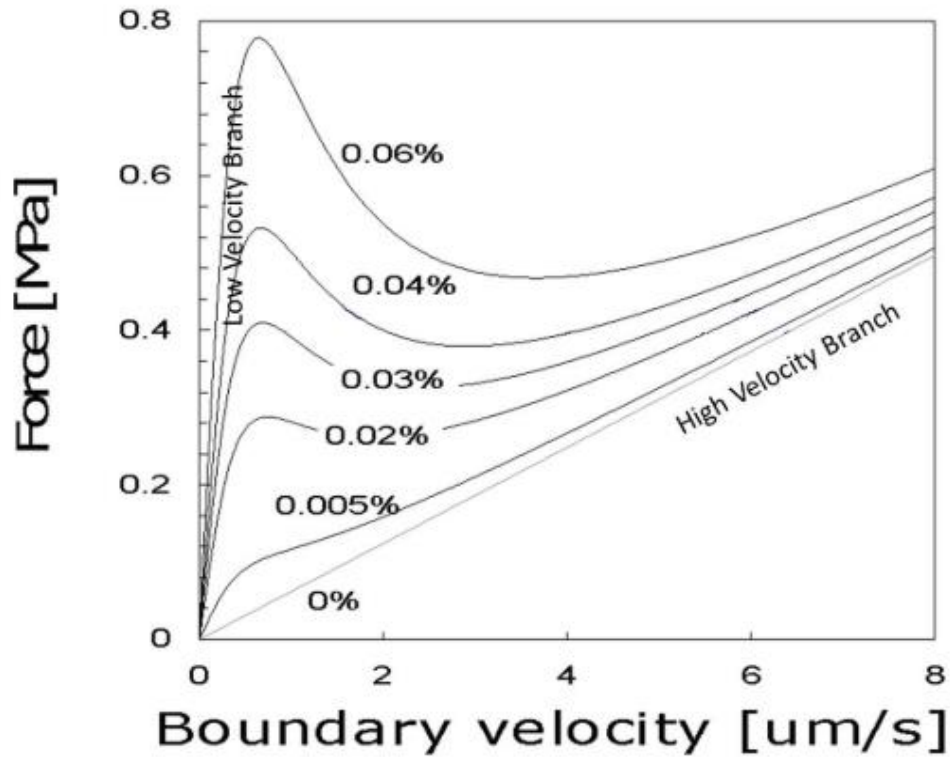
Figure 24 – Cahn's solute drag plot for different values of Nb, showing both low velocity and high velocity branch[16].

2.5.3.1 Zener pinning

It is known that the presence of finely dispersed hard second phase particles delay or stop recrystallisation completely[131], [132]. This is because when a moving boundary intersects a particle, a small portion of the grain boundary area disappears and as a result the potential energy of the system is reduced by an amount equal to the surface energy of the absent boundary (as displayed in **Figure 25**). Consequently for the boundary to break away from the particle it needs to create a surface, hence raising the overall energy. This difference in energy level is what is termed as Zener drag.
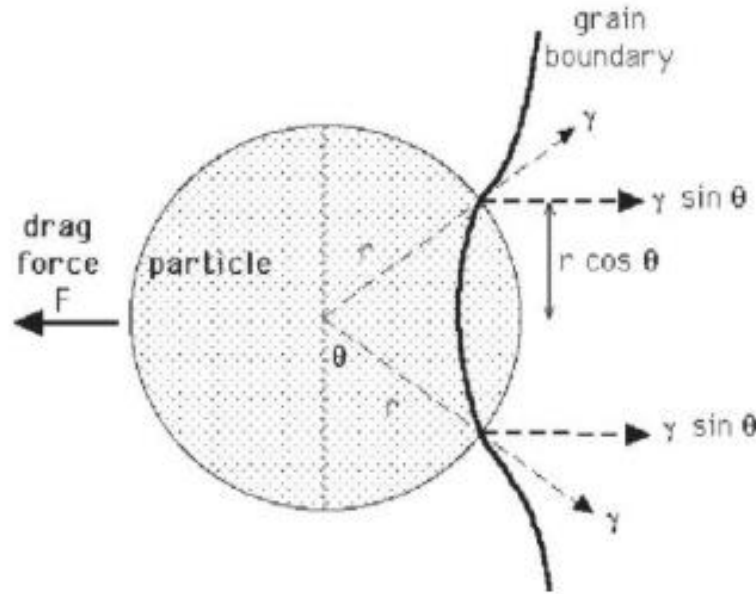
The net drag force on the surface boundary energy (γ) per unit area, due to a non-shearable particle of radius r is given by:

$$F = 2\pi r\gamma \, sin\,\theta \, cos\,\theta \qquad \text{Equation 2.30}$$

The maximum force experienced by the boundary is when $\Theta=45°$ and substituting this value into the above given equation, we have:

$$F = \pi r\gamma \qquad \text{Equation 2.31}$$

The number of random particles per unit volume in a random distribution is given by:

$$N_V = \frac{3F_V}{4\pi r^3} \qquad \text{Equation 2.32}$$

Where F_v is the volume fraction of the particles. The number of particles intersecting unit areas (N_s) of the grain boundary is the product of the diameter of the particles and N_s and is equal to:

$$N_s = \frac{3F_V}{2\pi r^2} \qquad \text{Equation 2.33}$$

Therefore the total drag force is N_s times F

$$P_z = \frac{3 F_V \gamma}{2 r}$$

Equation 2.34

Zener drag in a classical thermodynamic sense is not a drag force owing to its discontinuous nature, it is rather a kind of activation energy that the moving boundary needs to pass through an obstacle. Grain boundaries are preferential sites for precipitation since it takes place after deformation in a microalloyed steel. This means the grain boundaries experience a higher Zener drag than that calculated from the above equation, assuming a random distribution.

2.6 Modelling of recrystallisation kinetics

Various research has showed that the process of recrystallisation has a sigmoidal trend. Johnson, Mehl, Avrami and Kolmogorov (JMAK) model was one of the simplest and earliest models to show this. The main concept of this model is centred on the extended volume fraction[52][4] given by:

$$X_{ext} = \int_0^t V_t \dot{N} dt$$

Equation 2.35

Where, $\dot{N}$ is the nucleation rate (assumed constant) and V_t is the volume of the single recrystallised grain. Using the extended volume fraction does not take into consideration the impingement of one growing nuclei on another. Also new nuclei cannot form in an area that has already recrystallised. The actual recrystallised fraction for randomly distributed nuclei in a deformed material is given by:

$$X = 1 - exp(-X_{ext})$$

Equation 2.36

Merging **Equations 2.35 and 2.36** and replacing volume by $4\pi(vt)^3 / 3$ we have:

$$X = 1 - exp\left(-\frac{4\pi}{3} \int_0^t \dot{N} v^3 t^3 dt\right)$$

Equation 2.37

Where v is the interface velocity, and in most of the formulation of this equation it is assumed that the nucleation rate and growth velocity are constant and accordingly we can simplify the above equation as:

$$X = 1 - exp\left(-\frac{\pi}{3} \dot{N} v^3 t^4\right)$$

Equation 2.38

66

The equation above is the simplified JMAK equation for constant nucleation and growth rates. The simplified version of the JMAK equation is used in most empirical and quasi-physically based models and has assumed that both the nucleation and growth rate are constant and when put together, it is further simplified to:

$$X = 1 - exp(-Kt^n)$$

Equation 2.39

Where n and K are usually referred to as Avrami constants. These constants are fitting parameters as they are not calculated separately but derived from fitting the JMAK equation to the recrystallised kinetics from experimental data. As a result it is difficult to derive any physical meaning from these constants and therefore, Avrami constants are quasi-physical parameters at best.

Similarly, the above equation can be derived for the limiting case of site-saturation where the nuclei are formed before the recrystallisation growth starts and this assumption will lead to an exponent of n to have the value of 3. When nucleation decreases at finite rate, the JMAK exponent will lie between 4 and 3[52], also experimentally derived JMAK exponents can be less than 3 because the growth rate and dimensionality can change during recrystallisation[52].

Figure 26 showing the changes in Avrami exponent during recrystallisation. From the plot at 15µm even when the nuclei are at grain boundaries, they are still randomly distributed. However, by increasing the initial grain size to 50µm the distribution becomes non-random and this violates the JMAK assumption, resulting in a non-constant Avrami exponent.
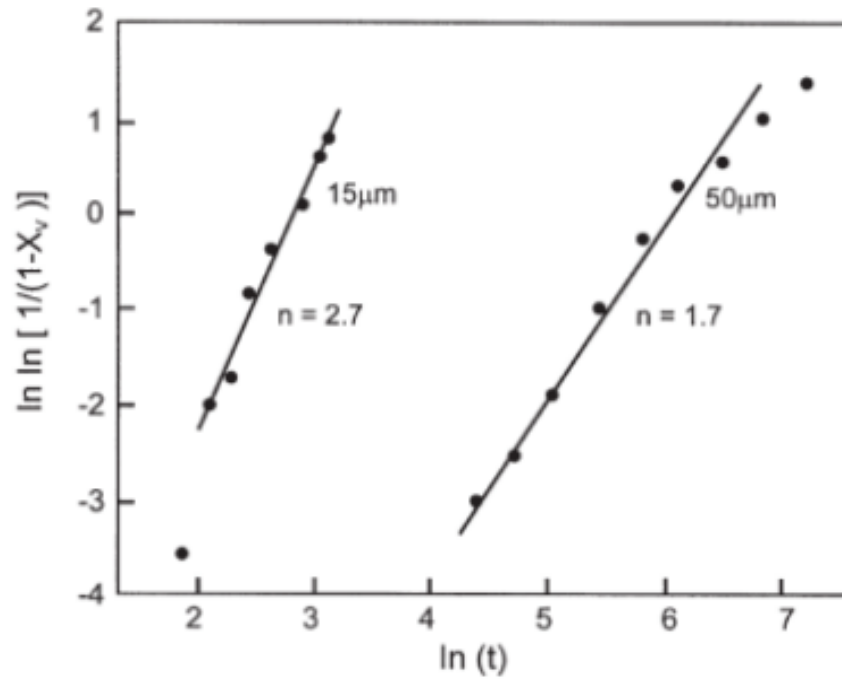
Figure 26 – Recrystallisation kinetics of copper at 225°C of different initial grain sizes cold rolled 93% [124][4].

The main objective of recrystallisation industrially is to refine the coarse austenite grains(~1500µm) and owing to this large grain size, the nucleation is non-random and therefore it is not applicable industrially to use constant Avrami exponent.

The theoretical calculated values of the Avrami exponent are shown in **Table 1** depending on the nucleation mechanism and growth dimensionality. As previously discussed in section 2.5.1 site saturation or constant nucleation are not usually true in most cases, since the rate of nucleation changes during recrystallisation. Also sample geometry or microstructural constraint can inhibit the recrystallised grain, which will result in dynamic change in the growth dimensionality and so the experimentally obtained Avrami constants are not integral values and evolve with time.

Table 1 – Theoretical calculated Avrami exponents[52][4][141].

Growth Dimensionality	Site Saturation	Constant Nucleation Rate
3-D	3	4
2-D	2	3
1-D	1	2

The most critical limitation in the JMAK model is in it assumptions that the nuclei are randomly distributed. This means it requires considerable modification to be applied to situations where the nucleation is supposed to start from some definite regions, like the grain boundary, twins etc.

To solve this problem the next generation model tries to make the Avrami exponent as a function of time, so as to fit the experimental data better. This is entirely an empirical approach, thereby limiting its application to the domain for which it was defined. This means that physical interpretation of the model is not possible.

Sellars *et al.* [133] proposed an empirical equation for predicting time for 50% recrystallisation but this equation is only valid for C-Mn steels.

$$t_{50\%} = 2.5 \times 10^{-19} D_0^2 \varepsilon^{-4} \, exp\left(\frac{300,000}{RT}\right) \qquad \text{Equation 2.40}$$

Where D_o is the initial modal grain size and ε is the applied strain .

Over the past decades this and other equations of a similar type are popularly used by researchers studying the effects of some influential parameters. They have developed a database for activation energy, strain exponent and other parameters for a wide variety of compositions and processing conditions. Medina *et al.* reported the values of the constants used in Sellar's equations by conducting torsion based experiments for a variety of steels of both microalloyed and C-Mn type[134]. Sellar's $t_{50\%}$ equation was used by other authors[135], [136] to compare steels of different chemistry and processing conditions and they discovered that Nb slows growth remarkably and even slows it further when it precipitates at a lower temperature. Sellar's model is used for comparing steels with different chemistry and processing conditions or parameters but it is not good enough to predict the complete recrystallisation kinetics.

Sun *et al.* [137] used Sellar's model to compare recrystallisation kinetics for steels having different chemistries and processing conditions, but acknowledged that physical based models are too complicated to develop but would provide further insight.

In a later development using the Sellar's model combined with the finite element method (FEM), more sophisticated models have been developed to capture the evolution of the microstructure and flow stress throughout the volume of the material. The flow stress is captured by combining the Sellar's equation with a Forest-Hardening

69

equation (**Equation 2.10**). These models were capable of predicting the evolution of recrystallisation in multi-pass deformation under continuous cooling and thus were better able to predict the evolution of austenite microstructure.

Zurob *et al.*[112] presented a model that used an identical idea to that of Humphreys [138] that the growth rate of an individual sub-grain is given by the product of mobility and the driving force. The driving force is the stored energy of deformation decreased by the amount of the Zener drag of precipitates. An individual grain is assumed to grow spherically and isotropically. Avrami's extended volume concept was utilised to calculate global recrystallisation kinetics and Dunlop *et al.* also further extended the modal and applied it to zirconium alloys[130].

The growth model for multi-pass rolling using non-isothermal conditions was developed from a single pass isothermal model by Pereda *et al.* [139] and the growth was modelled using the coupled Seller's and Avrami equations.

$$X = 1 - exp\left[-ln\,2\left(\frac{t}{t_{0.5X}}\right)^{n}\right]$$

Equation 2.41

Where t is time (s), $t_{0.5x}$ is the time to reach a 50% recrystallised fraction and n is the Avrami exponent.

$$t_{0.5RX} = 9.92 \times 10^{-11} D_0 \varepsilon^{-5.6\,D_0^{-0.15}} \dot{\varepsilon}^{-0.53} exp\left(\frac{180,000}{RT}\right)$$
$$\times exp\left[\left(\frac{275000}{T} - 185\right).[Nb]\right]$$

Equation 2.42

The Avrami exponent was modified to be applicable under various conditions, giving:

$$n = 155\,exp\left(-\frac{56485}{RT}\right)$$

Equation 2.43

These equations are solely valid for isothermal single pass rolling. Pareda *et al.* [139] boosted the application in non-isothermal conditions by discretising temperature in small isothermal steps and the corresponding recrystallised fraction in each step was calculated and added later on. To use this in a multi-pass deformation schedule, the

recrystallised fraction along with the effective grain sizes were calculated at the end of each pass. This was used as an input for the next pass.

Strain induced boundary migration (SIBM) nucleation is mostly neglected for a physical based model in the literature, primarily because almost all of the published work assumes site saturation since there is no physical based nucleation model to describe the nucleation process thereby removing the need for the assumptions of site saturation or constant nucleation rate and the overall kinetics is modelled using the Avrami equation, thereby removing the need for a separate nucleation model. The growth of recrystallisation can be measured microscopically unlike nucleation [117] and as such, in recrystallisation models and simulations, growth is treated in much detail and nucleation is overlooked. Therefore for a formidable recrystallisation model, a precise nucleation model is a pre-requisite.

The majority of nucleation takes place in a very short interval compared to the total time for recrystallisation (**Figure 21**) [117]. Thus a constant[16] for site saturation is used instead of the number density of recrystallisation nuclei and this is known as site saturation approach. The exclusion of a reliable nucleation model makes it challenging for predicting the incubation time and recrystallised grain size. The use of Bailey Hirsch criterion[140] to calculate the critical size of nucleation helps to overcome these limitations [112]. This criterion stipulates that a sub-grain with radius r(t) will start to grow inside the deformed structure in an unstable manner when the driving force for growth G(t) overcomes the capillary force $2\gamma_{SE}/r(t)$ where γ_{SE} is the surface energy and when the sub-grain size is greater than $2\gamma_{SE}/r(t)$ nucleation will kick in. It is the sub-grains that are greater than this in size, called the critical size, that will form a growing nuclei.

$$r_c(t) > \frac{2\gamma_{SE}}{G(t)}$$

Equation 2.44

Pairing the growth kinetics equation of sub-grain and high angle boundary growth rate allows prediction of the incubation time for nucleation and then the overall recrystallisation kinetics. Backe's [69] recrystallisation model assumed that the size of a sub-grain is proportional to the mean free distance of the dislocation slip. The sub-grain misorientation and low angle boundary energy both depend on the dislocation density. As recovery progresses the dislocation density decreases. It is assumed that

71

nucleation starts when a certain critical value of the ratio of recovered dislocation density to the original deformed dislocation density is reached. Backe suggested that the growth rate of sub-grains will be proportional to sub-grain boundary mobility, driving force and the sum of vacancy concentration in the deformed and recrystallised zone. The driving force used by Backe is the stored energy of deformation minus the Zener pinning force and solute drag forces[69] [4].

2.7 Summary of literature review

For modelling recrystallisation it is common practice to use average grain sizes. While this is sufficient for predicting some properties like tensile strength, it is not sufficient in predicting complex properties like toughness, which depends on the grain size distribution, rather than the average grain size.

Modelling recrystallisation using average grain sizes is also not widely applicable because it is limited to the specific steels and conditions upon which the model is based. This method could potentially be used for other steels or conditions if it can be assumed that the grain size distributions are log normal and that the grains all have the same shape. However, in reality the initial grain size distributions are made up of a range of grain sizes.

Furthermore, significant discrepancies related to the ability of recrystallisation models to predict final grain sizes correctly have been identified. Kundu *et al*. investigated this and concluded that grain size distributions should be used instead of average grain sizes[141].

Zurob *et al*. used grain size distributions for dynamic recrystallisation. However, the model did not fit well with the observed experimental dynamic softening behaviour at a strain rate of above $0.2s^{-1}$ because the nucleation rate was underestimated[53].

The Zurob model was then extended by Rehman *et al*. to model static recrystallisation with the potential to model recrystallisation inhomogeneity but there was no comparison between the predicted and experimental data[4].

Bos *et al*. built on the work of Rehman to describe metallurgical processes at the annealing stage of dual phase steels for recrystallisation and transformation using a 3D physical cellular automata model. This uses the austenite grain size distribution (rather than the frequently used empirical recrystallisation equations, where average grain

sizes are considered) to predict the recrystallised grain size distribution and recrystallisation kinetics. However, the model was not validated against experimental data for recrystallisation to predict the recrystallised full grain size distribution[142].

3 Current modelling capability

An internal model has been developed with Tata Steel Europe R&D for grain evolution during processing. This model has initially focused on the austenite to ferrite transformation[143].

This model is Cellular automata based and will be discussed in this chapter along with an assessment and sensitivity analysis of the initial state of play of the model.

3.1 Cellular automata (CA) modelling state of the art for recrystallisation

Cellular automata models are made up of algorithms that describe the discrete spatial and temporal evolution of complex systems by applying local transformation rules to the lattice cells that typically represents volume portions. For recrystallisation models, each lattice site assumes one of a finite set of possible discrete states and the state of a lattice site is characterised in terms of internal state variables such as lattice defect quantities (stored energy), precipitation density or crystal orientation. By mapping the initial distribution values for the chosen state variables onto the lattice [180]-[193], the opening state of automaton is defined.

As deterministic or probabilistic transformation rules, known as switching rules are applied, they act on the state of each lattice point so that its state is a function of its previous state and that of neighbouring sites.

Cellular automata operate in discrete time steps. The values of the state variables update for every point simultaneously after each time interval. Therefore, cellular automata simulate the evolution of complex dynamical systems containing numerous similar components, based on their local interactions. Cellular automata are like other continuum models, requiring the definition of elementary units and transformation rules reflecting the kinetics addressed.

Achieving the correct common scaling of the entire system is necessary if some of the transformation rules refer to different real-time scales (like recrystallisation and recovery, grain boundary and bulk diffusion). By using a probabilistic transformation rule [144] predict the recrystallisation texture. Time and space are the independent variables and the space is discretised equally into shaped cells that describe stored deformation energy(mechanical driving force) and the crystal orientation(texture). The

inputs data in such cellular automata are extracted from plasticity theory (i.e crystal plasticity finite element simulations) or experiment (i.e micro texture map). The distribution of the crystal orientation and the driving force is commonly the initial state. In this cellular automata each mapped regions of identical crystal orientation is use to denote the grains or sub-grains however the driving force varies inside the areas. As the state of the cells changes the kinetics evolves from it and this takes place based on the transformation rule that governs the individual switching probability of each cell as a function based on its previous state and that of the state of its neighbouring cells. The transformation rule ensures that the phenomenon of static recrystallisation is mapped. The state of the non-recrystallised cell that belongs to the deformed grain may change as a result of the expansion of the recrystallised neighbouring grain that expands based on the local driving force and the boundary mobility. The stored dislocation energy of a non-recrystallised cell drops to zero when the expanding recrystallised grain sweeps through it and a new orientation is mapped onto it and it then becomes that of the expanding neighbour grain [145]. The progress in recrystallisation can be defined as a function of the local driving forces (stored deformation energy) and interface properties (grain-boundary mobility). The difficult aspect of such simulations is to identify an appropriate rule for nucleation events.

Figure 27 shows an example of a coupling of a cellular automaton with a crystal plasticity finite element model for predicting recrystallisation textures in aluminium [146]. The change both in dislocation density (upper figures) and in micro texture (lower figures), as a function of the annealing time during isothermal recrystallisation. The grey areas in the upper figures indicate a stored dislocation density of zero, i.e. these areas are recrystallised [146].

The major advantage of such an approach is the fact that it considers the inherited heterogeneity in the deformed material instead of material homogeneity.

In this coupled model the nucleation is considered at a level above the sub grain length scale as it does not describe explicitly the cell walls and sub grain coarsening phenomenon it alternatively assimilate the nucleation on the basis of the kinetic and thermodynamic instability criteria known from classical recrystallisation theory. The kinetic criterion implies that the formation of a high angle grain boundary that can sweep the neighbouring deformed matrix is due to a successful nucleation process while the thermodynamic criterion implies that the driving force is provided by the

stored energy changes in the newly formed high angle grain boundary that drives it into the deformed matrix.
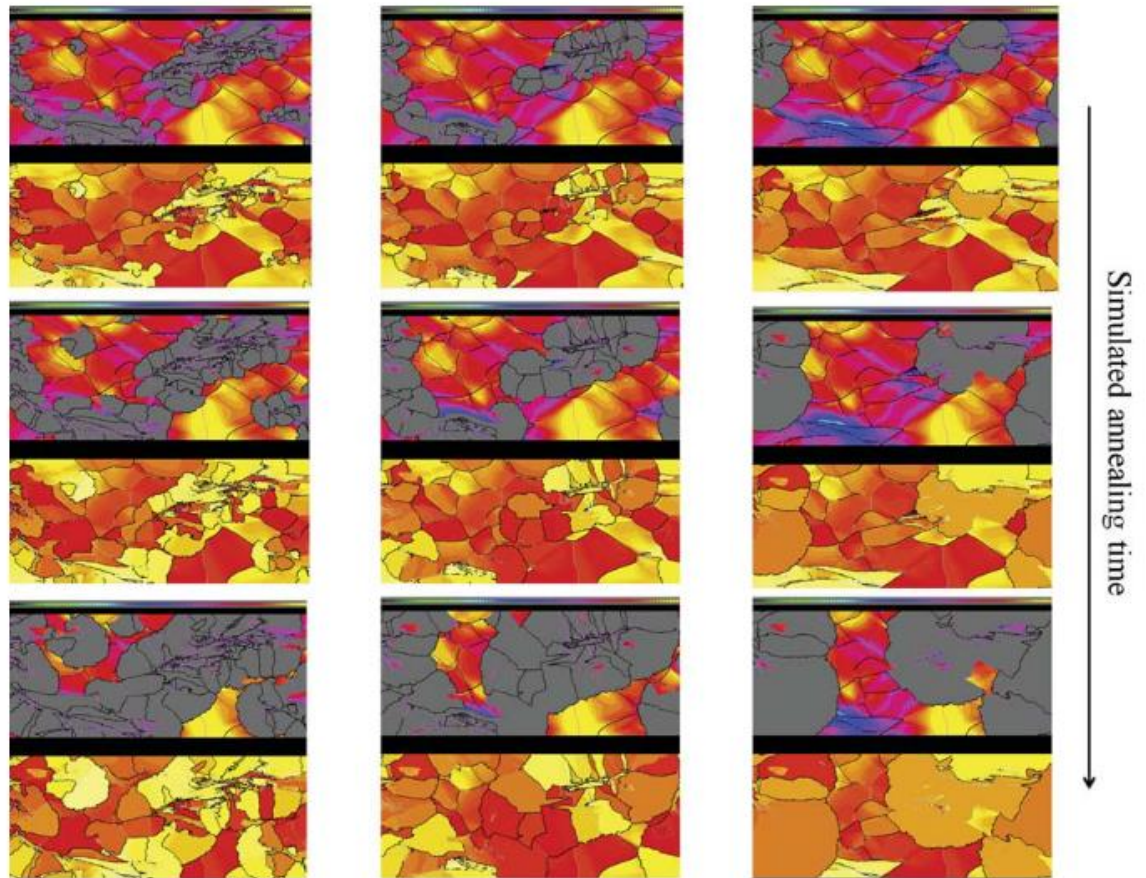
Figure 27 – Series of subsequent stages of a 2D cellular automaton simulation of primary static recrystallisation in a deformed aluminium polycrystal on the basis of crystal plasticity finite element data .The figure shows the change both in dislocation density (upper figures) and in macrotexture (lower figures), as a function of the annealing time during isothermal recrystallisation. The grey areas in the upper figures indicate a stored dislocation density of zero, i.e. these areas are recrystallised, the black lines in both figures indicate misorientations above 15∘ and the thin grey lines indicate misorientations between 5∘ and 15∘, irrespective of the rotation axis. [139].

Bos *et al.* reported the development of a 3D cellular automata model, which is able to simulate the microstructure development throughout the annealing stage using the starting grain size distribution instead of the modal grain size. This includes austenite to ferrite phase transformation with physical a nucleation model that describe the nucleation process hence no need for site saturation assumptions or constant nucleation

rate, austenite and ferrite recrystallisation, pearlite to austenite transformation, ferrite to austenite transformation, finite difference description of carbon diffusion and an improved nucleation model for recrystallisation [143]. The model can simulate the microstructure development based on the local grain-boundary and interface velocity, the latter controlled by both interface mobility and carbon diffusivity. It also provides information on the carbon gradient in austenite at the end of the cycle, which is relevant for the prediction of martensite formation during any subsequent quenching. The simulated structure **Figure 28** thus provides a realistic representation of many microstructural aspects [143][142].
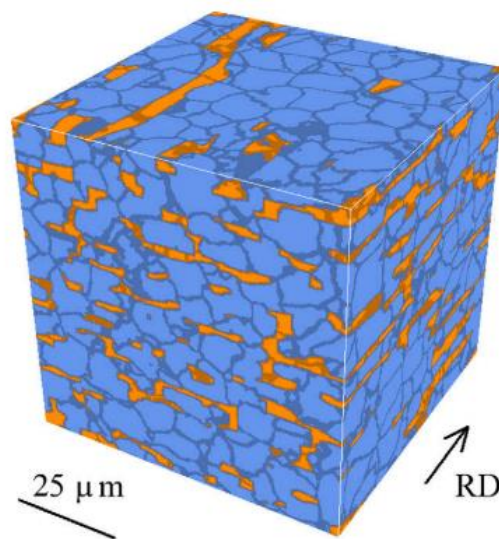
Figure 28 – A three dimensional final microstructure of a dual phase annealing cycle simulation: the orange colour is the austenite, blue is ferrite and RD is the rolling direction[142].

3.2 Cellular automata modelling framework

A cellular automata (CA) model was received from TATA steel Europe. This had been used to model recrystallisation kinetics and phase transformation behaviour, giving good agreement to the commercially produced microstructures with less attention having been given to the full grain size distribution predictions[142][143].

In this chapter, I will describe the new work carried out to analyse the suitability of this model for its application to model 3D recrystallisation in hot rolled steel.

The following sections will focus on the work I did to assess the applicability of the CA starting model as I received it. Important characteristics of the model relevant to adapting it as a recrystallisation model for hot rolled steel will be presented. Elements including creating the initial microstructure, grid spacing and hot deformation. Also pertinent to this is the work of Rehman *et al.* [4] as this collection of research provides key fundamental models used to inform the analysis of the CA model undertaken.

The Cellular automata basically work using the following algorithm, for every time step:

I.   Nucleate new grains

II.   Calculate interface velocity for all interface cells

III. Grow interface cells: $r_i(t+\Delta t) = r_i(t)+ \Delta t\, v_i$, where t is the time, r growth radius and v_i is the interface velocity

IV.   Update transformed cells and interface cells

3.2.1   Creating initial microstructure in cellular automata

Numerical analysis of the microstructure is enabled by modelling the properties and geometrical shape of grain size. The distribution of grain size and the geometrical shape of the grains are the relevant properties to model. For any further meaningful analysis to be done, a mathematically analytic description of a microstructure that is similar enough to the real structure of the material is needed. One way of approximating the microstructure in polycrystalline materials is with the Voronoi tessellation. This Voronoi diagram is a partitioning of a plane into regions based on distance to points in a specific subset of the plane. That set of points (seeds) is specified beforehand, and for each seed there is a corresponding region consisting of all points closer to that seed than to any other. These regions are called Voronoi cells. **Figure 29** shows the 3D Voronoi microstructure of the initial grain size distributions, the 2D microstructure of the starting microstructure used in the model and the initial grain distribution output from the model with a modal grain size of 160µm.
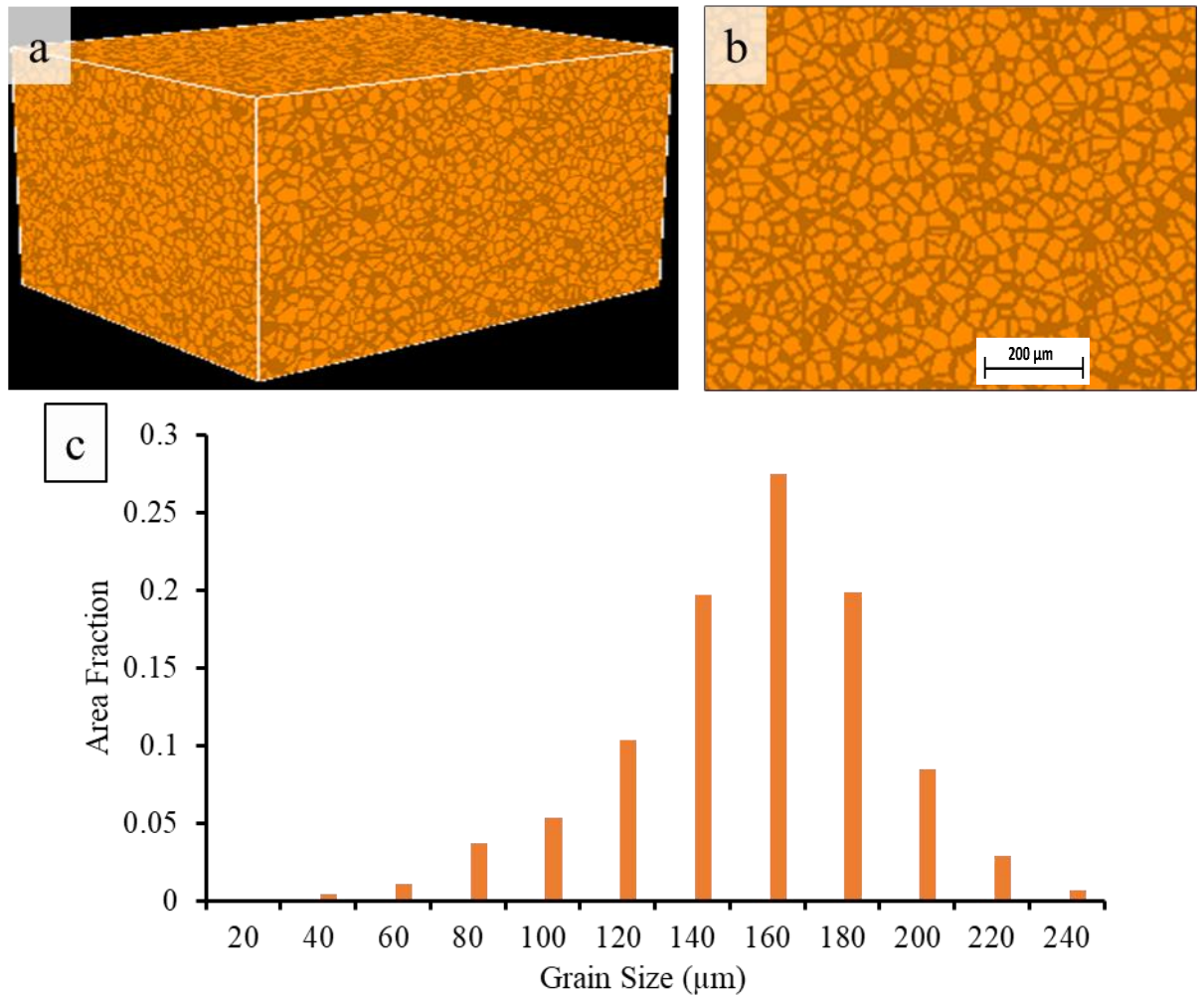
Figure 29 – Shows the austenite starting microstructure with a modal grain size of 160µm for Fe-30Ni-0.044%Nb, system dimension of 400x400x400 with a grid spacing of 6µm and 3D grain density of $4.666000E+11m^{-3}$ (a) 3D starting microstructure in the simulation system. (b) 2D-Cut from the 3D starting microstructure. (c) Initial grain size distribution.

3.3 Hot Deformation in cellular automata

After the initial microstructure is generated, which is shown in **Figure 30**, it is then hot deformed to a given strain. The example shown in **Figure 30**, the deformation at the end is set by subtracting the strain from one $(1.0 – 0.35 = 0.65)$, so the deformation is carried out to a strain of 0.35. The system applies the specified deformation to the system, which is purely geometric plane strain compression. The deformation is always in the Y–direction and it is compensated by the deformation in the X–direction and the Z–direction is unchanged. The strain energy that is assigned to the deformed

austenite can either be a constant value for all the grains (the deformation parameter) or the user can specify a strain energy distribution file. This file is a simple text file (ASCII) that contains the strain energy and the relative intensity, which add together to make one.
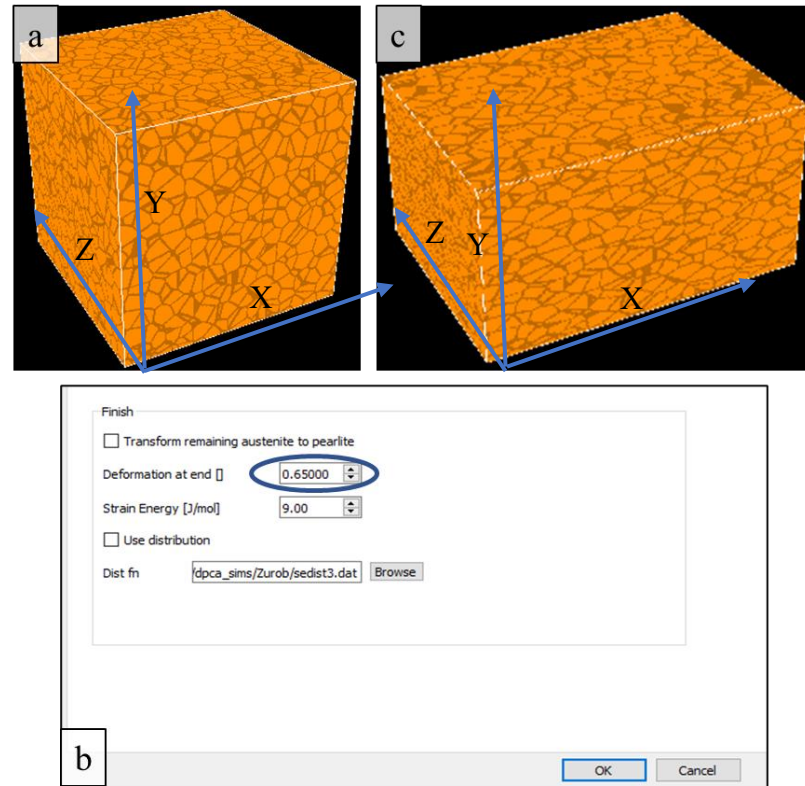
Figure 30 – (a) The initial 3D austenite microstructure. (b) The cellular automata console applying constant deformation equal to 0.35 strain at the end. (c) The deformed austenite structure at 0.35 strain, for Fe-30Ni-0.044%Nb hot deformed at 950°C with a starting modal size of 160µm.

The 'deformation at end' is a scaling factor that is multiplied with the original 'height of your system (the size of your system in the y–direction). So with a factor of 0.65, as shown in **Figure 30**, your new height is 0.65 times your original height. This corresponds roughly with a strain of 0.35. The exact value is given by this relationship:

$$\varepsilon = \ln(\frac{\Delta Y}{Y}) = \ln(1 - \varepsilon) \qquad \text{Equation 3.1}$$

Where ε is strain, ΔY is the change in thickness in the Y–direction. The system is scaled by the factor specified. The deformed sample is then run for recrystallisation.

3.4 Spatial components (Grid size and volume)

Grid spacing is the measured distance between two discrete points in the software. By increasing the distance then computationally the simulation is much quicker, however ensuring that features can be encapsulated by the grid spacing is important. Depending on the used grid spacing a nucleus is either smaller or larger than one cell. With grid spacings of 1 and 3 micron a nucleus is typically larger than one cell. We can deal with this in two ways. Either a nucleus larger than one cell can be introduced. Alternatively , a nucleus can be introduce as one cell which is allowed to grow a bit faster until it reaches its (original) critical size. The latter of these two methods was implemented in this model.

Several simulations were run for recrystallisation with a grid spacing of 1µm, 3µm, 6µm, 9µm and 12µm (**Figure 31**). The initial microstructure was generated for each of the grid spacing and then deformed at 0.3 strain then each of the deformed microstructures was then allowed to recrystallized. The results were analysed for the initial grain size distribution, grain size distribution after recrystallisation and the recrystallisation kinetics.
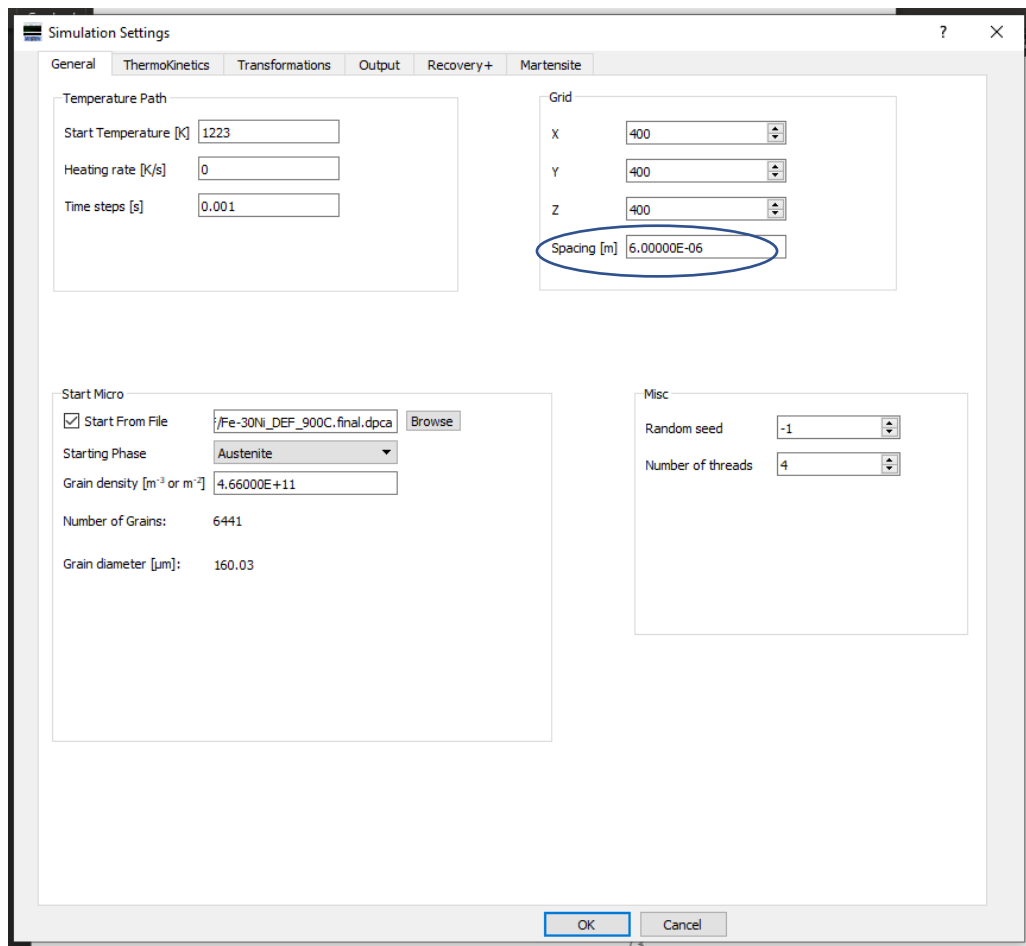
Figure 31 – The encircled box is the grid spacing in the simulation console.

Figure 32 shows the initial grain size distribution for the various grid spacing of 1µm, 3µm, 6µm and 12µm. The initial distribution from 3–12µm grid spacing has the same modal grain size of 160µm but the 1µm grid spacing has a modal grain size of 140µm, which is different from the starting modal grain size of 160µm that was input into the simulations. This is due to the fact that statistically there are a lower number of grains created using a grid spacing of 1µm. Across all values of the grid spacing, the range of grain size is the same (from 20µm to 260µm).
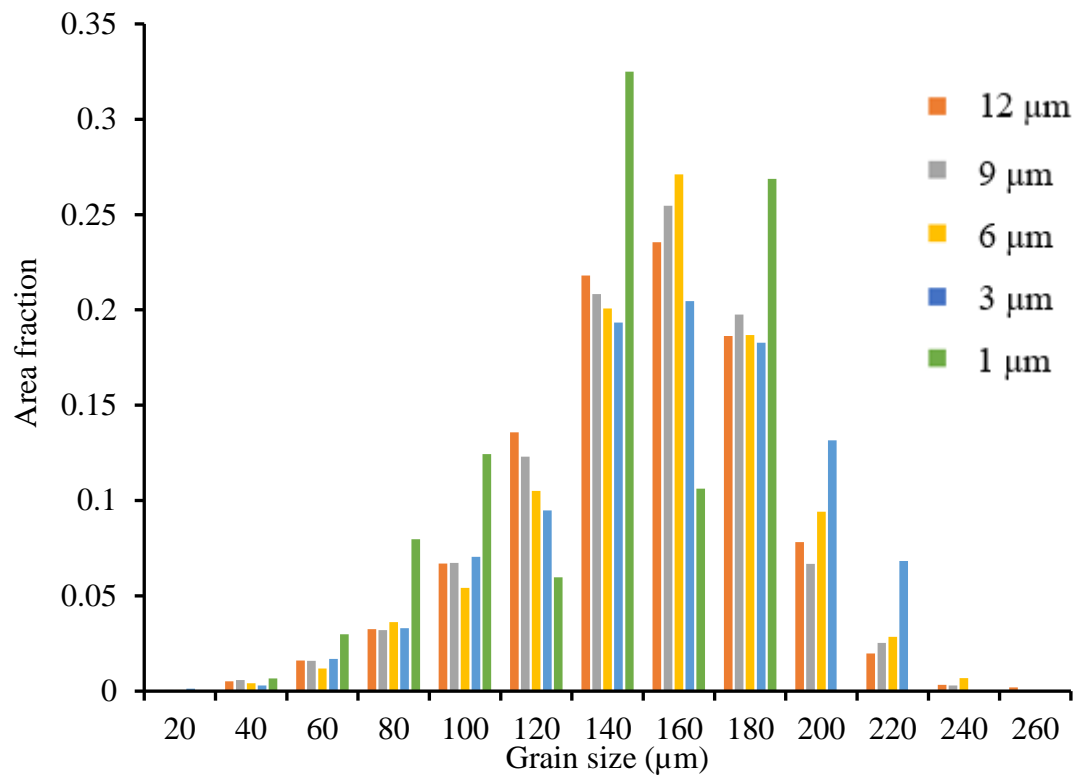
Figure 32 – Initial grain size distribution using different spacing for 160µm modal grain size for Fe-30Ni-0.044%Nb.

3.4.1 The grain size distribution after recrystallisation

Figure 33 shows the various grain size distributions after recrystallisation for the different grid spacing (with values 1µm, 3µm, 6µm and 12µm). The grain size distribution after recrystallisation for 3µm, 6µm and 9µm grid spacing have approximately the same modal grain size. Whereas, the 1µm and 12 µm grid spacing gives rise to a different modal of grain size. The input data used for this simulation is given in **Table 2**.

Table 2 – Simulation input data for CA model for Fe-30Ni-0.044%Nb .

Parameters	CA model parameters
Austenite Burgers vector	2.50E-10 m
Debye Frequency	$2.00000E+12 \text{ s}^{-1}$
Activation Energy	$1.7315000E+05 \text{ J mol}^{-1}$
Initial dislocation density	$4.30000E+14 \text{ m}^{-2}$
Temperature	1223 K
Taylor Factor	3.1
Alpha parameter	0.15
C1	6.30000E+00
C2	4.20000E-02
K_{ad}	2.35
Grain Density(3D)	$4.66000E+11 \text{ m}^{-3}$
GB energy	0.5 J mol^{-1}
Strain	0.35
Shear Modulus	81GPa
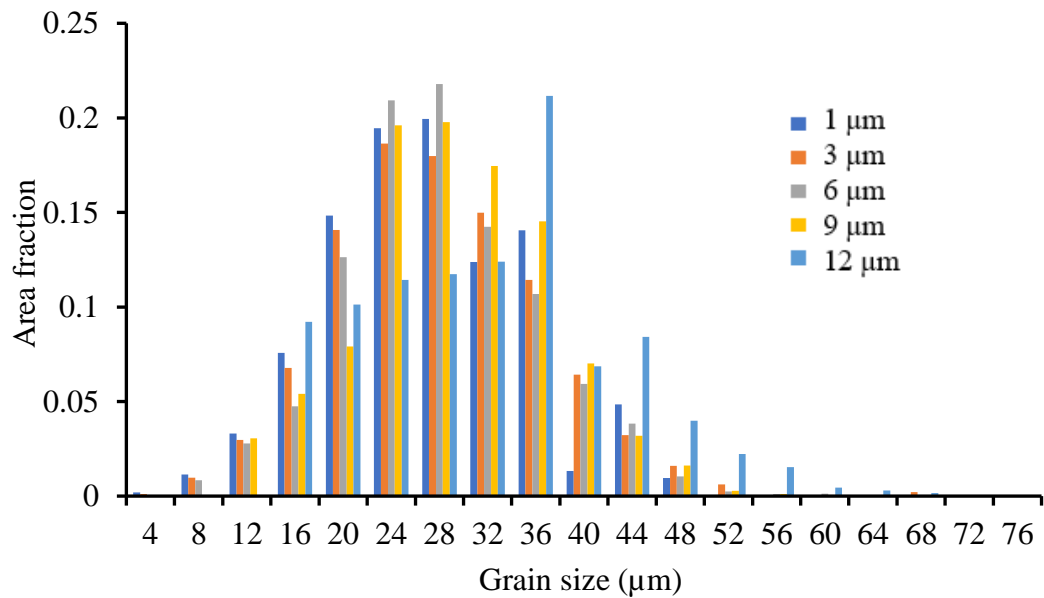
Figure 33 – Recrystallised grain size distribution using different spacing for 160µm modal grain size hot deformed at 950°C to a strain of 0.35 for Fe-30Ni-0.044%Nb.

Plotting the recrystallisation fraction against time shows that 1µm and 3µm grid spacing have the same recrystallisation kinetics. The 6µm grid spacing deviates slightly from these but 9µm and 12µm grid spacing have serious time stepping issues, which means that the timing is different for these. Hence, it is difficult to use 9µm and 12µm grid spacing values for the recrystallisation kinetics.
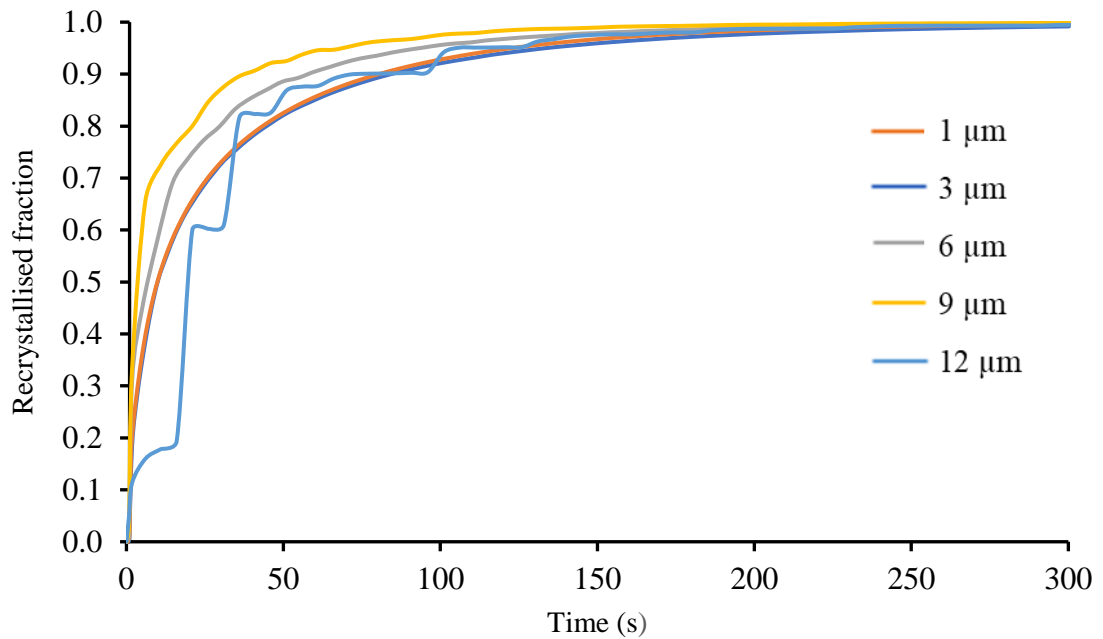
Figure 34 – Recrystallisation kinetics for different grid spacing for hot deformed at 950°C with a starting modal grain size of 160µm to a strain of 0.3 for Fe-30Ni-0.044%Nb.

In order to ascertain whether changing the system volumes would affect the initial grain size distribution (and subsequently affect the recrystallised grain size distribution and recrystallisation kinetics), the model was run for different system volumes under the same conditions. The results from this analysis are shown in **Figure 35** and the raw data is shown in **Table 3**. It can be seen that the modal grain sizes for the different volumes are the same for the initial grain size distributions. This is also shown for the recrystallised grain size distributions with the different system volumes giving the same modal grain sizes.
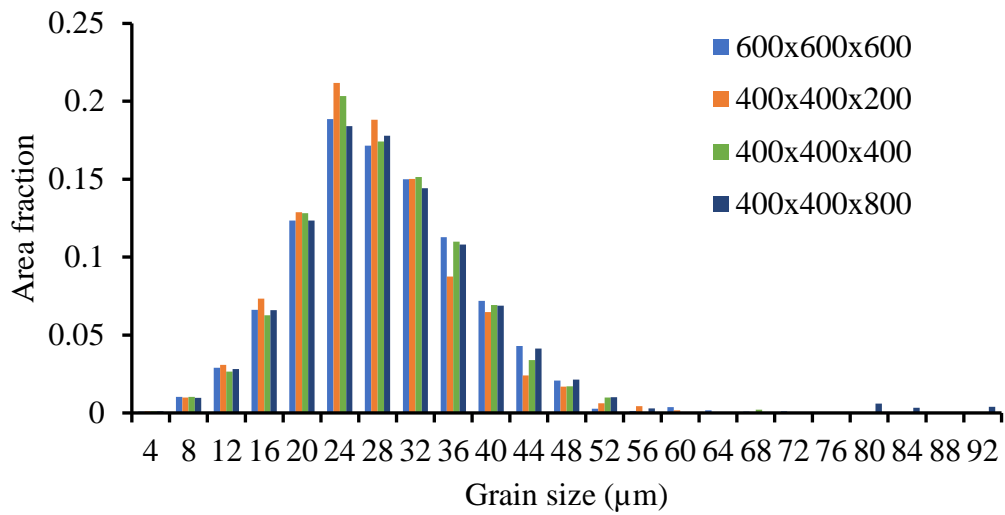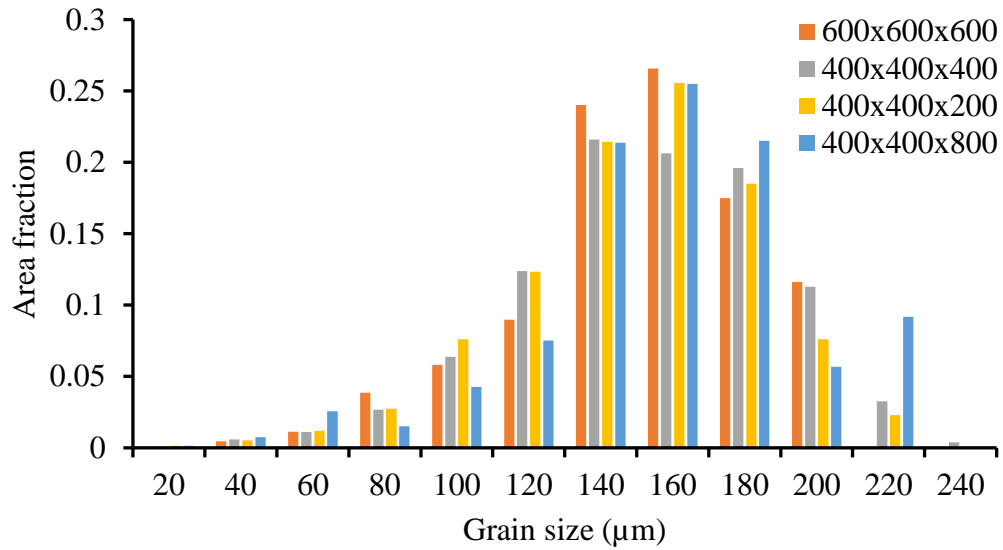
Figure 35 – Initial grain size distributions for different system volumes (top) and Recrystallised grain size distributions for different system volumes (bottom) with a starting modal grain size of 160µm at a strain of 0.3 and 6µm(default) grid spacing for Fe-30Ni-0.044%Nb.

Looking at the raw data for this analysis in **Table 3**, as the number of grains increases with increasing volume, the recrystallisation kinetics are not significantly affected. The results show that a starting number of grains of 395 gives the same results as 2670 grains. For example, the recrystallisation starting time (R_s) is 0.16s, 0.16s, 0.16s and 0.15s for 395, 791, 1582 and 2670 grains respectively. Hence, using more grains does not change the recrystallisation kinetics.

Table 3 – Summary of the recrystallisation kinetics for simulations using different system volumes with a starting modal grain size of 160µm at a strain of 0.3 and 6µm grid spacing.

Volumes	400x400x200 No of grains = 395	400x400x400 No of grains = 791	400x400x800 No of grains = 1582	600x600x600 No of grains = 2670
R_s (s)	0.16	0.16	0.16	0.15
R_f (s)	57.8	57.3	56.8	57
n	0.6108	0.6142	0.6128	0.6123
k	0.1592	0.1578	0.1596	0.1596
D50% (µm)	24	24	24	24
D5% (µm)	8	8	8	8
D95% (µm)	36	36	36	36

In summary, the results show that both the grain size distribution and the recrystallisation kinetics are similar for 1µm and 3µm and 6µm grid spacing. However, at values of 9µm and 12µm there is significant deviation between the recrystallisation kinetics.

During recrystallisation the growth of sub-grains are calculated empirically. Once a sub-grain reaches the critical radius and nucleates a "new" grain, this then appears in the CA model physically. The smallest feature within the CA model is therefore a newly nucleated grain of a size equal to the critical radius (around 6µm). Therefore, any grid spacing larger than this will result in a poor description of these features. During grain growth, the time taken between activating a new node is much longer, this results in a jerky measurement of recrystallisation fraction with time, albeit maintaining the prediction of the finish time.

3.5   Recovery module

The decay in the internal stress can be represented by a single parameter using the analysis of Verdier *et al.* [147], the recovery model is the modified version of Friedel's model [69] which is due to Verdier *et al.* [147] and by using the Verdier *et al.* model for static recovery the strain energy is reduced. Although not closely linked the sub grains growth is also calculated as part of this function **Equation 3.11**.

By combining **Equation 2.10** and **Equation 2.18** the differential equation for the dislocation density ρ:

$$\frac{d\rho}{dt} = -\frac{128\,\mu b v_D \rho^{3/2}}{9 M_T^2 \alpha_r E}\, exp\left(-\frac{U_a}{R_g T}\right) sinh\left(\frac{M_T \alpha_r \mu b V_a \sqrt{\rho}}{k_B T}\right) \qquad \text{Equation 3.2}$$

where, ρ is the dislocation density, U_a activation energy, U_D Debye frequency, V_a activation volume factor and $M_{(T)}$ mobility of grain boundaries.

The activation energy for microalloyed steels is assumed to be constant and is within the range value for the activation energy for pipe diffusion and bulk diffusion [74].The value of the activation energy chosen for this work does not treat cross-slip, climb or solute drag differently. A value of 285 kJ/mol is used which is equal to austenite self-diffusion [74]. V_a was originally used as a fitting parameter for the recovery model but the value of V_a can be determined as a function of Nb content and temperature obtained after fitting the experimental softening data **Figure 36**.
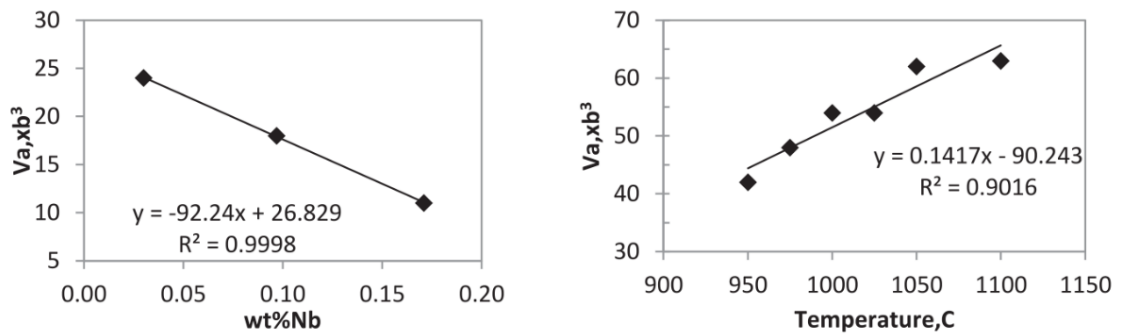
Figure 36 – Plot of activation volume as a function of solute Nb content. (b) Plot of activation volume as a function of annealing temperature for the same steel composition. The steel contains 0.03 Nb, 0.076C and 0.097 Nb, 0.002 C rolled to a strain of 0.3 at a strain rate of 10s-1 at 900ºC [125][148].

Through the activation volume (V_a) the effect of solute content on recovery is captured and from the data fit in **Figure 36** it shows that V_a has strong relationship with the content of the solute and the temperature.

Rehem *et al.* [4] developed a relationship between activation volume (V_a),solute Nb and temperature. In Verdier's mode the activation volume activation length or

distance(V_a/b^2) and that is the distance between pinning centres of a sub-grain boundary. But in the work of Rehman *et al.* it was assumed that the pinning centres can be either extrinsic dislocations, of which this spacing is proportional to $1/\sqrt[3]{\rho}$, or it could be the solute clusters of which the spacing is proportional to $1/\sqrt[3]{C}$ as calculated through dimensional analysis and both of these are treated as equivalent. Therefore the total spacing between pinning centres λ can be derived as :

$$\tfrac{1}{\lambda} = K_1\sqrt{\rho} + K_2\sqrt[3]{C_{Nb}}$$

Equation 3.2

Where K_1 and K_2 are proportionality constants, and the insight of these constants is crucial for modelling sub-grain growth. The values were back calculated from experimental results rather than from first principles[149]:

$$\frac{1}{\lambda} = 6.3\sqrt{\rho} + \frac{0.042}{b}\sqrt[3]{C_{Nb}}$$

Equation 3.3

Finally the activation volume λb^2 is given by;

$$V_a = \frac{b^2}{6.3\sqrt{\rho} + \frac{0.042}{b}\sqrt[3]{C_{Nb}}}$$

Equation 3.4

For a very small amount of solute Nb and low dislocation density **Equation 3.4** gives an unrealistically large activation volume. For instance Rehman *et al.*[4] for a 0.03 wt % Nb steel with dislocation density of 4×10^{15}/m^3, calculated the activation volume to be $23b^3$, where b is the magnitude of the Burgers vector and also when the solute Nb was reduced to 0.001 wt % and dislocation density was reduced to 4×10^{14}/m^3 activation volume was calculated to be $84b^3$. To capture other pinning points that will be included in **Equation 3.4** due to other solutes like Mn a minimum value of V_a from **Equation 3.4** with a value of $35b^3$ was used as the activation volume for the sub-boundary motion. The parameters chosen depend on the phase of the grains.

The dislocation energy is related to the stored energy ΔG as :

$$\rho = \frac{2\mu\Delta G}{\mu b^2}$$

Equation 3.5

By using this equation the stored energy is updated from time to time according to the change of the dislocation density (that is dislocation driven). The stored energy

is calculated for room temperature and if the dislocation energy is negative that is in the model not initialised the dislocation density is estimated from the strain energy which is converted from room temperature to the current temperature .It should be noted that this dislocation density is the average dislocation density both at the boundary and at the core of the grain.

3.6   Recrystallisation module

The model used in the CA is based on the model developed by Bos *et al.* [142] for dual phase steel which is capable to a good extent to describe recrystallisation and phase transformation process that occurs during the dual phase annealing cycle. The model employed in the CA model by Bos *et al.* [142] is the version of recrystallisation model developed by Rehman and Zurob [4] which is the modified version Dunlop *et al.* [130] who developed a model that includes the nucleation and growth of new grains during static recovery in Zircaloy-4   and that was adapted for modelling recrystallisation during hot rolling microalloyed austenite. The model can predict incubation time, nucleation rate, the recrystallised kinetics and the recrystallised grain size distribution.

In this model nucleation is assumed to occur by SIBM as discussed in 2.5.1 because of the reasonable low strain assumption and this is also supported by metallographic observation by Hansen *et al.* [150] that discovered that at high strain recrystallisation does nucleate at twin boundaries and deformation bands and the assumption for relatively low strain (0.1-0.4) experienced during roughing rolling is valid. In the classical JMAK equation it is assumed that nucleation is random and this becomes invalid during rough rolling of microalloyed steels as the austenite starting grain size is over 1500µm. Researchers have tried to solve this issue as can be seen from the literature by making the exponents of the JMAK equation a function of the processing parameters/conditions i.e. the modified JMAK equation. Nonetheless the issue with that is that specific events like impingement of nucleated new grains in proximity of one another along the grain boundary have not been taken into consideration. **Figure 37** gives a more detailed explanation of the nucleation and growth of recrystallisation. The nucleation only takes place at the grain boundaries and the growth of these nuclei is within the shell and as it grows it consumed the original deformed shell volume and when the whole shell volume has been consumed it switches over to pure growth stage in which the recrystallised surface shell grows progressively towards the centre and

consuming the deformed volume. The recrystallised volume fraction is the ratio of the shell volume to the original deformed volume at any point in time. The two stages will be further discussed in detail in the subsequent sections. It is assumed that the deformed grains are spherical and the nuclei to be hemispheres but in reality the deformed grains are elongated/pancaked(ellipsoid) and the nuclei have irregular shape.
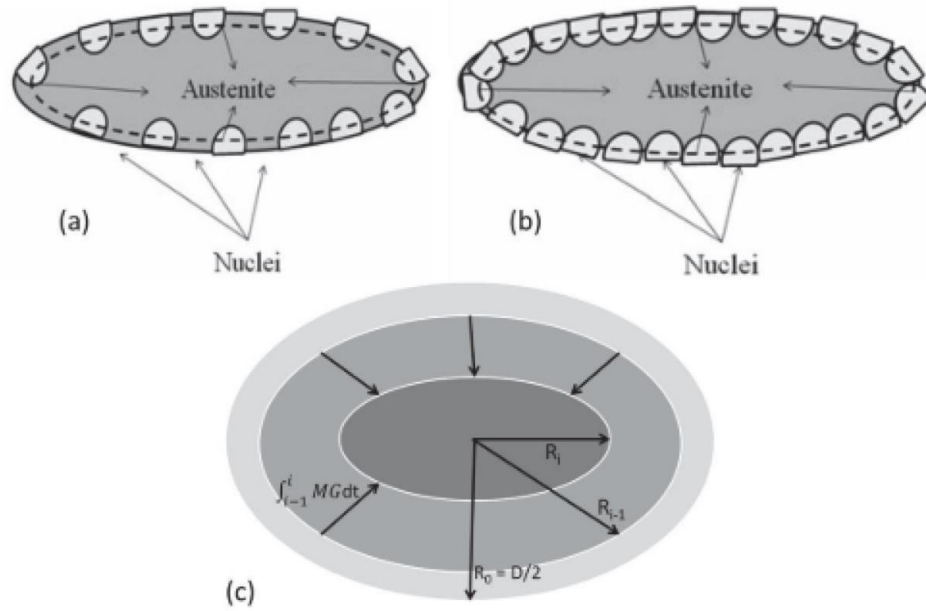
Figure 37 – (a) The beginning of nucleation and hemispherical nuclei formed at the grain boundary by SIBM. The recrystallised film position is represented by the dotted lines. (b) Site saturation is achieved and new hemispherical nuclei consume the original deformed HAGB. The equivalent recrystallised film position is shown by the dotted lines.(c) Schematic of the growth recrysallised front[4][37].

3.6.1 Sub-grain growth

The deformed austenite microstructure is assumed to be made of a statistical distribution of sub-grains or cells. It is also assumed that the sub-grain size distribution remains self-similar during the sub-grain growth i.e. the normalized sub-grain size distribution remains the same at all times.During rough rolling the average sub-grain size evolves in order to reduce the total stress of the system as discussed in 2.3.1 and **Figure 14** at rate that is proportional to the product of the sub-grain mobility and the driving force for sub-grain growth.

Winning *et al.* [151] in order to address the sub-grain boundary migration actually concluded that is the bowing out of the intrinsic dislocations(structural dislocations)

among extrinsic dislocations(structurally necessary dislocations) and these extrinsic dislocations act as the pinning centres. Winning *et al.* [151]analysis was restricted to pure material with low driving forces but in this work Rahman *et al.* [142] modified some parameters of the original work of Winning *et al.* [151]to apply it to microalloyed steels. From **Figure 38** $\eta\tau$ is the force experienced by each dislocation, η is the number of intrinsic dislocations between two extrinsic dislocations and the resolved shear stress is τ. In order to cause the pinning centres to climb the shear force and a chemical potential difference $\Delta\mu$ is needed. The diffusion flux is used to represent the movement of the extrinsic dislocations and is expressed as:

$$J = -\frac{2D}{\Omega\lambda} sinh\left(\frac{\Delta\mu}{2kT}\right)$$

Equation 3.6

Where D is the bulk self -diffusion coefficient, Ω is the atomic volume and λ is the spacing between the pinning centres(see **Figure 38**).

By replacing $\Delta\mu$ for $2\eta\tau\Omega$ in **Equation 3.7**:

$$J = -\frac{2D}{\Omega\lambda} sinh\left(\frac{\eta\tau\Omega}{kT}\right) = -\frac{2D}{\Omega\lambda} sinh\left(\frac{\lambda\theta\tau\Omega}{bkT}\right)$$

Equation 3.7

The number of dislocations between the pinning points η was estimated as $\lambda\left(\frac{\theta}{b}\right)$, where θ is the misorientation of low angle boundary. The value λ is calculated from **Equation 3.4**.

The work done by Rehman *et al.* [4] unifies the recovery and recrystallisation modules.
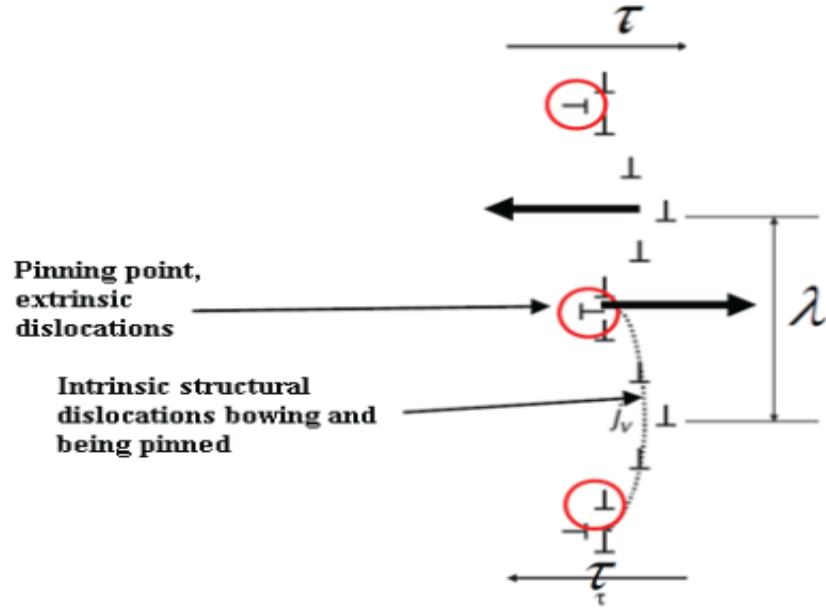
Figure 38-Schematic of the plot of sub-grain boundary bowing out while being pinned by extrinsic dislocations [4][152]

Lastly the sub-grain boundary velocity is expressed as:

$$V = -Jb^3 = -2\frac{Db^3}{\Omega\lambda}sinh\left(\frac{\lambda\theta\tau\Omega}{bkT}\right) \sim 2\frac{D}{\lambda}sinh\left(\frac{\lambda\theta\tau\Omega}{bkT}\right)$$

Equation 3.8

The assumption [4] is that $\tau\theta$ is equivalent to the increment of stress due to dislocations, σ_D as a result the sub-grain velocity is given as:

$$V = 2\frac{D}{\lambda}sinh\left(\frac{K_{ad}\sigma_D\lambda\Omega}{bkT}\right)$$

Equation 3.9

K_{ad} in **Equation 3.9** is an adjustable fitting parameter to experimental data and the equation above is identical to Friedel *et al*.[69] equation for dislocation motion with the existence of solute clusters. Considering that the sub-grain boundary velocity is $\langle r_t \rangle / dt$, then the sub-grain evolution or growth is expressed as :

$$\langle r_t \rangle = \langle r_0 \rangle + \int_0^t 2\frac{D}{\lambda}sinh\left(K_{ad}\sigma_D b^2 \frac{\lambda}{kT}\right)dt$$

Equation 3.10

Rehman *et al.* [4] assumed that the sub-grain sizes are distributed according to a Rayleigh distribution with a fixed width/standard deviation.

3.6.2 Recrystallisation nucleation

Bailey-Hirsch criterion states that a nucleus is formed just after the driving force for growth overcome the capillary forces $(2\gamma_{SE}/R_{SG})$, where γ_{SE} is the grain boundary energy and R_{SG} is the sub-grain radius. At the beginning the sub-grain growth are really small and the driving force is not sufficient to overcome the capillary force that can cause bulging into the neighbouring grains. The critical size for bulging to happen is given as:

$$r_c = \frac{2\gamma_{SE}}{\Delta G_t}$$

Equation 3.11

And the grain boundary energy is expressed as function of temperature

$$\gamma_{SE} = 1.11150 - 0.0005T$$

Equation 3.12

where T is the temperature in degree Kelvin

ΔG_t is the sub-grain growth driving force and is expressed as:

$$\Delta G_t = \frac{1}{2}\Delta\rho'\mu b^2$$

Equation 3.13

Where the dislocation density difference between the two sides of the grain boundary is $\Delta\rho'$. The $r_c \rightarrow \infty$ when the dislocation density difference is the same on both sides of the grain boundary. $\Delta\rho' = \rho$, with the assumption that the recovered substructure is dislocation free and ρ is the global dislocation density. Rehman and Zurob [153] used an intermediate value of $\Delta\rho' = \rho/2$ because of the absence of the exact numbers on the dislocation density difference.

ΔG_t in **Equation 3.12** diminishes over time owing to static recovery taking place continuously and this lead to the critical radius for the sub grain bulging as an increasing function of time. The increase in the sub grain size cannot overcome the capillary drag forces as shown in **Figure 39** if the applied strain is less than the critical

strain, although the sub grain will be able to overcome the critical conditions leading to recrystallisation nucleation if the strain is higher than the critical strain. The incubation time is determined by the time it takes for the largest sub grain to overcome the capillary drag force. In the sub grain size distribution the largest sub grain bulges out first and hence it is important to have knowledge of the sub grain size distribution in order to be able to predict the incubation time accurately.
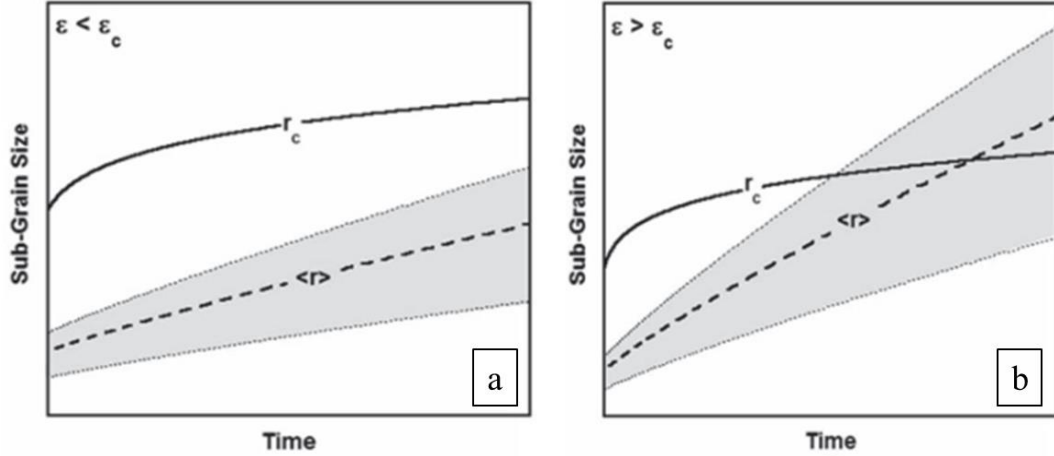
Figure 39 – The evolution of sub grain size and the critical radius for nucleation (a) applied strain less than the critical strain for nucleation (b) applied strain greater than the critical strain for nucleation[4][33].

The measured sub grain size distribution for variation of metals by Hughes *et al.* [154], [155] found that it follows a Rayleigh distribution.

$$P(\chi) = \frac{\pi}{2} \chi \, exp\left(-\frac{\pi \chi^2}{4}\right)$$
  Equation 3.14

Where χ is the normalised sub grain size by the average sub grain size $\langle r_t \rangle$,

$$\chi = \frac{r}{\langle r_t \rangle}$$
  Equation 3.15

Therefore the normalised critical sub-grain size is expressed as:

$$\chi_{c,t} = \frac{R_{c,t}}{\langle r_t \rangle}$$
  Equation 3.16

95

And the fraction sub grains $f(t)$ which are bigger than the critical size χ_c is express as :

$$f(t) = \int_{\chi_{c,t}}^{\infty} P(\chi)d\chi \qquad \text{Equation 3.17}$$

And the analytical value for **Equation 3.18** is given by:

$$f(t) = exp\left(-\frac{\pi}{4}\chi_{c,t}^2\right) \qquad \text{Equation 3.18}$$

Since the assumption was that the recrystallisation occurs entirely by SIBM therefore only the sub grains at the grain boundary will develop into nuclei. The number of potential nuclei is calculated by dividing the deformed grain boundary area per unit volume, S_v by the critical sub grain cross sectional area. The nucleation rate is derived by pairing **Equation 3.18** for the fractions of sites that have recrystallised over time and this is express as:

$$\frac{dN}{dt} = \frac{df}{dt}\frac{S_v}{A_{nucl}}F_n(t) \qquad \text{Equation 3.19}$$

Where A_{nucl} is the average area of the viable nucleus and the empirical equation by Yoshie *et al.* [156] is used to calculate S_v which is the deformed grain boundary area per unit volume :

$$S_v = \left(\frac{24}{\pi D_i}\right)\left(0.491e^{\varepsilon} + 0.155e^{-\varepsilon} + 0.143e^{-3\varepsilon}\right) \qquad \text{Equation 3.20}$$

and $F_n(t)$ is the function that captures the continuous decay of the nucleation sites and show the fraction of the outer grain boundary shell that is free for nucleation. It serves as the fraction of the non-recrystallised fraction of the surface shell :

$$F_n(t) = 1 - \frac{V_{rex}}{4\pi R_i^2 \delta} \qquad \text{Equation 3.21}$$

Where R_i is the initial radius of the deformed grain, V_{rex} is the total volume of the recrystallised grains in the outer shell of the deformed grain and δ is the grain boundary shell thickness see **Figure 37.** The nucleation rate is zero when $Fn(t)$ is zero i.e. site saturation has occurs.

The shape of the nuclei is assumed to be hemispherical and they emerge from the boundary and grows inwards. Therefore, the recrystallising nucleus volume is derived as:

$$V = \frac{1}{2}\left[\frac{4}{3}\pi\langle R_t\rangle^3\right]$$

Equation 3.22

And the radius of the spherical cap $\langle R_t\rangle$ is derived as:

$$\langle R_t\rangle = \langle R_0\rangle + \int_0^t M_{GB}G_t dt$$

Equation 3.23

Where G_t indicates the stored energy deformation and M_{GB} the mobility of high angle grain boundary. And lastly the recrystallised volume fraction is derived as :

$$X_t = \frac{N_t V}{V_0}$$

Equation 3.24

where V_0 is the volume of the deformed grain, N_t is the number of new grains which is determined by integrating Equation 3.18 and V is the volume of a new recrystallized grain. The nucleation rate will reduce to zero when the recrystallised volume is greater than the volume of the outer spherical shell ($4\pi R_i^2\delta$) because all the nucleation sites have been consumed and at this stage the recrystallised volume evolves only as a result of the growth of this outer recrystallised shell toward the centre of the grain[37].

In the CA model for each grain pair the grain boundary is calculated by counting the number of cells on the boundary. This number of cells is then multiplied with the cross section area of a cell which is equal to the square of the grid spacing(δ^2) or the length of the a single cell (δ) and is expressed as :

$$A_{GB} = N_{GB}\delta^2$$

Equation 3.25

Where A_{GB} is the grain boundary area and N_{GB} is the number of cells on the boundary.

3.6.3 Recrystallisation growth kinetics

The pure growth starts when the recrystallising nuclei reaches the critical grain size that is at the point when it has entirely devoured the shell volume **Figure 37**. The kinetics of recrystallisation is modelled in terms of the spherical shrinking of the grain(shell of the recrystallised material) because it is the shrinking grain that determines the driving force and hence the interface velocity.

Therefore, the increase in the shell thickens in time step dt which is given as $\int_0^{dt} M_{GB} G_t dt$. The increase in the recrystallised volume is expressed as:

$$dV = 4\pi R_t^2 M_{GB} G_t dt$$

Equation 3.26

Where the radius of the non-recrystallised core is R_t. The overall recrystallisation kinetics (X_t) is finally expressed as:

$$X_t = 1 - \frac{\frac{4}{3}\pi R_t^3}{V_0}$$

Equation 3.27

V_0 is the initial deformed grain volume.

The cells of course represent a discretization of space (in 3-dimensions). However a cell grows continuously. In fact the growth of an interface cell is implemented as the growth of a spherical particle. Therefore the radius of the interface cell is stored and updated as the cell grows. When the cell radius has become so large that a neighbouring cell is completely within the radius of the growing cell, the neighbouring cells transforms (and becomes part of the grain of the growing cell and usually becomes a growing interface cell itself). When all neighbouring cells have been transformed (diagonal neighbours transform later than the nearest neighbours) an interface cell is no longer an interface cell and it stops growing.

3.6.4 High angle boundary mobility

In the CA model the recrystallisation uses the term M_{GB} which denotes the high angle grain boundary mobility(HAGB). It is a constant of proportionality between the interface velocity and the driving force and the units is m^4/J s.

The mobility of HAGB in C-Mn has been taken as pure in the microalloyed austenite steel in the model. The high angle boundary mobility is the highest for pure material and a reasonable estimate can be calculated from Turnbull's **Equation 2.20**. The significant boundary retardation effect by Mn is excluded from the CA model because it is always present in all steel grades except in some rare cases such as interstitial free steel etc. Therefore mobility from Zhou *et al.* [157] from experimental study of grain coarsening is used in the model presently:

$$M_{C-Mn} = \frac{0.1920}{T} exp\left(-\frac{20837.14}{T}\right)$$ Equation 3.28

Cahn's solute drag model is used to capture the retardation of the boundary due to solute Nb and is given by:

$$\frac{1}{M_{GB,eff}} = \frac{1}{M_{pure}} + \alpha_m C_{Nb}$$ Equation 3.29

and $$\alpha_m = \frac{\beta N_v (kT)^2}{E_b D_X}\left(sinh\left(\frac{E_b}{kT}\right) - \frac{E_b}{kT}\right)$$ Equation 3.30

N_v is the number of atoms per unit volume, E_b is the solute-boundary binding energy (20 kJ/mol) , β is the grain boundary thickness (~1 nm) and D_X is the trans-interface boundary diffusion which is equal to twice the bulk diffusion coefficient of Nb in austenite [37].

M_{pure} in Cahn's model originally refers to mobility of pure materials but as explained earlier mobility of C-Mn steel is used in the CA model.

E_b (binding energy) which captures the effect of solute Nb in the model through and D_X (cross boundary diffusion coefficient). E_b is a well-known which is estimated to

vary between 20-38 kJ/mol compared to D_X which a value of twice the bulk coefficient is used based on the best fit from experimental results[2][33] and also with good agreement with values from literatures [16][158].

3.6.5 Driving force for recrystallisation growth

The stored energy of deformation between the recrystallisation and non-recrystallisation region is the driving force for recrystallisation growth and this is given as:

$$G(t) = \frac{1}{2}\rho\mu b^2$$

Equation 3.31

Where μ is the shear modulus. As recovery takes place the dislocation density in the non-recrystallised region will continuously decrease and this effect is captured in **Equation 3.23** and **Equation 3.24** by making *G* a function of time. Recovery is already modelled using the modified version of Friedel's model as discussed in section 3.5 using **Equation 3.2**

The dislocation density evolution can be calculated using the Forest-Hardening relationship.

$$\sigma = \alpha M \mu b\sqrt{\rho}$$

Equation 3.32a

$$\rho = \left(\frac{\sigma}{\alpha M \mu b}\right)^2$$

Equation 3.33b

3.6.6 Calculation of the fitting parameters used in the model

The model has range of values of parameters when compared to the domain of strain, operating temperature and solute content that the reliability is not well known. Some of the parameters were back calculated from experimental data like the activation volume used in recovery, sub grain boundary mobility, cross boundary diffusion coefficient to calculate the constants in the model. Rehman *et al* .[2,33], used various experimental data base to fit the variety of parameters by calculating the simple parameters first and then increased the complexity.

100

The parameter K_1 in the sub grain growth model and activation volume for recovery calculation in Equation 3.3, the experimental database used was that of Kwon and DeArdo [149] at 1000°C and 900°C. K_{ad} in the sub grain growth parameter in Equation 3.10 was calculated from the database of 900°C because no dynamic recrystallisation was reported. K_2 in Equation 3.3 was calculated also from the Kwon and DeArdo [201] database for a 0.042 wt % Nb steel deformed at 1000°C.

The kinetics of precipitation at this temperature is feasible but will be far slower than that of recrystallisation under these conditions. Calculation of K_2 is possible by fitting this data. And the values of K_1 , K_2 and K_{ad} were further refined by simultaneously fitting all of the available experimental data [2][4].

3.6.7 Modelling recrystallisation with grain size distribution

Using the original input parameters for Fe-30Ni-0.044 wt% Nb as described (**Table 3**) a typical final output after running the CA model is shown in **Figure 40**. The nucleation can be seen at the deformed grain boundary and it is continuous until all the sub grains that have reached the critical radius have recrystallised. When they appear at the grain boundary, they start to grow inwards spherically.
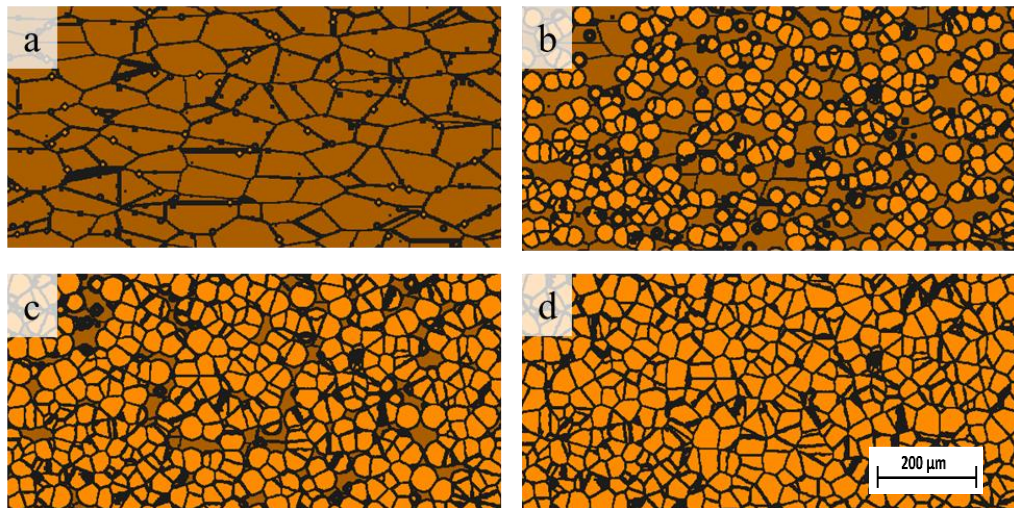
Figure 40 – Microstructure at different stages of recrystallisation. a) 5% recrystallised after 10s b) 50% recrystallised after 18s c) 85% recrystallised after 27s d) 99.9% recrystallised after 60s – the final microstructure, for Fe-30Ni-0.044%Nb hot deformed at 950°C to a strain of 0.3 with a starting modal size of 160µm.

A recrystallised grain size distribution graph can be plotted using the output data from the model, which is a key feature of this specialised model. A typical graph of grain size in microns against the recrystallised area fraction shows the recrystallised grain distribution (**Figure 41).** It gives a modal grain size of 80µm from a starting modal grain size of 160µm.
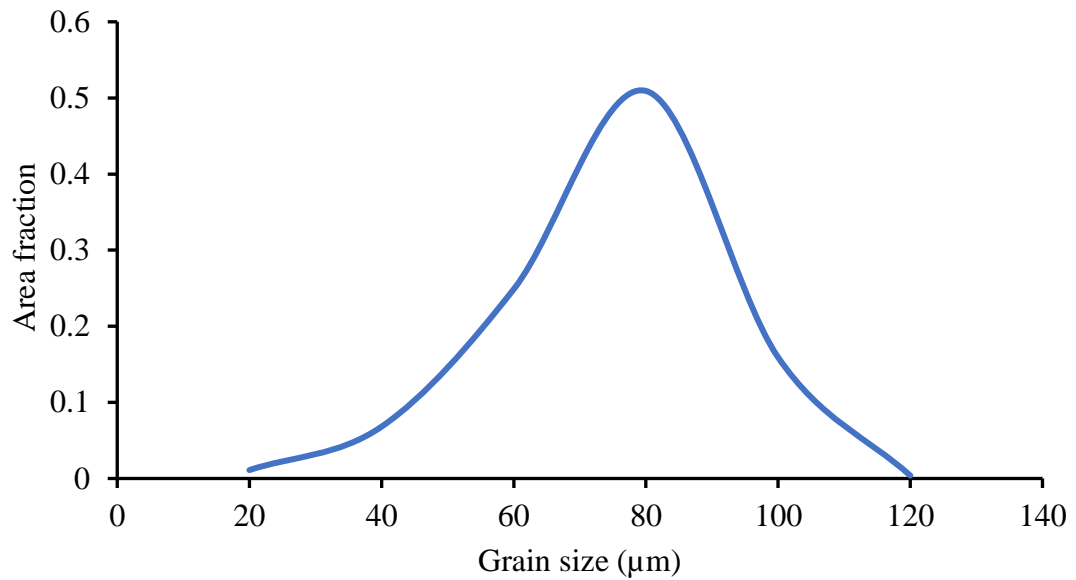
Figure 41 – Recrystallised grain size distribution from a starting modal grain size of 160µm hot deformed at 0.3 strain and 950ºC for Fe-30Ni-0.044%Nb.

The predicted recrystallisation kinetics and the predicted Avrami constant is in line with 3D particle(**Figure 42**). The model reproduces the general trend as described in literature with respect to grain size as a function of time. The model data can also be used to plot the recrystallisation kinetics as shown in **Figure 43**.

y = 3.277x -9.8894
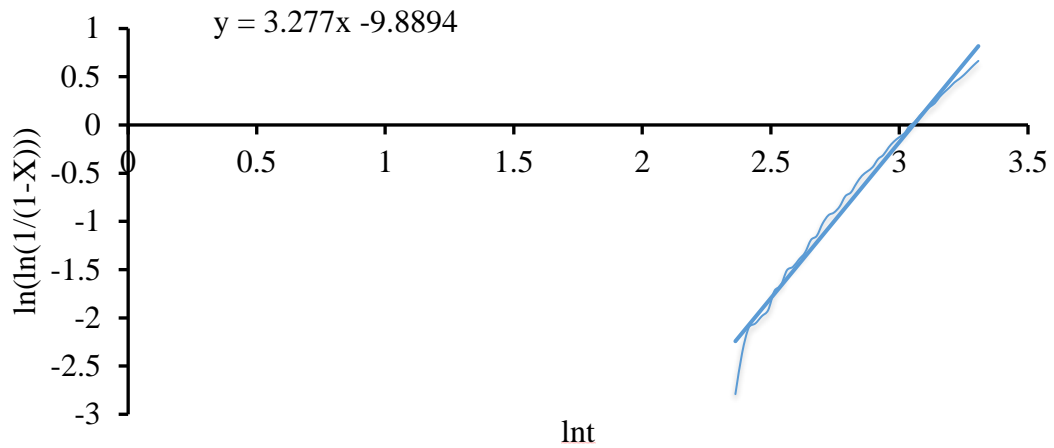
Figure 42 – Graph showing the evolution of the Avrami value (n) for Fe-30Ni-0.044%Nb hot deformed at 950°C to a strain of 0.3 with a starting modal size of 160μm.
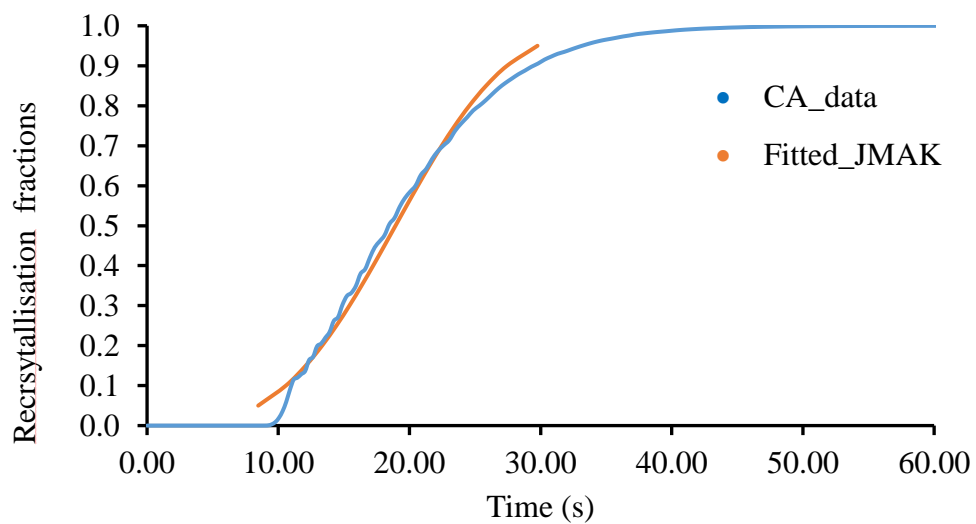
Figure 43 – Predicted recrystallisation curve (s): Orange circles show the fitted JMAK and blue the actual recrystallised fraction curve from the CA with an initial grain size distribution with a modal grain size of 160μm and hot deformed at 950°C at 0.3 strain for Fe-30Ni-0.044%Nb.

3.6.7.1 Initial comparison between experimental and modelled data

For an initial assessment of the CA model the experimental details were used[149]. These relate to Fe-30Ni-0.044wt%Nb, which retains austenite grain structure at room temperature. The input parameters from the experimental data used for the simulation

are shown in **Table 4**, which also includes those parameters specific to the CA model (sub-grain growth parameters *C1*,*C2* and K_{ad}).

Table 4 – The simulation input parameters for Fe-30Ni-0.044%Nb.

Parameters	CA model parameters	Experiment data parameters
Austenite Burgers vector	2.520E-10 m	2.52E-10 m
Debye Frequency	2.00000E+12 s^{-1}	
Activation Energy	2.85000E+05 J mol^{-1}	2.85000E+05 J mol^{-1}
Temperature	1223 K	1223 K
Taylor Factor	3.1	3.1
Alpha parameter	0.15	0.15
C1	6.30000E+00	
C2	4.20000E-02	
K_{ad}	2.35	
Grain Density(3D)	4.57872E+11 m-3	
Dislocation density	4.50000E+14 m-2	4.50000E+14 m^{-2}
GB energy	0.5 J mol^{-1}	0.5 J mol^{-1}
Mo (boundary mobility pre-exponent)	50 mol.m.J^{-1}.s^{-1}	50 mol.m.J^{-1}.s^{-1}
Interface mobility activation energy of gamma to gamma transformation	1.95000E+05J/mol	1.95000E+05J/mol
Shear Modulus	70Gpa	70Gpa
Strain	0.3	0.3

The initial grain size distribution shown in **Figure 44**, shows that experimental data has an initial grain size range of 20-340µm and modal grain size of 160µm. This is comparable to that generated by the CA model between 20-240µm within the experimental range and also generates a modal grain size of 160µm. Further work on the impact of discrepancies at the upper end of the experimental initial grain size range was carried out (see Chapter 6).
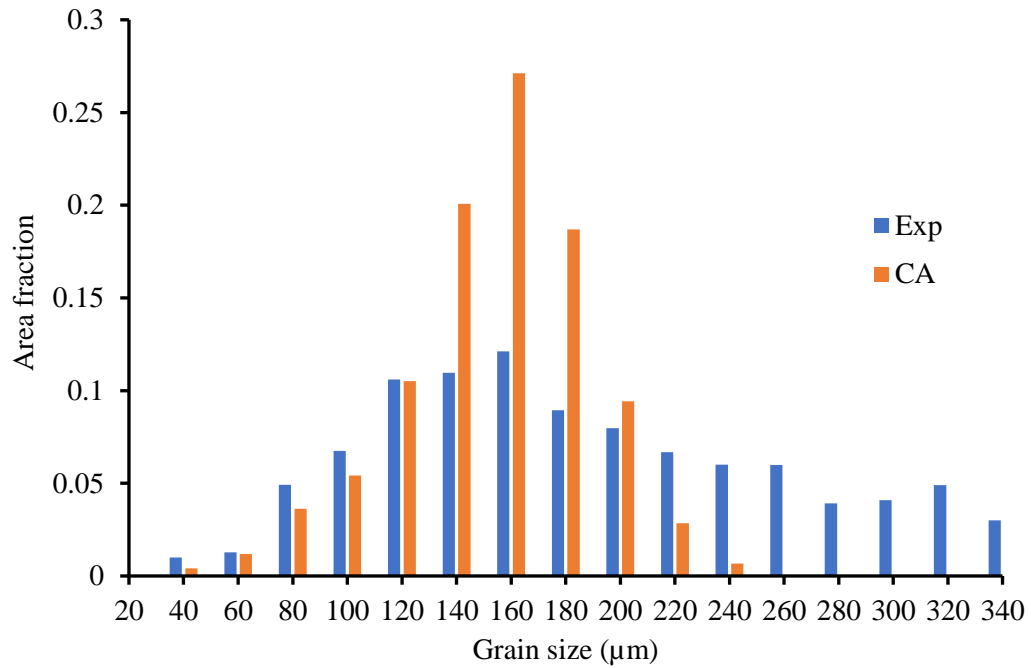
Figure 44 – Initial grain size distributions for hot deformed Fe–30Ni–0.044wt%Nb at 950°C to a strain of 0.3 for the experiment and the CA model with a modal grain size of 160µm.

The resulting recrystallised grain size distributions are shown in **Figure 45**. It can be seen that the recrystallised grain size range for the CA model is from 20-120µm whereas the experimental range if from 20-140µm. The modal recrystallisation grain size is in good agreement.

D5%, D50% and D95% are the grain sizes at the 5%, 50% and 95% cumulative area fraction respectively. These are included in the recrystallisation data tables.
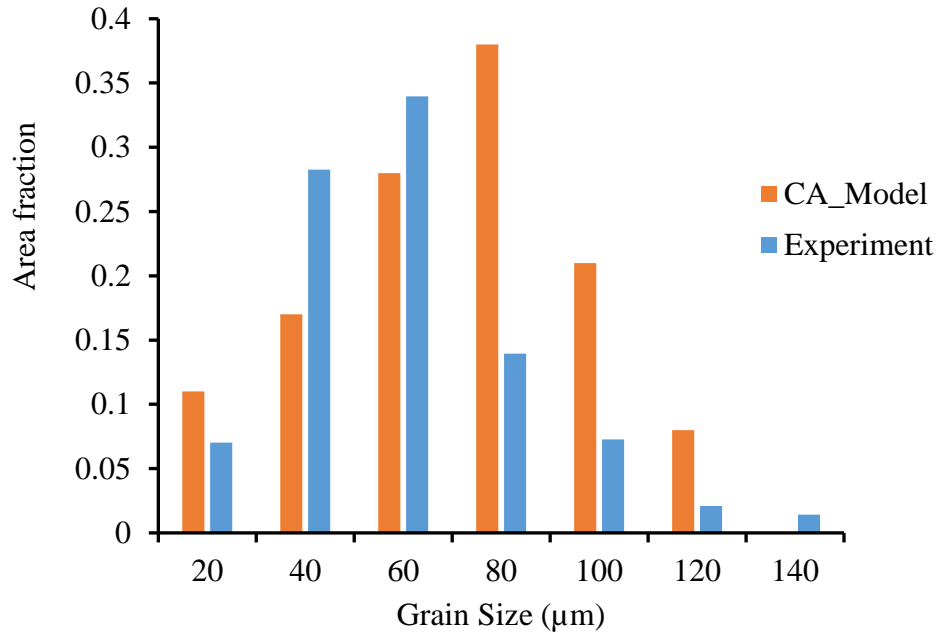
Figure 45 – Recrystallised grain size distribution for hot deformed Fe-30Ni-0.044%Nb at 950°C to a strain of 0.3 with a starting modal grain size of 160µm for the CA model and the experiment.

The recrystallisation kinetics, for the comparison of the CA model with the experimental data, is shown in **Table 5** and **Figure 46**. The recrystallisation kinetics for the CA model simulation and the experimental data are different. It can be seen that the recrystallisation starting time (R_s), which is time at 5% recrystallisation, is later for the CA model than the experimental data (12.5s and 2.35s respectively), a step in the model is seen at around every 1s during the simulation **(Figure 46)**. The recrystallisation finishing time (R_f), which is the time at 85% recrystallisation is 36.6s for the CA model and 43.37s for the experimental data. As the starting time for the CA model is later than for the experimental data, it may be anticipated that the finishing time would also be later and this is not the case. This may be because the initial grain size distribution range is different and smaller grains recrystallise before larger grains. Also the CA model assumes uniform strain (homogeneous microstructure), which is not the case in reality. The CA model gave an Avrami exponent (n) of 3.0658 (which is in line with that expected for 3D simulations), while the Avrami exponent from the experimental data[3] was 1.2383. This difference maybe due to the fact that the CA model assumes uniform strain and in reality we see strain inhomogeneity. The computational time for the simulation on average is 16s.

Table 5 – Comparison of the recrystallisation data for the CA model simulation of hot deformed Fe-30Ni-0.044%Nb at 950°C with a starting modal grain size of 160µm to a strain of 0.3.

Recrystallisation kinetics / parameter	Recrystallisation data	
	CA model	Experimental data
R_s (s)	12.5	2.35
R_f (s)	36.6	43.37
n	3.0658	1.2383
k	3.6253e-5	0.00178
D50%	100	60
D5%	44	20
D95%	105	40
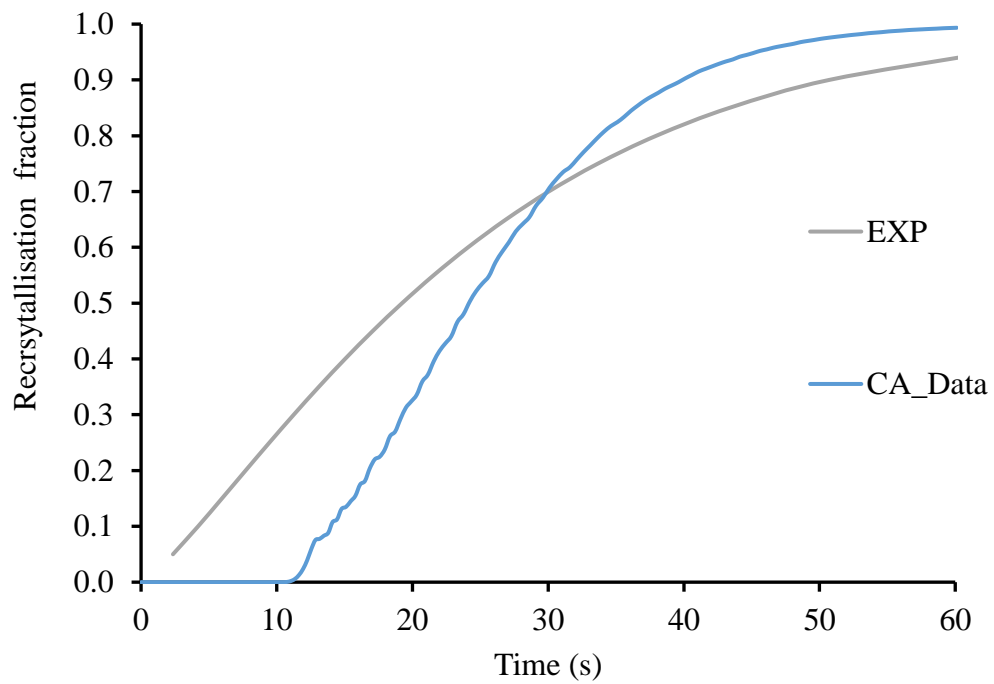
Figure 46 – Recrystallisation kinetics of hot deformed Fe-30Ni-0.044%Nb at 950°C to a strain of 0.3 with a starting modal grain size of 160µm.

3.7   Summary of the current state of the model

The as-received CA model can be used to model recrystallisation starting from any realistic microstructure and this 3D model is able to produce equivalent 2D modal grain sizes.

The shape of the initial grain size distribution, while not a log-normal shape, produces recrystallisation data for smaller recrystallised grain sizes (D5%) and the recrystallised modal grain size (D50%) that is in good agreement with experimental data. As it is, the CA model can be used to generate recrystallised grain size distributions and recrystallisation kinetics.

However, the shape of the distribution given by the Voronoi method used in the CA model is not log-normal. This means that larger grain sizes from the experiment are not captured in the starting microstructure and hence the recrystallised grain size distribution produced by the CA model.

Full grain size distributions are also generally not well predicted due to the need to take into account strain inhomogeneity accurately i.e. fine grains in a distribution have higher stored energy on deformation and recrystallise first, which affects the available nucleation sites for subsequent recrystallisation of the larger grains.

Variation in the output grain size from the 3D model may be caused by the calculation of the grain size which is done using equivalent volume diameter rather than equivalent area diameter.

Differences between the CA model and the experimental data recrystallisation kinetics may be due to different factors and assumptions within the as received CA model. It assumes uniform dislocation density and that the grains are spherical (while in actuality they are elongated).

4 Sensitivity analysis on the recrystallisation parameters

Chapter 3 presents the initial work carried out to analyse the suitability of the CA model for its application to model 3D recrystallisation in hot rolled steel. This Chapter will describe a set of sensitivity analysis investigations carried out on the same model. This work was done to ascertain the sensitivity of key parameters used in the CA model and what aspects of the recrystallisation process these parameters affect. The studies build upon those specific gaps in the model's capabilities that came to light during the initial work (3.7).

A set of baseline values for key parameters based on work from the literature were used as a benchmark. By making changes to one parameter at a time in the CA model and simulating recrystallisation, its affect on the recrystallisation grain size and kinetics was investigated. Results were generated for the pre-exponential mobility factor, the magnitude of the austenite Burgers vector, temperature, the applied strain, sub-grain growth parameter (K_{ad}), shear modulus, activation energy, activation volume factor and the grain boundary surface energy.

4.1 Sensitivity analysis on the baseline data

The input parameters in **Table 6** were used as a baseline set of data to then carry out a sensitivity analysis to determine how each parameter influences the recrystallisation kinetics and resulting grain size distribution. These input parameter values were taken from the literature[37][142][3].

Table 6 – Baseline input simulation settings for Fe-30Ni-0.044%Nb.

Parameters	CA model parameters
Austenite Burgers vector	2.520E-10 m
Debye Frequency	$2.00000E+12 \ s^{-1}$
Activation Energy	$2.85000E+05 \ J \ mol^{-1}$
Temperature	1223 K
Taylor Factor	3.1
Alpha parameter	0.15
C1	6.30000E+00
C2	4.20000E-02
K_{ad}	2.35
Grain Density(3D)	$4.666000E+11 \ m^{-3}$
Dislocation density	$4.50000E+14 \ m^{-2}$
GB energy	$0.5 \ J \ mol^{-1}$
Mo (boundary mobility pre-exponent)	$50 \ mol.m.J^{-1}.s^{-1}$
Interface mobility activation energy of gamma to gamma transformation	$1.95000E+05 \ J \ mol^{-1}$
Shear Modulus	70GPa
Strain	0.3

To complete the benchmark, simulations using the baseline data in the CA model were run with a modal grain size of 160µm. The grain size distributions for this benchmark simulation are given in **Figure 47**.
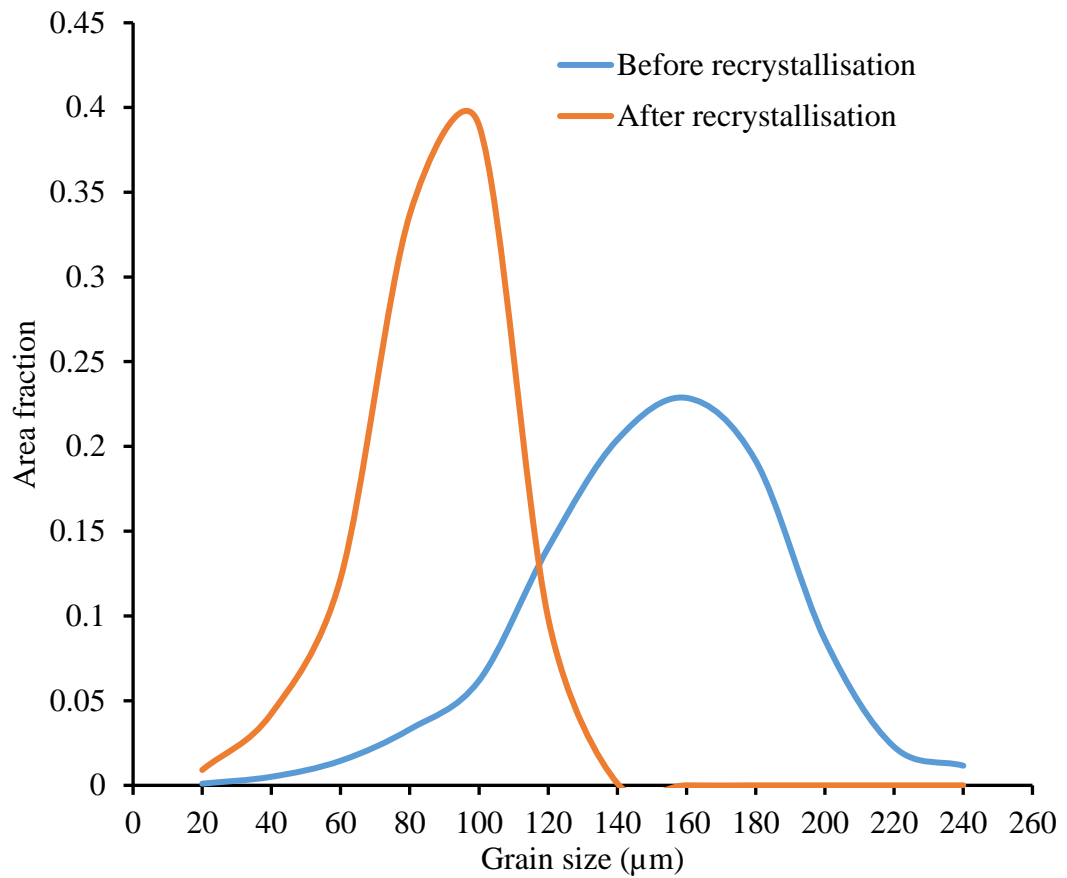
Figure 47 – Grain size distribution for the baseline data before and after recrystallisation with a modal grain size of 160µm and hot deformed at 950°C at 0.3 strain for Fe-30Ni-0.044%Nb.

The baseline data(BLD) was run for six different simulations (BLD, BLDSIM1, BLDSIM2, BLDSIM3, BLDSIM4 and BLDSIM5) with different random seed for the starting Voronoi to see if there was any variation in the recrystallisation kinetics. The results are shown in

Figure 48. It can be seen from the graph that the recrystallisation curve for all simulations overlay each other, showing no deviation from one another. Therefore, should a deviation be observed when alterations are made to model parameter values, this may be attributed to those changes with confidence.
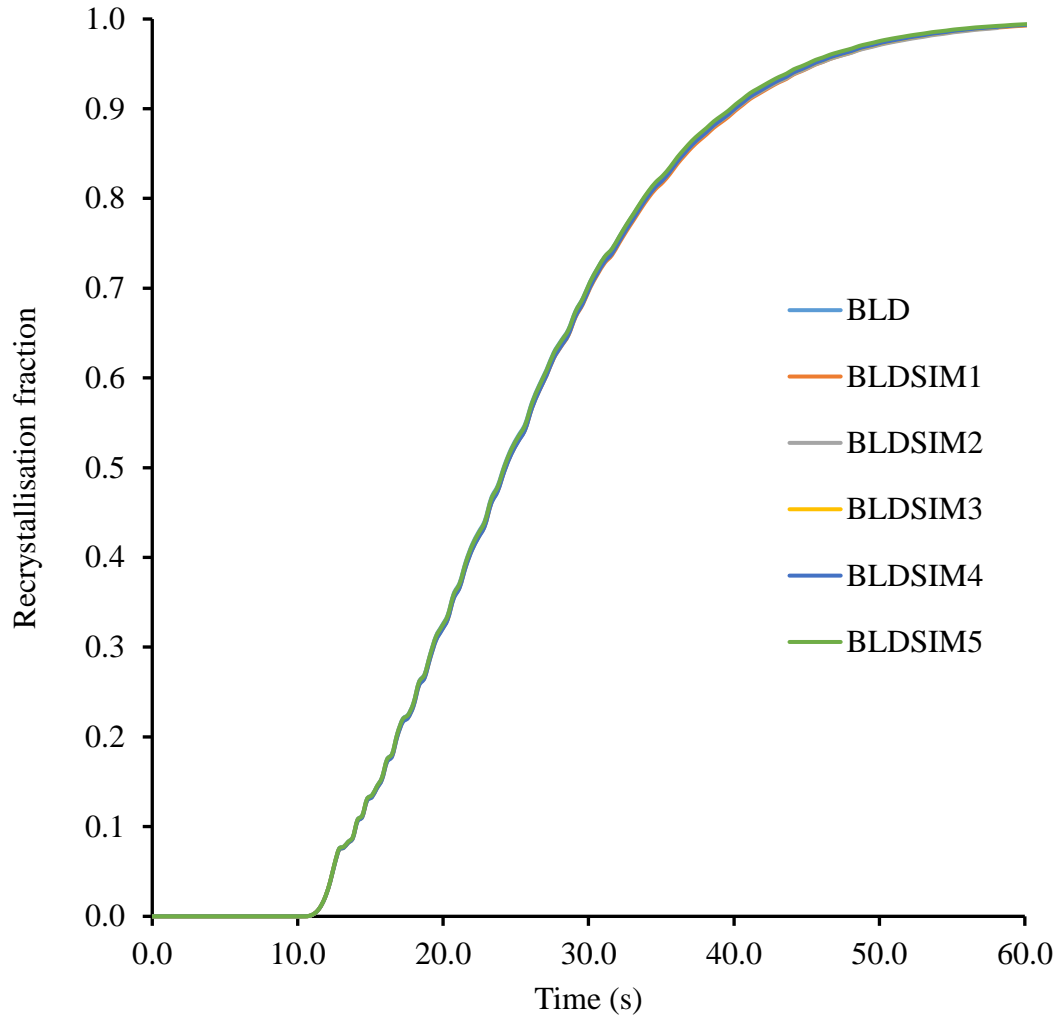
Figure 48 – Benchmark recrystallisation kinetics for six nominally identical simulations(BLDSIM1-BLDSIM5) of the baseline data (BLD) in the CA model for Fe-30Ni-0.044%Nb hot deformed at 950°C to a strain of 0.3 with a starting modal size of 160µm.

For the starting microstructures in all of the six identical benchmark simulations (BLD, SIM1-SIM5), the almost identical grain size distributions after recrystallisation were obtained. This is shown in **Figure 49**. Therefore, if a deviation in the recrystallised grain size distribution is observed when alterations are made to the parameter values, this may be attributed to those changes with confidence.

Figure 48 and **Figure 49** supports the ability of the CA model to continue to reproduce similarly the same results from the same set of input conditions.
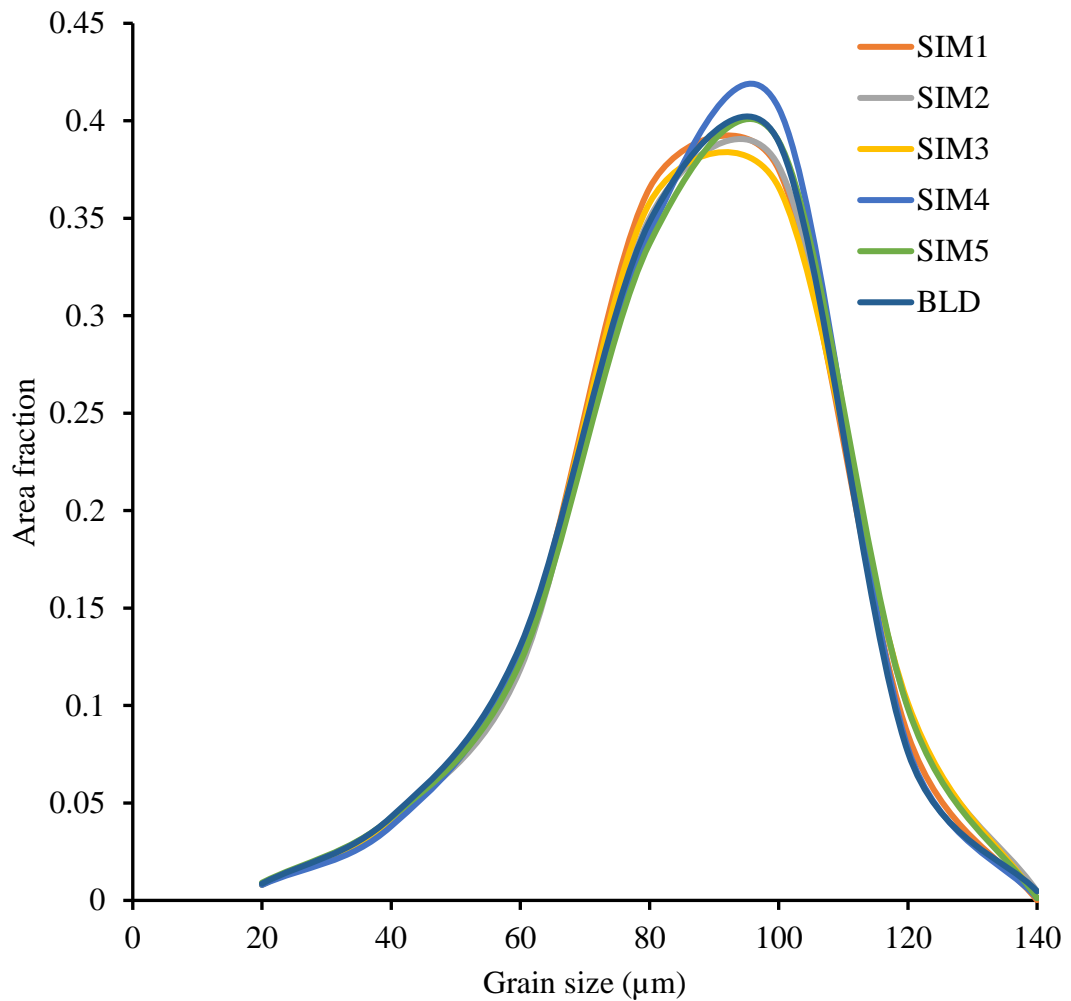
Figure 49 – Benchmark recrystallised grain size distributions for six identical simulations(BLD,SIM1-SIM5) of the baseline data (BLD) in the CA model for Fe-30Ni-0.044%Nb hot deformed at 950°C to a strain of 0.3 with a starting modal size of 160µm.

The raw data output from the six identical parameters baseline simulations is shown in **Table 7**. This confirms the reproducibility in the CA model numerically and provides benchmark recrystallisation data for reference.

Table 7 – Benchmark recrystallisation data for six nominally identical simulations of the baseline data (BLD) in the CA model for Fe-30Ni-0.044%Nb with a starting modal grain size of 160 µm.

Recrystallisation data	BLDSIM1	BLDSIM2	BLDSIM	BLDSIM3	BLDSIM4	BLDSIM 5
R_s (s)	12.5	12.5	12.5	12.5	12.5	12.5
R50%	24.2	24.2	24.2	24.6	24.7	24.2
R_f (s)	36.6	36.6	36.6	36.6	36.6	36.6
n	3.0658	3.0565	3.0658	3.0709	3.0720	3.0698
K	3.6253e-5	3.7059e-5	3.6253e-5	3.5111e-5	3.4936e-5	3.5749e-5
D5% (µm)	44	44	43	43	45	43
D50% (µm)	100	100	100	100	100	100
D95% (µm)	104	105	105	106	104	106

For further confirmation, the % difference between the recrystallisation data values from the first simulation and the other five simulations are given in **Table 8**. The recrystallisation starting time (R_s), which is the time at 5% recrystallisation and the recrystallisation finishing time (R_f), which is the time at 85% recrystallisation, shows no variation for the six different simulations. Slight variations of less than ±10% in recrystallisation time at 50% (R_{50}%), Avrami exponent (n) and rate constant (k) are within an acceptable percentage error (see **Table 8**). The predicted and measured recrystallisation kinetics are different, which is down to the problem from the initial grain size distribution since it did not capture the tail end the grain size distribution when compared to the experiment (**Figure 44**). In addition a 'step' in the model prediction is seen at approximately 1 second which gave rise to a rounding error (**Figure 46**). In modelling the sensitivity of the parameters to variation in changes of the value of parameters, a standard ±10% is used to determine the impact of increasing or decreasing a parameter on the material microstructure or kinetic properties . The error shown in table 8 is due to rounding error not an error as result of variation of the single parameter by ±10% . Even though the some of the parameters is varied by ±10% because of lack of data in literature for various ranges of measurement of some the parameters used in Table 6 this ±10% is not carried forward in all the calculations only used where there are insufficient ranges from literature for the specific parameters

Table 8 – Summary data showing the percentage variations for the baseline recrystallisation data for the different simulations of the baseline data. The first row shows the recrystallisation data from the first baseline simulations and subsequent rows show the % difference between the other baseline simulation values and those of the first one.

Benchmark simulations	Recrystallisation data							
	Rs (s)	R50% (s)	R_f (s)	n	k	D50% (μm)	D5% (μm)	D95% (μm)
BLDSIM	12.5±0.2s	24.2±2s	36.6±4s	3.0658	0.00004	100	43	105
	% Difference from the BLDSIM benchmark recrystallisation data							
BLDSIM1	0.0	0.0	0.0	0.0	-9.4	0.0	1.4	-1.0
BLDSIM2	0.0	0.0	0.0	-0.3	-7.4	0.0	1.4	0.0
BLDSIM3	0.0	1.7	0.0	0.2	-12.2	0.0	-0.9	1.0
BLDSIM4	0.0	2.1	0.0	0.2	-12.7	0.0	3.7	-1.0
BLDSIM5	0.0	0.0	0.0	0.1	-10.6	0.0	-0.9	1.0

4.2 Sensitivity analysis on the pre-exponential mobility parameter

The pre-exponential mobility affects how fast the grain boundary is moving. A sensitivity analysis was carried out for this parameter. CA model simulations were run using the baseline data with pre-exponential mobility values ranging from 25 to 280 mol.m.J^{-1}.s^{-1}. Note that the pre-exponential mobility value for the benchmark baseline data is 50 mol.m.J^{-1}.s^{-1}, shown as 'BLD (50) and the effect of varying the pre-exponential mobility value on the recrystallisation data is shown in **Table 9.**

Table 9 – Recrystallisation data obtained for CA simulations run with baseline data and pre-exponential mobility values ranging from 25 to 280 mol.m.J^{-1}.s^{-1}, with the baseline benchmark value at 50 mol.m.J^{-1}.s^{-1}, BLD(50).

Recrystallisation kinetics / parameter	Recrystallisation data for different pre-exponential mobility values				
Pre-exponential mobility (M_o) in mol.m.J-1.s-1	25	BLD(50)	55	100	280
R_s (s)	14	12.5	12.3	11.5	10.9
R50% (s)	45.0	24.2	22.7	16.7	12.5
R_f (s)	93.0	36.6	33.3	21.2	13.8
n	1.6927	3.0658	3.3301	5.4656	13.599
k	1.e-3	3.6253e-5	2.0e-5	0.0000001	7.4e-16
D50% (μm)	100	100	100	100	100
D5% (μm)	43	43	44	45	45
D95% (μm)	104	105	103	106	106

4.2.1 Effects of pre-exponential boundary mobility on the microstructure

Looking at the effect on D50%, the average grain size, would be indicative of any notable difference in microstructure.

From **Table 9** it can be seen that changing the pre-exponential boundary mobility has little effect on the recrystallized average grain size (D50%). At values from 25 to 280 mol.m.J^{-1}.s^{-1} inclusive, D50% is 100 μm.

To look at the microstructure in more detail, a comparison of the recrystallised grain size distribution can be made. **Figure 51** shows the recrystallised grain size distributions of each of the simulations using different pre-exponential boundary mobility (M_o) values. These distributions are almost identical, showing that increasing the pre-exponential boundary mobility value, has no significant effect on the

recrystallised grain size distribution. Therefore, changing the pre-exponential boundary mobility value does not change the final microstructure and by extension the mechanical properties of the steel.

This is further supported by the 2D microstructure images shown in **Figure 50**, in which the final microstructures obtained appear the same for pre-exponential values of 50, 100 and 280 mol.m.J^{-1}.s^{-1}. This may be because the critical grain size is the same, so they all attain a stable nuclei at the same time.
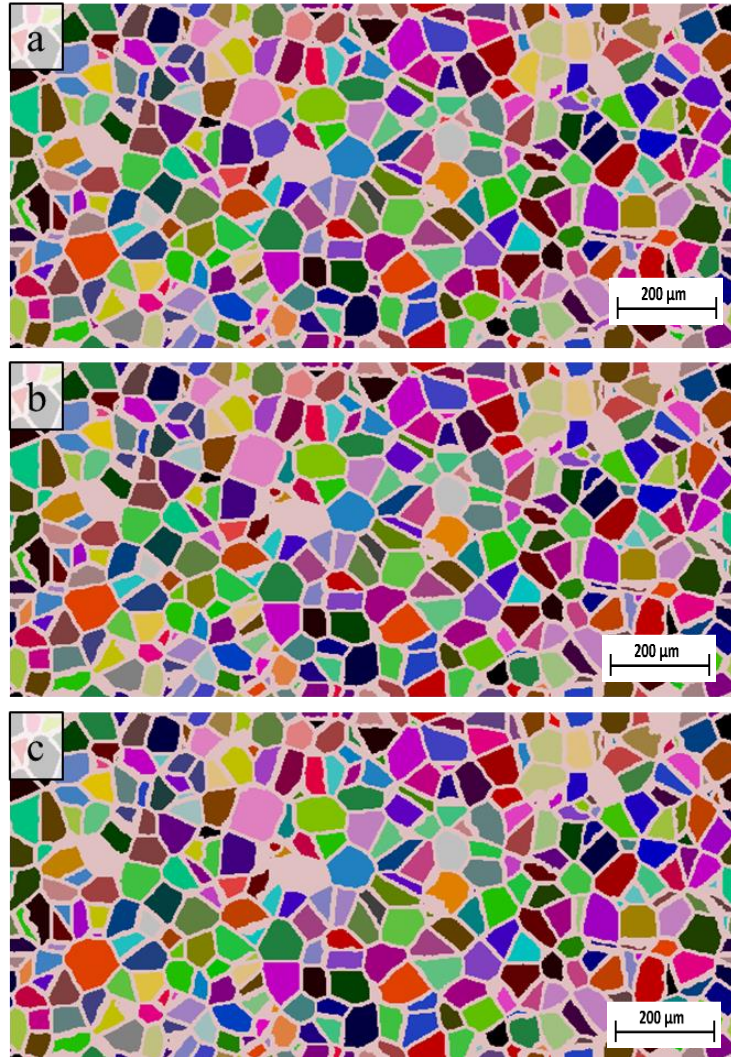
Figure 50 – 2D Final microstructure for CA model baseline simulations run using different pre-exponential mobility (M_o) values of (a) 50 mol.m.J^{-1}.s^{-1} (b) 100 mol.m.J^{-1}.s^{-1} and (c) 280 mol.m.J^{-1}.s^{-1}, the different colours represent different grain sizes within the microstructure, for Fe-30Ni-0.044%Nb hot deformed at 950°C to a strain of 0.3 with a starting modal size of 160µm.
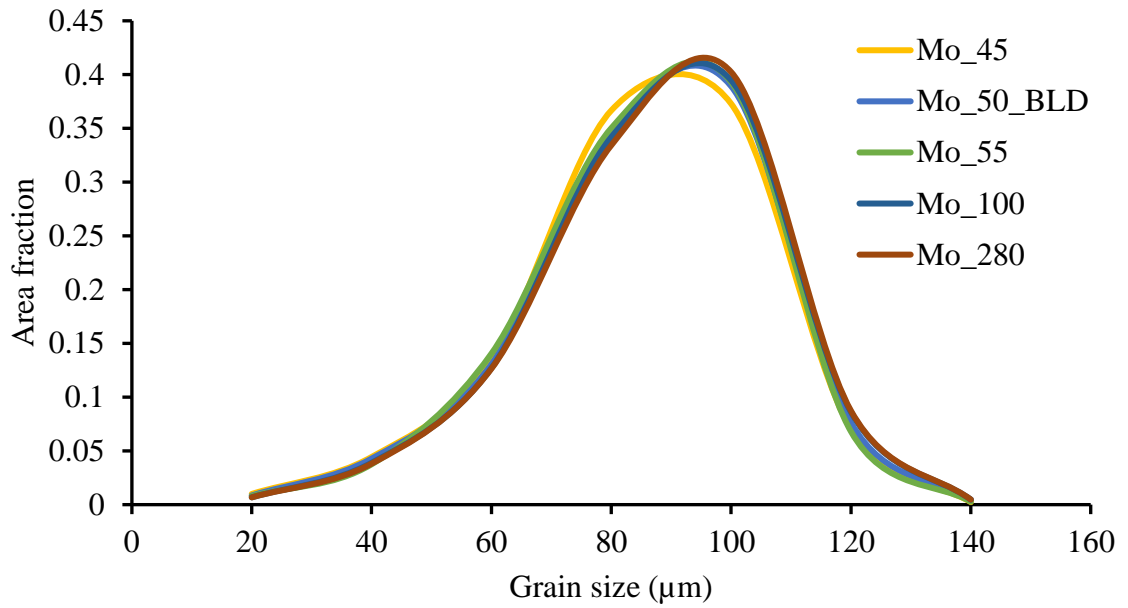
Figure 51 – Recrystallised grain size distributions for CA model simulations run with baseline data using different pre-exponential mobility (M_o) values ranging from 25 to 280 mol.m.J-1.s-1. The baseline benchmark value is at 50 mol.m.$J^{-1}s^{-1}$, M_o_50_BLD, for Fe-30Ni-0.044%Nb hot deformed at 950°C to a strain of 0.3 with a starting modal size of 160µm.

4.2.2 Effects of pre-exponential mobility on the recrystallisation kinetics

Following the sensitivity analysis shown in **Table 9**, the percentage deviation of the kinetics parameters from the baseline data was calculated for each value of pre-exponential mobility.

These numbers, shown in **Table 10**, in addition to the recrystallisation kinetics plotted in **Figure 52**, highlight differences in the reaction kinetics brought about by changing the pre-exponential mobility.

It can be seen that varying the pre-exponential boundary mobility causes changes in the recrystallisation kinetics. The recrystallisation starting time (R_s) for M_o values between 45 and 100molm/Js deviate by ±8%, with a greater deviation of approximately ±12% for M_o with the wider range of 25 to 280 mol.m.J-1.s-1. The small deviation for most M_o values is probably due to a similar delay time because they contain the same amount of Nb.

118

For the time at 50% recrystallisation, R50%, there is significant variation across the range of pre-exponential mobility (M_o) values. This is to be expected as the M_o affects the frequency of collisions. This same trend is apparent for the recrystallisation finishing time (R_f), the Avrami exponent (n) and the rate constant (k).

Table 10 – Calculated percentage deviation of the recrystallisation kinetics parameters from the benchmark baseline data, BLD(50) for different pre-exponential mobility values.

pre-exponential mobility (M_o) value in mol.m.J^{-1}.s^{-1}	Recrystallisation data							
	Rs(s)	R50% (s)	R_f (s)	n	k	D50% (µm)	D5% (µm)	D95% (µm)
BLD(50)	12.5	24.2	36.6	3.065	0.00004	100	43	105
	% Difference from the BLD(50) benchmark recrystallisation data							
25.0	12.0	86.0	154.1	-44.8	2400.0	0.0	-0.9	-1.0
55.0	0.0	0.0	-9.0	8.6	-50.0	0.0	2.1	-1.9
100.0	-8.0	-31.0	-42.1	78.3	-99.8	0.0	3.0	1.0
280.0	-12.8	-48.3	-62.3	343.6	-100.0	0.0	3.2	1.0

The recrystallisation kinetics in **Figure 52** shows that the recrystallisation rate is affected by the pre-exponential mobility (M_o). As the M_o increases from 50molm/Js to 280molm/Js, the recrystallisation rate increases along with more frequent collisions.
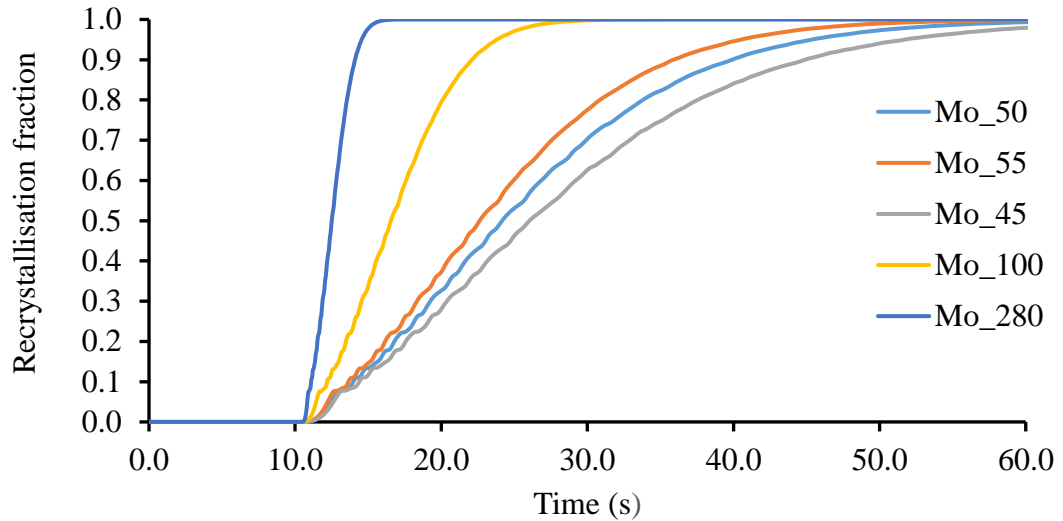
Figure 52 – Recrystallisation kinetics for CA model simulation run using the baseline data for different pre-exponential mobility values for Fe-30Ni-0.044%Nb hot deformed at 950°C to a strain of 0.3 with a starting modal size of 160µm.

There is a consistent trend as the pre-exponential mobility is increased. As the mobility is increased, the time at 50% of recrystallisation ($R50\%$) and the recrystallisation finishing time (R_f) decreases since the grain boundary moves faster and the growth of recrystallisation is faster. With increasing M_o, the sub-grains reach a stable nuclei at the same time, after which the growth of the stable nuclei then depends on the varying grain pre-exponential boundary mobility. So, the greater the pre-exponential boundary mobility, the greater the grain boundary velocity and therefore, the faster the recrystallisation kinetics.

4.2.3 Summary on sensitivity analysis of the pre-exponential boundary mobility

Varying the pre-exponential boundary mobility, which affects the grain boundary velocity, will not change the microstructure and hence the mechanical properties of the final product will not be affected.

The pre-exponential boundary mobility will play a significant role in terms of the process conditions, since the recrystallisation kinetics are significantly affected by changes of more than ±10%. An accurate determination of the pre-exponential mobility value for the recrystallisation kinetics is therefore necessary.

4.3 Sensitivity analysis on the magnitude of the austenite Burgers vector parameter.

In the model, the Burgers vector appears in many equations. The recovery rate **Equation 3.2** depends on it through the activation volume **Equation 3.5**. It also appears in the critical radius **Equation 3.12** , the sub-grain growth rate **Equation 3.11** and the stored energy **Equation 3.14**.

Since the Burgers vector appears in various equations in the model, it plays an important role in terms of the nucleation and driving the growth of recrystallisation.

A sensitivity analysis was carried out for this parameter. CA model simulations were run using the baseline data with Burgers vector values ranging from 2.23e-10m to 2.73e-10m. Note that the Burgers vector value for the benchmark baseline data is 2.52e-10m gotten from literature[141], shown as 'BLD(2.52)' in **Table 11**. The effect of varying the Burgers vector value on the recrystallisation data is shown in **Table 11**.

Table 11- Recrystallisation data obtained for CA simulations run with baseline data and Austenite Burgers vector values ranging from 2.23e-10m to 2.73e-10 m, with the baseline benchmark value at 2.52e-10 m, BLD(2.52).

Recrystallisation kinetics / parameter	Recrystallisation data for different Burgers vector values				
Austenite Burgers vector (x E-10m)	2.23	BLD(2.52)	2.54	2.57	2.73
R_s (s)	No recrystallisation	12.5	9.55	7.16	1.3
R50%(s)	No recrystallisation	24.2	17.9	12.7	2.68
R_f (s)	No recrystallisation	36.6	32.8	18.8	6.59
n	No recrystallisation	3.0658	3.1845	3.0746	1.134
k	No recrystallisation	3.6253e-5	6.4859e-5	2.7808e-4	2.361e-1
D50% (µm)	No recrystallisation	100	100	100	40
D5% (µm)	No recrystallisation	43.4	44.3	44.7	15.1
D95% (µm)	No recrystallisation	105	103	106	43.2

4.3.1 Effects of the magnitude of the Burgers vector on the microstructure

Changing the magnitude of the Burgers vector between 2.52 and 2.57e-10m has little effect on the average recrystallised grain size ($D_{50\%}$) but with a Burgers vector magnitude of 2.73e-10 m, it is significantly smaller (see **Table 11**) and there is no recrystallisation using a Burgers vector of 2.23e-10 m, which is most likely because the sub-grains did not reach the critical grain size. Decreasing the Burgers vector increases the size of the critical grain size (see 3.6.2). The recrystallised grain size distributions are shown in **Figure 53**. The recrystallised grain size distributions for the CA model simulations with a Burgers vector of 2.54e-10m and 2.57e-10m are overlaid and closely match the grain size distribution using a Burgers vector of 2.52e-10m (the benchmark CA simulation). However, using a Burgers vector of 2.73e-10m, shifts the recrystallised grain size distribution significantly to the left.
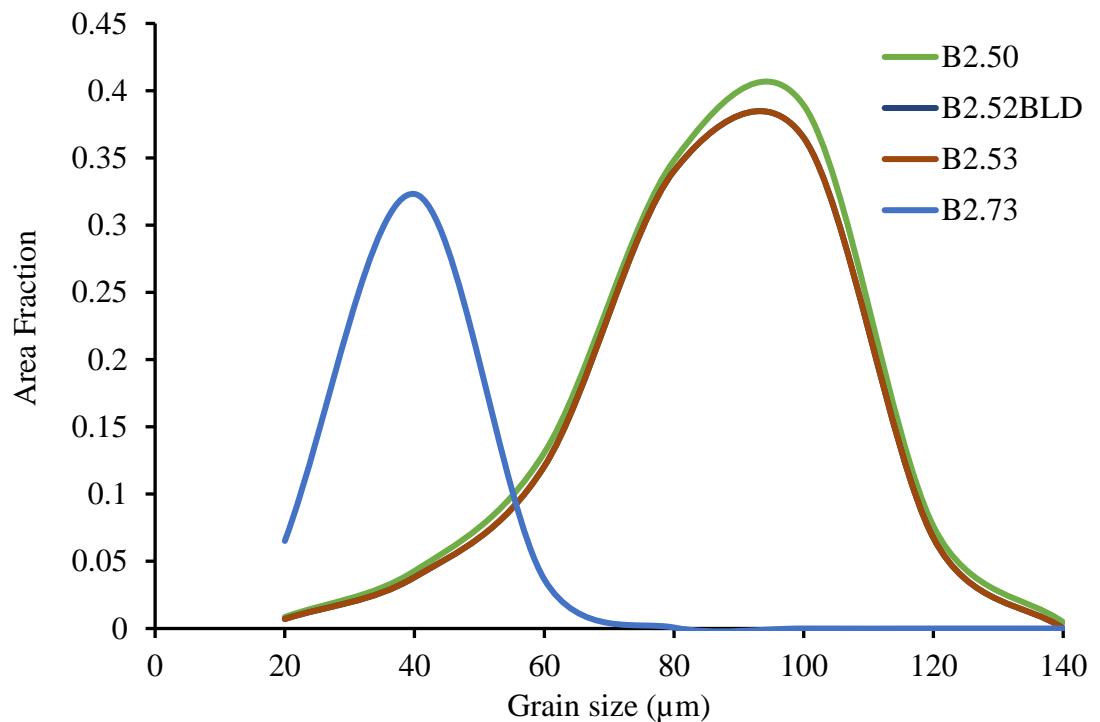
Figure 53 – Grain size distribution after recrystallisation for baseline CA model simulations using a different magnitude of Burgers vector, with the benchmark simulation at 2.52e-10m (B2.52BLD) for Fe-30Ni-0.044%Nb hot deformed at 950°C to a strain of 0.3 with a starting modal size of 160µm.

The 2D recrystallised final microstructure images resulting from baseline CA model simulations using the different Burgers vectors are shown in **Figure 54**. The

appearance of the final microstructure for Burgers vector values between 2.52e-10 m and 2.57e-10 m is similar and significant changes can be seen when using a Burgers vector value of 2.73e-10 m.
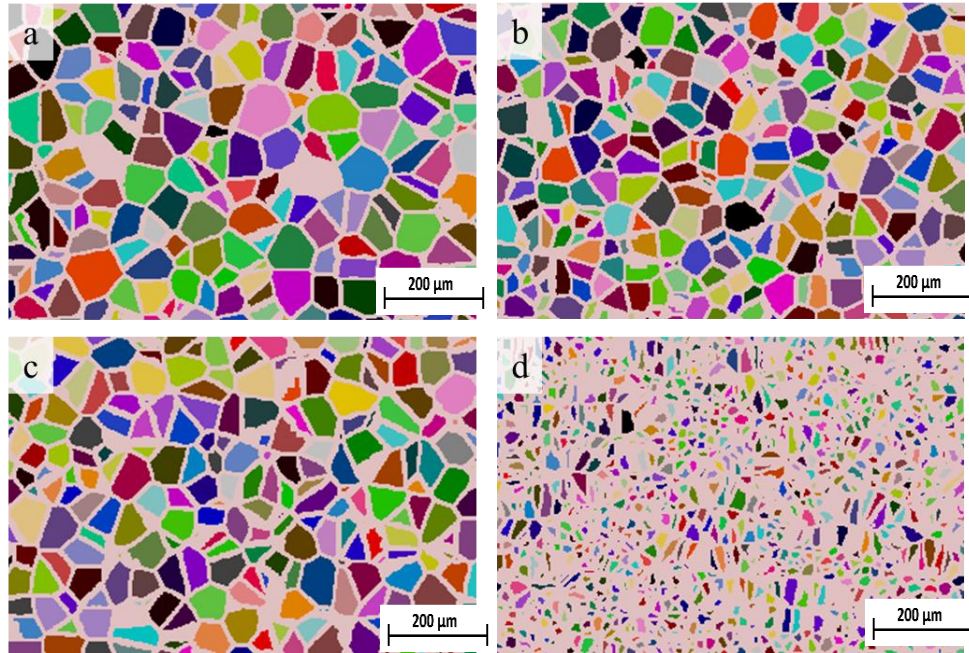
Figure 54 – 2D Final recrystallised microstructure for baseline CA model simulations with different Burgers vector magnitudes: (a) Burgers vector of 2.52e-10 m, (b) Burgers vector of 2.54e-10 m, (c) Burgers vector of 2.57e-10 m and (d) Burgers vector of 2.73e-10 m, for Fe-30Ni-0.044%Nb hot deformed at 950°C to a strain of 0.3 with a starting modal size of 160µm.

Therefore, changing the magnitude of the Burgers vector by more than ±10% will induce significant changes in the final microstructure and hence affect mechanical properties.

4.3.2 Effects of the magnitude of the Burgers vector on the recrystallisation kinetics

Changing the magnitude of the Burgers vector causes more pronounced changes in the recrystallisation kinetics (**Figure 55**). The recrystallisation starting time (R_s), time at 50% recrystallisation ($R_{50\%}$) and the recrystallisation finishing time (R_f) all decrease as the magnitude of the Burgers vector increases from 2.52e-10m (see **Table 11**). This is due to the fact that some of the sub-grains in the sub-grain distribution attain the critical

123

grain size faster, so that the start of the nucleation of recrystallisation begins earlier. This is because the critical grain size reduces as the Burgers vector value increases (see **Equation 3.12, Equation 3.10 and Equation 3.14**). It is notable that the Burgers vector is often squared and this implies that the results from the recrystallisation finishing time (R_f) might come from this non-linearity.

However, with all the various interactions between the parameters in the equations, it is difficult to come to a definite conclusion.
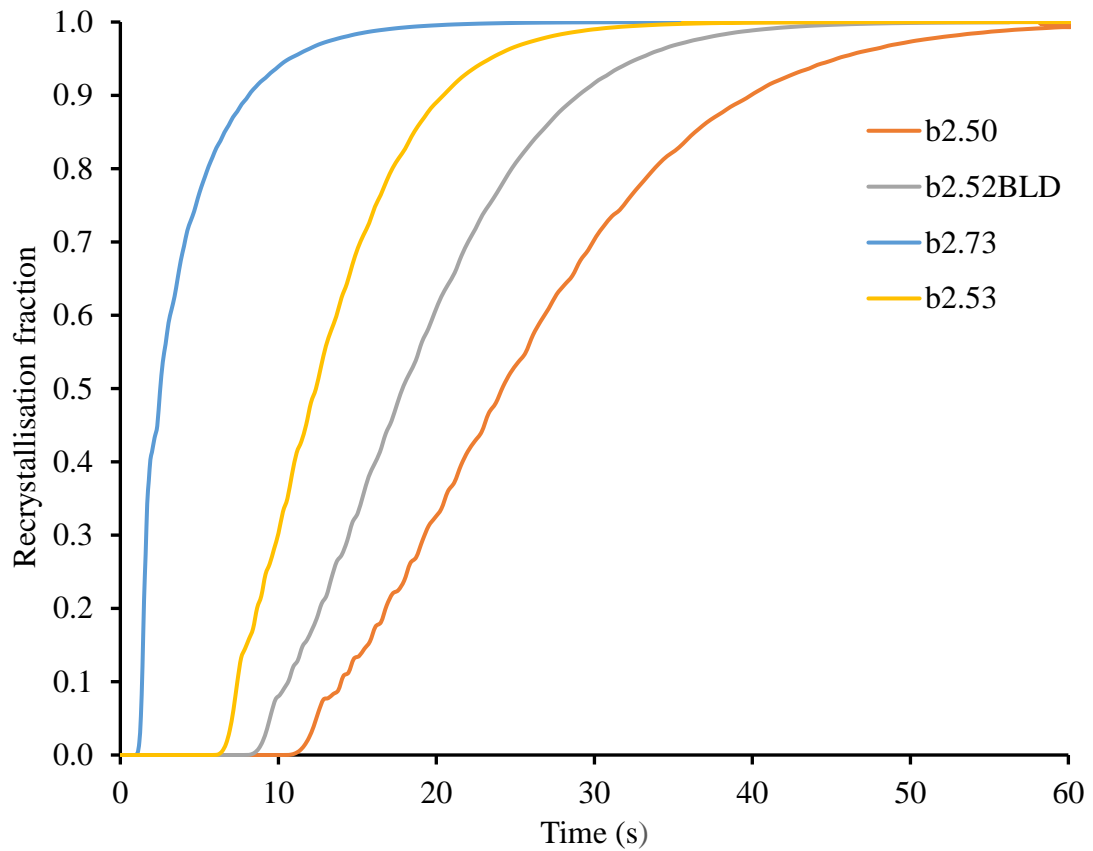
Figure 55 – Recrystallisation kinetics for baseline CA model simulations using a different magnitudes of Burgers vector, with the benchmark simulation at 2.52e-10m (B2.52BLD), for Fe-30Ni-0.044%Nb hot deformed at 950°C to a strain of 0.3 with a starting modal size of 160μm.

Following the sensitivity analysis shown in **Table 11**, the percentage deviation of the kinetics parameters from the baseline data was calculated for each Burgers vector value. These numbers, shown in **Table 12** in addition to the recrystallisation kinetics

plotted in **Figure 55**, highlight differences in the reaction kinetics brought about by changing the Burgers vector.

Table 12 – Calculated percentage deviation of the recrystallisation kinetics parameters from the benchmark baseline data, BLD(2.52) for different Burgers vector values.

Austenite Burgers vector (x E-10m)	Recrystallisation data							
	Rs(s)	R50% (s)	R_f (s)	n	k	D50% (μm)	D5% (μm)	D95% (μm)
BLD(2.52)	12.5	24.2	36.6	3.0658	0.00004	100	43	105
	% Difference from the BLD(2.52) benchmark recrystallisation data							
2.23	NA	NA	NA	NA	NA	NA	NA	NA
2.54	-23.6	-26.0	-10.4	3.9	60.0	0.0	3.0	-1.9
2.57	-42.7	-47.5	-48.6	0.3	600.0	0.0	3.0	1.0
2.73	-89.6	-88.9	-82.0	-63.0	590150.0	-60.0	-65.2	-58.9

4.3.3 Summary of the sensitivity analysis for the magnitude of the Burgers vector

Varying the magnitude of Burgers vector by more than ±10% significantly affects the critical grain size, which affects the final microstructure and so the mechanical properties of the final product will be affected.

The magnitude of Burgers vector will play a significant role in terms of the process conditions since the recrystallisation kinetics are significantly affected by this parameter. There is significant deviation from the benchmark CA simulation for all values (from 10.4% to 89.6% as the Burgers vector increases), shown in **Table 12**. An accurate determination of the Burgers vector value for the recrystallisation kinetics is therefore necessary.

4.4 Sensitivity analysis on varying the temperature of the baseline data.

In the model, temperature appears in many equations. The recovery rate depends on it (**Equation 3.2**). The critical radius (**Equation 3.12**) depends on temperature through the grain boundary energy γ_{SE} (**Equation 3.13**), expressed as a function of temperature. Also, the boundary velocity and sub-grain growth rate depend on temperature.

A sensitivity analysis was carried out for temperature to determine how the data is influenced by temperature. CA model simulations were run at different temperatures using the baseline data, with the benchmark simulation at 950°C. The temperature range analysed was between 850°C and 1100°C but there was no recrystallisation at 850°C.

The initial grain size distributions for the baseline CA model simulations at temperatures from 850°C and 1100°C is shown in **Figure 56**. It can be seen that all of initial grain size distributions for the starting microstructure are overlaid for temperatures between 850°C and 1100°C used in the simulations.
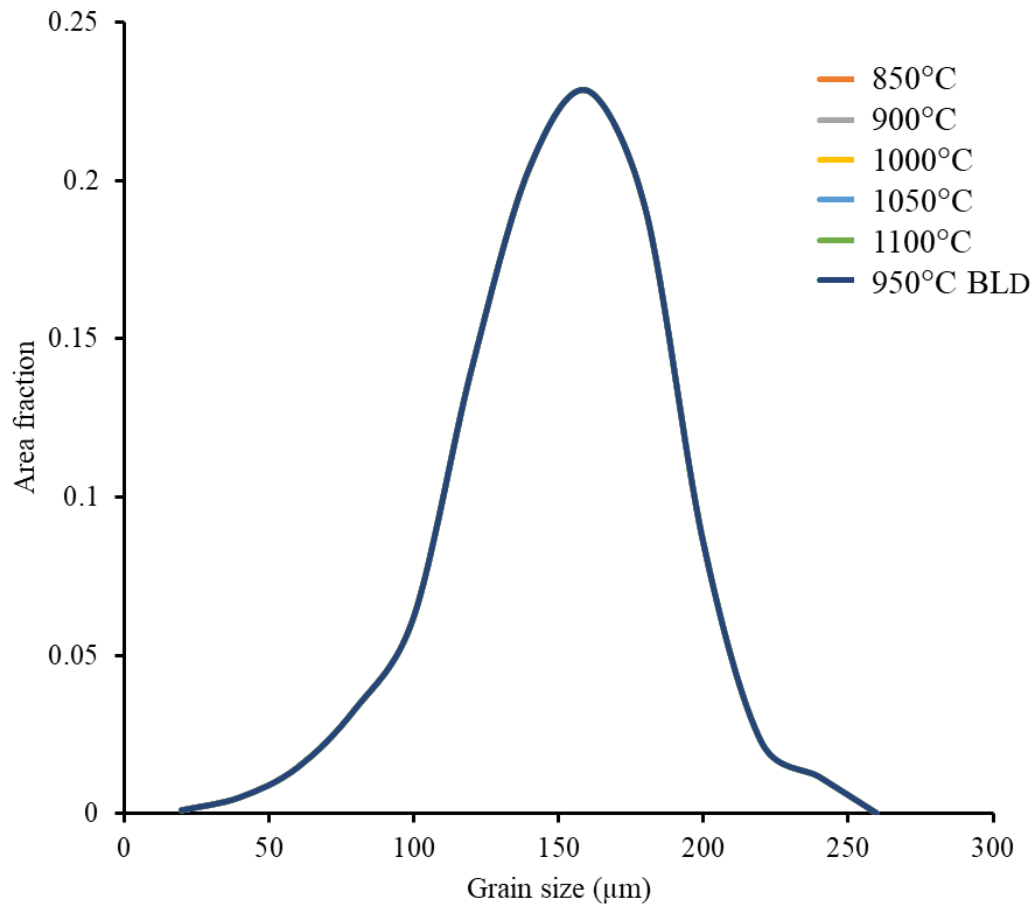
Figure 56 – Initial grain size distributions for the starting microstructure for baseline CA simulations at different temperatures. The benchmark simulation is at 950°C (950°CBLD),for Fe-30Ni-0.044%Nb hot deformed at 950°C to a strain of 0.3 with a starting modal size of 160µm.

The effect of varying the temperature value on the recrystallisation data is shown in **Table 13**.

Recrystallisation kinetics / parameter	Recrystallisation data for CA simulations using different temperatures					
Temperature (°C)	850	900	BLD(950)	1000	1050	1100
R_s (s)	No recrystallisation		12.5	3.5	0.9	0.4
R50% (s)	No recrystallisation		24.2	5.8	1.7	0.6
R_f (s)	No recrystallisation		36.6	9.4	3.5	1.7
n	No recrystallisation		3.0658	2.8361	1.868	1.4993
k	No recrystallisation		3.6253e-5	4.2890e-3	2.3070e-1	8.4570e-1
D50% (μm)	No recrystallisation		100	60	40	40
D5% (μm)	No recrystallisation		43	26	20	13
D95% (μm)	No recrystallisation		104	65	54	40

The recrystallised grain size distributions for the baseline simulations at different temperatures are shown in **Figure 57**. It can be seen from **Table 13**, that there is a significant variation in D5%, D50% and D95%, with the values decreasing with increasing temperature. Significant variation in the recrystallised grain size distributions supporting this can be seen in **Figure 57**.

This unwanted variation in the recrystallised grain sizes with temperature is inconsistent with the published work in the literature, as there is no temperature dependence for the grain size[141].

One effect of increasing the temperature is that this reduces the grain boundary energy making it easier for the grains to overcome the capillary force. This means that there are an increased number of nucleated grains that will recrystallise because the sub-

grain growth is faster at higher temperatures. Hence, finer recrystallised final microstructure will result at higher temperatures.

However another opposing effect of temperature is that when the temperature is increased the rate of recovery will increase because the grains will have less stored energy meaning it is less likely that they will nucleate new grains.

Due to these two opposing effects, the temperature is not expected to affect the recrystallised grain size distributions.
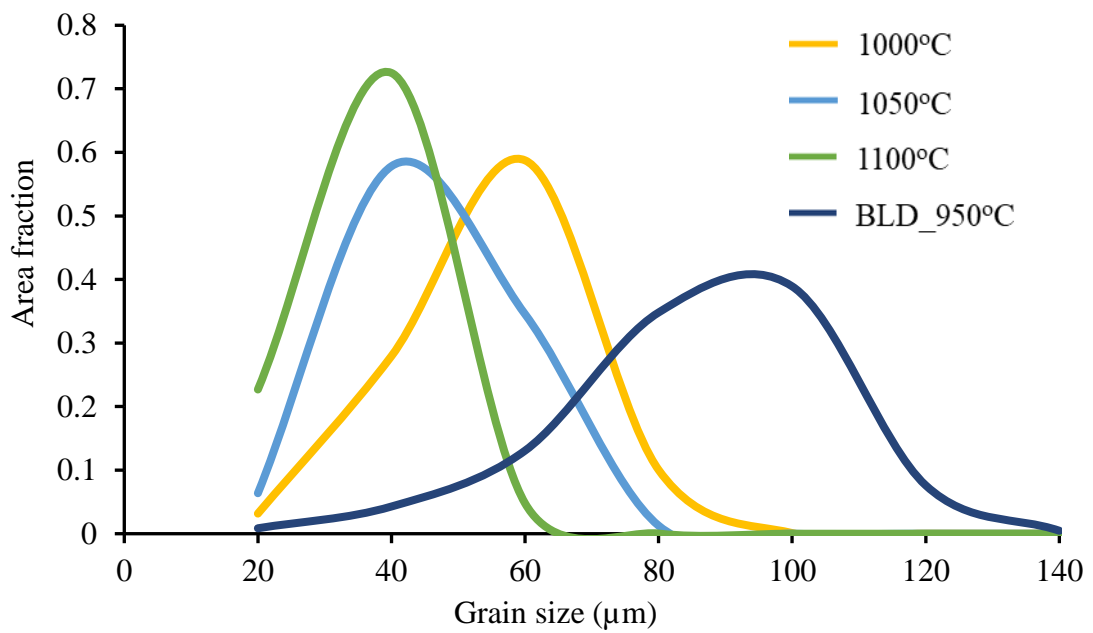
Figure 57 – Recrystallised grain size distributions for CA model simulations run with baseline data at different temperatures. The benchmark simulation is at 950°C (BLD_950C), for Fe-30Ni-0.044%Nb hot deformed at 950°C to a strain of 0.3 with a starting modal size of 160µm.

Following the sensitivity analysis shown in **Table 13**, the percentage deviation of the kinetics parameters from the baseline data was calculated for each temperature value. These numbers, shown in **Table 14**, in addition to the recrystallisation kinetics plotted in **Figure 58**, highlight differences in the reaction kinetics brought about by changing the temperature. **Table 13** shows the recrystallisation starting time (R_s), time at 50% recrystallisation ($R_{50\%}$) and the recrystallisation finishing time (R_f) all increase as the

temperature increases. **Figure 58** shows that the recrystallisation rate increases as the temperature increases.
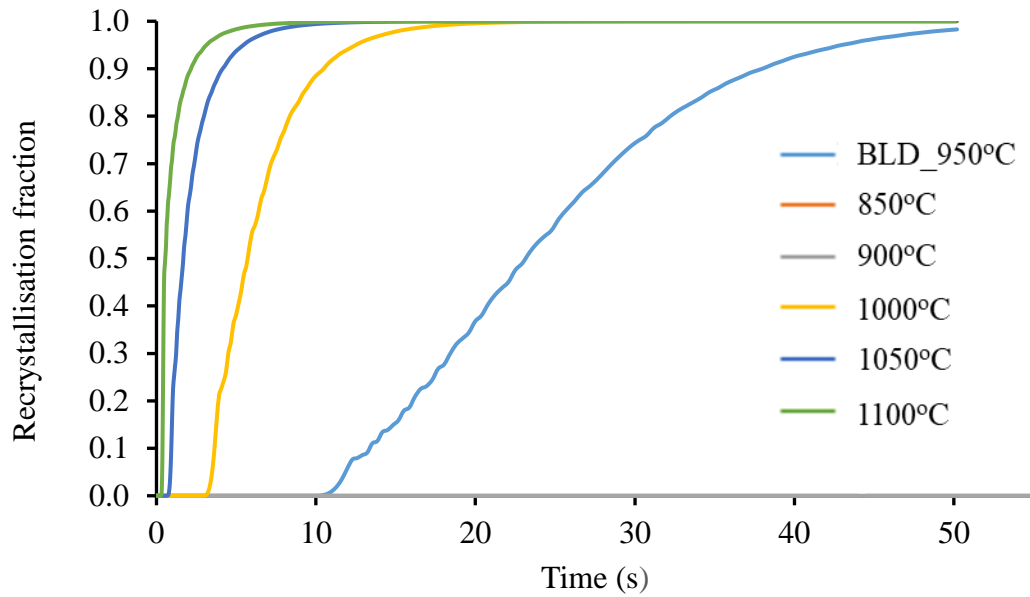
Figure 58 – Recrystallisation kinetics for CA model simulations run using the baseline data for different temperature values, with the benchmark simulation at 950°C (BLD_950C), for Fe-30Ni-0.044%Nb hot deformed at 950°C to a strain of 0.3 with a starting modal size of 160µm.

The large, significant variation in R_s, $R_{50\%}$, R_f , n and k can be seen in **Table 14**. For example, a 50°C increase from the benchmark temperature yields a 72% change in the R_s increasing to 97% when increased by 150°C. Therefore, varying temperature by more than ±10% has a significant effect on the recrystallisation kinetics.

Temperature (°C)	Recrystallisation data							
	Rs(s)	R50%	R_f	n	k	D50%	D5%	D95%
BLD(950)	12.5	24.2	36.6	3.0658	0.00004	100	43	105
	% Difference from the BLD(950) benchmark recrystallisation data							
850	NA	NA	NA	NA	NA	NA	NA	NA
900	NA	NA	NA	NA	NA	NA	NA	NA
1000	-71.9	-76.0	-74.3	-7.5	10622.5	-40.0	-40.1	-38.1
1050	-92.6	-92.8	-90.5	-39.1	576650.0	-60.0	-53.9	-48.6
1100	-97.1	-97.7	-95.4	-51.1	2114150.0	-60.0	-70.0	-61.9

4.4.1 Summary on sensitivity analysis for the effects of temperature

Varying the magnitude of temperature by more than ±10% significantly affects the critical grain size, which affects the final microstructure and so the mechanical properties of the final product will be affected.

The temperature will play a significant role in terms of the process conditions since the recrystallisation kinetics are significantly affected by this parameter. There is significant deviation from the benchmark CA simulation for all values, shown in **Table 14**.

4.5 Sensitivity analysis on varying the strain

A sensitivity analysis was carried out to determine the effect of strain on the recrystallised microstructure and recrystallisation kinetics. Baseline CA model simulations were run at two different temperatures (950°C and 1100°C) to a strain of 0.3 and 0.6. The resulting recrystallised grain size distributions are given in **Figure 59**.
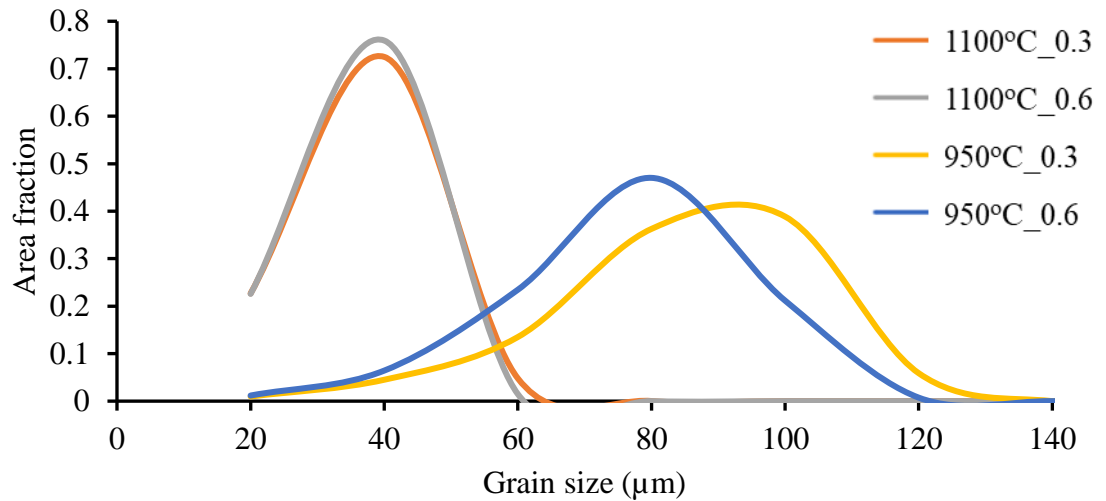
Figure 59 – Recrystallised grain size distributions for baseline CA simulations run at 950°C to a strain of 0.3 and 0.6 and at 1100°C to a strain of 0.3 and 0.6, for Fe-30Ni-0.044%Nb with a starting modal size of 160µm.

For baseline CA model simulations at 950°C, the recrystallised grain size distribution shifts to the left when the strain is increased from 0.3 to 0.6 and the recrystallised modal grain size decreases. However, at 1100°C, the strain has no effect on the recrystallised grain size distribution.

Changes in the recrystallisation grain size distribution for the same temperature to different strain arise as the modal grain size gets finer with increasing strain due to higher stored energy. This trend has be observed in the literature. The results from the CA simulations at 950°C show this pattern, while the results at 1100°C do not.

In addition to the recrystallised grain size distributions, the recrystallisation kinetics for the CA model simulations at different temperatures and strain were analysed. Results are given in **Figure 60**.
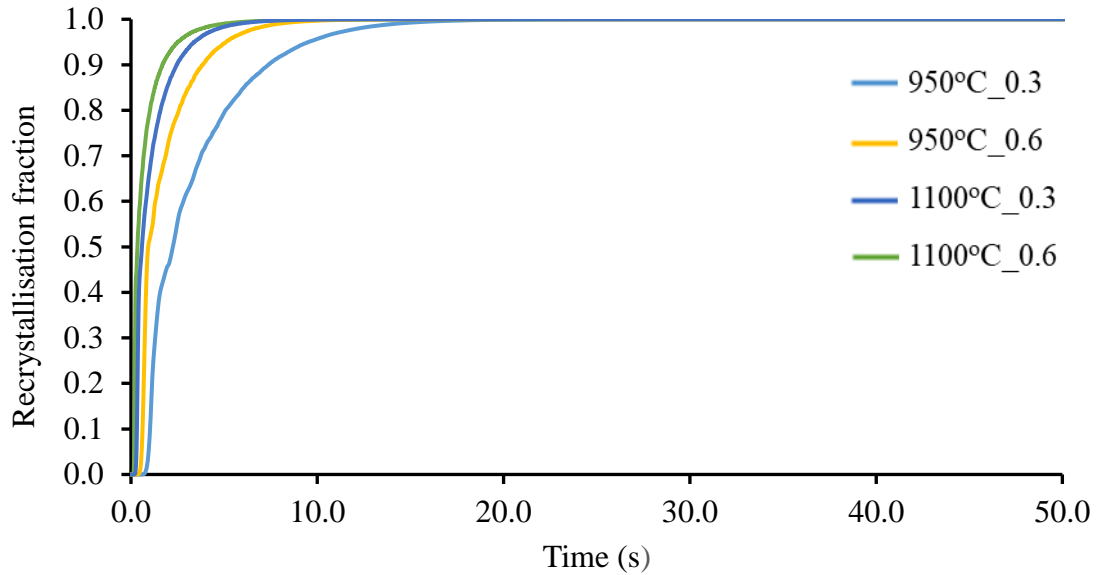
Figure 60 – Recrystallisation kinetics for the baseline CA model simulations at 950°C and 1100°C to a strain of 0.3 and 0.6, for Fe-30Ni-0.044%Nb hot deformed with a starting modal size of 160μm.

It can be seen that the results for the recrystallisation kinetics obtained are as expected. The recrystallisation rate increases with temperature and for each temperature it increases with increasing strain (**Figure 60**). At a given temperature the stored energy increases as the strain increases, which means there is a higher driving force for recrystallisation.

Varying the strain will affect the recrystallised grain size distribution, which affects the final microstructure and so the mechanical properties of the final product will be affected.

The strain will play a significant role in terms of the process conditions since the recrystallisation kinetics are significantly affected by this parameter.

This sensitivity analysis indicates, therefore, that the CA model needs to be designed so that it is strain dependent as seen in the literature.

4.6 Sensitivity analysis on varying the sub-grain factor (K_{ad})

The sub-grain factor in the CA model (K_{ad}) affects the speed at which the sub-grain reaches the critical size because it is a constant for nucleation. The K_{ad} baseline value

of 2.35 used in the model was derived by Rehman *et al.*[37] by fitting it to experimental data with no dynamic recrystallisation and the absence of precipitation at the recrystallisation temperature.

A sensitivity analysis was carried out to see the impact of varying the K_{ad} value on the baseline data at 950°C and 1100°C. CA model simulations were run using baseline data with the benchmark simulation using a K_{ad} of 2.35.

The recrystallised grain size distributions for baseline CA simulations using the same K_{ad} of 2.35 at 950°C and 1100°C are shown in **Figure 61**. The recrystallised modal grain size decreases significantly from 100µm at 950°C to 40µm at 1100°C. One possible explanation for this is that in the model, the temperatures appears in many equations. The recovery rate, the critical radius (through the grain boundary energy) and the boundary velocity. So sat higher temperatures, the boundary velocity is higher and the rate of nucleation. As more nuclei are formed with smaller grain sizes.
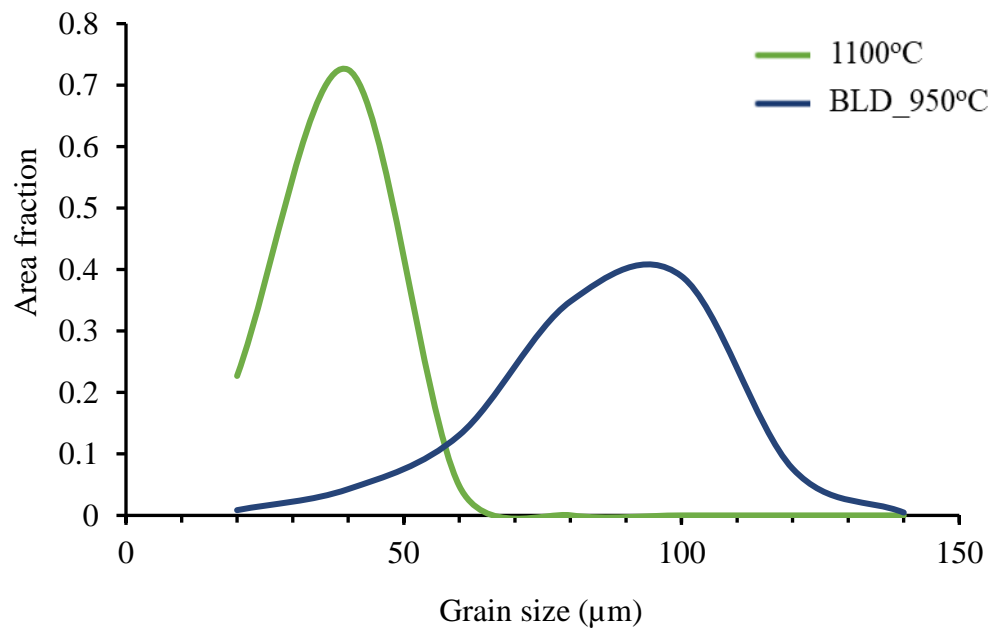
Figure 61 – Recrystallised grain size distributions of the baseline CA simulations at 950°C and 1100°C both with a K_{ad} value of 2.35, for Fe-30Ni-0.044%Nb hot deformed to a strain of 0.3 with a starting modal size of 160µm.

Baseline CA model simulations were then run at 950°C using K_{ad} values of 2.35 and 3.35. **Figure 62** shows that at a K_{ad} values of 2.35 and 3.35, the recrystallised modal grain size is 40µm and 100µm with a significant difference of 60µm. Therefore, changing the K_{ad} value has a significant effect on the recrystallised grain size distribution.
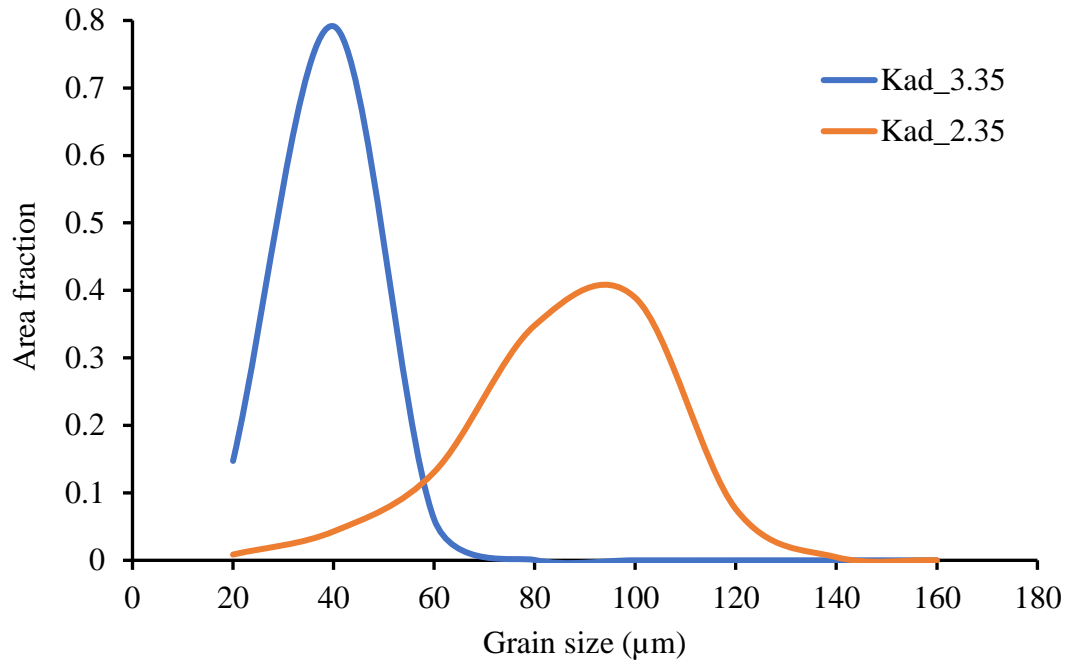
Figure 62 – Recrystallised grain size distribution for the baseline data at Kad values of 2.35 and 3.35, for Fe-30Ni-0.044%Nb hot deformed at 950°C to a strain of 0.3 with a starting modal size of 160µm.

Further work on the sensitivity analysis using the higher K_{ad} value. CA model simulations were carried out to a strain of 0.3 and 0.6 using a K_{ad} value of 3.35 at 950°C and 1100°C. Results are shown in **Figure 63**.
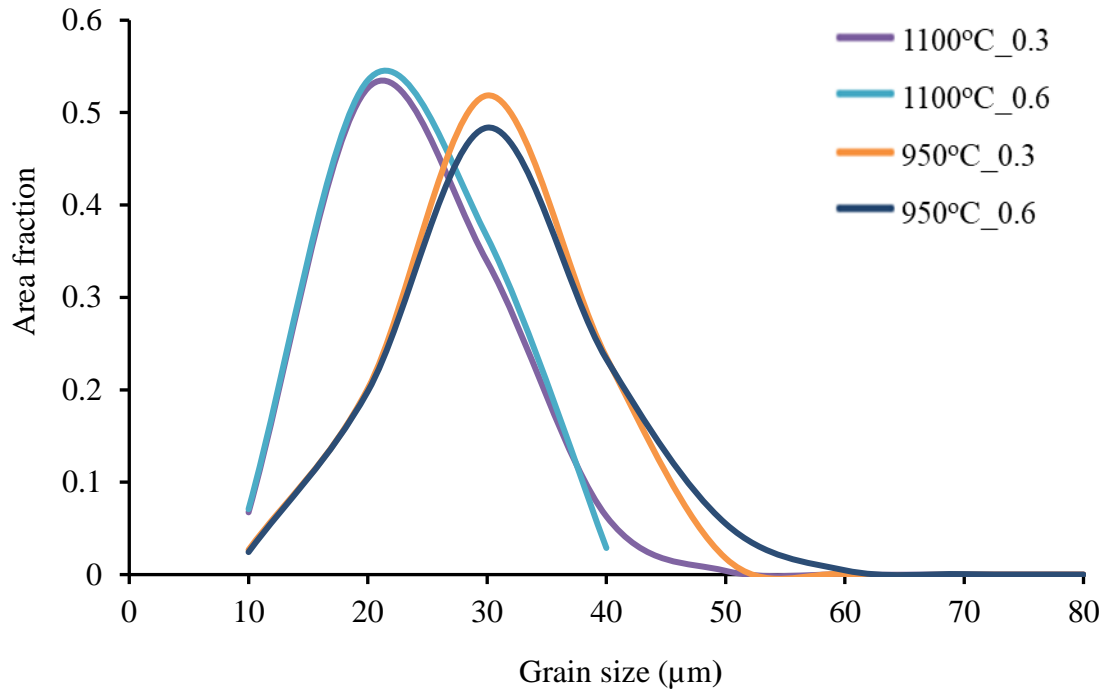
Figure 63 – The recrystallised grain size distributions for baseline CA model simulations at temperatures of 950°C and 1100°C to a strain of 0.3 and 0.6 using a K_{ad} value of 3.35 for all simulations, for Fe-30Ni-0.044%Nb hot deformed with a starting modal size of 160µm.

Using a K_{ad} value of 3.35 the recrystallised grain size distributions at 950°C were both the same to a strain of 0.3 and 0.6 with the same recrystallised modal grain size. This trend was repeated at 1100°C thus showing strain insensitivity at both temperatures. Increasing K_{ad} means the more nuclei are formed and sub-grains grow more quickly so that more sub-grains reach the critical radius and hence more sub-grains becomes stable and grows at the same time.

The percentage deviation of the kinetics parameters from the benchmark baseline data (using a K_{ad} value of 2.35) was calculated for the CA simulations carried out using a K_{ad} value of 3.35. These numbers, shown in **Table 15**.

Table 15 – Summary of the percentage deviation of the recrystallisation kinetics with K_{ad} of 3.35 value from the baseline data.

	Recrystallisation data							
	R_s (s)	R50% (s)	R_f (s)	n	k	D50% (μm)	D5% (μm)	D95% (μm)
BLD(2.35)	12.5	24.2	36.6	3.0658	0.00004	100	43	105
Baseline CA simulations with a K_{ad} of 3.35	% Difference from the BLD(2.35) benchmark recrystallisation data							
950°C to a strain of 0.3	-90.4	-91.0	-83.2	-60.2	559345.0	-60.0	-67.7	-61.0
950°C to a strain of 0.6	-91.2	-93.0	-89.0	-36.6	445687.5	-60.0	-67.7	-64.8
1100°C to a strain of 0.3	-97.2	-97.7	-94.7	-60.3	3010050.0	-80.0	-77.0	-69.5
1100°C to a strain of 0.6	-99.6	-99.3	-98.4	-67.9	9244050.0	-80.0	-77.0	-76.2

It can be seen that there is a significant percentage deviation in the reaction kinetics at a K_{ad} value of 3.35 for 950°C and 1100°C to a strain of both 0.3 and 0.6 compared to the benchmark baseline data.

Baseline simulations using K_{ad} values below 2.35 (ranging from 0.1 to 2.0) were also carried out and the recrystallisation kinetics are given in **Figure 64**. Looking at the trend, it can be concluded that increasing the k_{ad} value from 1.0 to 2.0 leads to faster recrystallisation kinetics but at k_{ad} values between 0.1 and 0.5 there is no difference in terms of recrystallisation kinetics. One possible explanation is that the evolution of the sub-grain is slow, as there is no noticeable difference in the speed at which it evolves to the critical size.
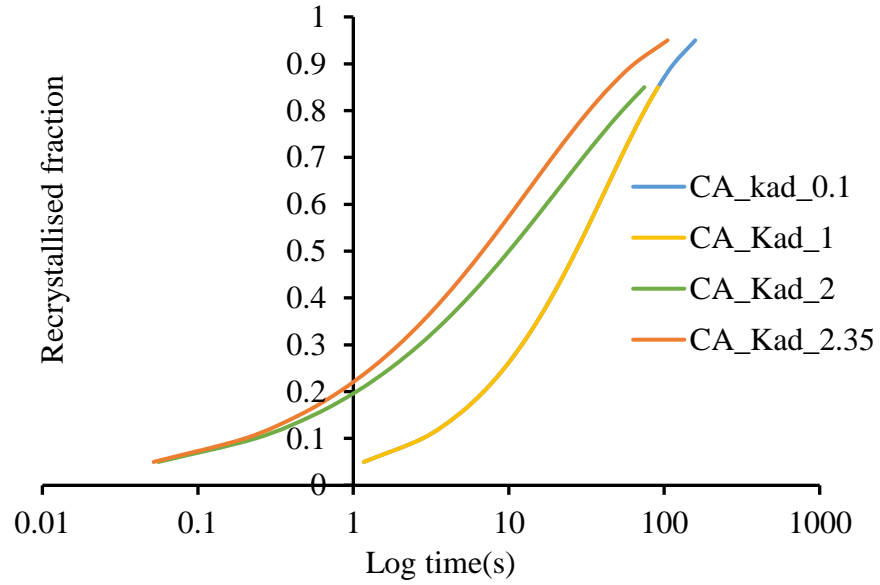
Figure 64 – Recrystallisation kinetics for baseline CA model simulations at lower K_{ad} values for Fe-30Ni-0.044%Nb hot deformed at 950°C to a strain of 0.3 with a starting modal size of 160µm.

4.7   Sensitivity analysis on varying the shear modulus

The shear modulus is a function of temperature and the most common values of shear modulus reported at room temperature in the literature are 70GPa, 81Gpa and 87Gpa. These commonly reported values for steels were used in baseline CA model simulations and compared to the benchmark (using a shear modulus value of 70GPa).

The recrystallisation data is given in **Table 16**. It can be seen that increasing the shear modulus gives rise to decreasing R_s, R_f and n. **Figure 65** shows the recrystallisation kinetics. As the shear modulus increases the recrystallisation rate increases. The critical radius decreases with increasing shear modulus and therefore there is an increase in the number of nuclei formed. The stored energy also increases with the shear modulus. The trend in the recrystallisation kinetics is consistent with what is observed in literature.
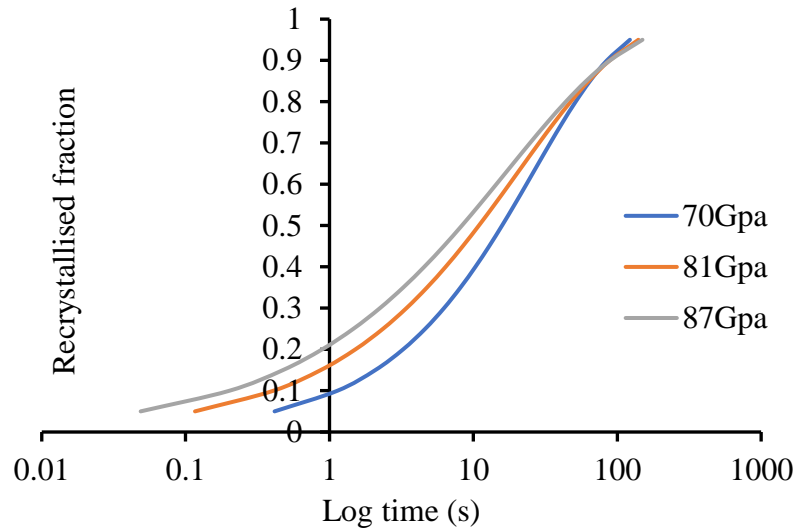
Figure 65 – Recrystallisation kinetics for baseline CA model simulations using different shear modulus values of 70GPa (benchmark value), 81Gpa and 87Gpa for Fe-30Ni-0.044%Nb hot deformed at 950°C to a strain of 0.3 with a starting modal size of 160µm.

The microstructure at 70GPa, 81GPa and 87GPa at the same temperature and strain shows similar microstructure (see **Table 16**), as D5%, D50% and D95% are similar for all shear modulus values. Therefore, increasing the shear modulus does not significantly affect the final microstructure.

Table 16 – Recrystallisation data for baseline CA model simulations using different shear modulus values of 70GPa, 81GPa and 87GPa for Fe-30Ni-0.044%Nb hot deformed at 950°C to a strain of 0.3 with a starting modal size of 160µm.

Recrystallisation kinetics/parameters	Recrystallisation data for baseline CA simulations using different shear modulus values		
Austenite Shear modulus (GPa) at room temperature	BLD(70)	81	87
R_s (s)	12.5	3.71	3.46
R_f (s)	36.6	33.7	30.36
n	3.0658	1.0754	1.0413
k	0.0004	0.0125	0.0143
D5% (µm)	43	43	43
D50% (µm)	100	90	84
D95% (µm)	105	104	101

138

4.8 Sensitivity analysis on varying the activation energy

The activation energy affects the driving force in the model through the rates of recovery. Sensitivity analysis was carried out to determine the influence of activation energy on recrystallisation kinetics and recrystallised grain size distribution. Values of the activation enthalpy for the operating recovery process reported in the literature were 195kJ/mol, 285kJ/mol (the value used in the benchmark baseline simulation i.e. the activation energy for self-diffusivity) [37] and 485kJ/mol[3], [19], [20].

Baseline CA simulations were carried out using these activation enthalpy values. The resulting recrystallisation data and recrystallisation grain size distribution are given in **Table 17** and **Figure 66** respectively. There is a significant difference between the recrystallised grain size distributions for 285kJ/mol and 485kJ/mol and there was no recrystallisation using an activation energy value of 192kJ/mol. The recrystallised modal grain sizes using an activation energy of 485kJ/mol is 40µm (compared to 100 µm for the benchmark using 285kJ/mol), see **Table 17**.
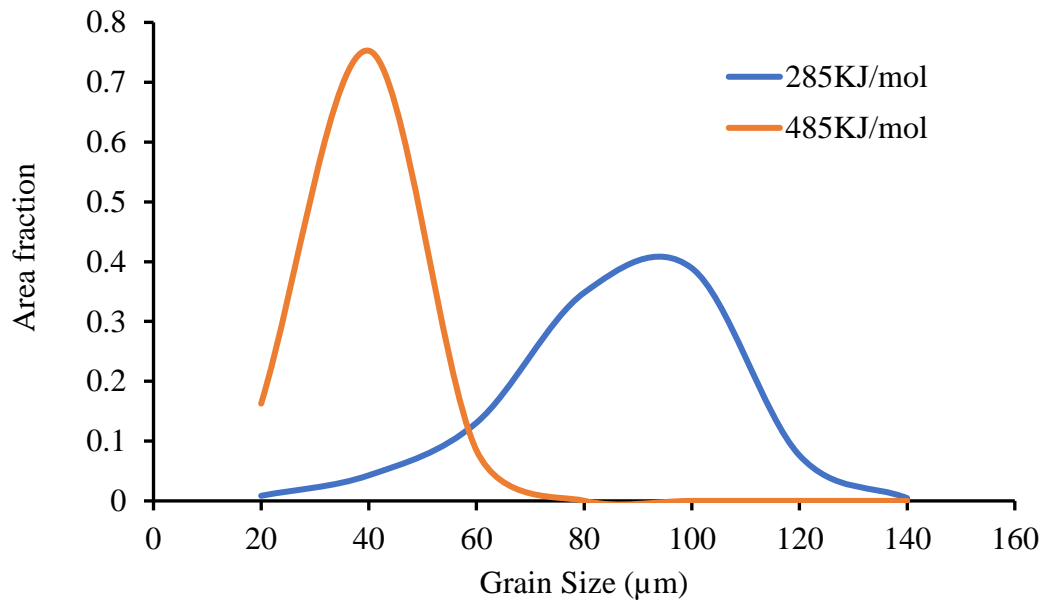
Figure 66 – Recrystallised grain size distribution for the baseline CA model simulations using activation energy values of 192kJ/mol, 285kJ/mol (benchmark value) and 485kJ/mol for Fe-30Ni-0.044%Nb hot deformed at 950°C to a strain of 0.3 with a starting modal size of 160µm.

At 195kJ/mol there was no recrystallisation which is possibly due to the fact that the recrystallisation nucleation activation energy for the model steel (192kJ/mol) used is very close to the activation energy of self-diffusion used in the recovery rates equation (195kJ/mol) and these two processes are in competition.

Table 17 – Recrystallisation data for baseline CA model simulations using different activation energy values of 195kJ/mol, 285kJ/mol (benchmark value) and 485kJ/mol for Fe-30Ni-0.044%Nb hot deformed at 950°C to a strain of 0.3 with a starting modal size of 160µm.

Recrystallisation kinetics/parameters	Recrystallisation data for baseline CA simulations using different activation energy values		
Activation energy (KJ/Mol)	195	285	485
R_s (s)	No recrystallisation	12.5	4.95
R50% (s)	No recrystallisation	24.2	6.01
R_f (s)	No recrystallisation	36.6	8.89
n	No recrystallisation	3.0658	3.6058
k	No recrystallisation	3.6253e-5	0.0008643
D5% (µm)	No recrystallisation	43	20
D50% (µm)	No recrystallisation	100	40
D95% (µm)	No recrystallisation	105	60

Recrystallisation kinetics for this sensitivity analysis of activation energy is given in **Figure 67**, which shows that at higher activation energy the recrystallisation kinetics are faster. The resulting R_s and R_f using an activation energy of 485kJ/mol is faster compared to the those using an activation energy of 285kJ/mol **Table 17**.
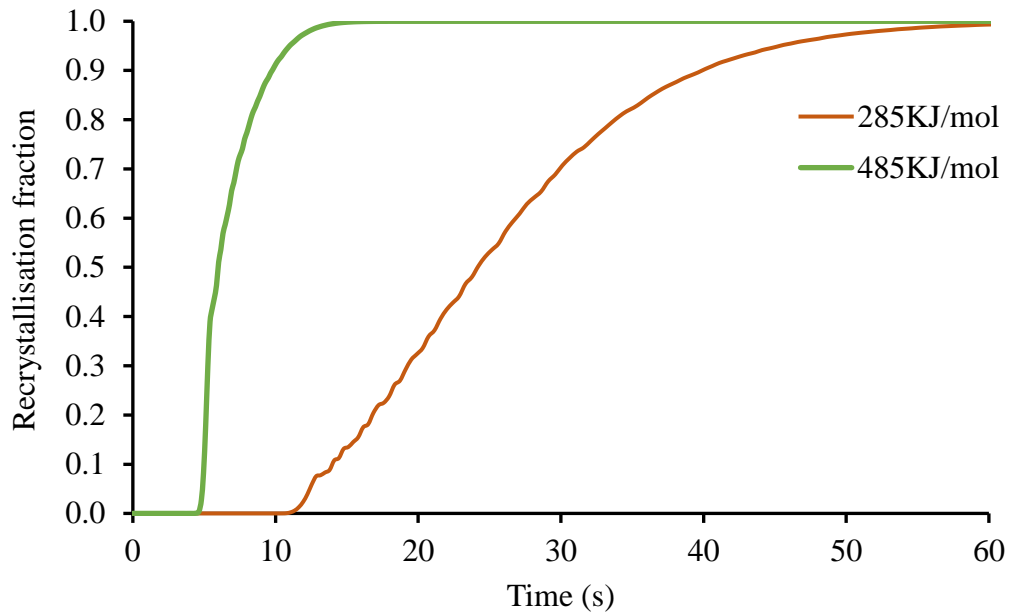
Figure 67 – Recrystallisation kinetics for baseline CA model simulations using different activation energy values of 285kJ/mol (benchmark value) and 485kJ/mol for Fe-30Ni-0.044%Nb hot deformed at 950°C to a strain of 0.3 with a starting modal size of 160µm.

In summary, the activation energy value affects both the final microstructure and the recrystallisation kinetics. Hence, an increase in activation energy from the benchmark baseline value (285kJ/mol) for the model steel will have a significant effect on the mechanical properties and the processing conditions of the steel.

4.9   Sensitivity analysis activation volume factor

The most common values reported in the literature for activation volume factor are between 15 to 61[16]. The activation volume factor is used in the recovery process. A sensitivity analysis was carried out for this parameter. CA model simulations were run using the baseline data with activation volume factor values ranging from 15 to 61. Note that the activation volume factor value for the benchmark baseline data is 35. **Table 18** and **Figure 68** show the recrystallisation data and the recrystallisation kinetics for the baseline CA model simulations using different activation volume factor values.

141

Table 18 – Recrystallisation data for the baseline CA model simulations using different activation volume factor values (15, 35 and 61) for Fe-30Ni-0.044%Nb hot deformed at 950°C to a strain of 0.3 with a starting modal size of 160µm.

Recrystallisation kinetics/parameters	Recrystallisation data for baseline CA simulations using different activation volume factor values		
Activation volume factor	15	35	61
R_s (s)	12.5	12.5	12.5
R50% (s)	24.2	24.2	24.2
R_f (s)	36.6	36.6	36.6
n	3.0658	3.0658	3.0658
k	3.6253e-5	3.6253e-5	3.6253e-5
D5% (µm)	43	43	43
D50% (µm)	100	100	100
D95% (µm)	105	105	105

It can be seen from **Table 18** that D5%, D50% and D95% are unaffected by changing the activation volume factor between 15 and 61, giving 43µm, 100µm and 105µm respectively for all values.
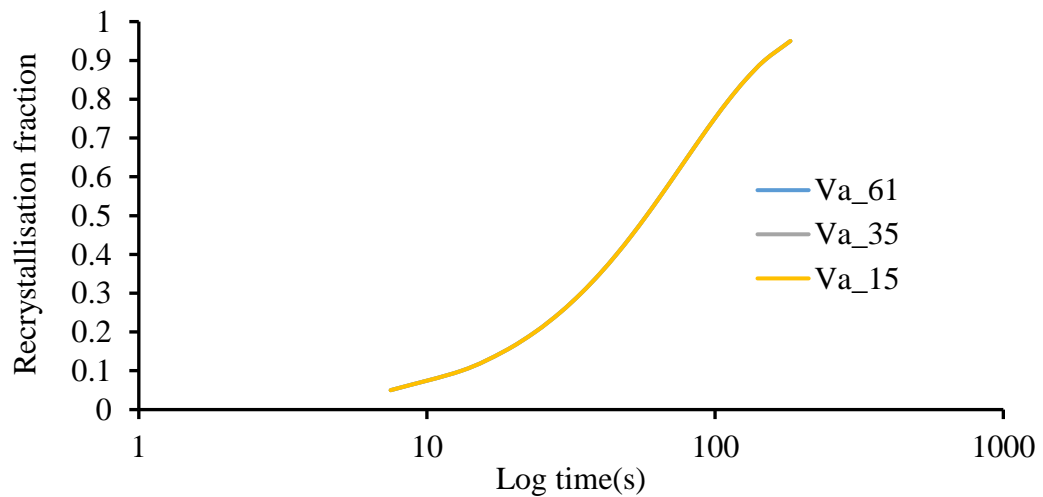
Figure 68 – Recrystallisation kinetics for the baseline CA model simulations using different activation volume factor values (15, 35 and 61) for Fe-30Ni-0.044%Nb hot deformed at 950°C to a strain of 0.3 with a starting modal size of 160µm.

Figure 68 shows that recrystallisation curves are the same for all values of activation volume factor.

In summary, changing the activation volume factor value within the range 15-61 has no effect on the final microstructure or the recrystallisation kinetics.

4.10 Sensitivity analysis of grain boundary surface energy

The grain boundary energy affects the critical radius. The most common grain boundary surface energy values reported in the literature for grain boundary surface energy are 0.5J/mol, 0.52J/mol, 0.3J/mol and 0.7J/mol.

A sensitivity analysis was carried out for this parameter. CA model simulations were run using the baseline data using grain boundary surface energy values 0.5J/mol, 0.3J/mol and 0.7J/mol. Note that the grain boundary surface energy value for the benchmark baseline data is 0.5J/mol.

Table 19 and **Figure 69** show the recrystallisation data and the recrystallisation kinetics for the baseline CA model simulations using different grain boundary surface energy values.

Table 19 – Recrystallisation data for the baseline CA model simulations using different grain boundary surface energy values of 0.3J/mol, 0.5J/mol (benchmark value) and 0.7J/mol for Fe-30Ni-0.044%Nb hot deformed at 950°C to a strain of 0.3 with a starting modal size of 160μm.

Recrystallisation kinetics/parameters	Recrystallisation data for baseline CA simulations using different grain boundary surface energy values		
Grain boundary surface energy (J/mol)	0.3	0.5	0.7
R_s (s)	12.5	12.5	12.5
R_f (s)	36.6	36.6	36.6
n	1.319	1.319	1.319
k	0.0004	0.0004	0.0004
D5% (μm)	43	43	43
D50% (μm)	100	100	100
D95% (μm)	105	105	105

It can be seen from **Table 19** that D5%, D50% and D95% are unaffected by changing the grain boundary surface energy values between 0.3 and 0.7J/mol, giving 43µm, 100µm and 105µm respectively for all values.
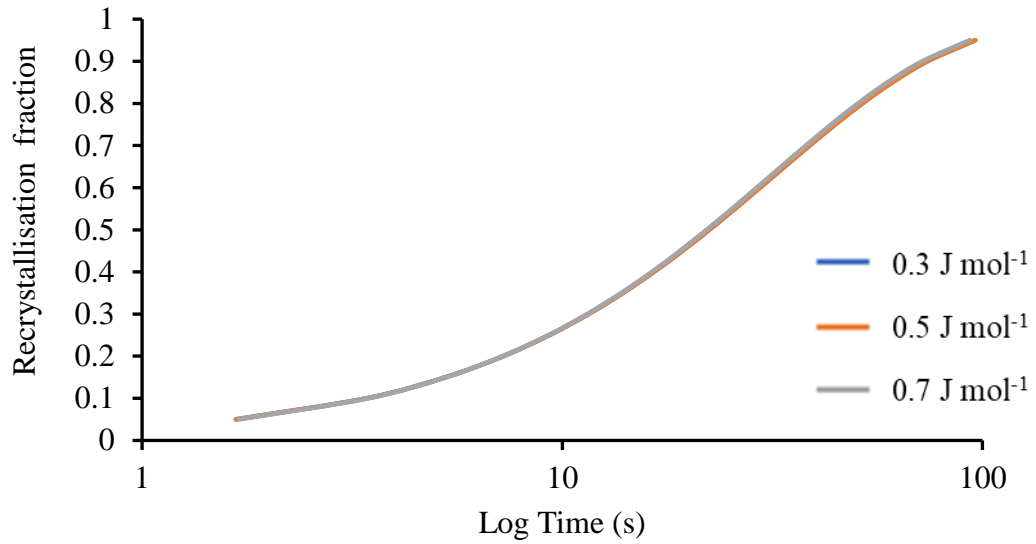
Figure 69 – Recrystallisation kinetics for the baseline CA model simulations using different grain boundary surface energy values of 0.3J/mol, 0.5J/mol (benchmark value) and 0.7J/mol for Fe-30Ni-0.044%Nb hot deformed at 950°C to a strain of 0.3 with a starting modal size of 160µm.

Figure 69 shows that recrystallisation curves are the same for all values of grain boundary surface energy used.

In summary, changing the grain boundary surface energy within the range 0.3-0.7J/mol has no effect on the final microstructure or the recrystallisation kinetics.

4.11 Sensitivity analysis on the initial dislocation density

The CA model is dislocation density driven (stored energy of deformation). The recovery rates and the critical radius depend on the dislocation density and it is the driving force for recrystallisation.

A sensitivity analysis was carried out for this parameter. CA model simulations were run using the baseline data using dislocation density values of $3.37 \times 10^{14} m^{-2}$, $4.5 \times 10^{14} m^{-2}$, $5.8 \times 10^{14} m^{-2}$, $1.5 \times 10^{15} m^{-2}$ and $4.13 \times 10^{15} m^{-2}$. Note that the dislocation density value for the benchmark baseline data is $4.5 \times 10^{14} m^{-2}$.

Figure 70 shows the grain size distribution for the baseline CA model simulations using different initial dislocation densities values. The figure shows significant variation in the recrystallised grain size distributions for the different values of the initial dislocation density. At a dislocation density of $3.37 \times 10^{14} m^{-2}$, there is no recrystallisation using the baseline data and this may be due to the fact that there is not sufficient stored energy left to drive the growth of recrystallisation.

It can be seen that the grain size gets finer with increasing dislocation density (stored energy), meaning the heavily deformed microstructure produces a finer recrystallised grain size distribution. The final microstructures are significantly affected by increasing dislocation densities.
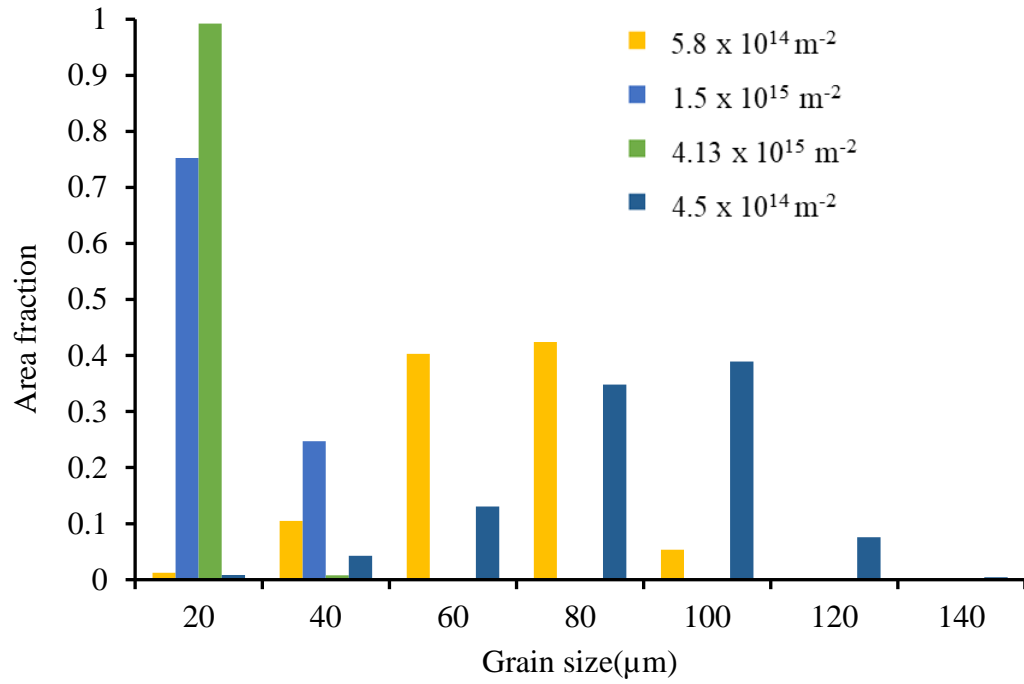
Figure 70 – Recrystallised grain size distribution for the baseline CA model simulations using initial dislocation density values of $4.5 \times 10^{14} m^{-2}$ (benchmark value), $5.8 \times 10^{14} m^{-2}$, $1.5 \times 10^{15} m^{-2}$ and $4.13 \times 10^{15} m^{-2}$ for Fe-30Ni-0.044%Nb hot deformed at 950°C to a strain of 0.3 with a starting modal size of 160µm.

Figure 71 shows the recrystallisation kinetics for the baseline CA model simulations using different dislocation density values. Looking at the recrystallisation curves, it can be seen that as the dislocation density increases the rate of recrystallisation increases.
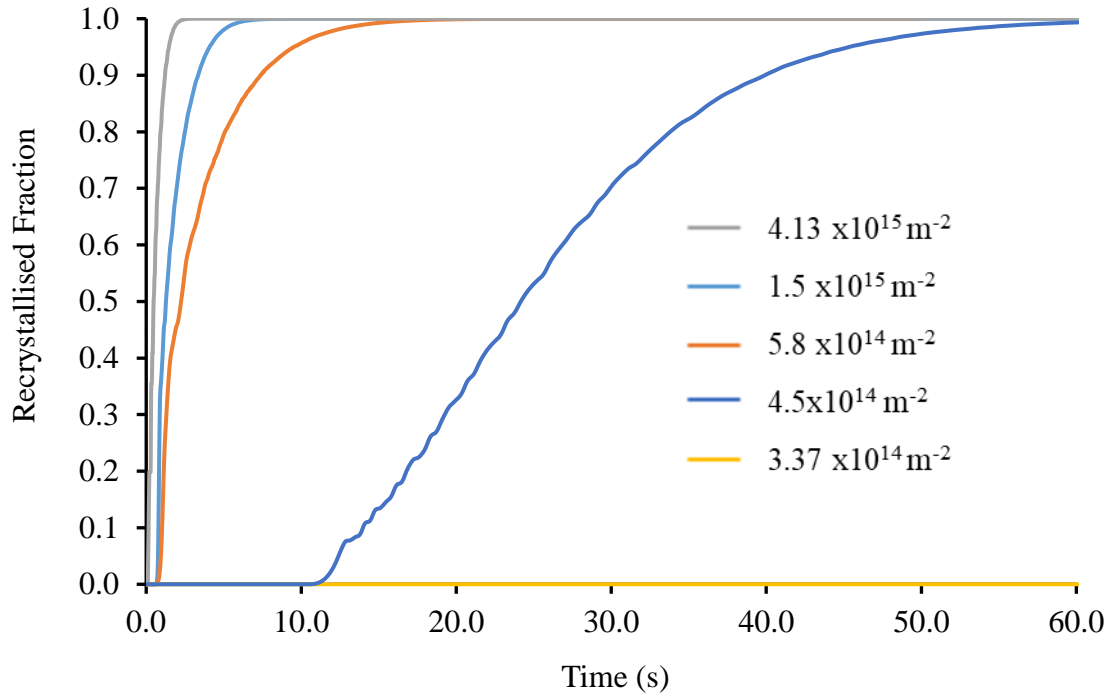
Figure 71 – Recrystallisation kinetics for the baseline CA model simulations using initial dislocation density values of $3.37 \times 10^{14}\text{m}^{-2}$, $4.5 \times 10^{14}\text{m}^{-2}$ (benchmark value), $5.8 \times 10^{14}\text{m}^{-2}$, $1.5 \times 10^{15}\text{m}^{-2}$ and $4.13 \times 10^{15}\text{m}^{-2}$ for Fe-30Ni-0.044%Nb hot deformed at 950°C to a strain of 0.3 with a starting modal size of 160μm.

The percentage deviation of the kinetics parameters from the benchmark baseline data (using a initial dislocation density value of 4.5×10^{14} m^{-2}) was calculated for the CA simulations carried out in this sensitivity analysis. From the numbers, shown in **Table 20**, it can be seen that there is significant deviation from the baseline benchmark data for all other initial dislocation density values.

– Summary of the percentage deviation of the recrystallisation kinetics using initial dislocation density values of $4.5 \times 10^{14} m^{-2}$ (benchmark value), $5.8 \times 10^{14} m^{-2}$, $1.5 \times 10^{15} m^{-2}$ and $4.13 \times 10^{15} m^{-2}$ for Fe-30Ni-0.044%Nb hot deformed at 950°C to a strain of 0.3 with a starting modal size of 160µm.

Initial dislocation density (m^{-2})	Recrystallisation data							
	R_s (s)	R50% (s)	R_f (s)	n	k	D50% (µm)	D5% (µm)	D95% (µm)
BLD(4.5×10^{14})	12.5	24.2	36.6	3.0658	0.00004	100	43	105
	% Difference from the BLD(4.5×10^{14}) benchmark recrystallisation data							
5.8×10^{14}	-92.5	-90.8	-83.4	-57.6	522350.0	-60.0	-67.7	-42.9
1.5×10^{15}	-93.9	-94.5	-92.1	-53.7	1138650.0	-80.0	-81.6	-71.4
4.13×10^{15}	-99.2	-98.0	-97.1	-53.3	4569900.0	-90.0	-90.8	-81.0

In summary, changing the dislocation densities significantly influences the recrystallised grain size distribution and the rate of recrystallisation. Hence, dislocation density will affect the final microstructure and the recrystallisation kinetics.

4.12 Summary of sensitivity analysis

To summarise, the parameters can be grouped into three categories based on their effect on the final microstructure, the recrystallisation kinetics and on both.

Parameters found to significantly affect neither the final microstructure nor the recrystallisation kinetics were the activation volume factor (V_a) and the grain boundary surface energy (γ_{SE}). Therefore, these parameters were not deemed significant in terms of the determination of the mechanical properties or processing conditions.

Parameters found to affect just the recrystallisation kinetics were the shear modulus (μ), pre-exponential mobility (M_o) and the sub-grain growth factor (K_{ad}). Therefore, these parameters are expected to affect the processing conditions but not the mechanical properties.

Parameters found to have a significant impact affecting the recrystallisation kinetics and the final microstructure include: the Burgers vector (b), temperature (T), applied strain (ε), activation energy (Q) and the initial dislocation density (ρ_{init}). The correct values for the CA model for these parameters is essential for accurate determination of the processing conditions and therefore the resulting mechanical properties.

5 Aims and objectives of the present work

The aim of the work is to assess and develop a 3D cellular automata model for predicting the recrystallisation kinetics and recrystallised grain size distribution during hot rolling of steel. Initial simulations using the 3D cellular automata model developed for hot rolling and subsequent phase transformation on cooling showed that it did not correctly predict the recrystallised grain size distribution. The existing model predictions showed temperature sensitivity for the predicted recrystallised grain size distribution and also a strain insensitivity, both of which do not exist for experimental results in the literature. Therefore the objectives of the present work are:

- To carry out a sensitivity analysis for the different input parameters in the existing 3D cellular automata model developed for hot rolling and subsequent phase transformation to determine their influence on the recrystallised grain size distribution prediction.

- To remove temperature sensitivity from the recrystallised grain size distribution by considering the separate nucleation and growth conditions for the critical sub-grain, based on the literature observations of inhomogeneous dislocation (and hence stored energy) distribution within deformed grains.

- To remove strain insensitivity on the recrystallised grain size distribution by consideration of the stored energy affecting the number of sub-grain nuclei and their growth to critical size.

- To use the modified 3D cellular automata model to predict recrystallisation kinetics and grain size distributions for different starting grain sizes, applied strain and deformation temperatures and validate against data from the literature.

- To identify any limitations and future areas for improvement for the modified 3D cellular automata model for recrystallisation prediction after hot deformation.

6 New development and improvement in the model

After the sensitivity analysis was carried out in chapter 4 for the impact of the various parameters to see how variation of the parameters have on modelling recrystallisation with the CA model some gaps were determined that were not in line with what was observed in literature examples include variation of recrystallised grain size with temperature, the predicted recrystallised grain size was also not sensitive to varying strain. A number of different parameters within the model were investigated to determine whether they gave rise to the temperature sensitivity in the model.

In order to resolve these problems various factors were looked at initially and below are some of the key factors that were further investigated.

6.1 Factor one: Critical radius

The critical radius (r_c) is incredibly hard to measure (the point where a sub grain turns to a high angle boundary) and therefore currently the model predict it as a function of the grain boundary energy and the stored energy. A nucleation to a high angle grain boundary occurs once a sub grain grows past the critical sub grain size (r_c). The r_c is dependent on the dislocation density and therefore strain and stored energy. First we look at how the r_c grows over time at two different temperatures of the same model steel at 950°C and 1100°C **Figure 72**. We observed that r_c reaches over 10µm in few seconds and it was therefore decided to select a nominal value of 3µm because it is the critical radius where the first grain appears.
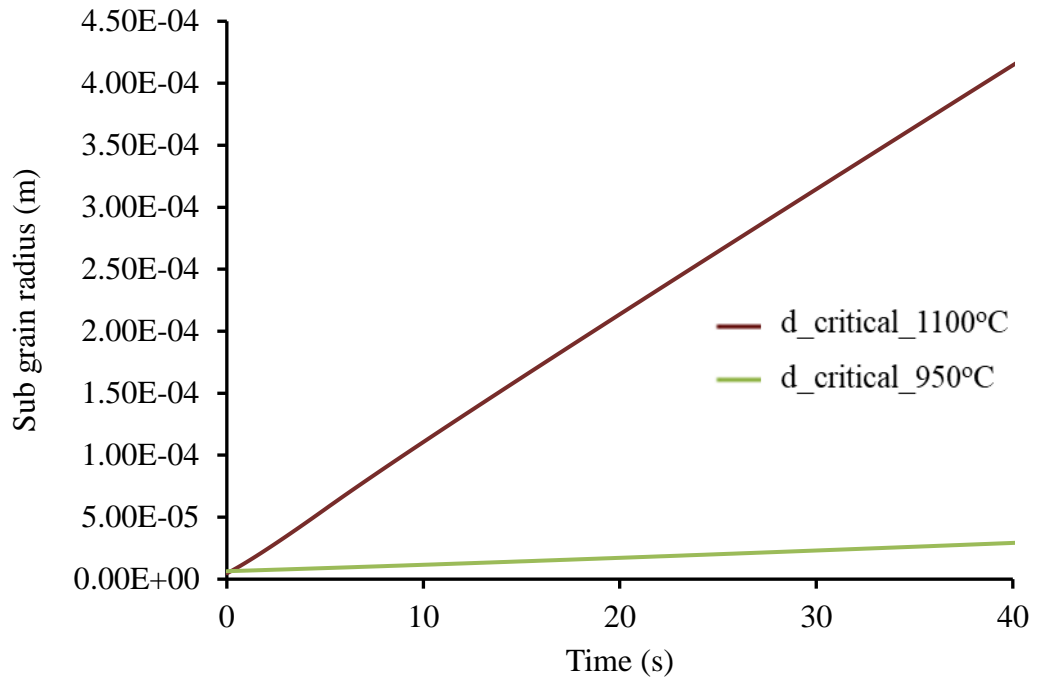
Figure 72 – Plot showing the growth of sub-grain with time at 950°C and 1100°C for Fe-30Ni-0.044%Nb   hot deformed to a strain of 0.3 with a starting modal size of 160µm.

With the nominal value of 3µm as the r_c effectively making it a constant value just to fix and to see if we can lose the temperature sensitivity in the model. The simulation was run keeping the other parameters the same at both temperatures and r_c a constant of 3µm. More sub grains reach the critical size from the sub grain distributions and hence the number of nucleated sites increases. The results in **Figure 74** shows that by making r_c a constant value in the model helps remove the temperature dependency in the model by bringing the modal grain sizes closer. This also makes the grain size

151

distributions smaller compared to **Figure 73** when r_c is a function of the grain boundary energy and the stored energy.
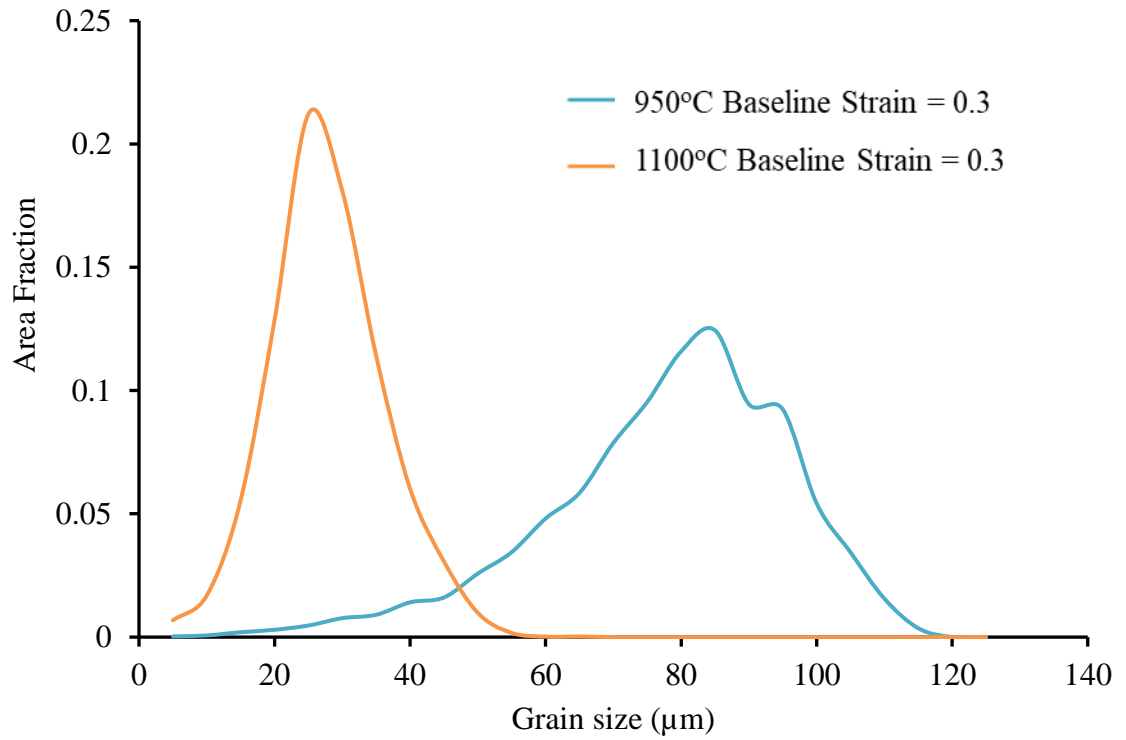
Figure 73 – Recrystallised grain size distribution with critical radius a dependent variable for Fe-30Ni-0.044%Nb hot deformed at 950°C to a strain of 0.3 with a starting modal size of 160µm .
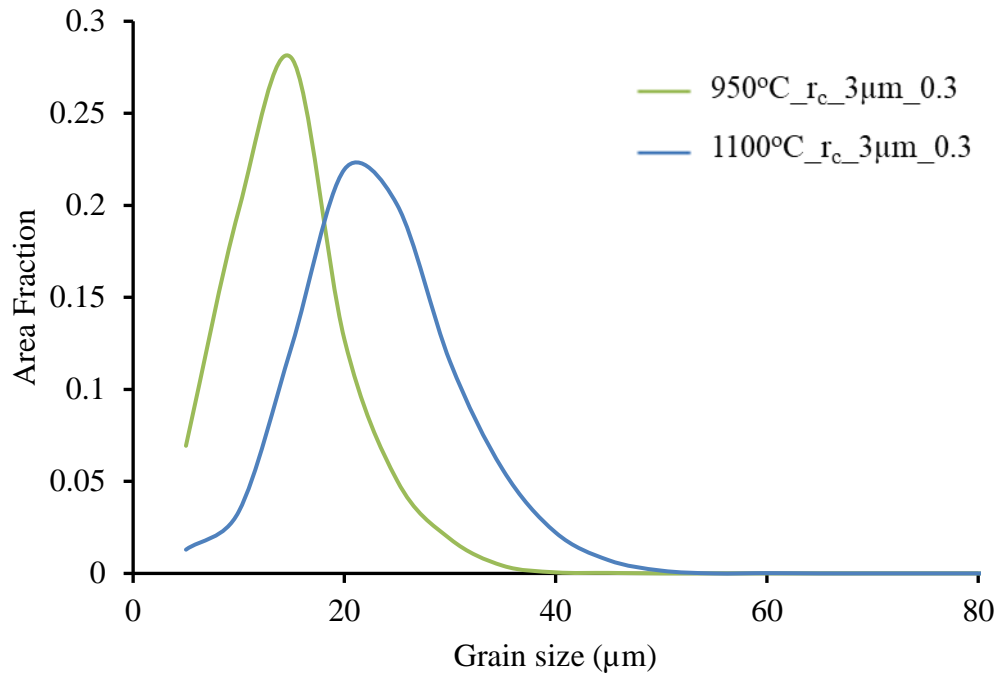
Figure 74 – Recrystallised grain size distribution as critical radius a constant value of 3µm, for Fe-30Ni-0.044%Nb hot deformed at 950°C and 1100°C to a strain of 0.3 with a starting modal size of 160µm.

And the impact of making r_c a constant was also investigated into how it changes the grain size distributions at different strain. **Figure 75** shows increasing the strain component at each temperature makes no difference to the recrystallised grain size distribution because we expect the grain size distribution to get finer as the strain component is increased as seen in the literatures[32]. Thus, making r_c a constant also removes the strain component in the model and we need to keep the strain dependence in the model.

Consequently it was determine that making r_c constant was not the answer and should be made a variable that will continue to be affected by the stored energy and grain boundary energy but this parameters need further investigation on the impact of the progression of change in the stored energy over time during the course of recrystallisation and the impact of grain boundary energy as it is a function of the temperature.
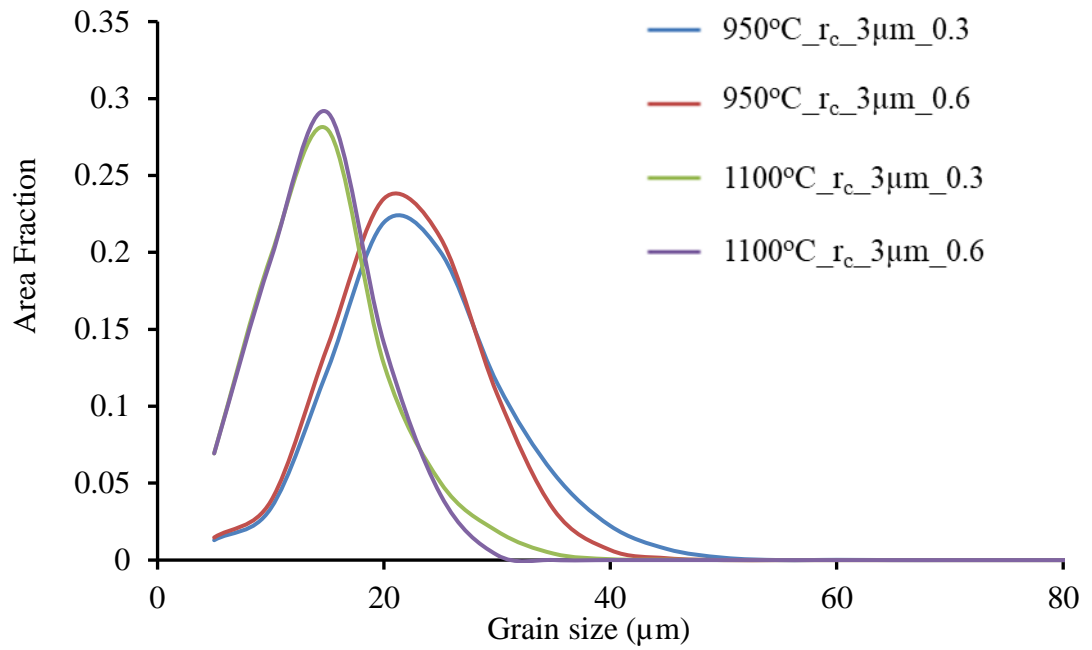
Figure 75 – Recrystallised fraction plot at different strain with critical radius a constant of 3µm for Fe-30Ni-0.044%Nb hot deformed at 950°C to a strain of 0.3 with a starting modal size of 160µm.

6.2   Factor two: Grain boundary energy

The next aspect was to look at the grain boundary energy which is a function of temperature as seen in **Equation 3.13** and how does the grain boundary energy affect the grain size distributions at different temperatures. To test this we made the grain boundary energy constant and ran the simulations at different temperatures of the baseline data **Figure 76**. Shows the grain size distributions changes with increasing temperatures as it gets finer.

Therefore making the grain boundary energy constant does not bring the grain size distributions together and hence this parameter was not the most suitable one for giving rise to temperature sensitivity and therefore no changes were made to the model for the remainder of the analysis.
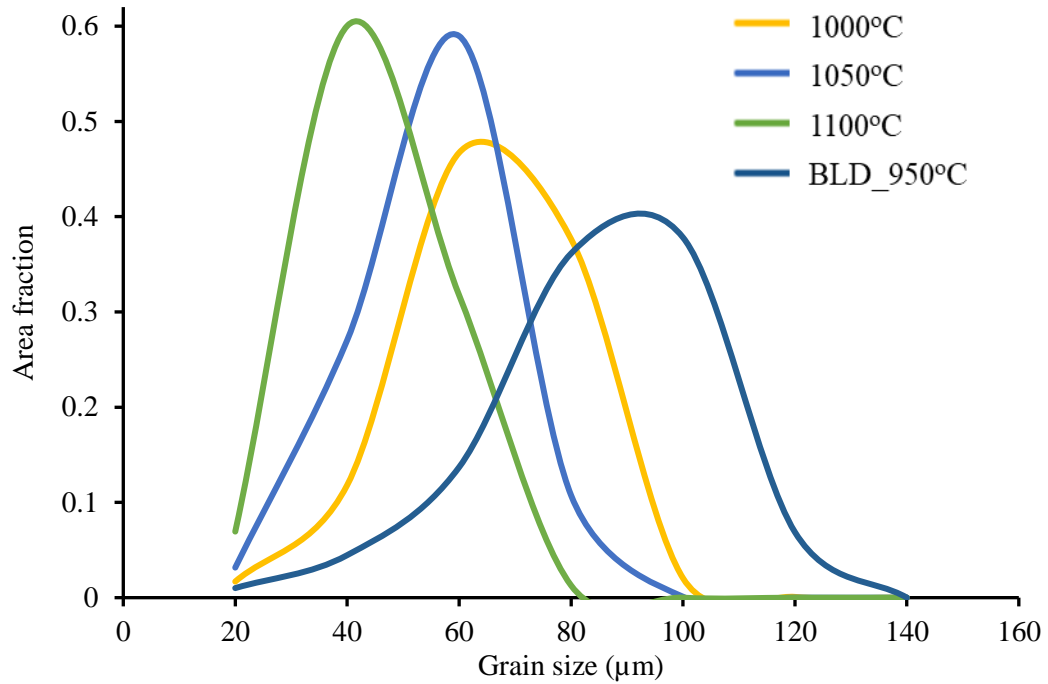
Figure 76 – Recrystallised fraction at different temperatures with a constant grain boundary energy of 0.5J/mol for Fe-30Ni-0.044%Nb hot deformed with a starting modal size of 160µm.

6.3 Factor three: Grain boundary strain intensity factor

Another factor looked into was the possibility the critical radius is poorly defined as seen section 6.1 from the paragraphs when the r_c is made constant. This all suggests that the critical radius is poorly predicted. The critical radius uses dislocation density. This is assumed uniform across the CA model. However in practise we do not see this in literature. The solution could be to use a strain intensity factor at the boundary i.e. at the grain boundary's to have an increase in the dislocation density for the purpose of the critical radius to have a multiplier . By increasing the strain intensity factor and looking for a point when the modal or the D50% is equal at two different temperatures in this case at 950°C and 1100°C. **Figure 77** shows that at a multiplier of 8 (the strain intensity factor) we observed that at temperature of 950°C and 1100°C of the baseline data both modal grain sizes are equal.

Therefore we can see that we need to get the macroscopic strain right because otherwise we do not get the times right the only thing we could consider is that the

distribution of the strain within the sample is different and therefore we can introduce a higher stored energy at the boundary and from now on will be referred to as the boundary intensity factor (BIF).
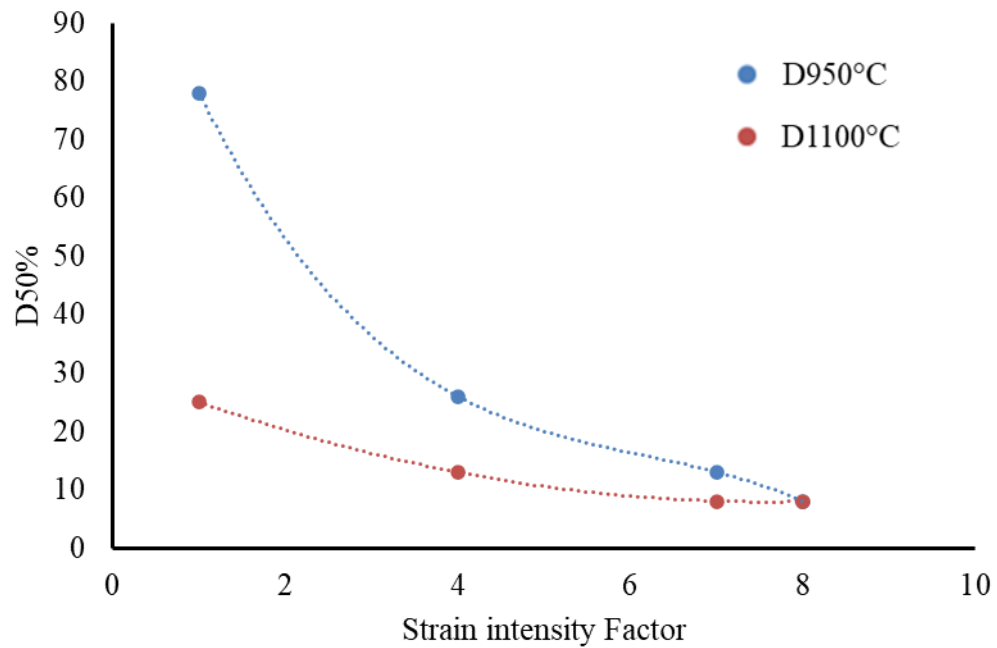
Figure 77 – Plot showing the convergence of the D50% at 950°C and 1100°C with increasing strain intensity factor for Fe-30Ni-0.044%Nb hot deformed and to a strain of 0.3 with a starting modal size of 160μm.

6.4 Boundary intensity factor (BIF)

The boundary intensity factor (BIF) is related to the individual grain size to allow smaller grains to have a higher dislocation density representative of the higher grain boundary area.

The BIF means that sub grain nucleation and growth to critical size is affected by the applied strain (giving strain sensitivity) but is less dependent on temperature (temperature insensitivity). Ji Mo[141] has mentioned that at the boundary the dislocation density is higher compared to the core (interior) and to capture this therefore a fitting parameter that will be based on the modal grain size and the nucleation. To derive BIF it was fitted to an experimental data for Fe30Ni with grain size distribution and a modal grain size of 160μm[141] and run several simulations to match the starting grain size distributions to the recrystallised grain size distributions and run it at different temperatures.

156

To arrive at a BIF that will be able to bring the recrystallised grain size distributions together at different temperatures and match the recrystallisation kinetics to the initial grain size distributions we first of all start to increase the dislocation density at the boundary and see how the recrystallised grain size from the models compared to an experimental data [141].

Figure 78 shows the comparison between two different microstructures at each stage of recrystallisation of the model steel hot deformed at 950°C of the baseline data . On the left hand side are the microstructures with a boundary intensity factor (BIF=1) i.e when the dislocation density at the boundary and at the bulk is the same when compared to when a boundary intensity factor of 1.5 is introduced that is the dislocation at the boundary is one and half times bigger than the dislocation at the bulk. The two scenarios microstructures were compared at 5%,15% ,50% and 100% recrystallised. When the boundary BIF was equal to 1, which in essence means the bulk and the boundary dislocation density is the same, at 5% recrystallisation it shows fewer nuclei at the deformed grain boundary but bigger when compared to the BIF of 1.5 of the same sample with more nuclei at the deformed grain boundary but very tiny . At 15% recrystallisation the nucleated grain has grown bigger than at BIF 1 but more than double nucleated grain growing at BIF of 1.5 and similar trend observed at 50% recrystallised. The final microstructure (100%) recrystallised shows bigger and fewer grains at a BIF of 1 compared to the final microstructure with a BIF of 1.5. This implies that with a BIF affects the nucleation process and more nuclei formed at higher dislocation density at the boundary and hence the final microstructure is affected.
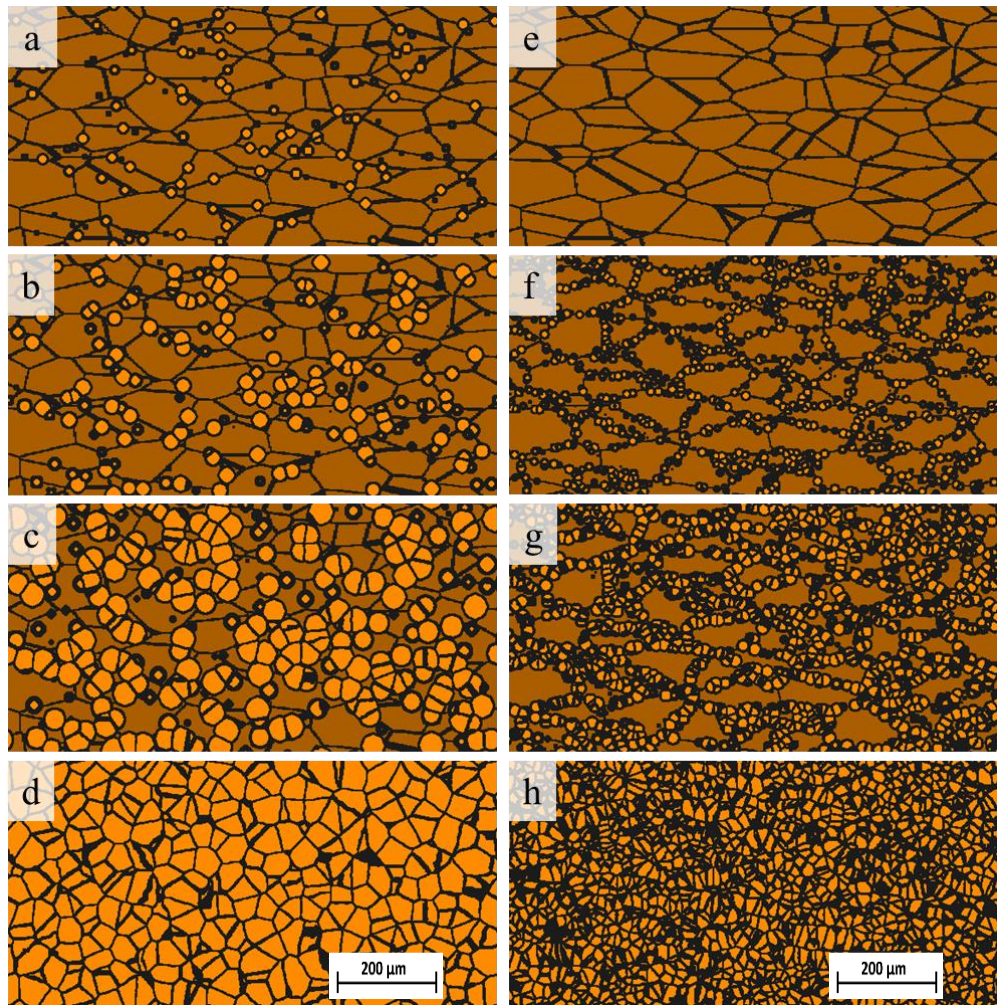
Figure 78-Images of recrystallised microstructure for BIF values of 1 and 1.5. Images on the left show the microstructure for a BIF of 1, with a % recrystallised of 5, 15, 50 and 100 for a, b, c and d respectively. Images on the right show the microstructure for a BIF of 1.5, with a % recrystallised of 5, 15, 50 and 100 for e, f, g and h respectively, for Fe-30Ni-0.044%Nb hot deformed at 950°C to a strain of 0.3 with a starting modal size of 160µm.

Given that the BIF value affects the microstructure, this parameter was altered for different hot deformed temperatures of 950ºC and 1050ºC in order to discover a value which may be used to obtain the same modal grain size. The results from these simulations are shown in **Figure 79** and **Figure 80** respectively.

At 950ºC, it can be seen that increasing the BIF values gave rise to smaller modal grain sizes and that BIF values of 1.5 and 1.3 both gave a modal grain size of 40µm (**Figure 79**). For 1050ºC, the same pattern was observed with the smallest modal grain sizes

also for the same BIF values. Modal grain sizes were 40μm and 30μm for a BIF of 1.3 and 1.5 respectively (**Figure 80**).
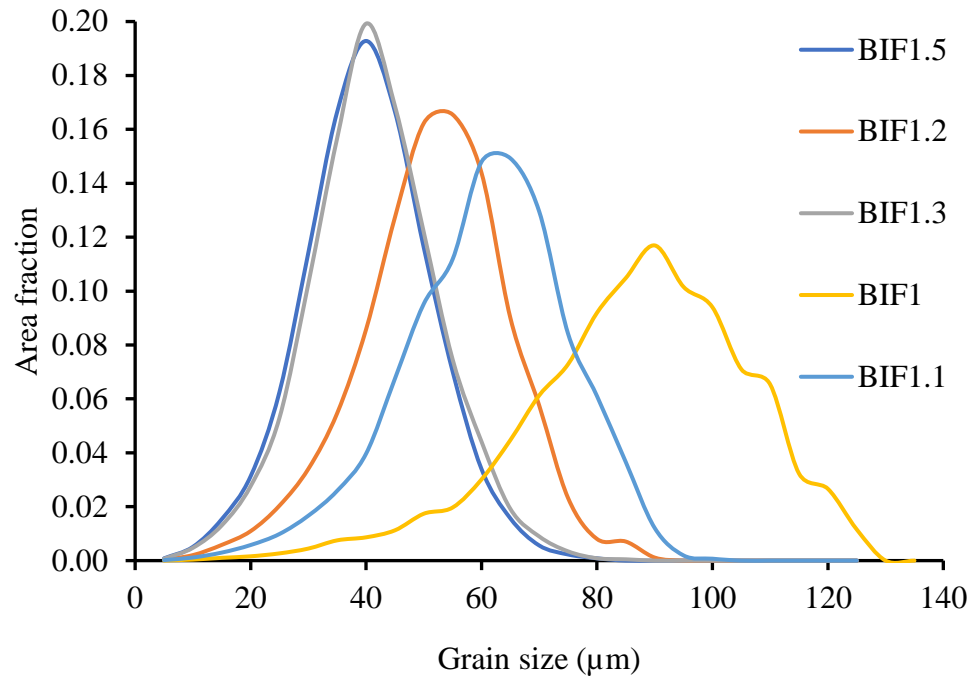
Figure 79 – Impact of varying boundary intensity factor(BIF) on the recrystallised grain size distribution hot deformed at 950°C to at strain of 0.3 and with a starting microstructure of modal grain size of 160μm for Fe-30Ni-0.044%Nb.
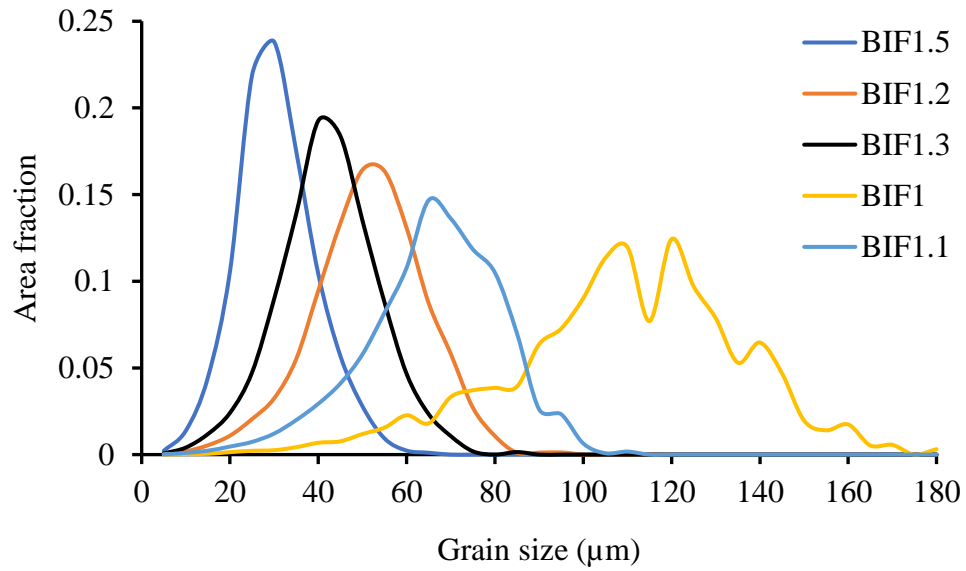
Figure 80 – Impact of varying boundary intensity factor (BIF) on the recrystallised grain size distribution hot deformed at 1050°C to at strain of 0.3 and with a starting microstructure of modal grain size of 160µm for Fe-30Ni-0.044%Nb.

While BIF values of 1.3 and 1.5 at both hot deformation of 950°C and 1050°C gave modal grain sizes (D50% shown in **Table 21** in blue) within a reasonable range of the experimental 60µm required (39µm and 38µm for a BIF of 1.3 and 1.5 respectively), the recrystallisation kinetics at these values were not close to the experimental data for a hot deformed Fe-30Ni-0.044%wt.Nb for 950°C. In **Table 21,** the recrystallisation starting time (R_s) is within a reasonable range at 950°C for the experimental data and the model (3.91s, 2.36s and 2.2s for a BIF of 1.3, 1.5 and the experiment respectively). However, the recrystallisation finishing time (R_f), Avrami value (n) and rate constant (K) are not.

As the recrystallised microstructure (D5%) for BIF 1.3 and 1.5 are 21µm, which is close to the experimental value of 20µm, it follows that R_s values would be within a reasonable range of the experimental data. However, the D95% (58µm and 56µm for a BIF of 1.3 and 1.5 respectively) is less than the experimental value (80µm). This may be attributable to the initial grain size distribution range (20–240µm) limitations of the model compared to that of the experiment (20–340µm).

The data for these recrystallisation kinetic parameters is significantly different to the experimental values most likely due to a poorly defined core dislocation density, which

assumes a constant value. It is expected that as recrystallisation progresses, the core dislocation density, which drives the growth of the nuclei, will decrease as the grain boundary thickens. In order to accommodate this expectation, a boundary thickness parameter may be introduced to the model.

Table 21-Recrystallisation data for hot deformed Fe-30Ni-0.044%Nb at 950°C and 1050°C for different BIF values compared to the experimental data at 950°C (in green).

		R_s (s)	R50%	R_f (s)	n	k	D50% (μm)	D5% (μm)	D95% (μm)
	Exp	2.20		43.50	1.2000	0.0178	50	20	80
950°C	BIF1/-1	8.87	15.01	20.45	4.7706	8.07E-06	86	50	115
	BIF=1.1	6.09	8.98	11.92	4.6766	2.07E-05	59	34	80
	BIF=1.2	4.42	6.74	9.17	4.2958	1.70E-04	50	28	69
	BIF=1.3	3.91	5.32	7.52	3.9691	8.02E-04	39	21	58
	BIF=1.5	2.36	3.92	5.91	3.2294	7.71E-03	38	21	56
1050°C	BIF1/-1	1.93	6.51	13.69	2.7812	0.02253	108	59	145
	BIF=1.1	1.04	2.48	4.12	2.4676	0.07299	65	36	86
	BIF=1.2	0.80	1.64	2.73	2.4255	0.19172	50	28	69
	BIF=1.3	0.64	1.20	2.18	2.3155	0.40289	40	22	59
	BIF=1.5	0.49	0.78	1.69	1.8853	0.8978	30	15	44

6.5 Boundary thickness

To develop a boundary thickness (δ) parameter, the electron back scatter diffraction (EBSD) images **Figure 81**, two different EBSD images with a mode grain sizes of 160μm and 150μm[141] for Fe-30Ni and electrical steel M250 respectively . The images where uploaded ImageJ software and converted to 16bit . The image is then calibrated by measuring the length of the scale bar on the uploaded image using the image J . A straight line is drawn over the length of the scale bar , then the scale is set using the distance in pixel measured ,the known distance which is 200μm and the unit length set as micron. Now with the scale set , several drawn straight lines were drawn across the grain boundaries of different grains within the microstructure and at each time, the lines are measured **Figure 82**. One hundred and thirty measurements were done to measure the thickness across the grain boundaries and the resulting thickness halved .

These measurements were plotted to give the boundary thickness distribution to ascertain the variation given by experimental data (**Figure 83**).
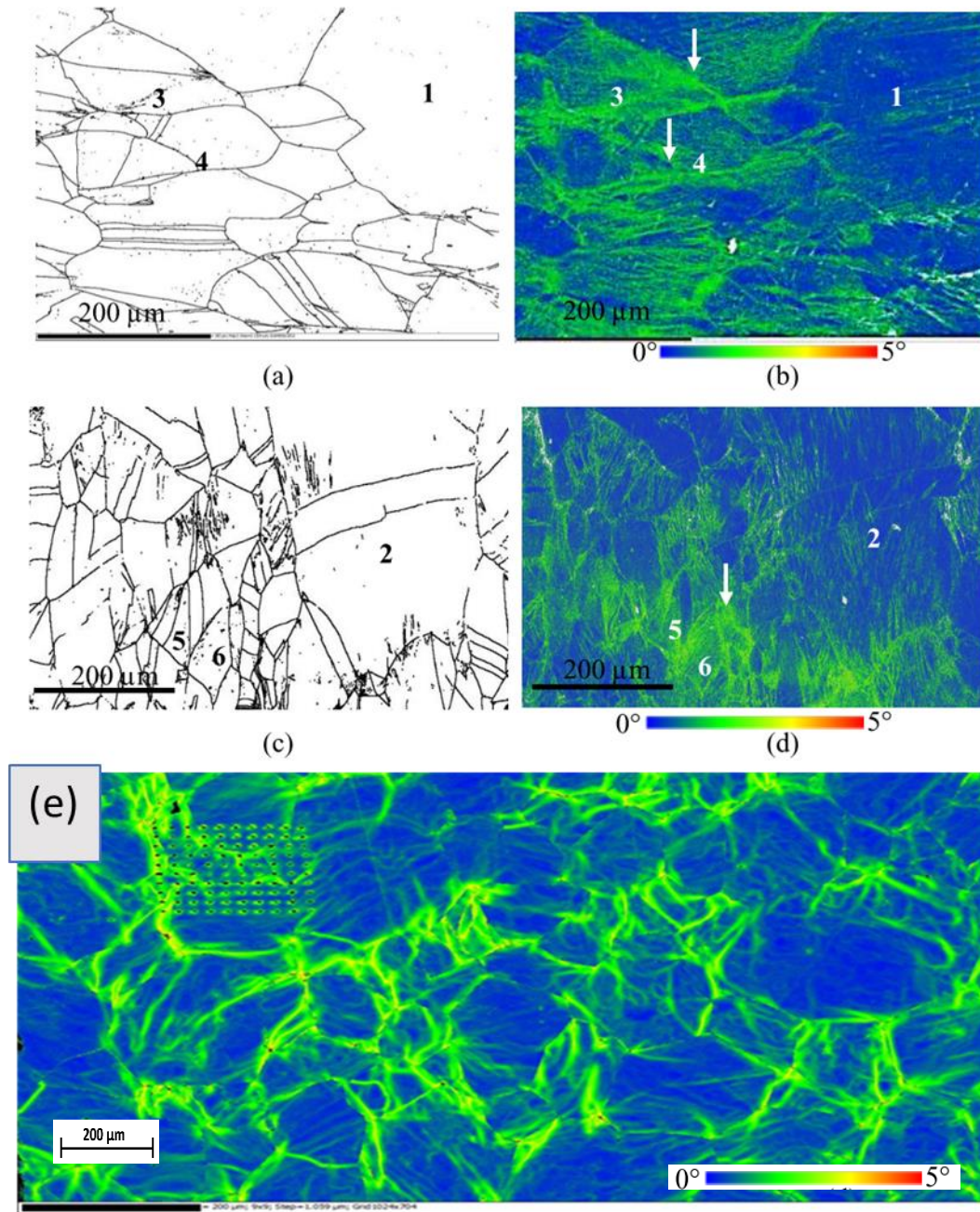
Figure 81 – (a),(c) Map of high angle grain boundaries (>10°) and local misorientation (b),(d) and EBSD image of Fe-30Ni-0.044%Nb deformed to a strain of 0.3 (e) EBSD image of an electrical steel M250 deformed to a strain of 0.3,green colour shows the stored energy distribution and the numbers point to grains [141].
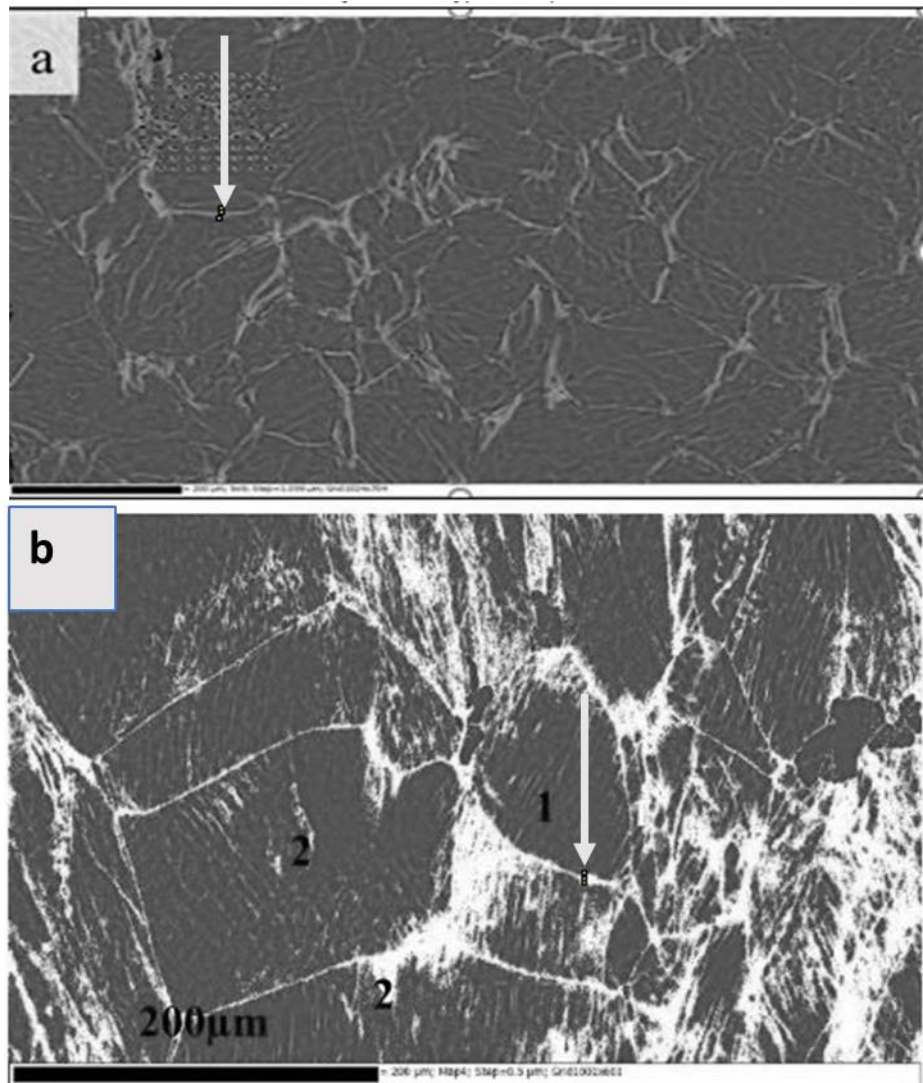
Figure 82 – A threshold image showing how the grain boundary width was determined using ImageJ for (a)-the Electrical steel M250 and (b)- Fe-30Ni EBSD image.
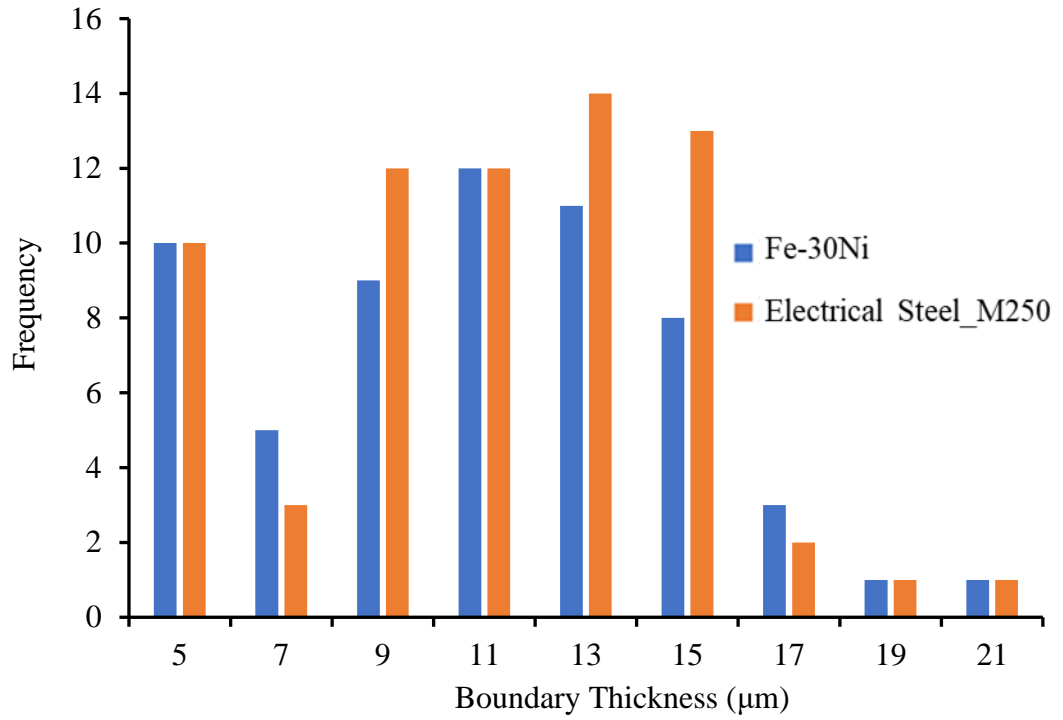
Figure 83 – Boundary thickness distribution using measurements from EBSD images shown in Figure 74.

In order to ascertain the effect of introducing a boundary thickness (δ) parameter into the model, simulations were set up for 900°C and 950°C using a boundary thickness of 6.6µm (based on the critical grain size) for BIF values between 1.0 and 1.5. The recrystallisation data is shown in **Table 22** along with the experimental data for cold deformation Fe-30Ni-0.044%Nb (in green). It should be noted that relevant reference experimental data is not readily available in the literature. This data was obtained from Ji's work on grain size distribution [141]. The trend that can be observed from the data shows a decrease in R_s, $R50\%$, R_f, n and K as the BIF increases for both temperatures.

Table 22 – Recrystallisation data using a boundary thickness of 6.6µm at 900°C and 950°C for BIF values between 1.0 and 1.5 compared to the experimental data for cold deformation Fe-30Ni-0.044%Nb (in green).

		R_s (s)	R50%	R_f (s)	n	k	D50% (µm)	D5% (µm)	D95% (µm)
900°C	Exp	5.0	35.30	75.2	1.300	0.006	60	20	80
	BIF=1	33.1	51.94	69.2	5.997	6.06E-09	124	70	165
	BIF=1.1	19.9	28.82	35.6	5.646	1.15E-09	78	44	102
	BIF=1.2	14.8	21.16	26.3	5.434	8.65E-09	62	35	83
	BIF=1.3	11.6	16.62	21.2	5.315	2.11E-07	54	30	73
	BIF=1.5	8.35	12.12	16.5	4.46	9.14E-06	40	22	58
950°C	Exp	7.0	19.2	43.5	1.2	0.0178	50	20	80
	BIF=1	10.4	19.11	27.4	4.618	1.59E-05	103	58	139
	BIF=1.1	6.76	10.54	14.1	4.471	1.70E-05	66	37	89
	BIF=1.2	5.09	7.83	10.4	4.358	8.34E-05	58	30	76
	BIF=1.3	3.95	6.01	8.38	3.995	4.85E-04	45	25	64
	BIF=1.5	2.82	4.47	6.86	3.309	4.28E-03	36	18	51

Simulations at 900°C and 950°C were then run using a range of values from the boundary thickness distribution for a BIF value of 1.5 (due to the previous work described in section 6.1) to see how the recrystallisation kinetics were affected. The results are shown in **Table 23.** It can be seen that different boundary thickness (δ) values do not affect the modal grain size, giving a D50% of 62µm for all δ values at 900°C and 58µm for all δ values at 950°C, which are in good agreement with the experimental data (60µm).

Table 23 – Recrystallisation data for a range of boundary thickness (δ) values at 900°C and 950°C using a BIF of 1.5 compared to the experimental data for cold deformation Fe-30Ni-0.044%Nb (in green) deformed to a strain of 0.3 with a starting modal size of 160µm.

		R_s (s)	R50%	R_f (s)	n	k	D50% (µm)	D5% (µm)	D95% (µm)
900°C	Exp	5.0	35.30	75.20	1.300	0.006	60	20	80
	d=6.6µm	14.8	21.16	26.32	5.434	8.65E-09	62	35	83
	d=13.2µm	15.0	21.87	27.51	5.588	2.10E-08	62	35	83
	d=19.8µm	15.4	23.88	31.15	4.796	1.56E-07	62	35	83
950°C	Exp	7.0	19.20	43.50	1.200	0.0178	50	20	80
	d=6.6µm	5.09	7.83	10.41	4.358	8.34E-05	58	30	76
	d=13.2µm	5.14	8.13	10.96	4.129	1.16E-04	58	30	76
	d=19.8µm	5.32	8.98	12.85	3.551	2.63E-04	58	30	76

Given that the boundary thickness (δ) that was most common from EBSD images (shown in **Figure 83**) was between 9µm and 15µm, further simulations concentrated around a boundary thickness of 12 – 13µm and an increased BIF to 2.2 to compensate for the increased grain boundary thickness(as increasing the thickness reduces the core dislocation density) were carried out to compare the reaction kinetics with experimental data for hot deformed Fe-30Ni-0.044%Nb at 950°C to a strain of 0.35[2]. Comparative results can be seen in **Figure 84**. The purpose of the comparison was to find the boundary thickness which gave a R50% (time at 50% recrystallised) closest to the experimental data. The optimum boundary thickness for this criteria was 13.0µm, as shown in **Figure 84** and **Table 24**, which gives a *R50%* value of 48.5s for 13.0µm compared to 48.8s for the experimental data.
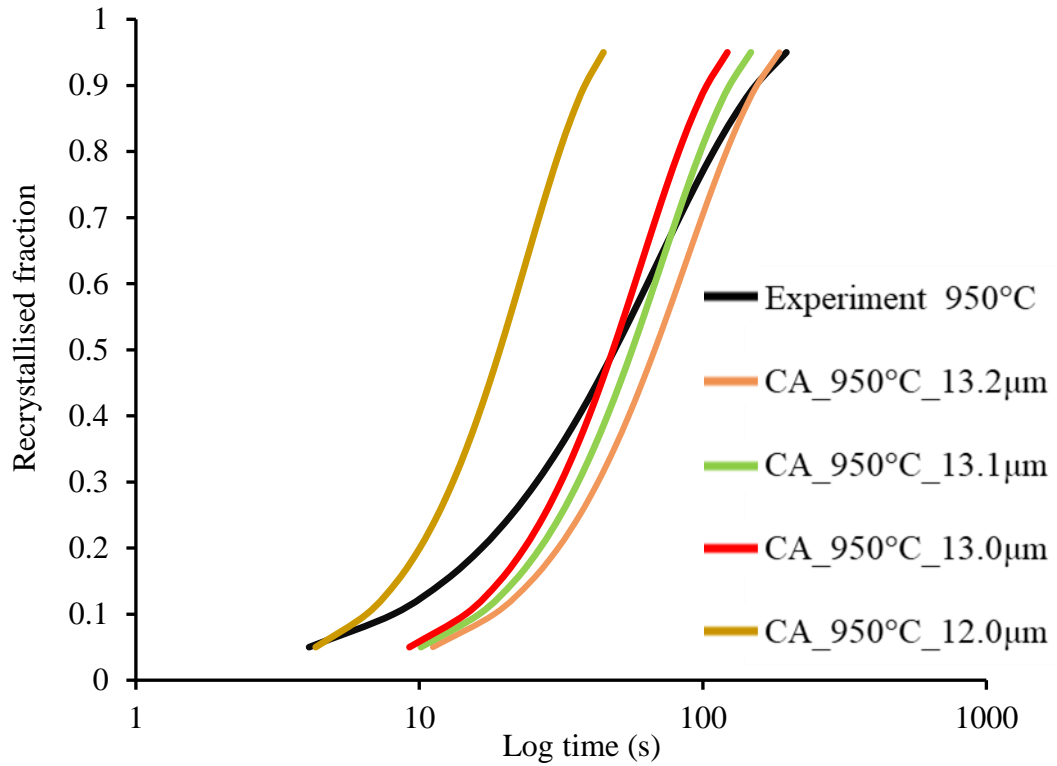
Figure 84 – Recrystallisation fraction curves for different boundary thicknesses (δ) hot deformed at 950°C to a strain of 0.35 at a BIF of 2.2, compared to experimental hot deformed Fe-30Ni-0.044%Nb at 950°C to a strain of 0.35.

Table 24 – Recrystallisation data for different boundary thicknesses (δ) hot deformed at 950°C to a strain of 0.35 at a BIF of 2.2 compared to experimental hot deformed Fe-30Ni-0.044wt %Nb at 950°C to a strain of 0.35.

		R_s (s)	R50%	R_f (s)	n	k	D50% (μm)	D5% (μm)	D95% (μm)
	Exp/Hot def	4.08	48.80	127.50	1.049	0.0117	50	20	80
	d = 6.6 μm	5.20	10.10	15.70	2.700	0.0001	46	26	66
950°C	d = 12.0 μm	6.50	19.00	35.50	1.740	0.0040	46	26	66
	d = 13.0 μm	8.50	48.50	91.50	1.575	0.0015	46	26	66
	d = 13.1 μm	9.00	57.00	108.00	1.517	0.0015	46	26	66
	d = 13.2 μm	9.50	68.00	133.50	1.445	0.0016	46	26	66

6.6 Core dislocation density

Introducing the grain boundary thickness (δ) affects the calculation of the core dislocation density. Prior to the generation of this parameter, the core dislocation density was the same as the initial dislocation density (average dislocation density within the system).

Following the introduction of the grain boundary thickness parameter (δ), the core dislocation density was calculated using the following **Equations 6.1-6.4**.

The CA model assume grains are spherical **Figure 85**. Therefore to calculate the grain boundary volume(V_{GB}), it is estimated from the CA model. In the CA model for each grain pair the grain boundary area (is calculated by counting the number of cells on the boundary). This number of cells is then multiplied with the cross section area of a cell which is simply taken to be Δ^2 where Δ is the side length of a single cell (Grid spacing):

$$V_{GB} = A_{GB} * \delta \qquad\qquad\qquad \text{Equation 6.1}$$

and

$$A_{GB} = N_{GB} * \Delta^2 \qquad\qquad\qquad \text{Equation 6.2}$$

Where N_{GB} is the number of sub-grains at a grain boundary (the area between a pair of grains as everything is calculated per grain pair).

The core volume (V_{core}) is calculated using the expression :

$$V_{core} = V_{tot} - V_{GB} \qquad\qquad\qquad \text{Equation 6.3}$$

and

The total grain volume (V_{tot}) is given by :

$$V_{tot} = N_X * N_Y * N_Z * \Delta^3 \qquad\qquad\qquad \text{Equation 6.4}$$

Where N_X is the number of cells in the X-direction, N_Y is the number of cells in the Y -direction and N_Z is number of cells in the Z -direction.
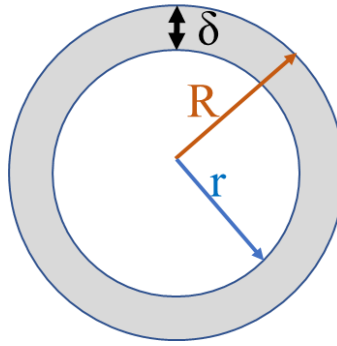
Figure 85 – Spherical representation of the grain showing the grain boundary thickness(δ).

The initial dislocation density (ρ_{init} is the system average dislocation density). Since the model is dislocation density driving ,it is pertinent to have an accurate initial dislocation density appropriate to the steel in question as this will affect the stored energy which affects the nucleation and driving force for growth of the nuclei and hence the recrystallisation kinetics and grain size distribution .The initial dislocation density is user supplied and can be calculated by combining the flow stress curve **Figure 86** and **Equation 2.10**.
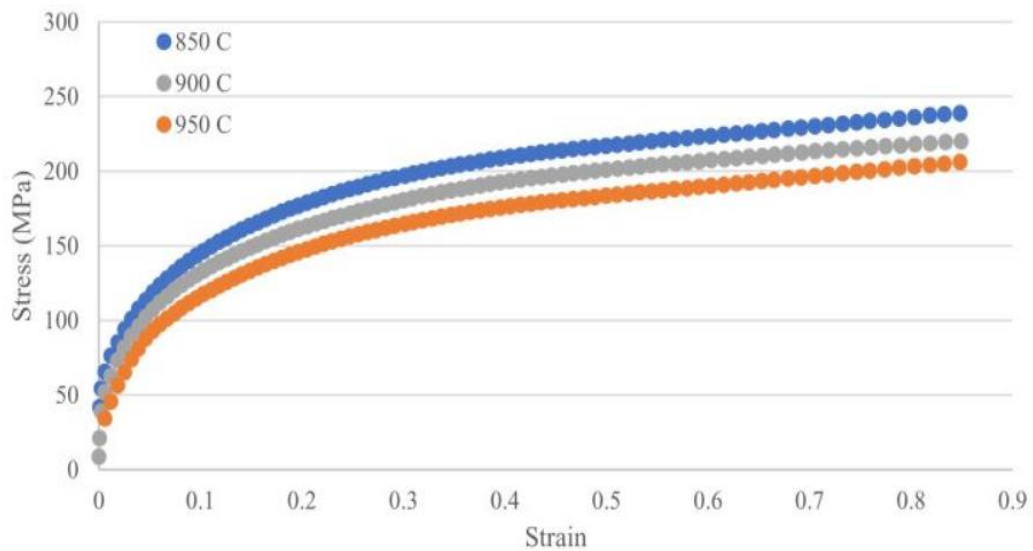
Figure 86 – Flow stress for Fe-30Ni-0.044%Nb steel that is uniaxially compressed at elevated temperature (850-950°C) [141].

The expression for the initial dislocation density can be expressed as:

$$\rho_{init} = \frac{V_{core} * \rho_{core} + V_{GB} * BIF * \rho_{init}}{V_{tot}}$$

Equation 6.5

Where ρ_{core} is the core dislocation density and can be derived by re-arranging(**Equation 6.5**) :

$$\rho_{core} = \frac{V_{tot} * \rho_{init} - V_{GB} * BIF * \rho_{init}}{V_{core}}$$

Equation 6.6

The grain boundary dislocation density (ρ_{GB}) is related to the initial dislocation density (ρ_{init}) using the **Equation 6.7**:

$$\rho_{GB} = BIF * \rho_{init}$$

Equation 6.7

The core dislocation density as stated earlier decreases with increasing grain boundary thickness **Figure 87**.
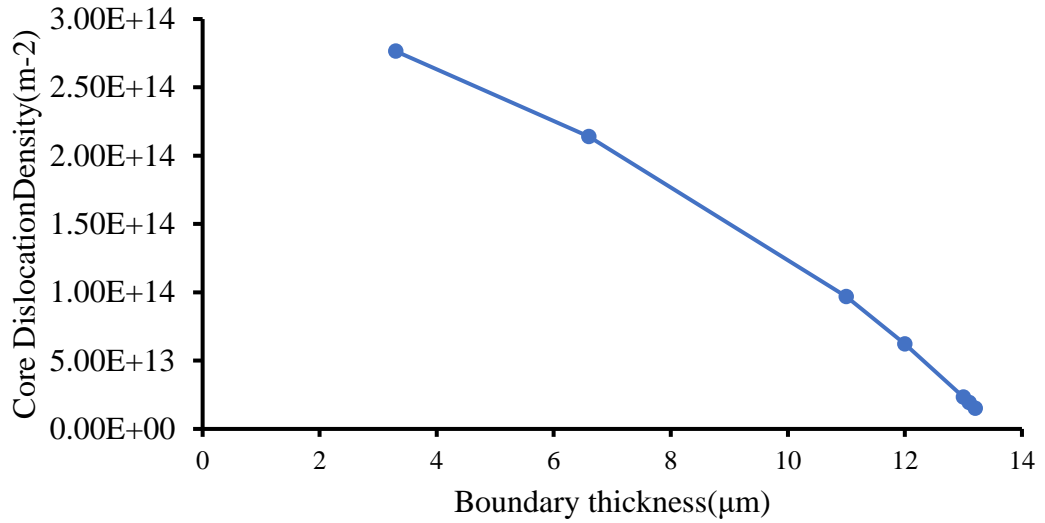
Figure 87 – The plot showing the impact of the grain boundary thickness on the core dislocation density for Fe-30Ni-0.044%Nb hot deformed at 950°C to a strain of 0.3 with a starting modal size of 160µm.

6.7 Burgers vector as a function of temperature

The initial model assumed a constant Burgers vector. However, when the magnitude of the Burgers vector is plotted against temperature using data from the data base of TCFE8 ThermoCalc version 2020b, it can be seen that the Burgers vector increases with increasing temperature (see **Figure 88**).
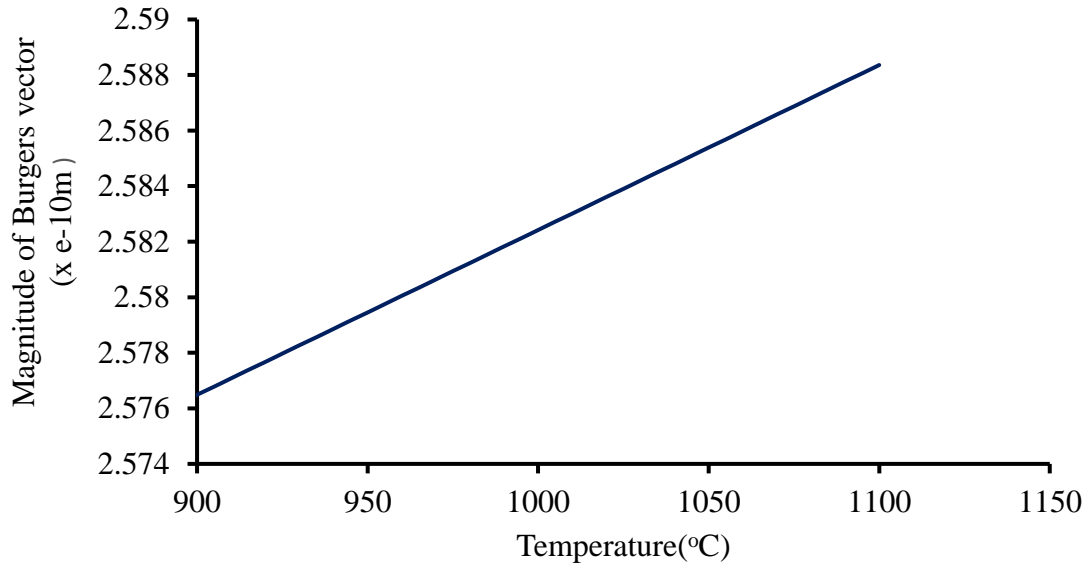
Figure 88 – Effect of temperature on the magnitude of the Burgers vector using data from the database of TCFE8 ThermoCalc version 2020b for Fe-30Ni-0.044%Nb.

6.8 Summary of the new developments in the model

Combining the work on the BIF, grain boundary thickness (δ) parameter and the Burgers vector as a function of temperature, the final BIF and grain boundary thickness (δ) used moving forward were 2.2 and 13.0μm respectively. These values gave rise to recrystallisation kinetics data closest to the hot deformed Fe-30Ni-0.044%Nb experimental data at different temperatures and strains (see **Figure 84** and **Table 24**).

It is notable, that BIF is fundamentally based on material science using a body of experimental data and it is not a arbitrary constant. So, there should be little requirement for further investigation to determine BIF values in alternative simulations since it is not specific to the steel it was fitted to.

7 Discussion/validation of the modified/improved cellular automata model

Improvements to the CA model as received (see Chapter 6) have been made by introducing BIF, a new grain boundary thickness parameter, making the Burgess factor a function of temperature and altering the core dislocation density calculations.

In order to validate the updated model, it was used to fit other experimental data in order to compare the predicted recrystallised grain size distributions and recrystallisation kinetics with those of the experiments. The model was fitted against the following for Fe-30Ni-0.044 wt % Nb steel (which preserves the austenitic structure):

- Hot deformed at 950°C to a strain of 0.2 and 0.3, with a starting modal grain size of 160µm

- Hot deformed at 950°C to a strain of 0.35 and with a starting modal grain size of 160µm

- Hot deformed at 950°C to a strain of 0.27 and with a starting modal grain size of 100µm

7.1 Validation for recrystallised grain size distribution

The one mechanism to refine grain size in a single phase in steel is recrystallisation. It is known that the grain size effects the recrystallisation kinetics but an average value is commonly used. This updated model uses a starting grain size distribution (see Chapter 3) rather than an average value. Good agreement can be seen between the modal grain size distribution results and those for the experimental data for Fe-30Ni-0.044%Nb hot deformed at 950°C to strain of 0.2 with a starting modal size of 160µm (**Figure 89**).
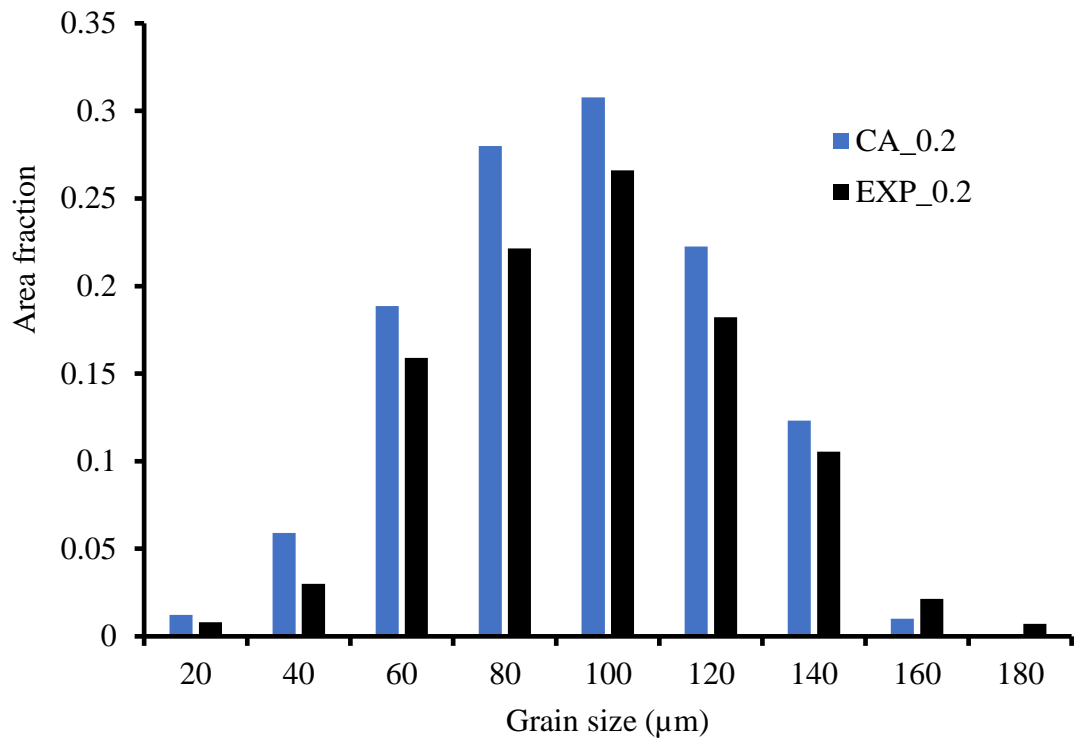
Figure 89 – Comparison of the resulting recrystallised grain size distributions for the model (above) and the experiment (below) for Fe-30Ni-0.044%Nb hot deformed at 950°C to a strain of 0.2 with a starting modal size of 160µm [141].

Good agreement can also be seen between the modal grain size distribution results and those for the experimental data for Fe-30Ni-0.044%Nb hot deformed at 950°C to strain of 0.3 with a starting modal size of 160µm (see **Figure 90**).
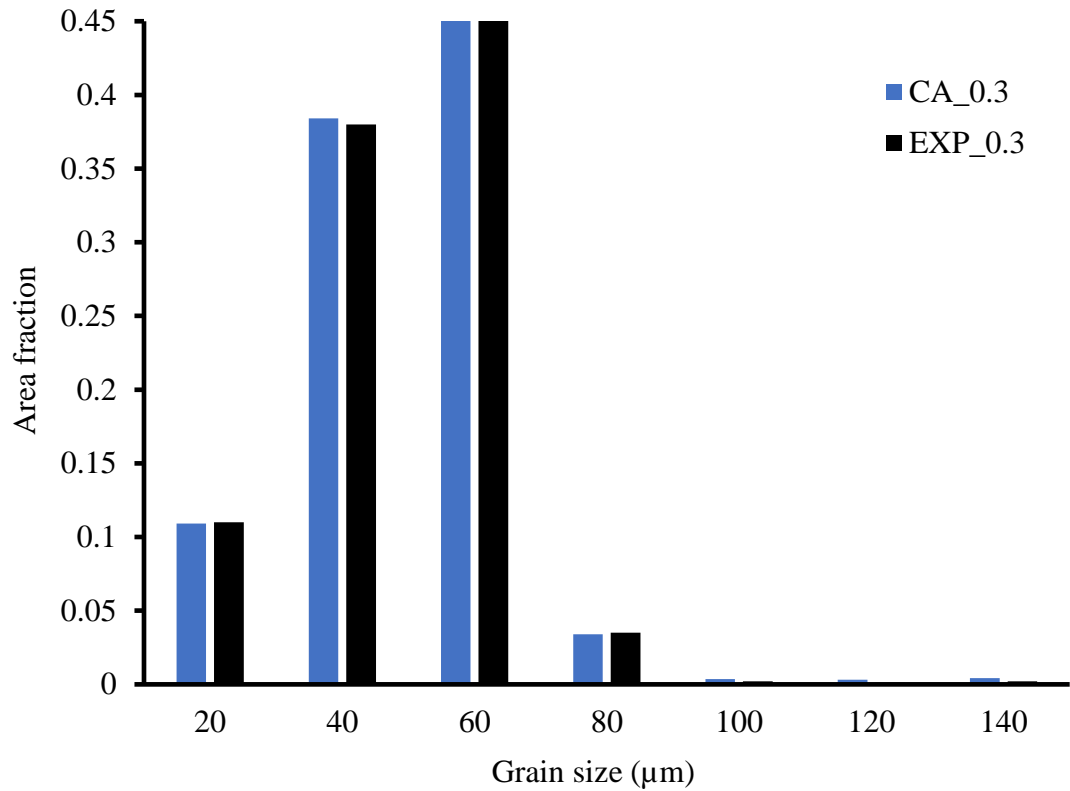
Figure 90-Comparison of the resulting recrystallised grain size distributions for the model (above) and the experiment (below) for Fe-30Ni-0.044%Nb hot deformed at 950°C to a strain of 0.3 with a starting modal size of 160µm [141].

Having validated the model against the grain size distribution at 950°C to 0.2 and 0.3 strain and a starting modal grain size of 160µm, the modal grain size for the recrystallisation distribution was 60µm (see **Figure 90**). This was used to validate the model at 0.3 strain for two different temperatures (900°C and 950°C). Results are shown in **Figure 91**.
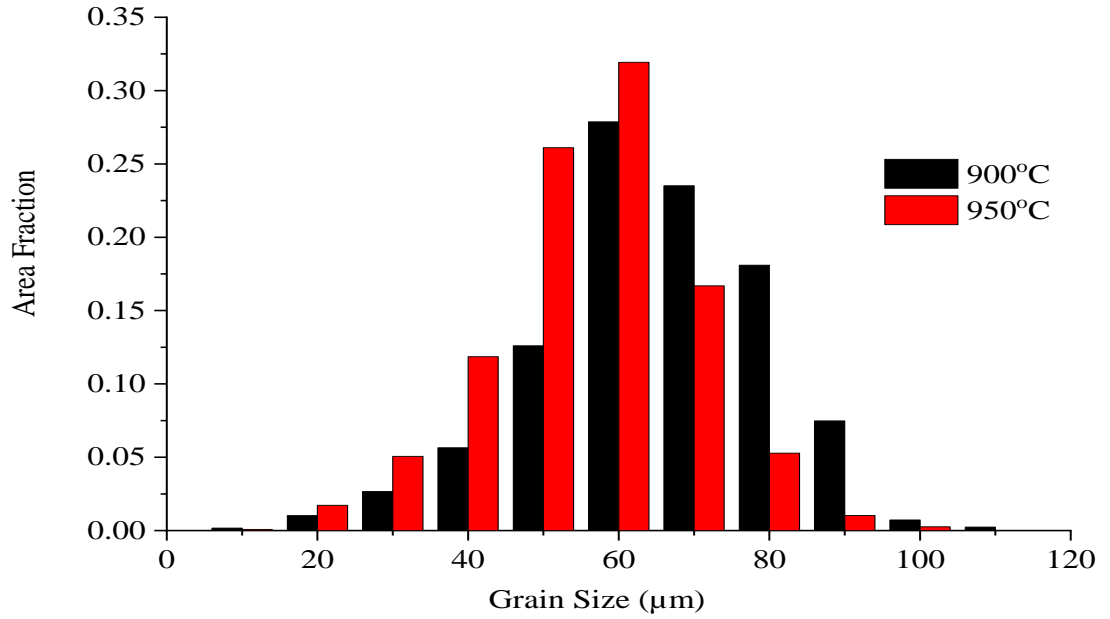
Figure 91 – Comparison of the resulting recrystallised grain size distributions for the model for Fe-30Ni-0.044%Nb hot deformed at 900°C (black) and 950°C (red) to a strain of 0.3 with a starting modal size of 160µm.

Results for both 900°C and 950°C both give a recrystallised modal grain size of 60µm, which supports the absence of temperature sensitivity for the updated model.

It is known from the literature that the recrystallised modal grain size decreases with increasing strain [28][25][21] due to the fact that the dislocation density (stored energy), the recrystallisation driving force, increases with strain[25][21]. Running the updated model at different strains and at different starting modal grain sizes, under the same conditions, also shows this same trend (**Figure 92**). This known trend of strain dependency seen in the updated model output data provides further validation for the model.
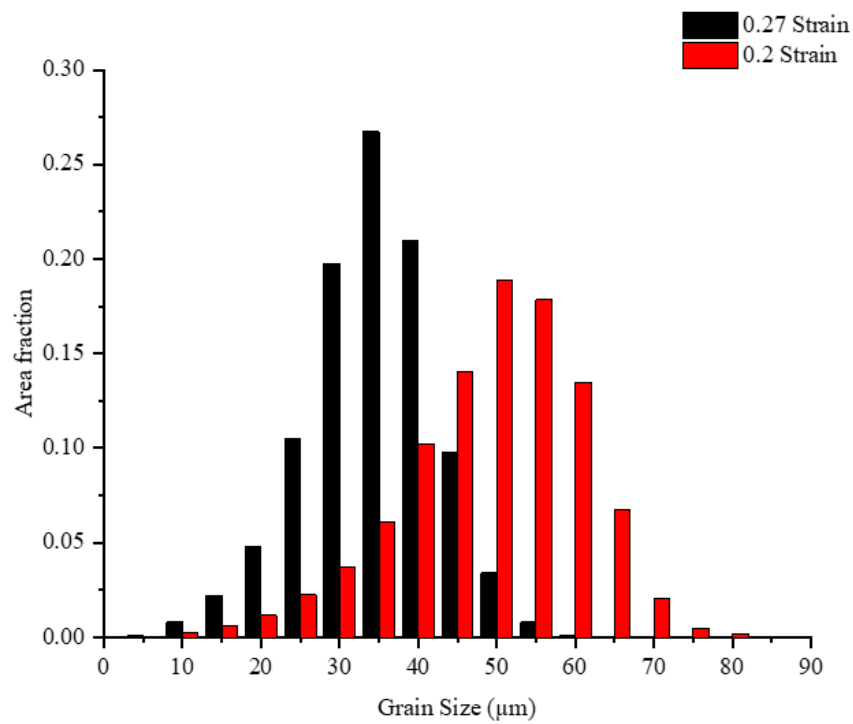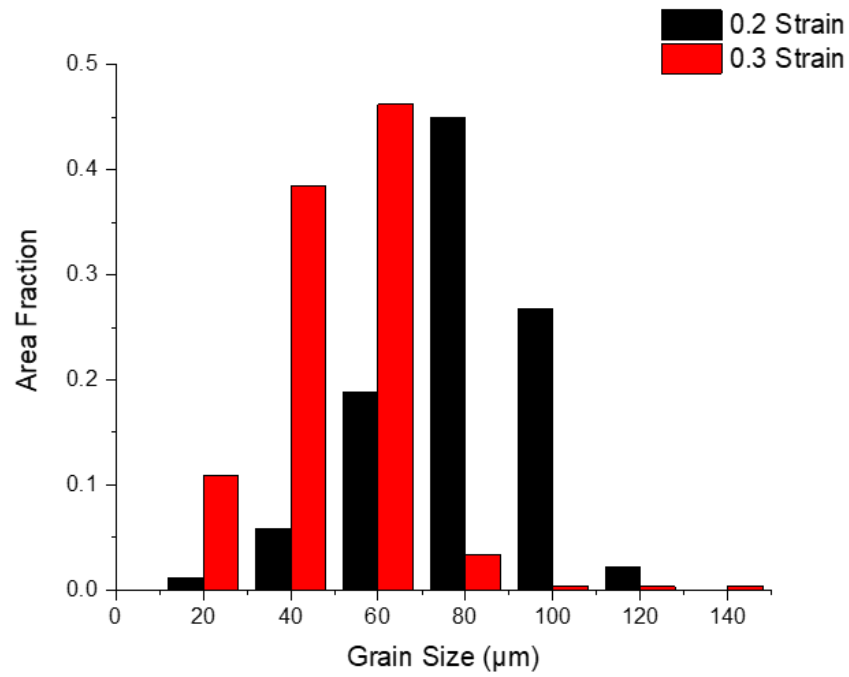
Figure 92 – Recrystallised grain size distributions for hot deformed Fe-30Ni-0.044%Nb at 950°C. The top graph compares strain 0.2 with 0.3 for a starting modal grain size of 160μm. The bottom graph compares strain 0.2 with 0.27 for a starting modal grain size of 100μm.

These results for the validation of the recrystallised grain size distribution support the idea that using the BIF has helped to introduce inhomogeneity in the model and enabled the replication of experimental recrystallisation grain size distributions by the updated model. Although the impact of the tail of the initial grain size distributions from the model CA that do not fit well with the initial grain size distributions from the experiment on the recrystallised grain size distributions was not pronounced at a strain of 0.3 but shows some deviation at a strain of 0.2.

The modifications made to include the BIF and core dislocation density have given rise to the same recrystallisation grain size distributions for different temperatures. This provides evidence that the recrystallised grain size distribution is no longer affected by temperature at the same strain. Also, with these modifications, the recrystallised grain size distribution is strain dependent.

7.2   Validation for recrystallisation kinetics

The progression of recrystallisation over time is given by plotting the recrystallisation fraction against time. A comparison of these graphs for the updated model and experimental data for hot rolled Fe-30Ni-0.044%Nb at 950°C, with different starting modal grain sizes and strain, show good agreement especially with the recrystallisation starting time(R_s) and   the time at 50% recrystallised $R_{50\%}$. The recrystallisation finishing time R_f do not agree well as explained in section 3.5.7(**Figure 93**).
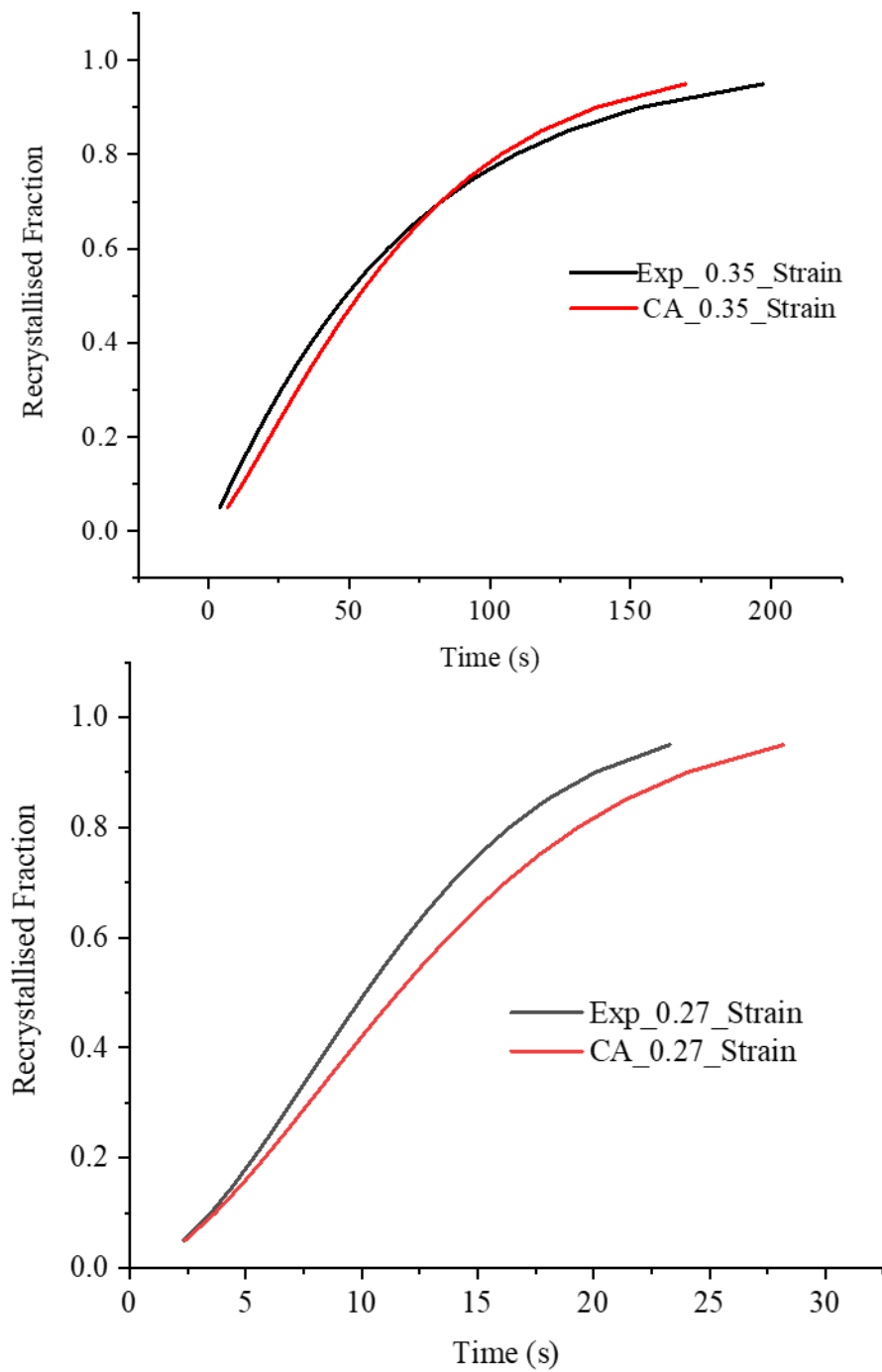
Figure 93 – Recrystallision kinetics for hot deformed Fe-30Ni-0.044%Nb at 950°C. The top graph compares the experimental data with the model at a strain of 0.35 and a starting modal grain size of 160μm. The bottom graph compares the experimental data with the modal at a strain of 0.27 for a starting modal grain size of 100μm[141].

The recrystallisation rate increases with increasing temperature since recrystallisation is a thermally activated process. This known pattern is also shown by the improved CA model providing further validation. At 950ºC the recrystallisation rate is faster than the recrystallisation rate at 900ºC. This can be seen in **Figure 94**.
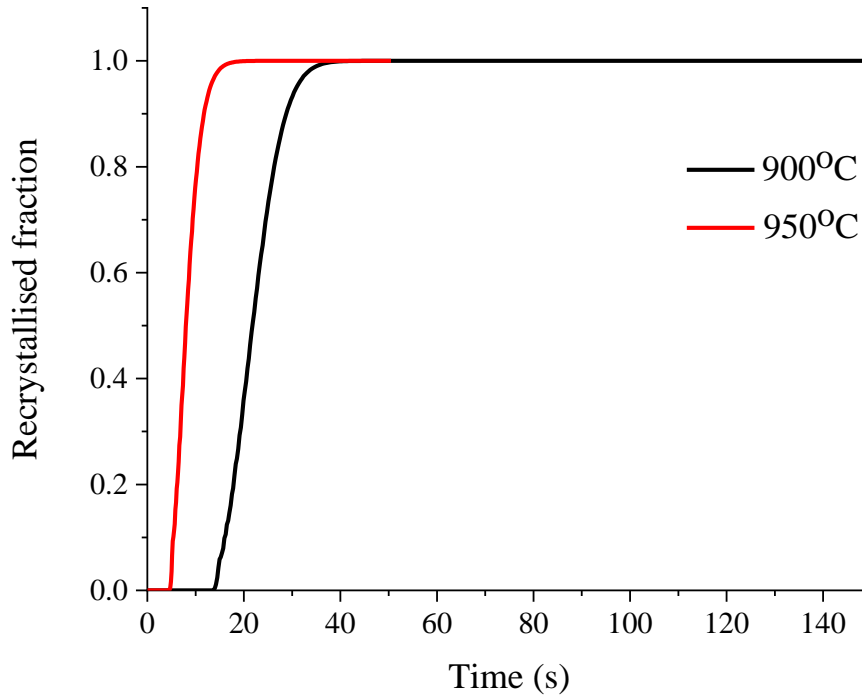
Figure 94 – Recrystallisation kinetics for hot deformed Fe-30Ni-0.044%Nb to a strain of 0.3 with a starting modal grain size of 160μm for 900°C and 950°C.

The recrystallisation is faster at higher strain. Running the modified model at different strains and at different starting modal grain sizes, under the same conditions, also shows this same trend (**Figure 95**). Thus providing further validation for the model.
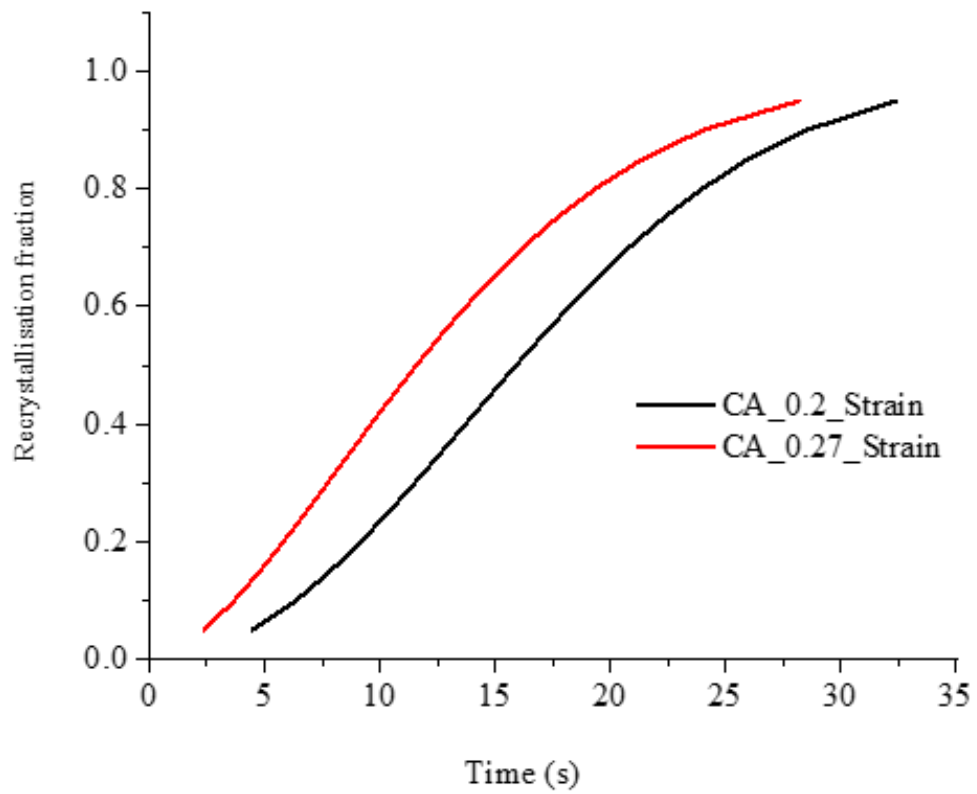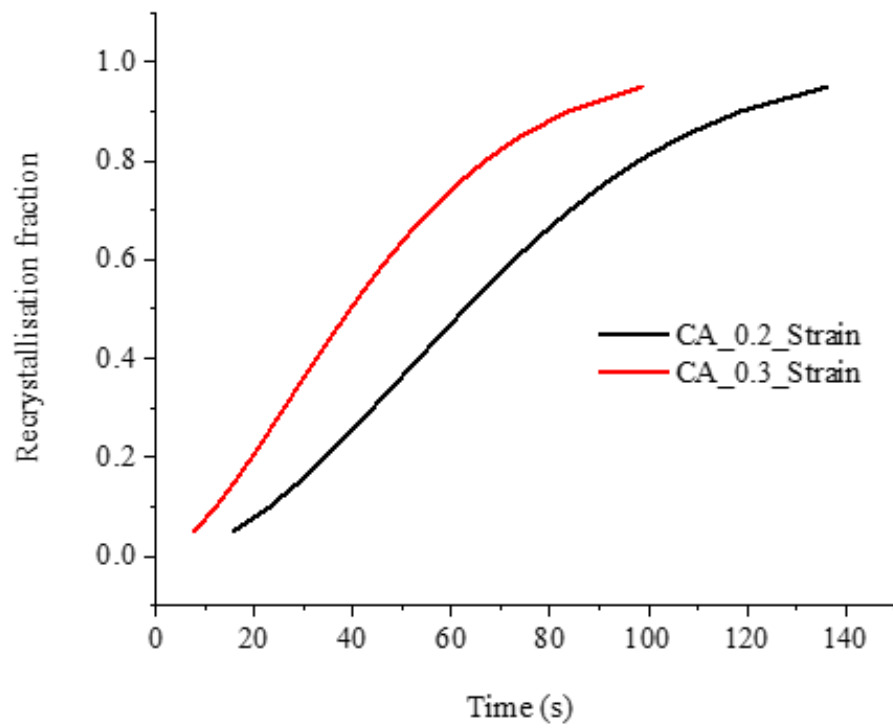
Figure 95 – Recrystallisation kinetics for hot deformed Fe-30Ni-0.044%Nb at 950°C. The top graph compares strain 0.2 with 0.3 for a starting modal grain size of 160μm. The bottom graph compares strain of 0.27 for a starting modal grain size of 100μm.

The stored energy increases for a decrease in initial grain size for a strain <0.5 [52] therefore faster recrystallisation rates as observed with the smaller initial modal grain size (100µm) compared to the larger grain size (160µm) since the coarser grains tend to be more inhomogeneous[52] and this trend is also captured in the model **Figure 96**.
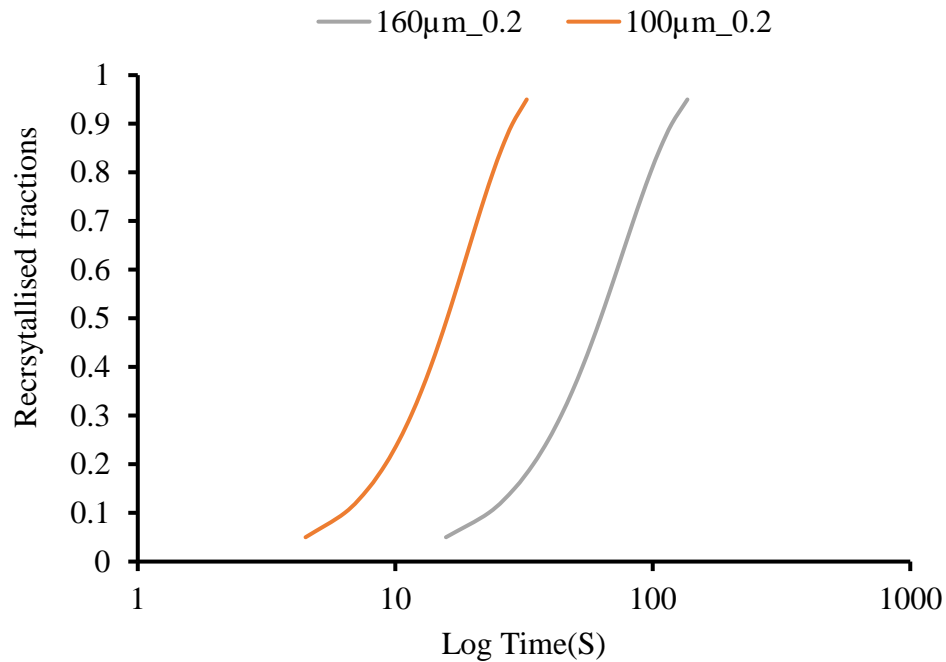
Figure 96 – Recrystallisation kinetics for hot deformed Fe-30Ni-0.044%Nb at 950°C to a strain of 0.2 with starting modal grain sizes of 100µm and 160µm.

7.3 Avrami Plot

From the recrystallisation curve **Figure 96,** it can be seen recrystallisation growth continuously changes over time and this depend on the nucleation rate, the driving force and the growth dimensionality. From the plot the predicted Avrami exponent is calculated shown in **Figure 97 (top)** from the starting grain size distribution with a modal grain size of 100µm, hot deformed at 950°C to a strain of 0.27 . The predicted Avrami value is in good agreement when compared to the experiment **Figure 97 (bottom)**.The predicted Avrami value of 1.6452 and that of the experiment as 1.7656. The Avrami exponent is less than 2 which supports the assumption that the nucleation is non-random, site-saturation assumption has not been made and the driving force is non-constant and decreases continuously due to recovery. Experimentally for the case of low carbon steels Avrami exponent has been found to be between 1 and 2.
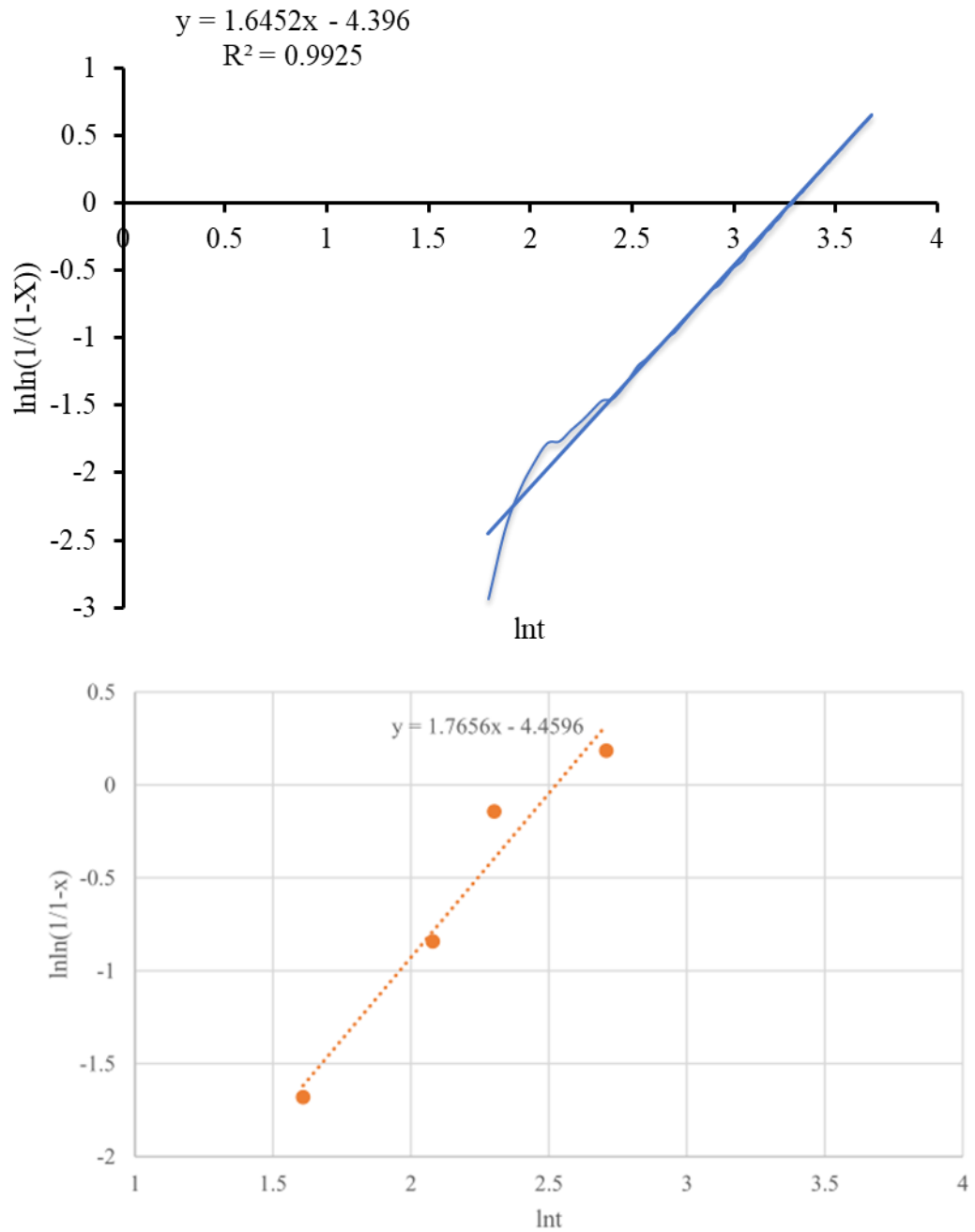
Figure 97 – Comparison of the Avrami plot for the model and the experiment for Fe-30Ni-0.044%Nb hot deformed at 950°C to a strain of 0.27 and a starting modal grain size of 100µm[141].

Figure 98 shows the impact of strain on Avrami exponent using the modified CA model. At a strain of 0.2 and 0.3 for the same modal grain size of 160µm,the Avrami exponent is 1.5964 for 0.3 strain compared to the value of 1.8836 for 0.2 strain. The Avrami value is lower at higher strain because at higher strain the recrystallisation

rate is faster. The faster the recrystallisation rate the smaller the Avrami value. Though Mo reported that within a strain of 0.2- 0.3 the Avrami exponent is independent of strain deformation level[133][141] but since strain is not homogeneously distributed , this affects recrystallisation kinetics and hence will affect the Avrami value [15][51].
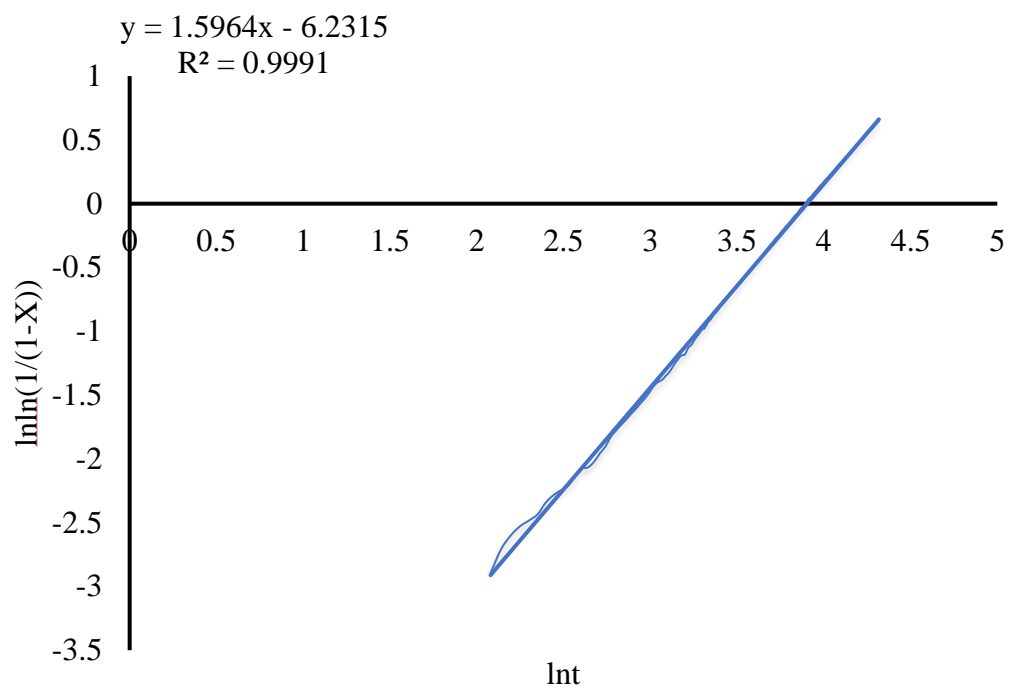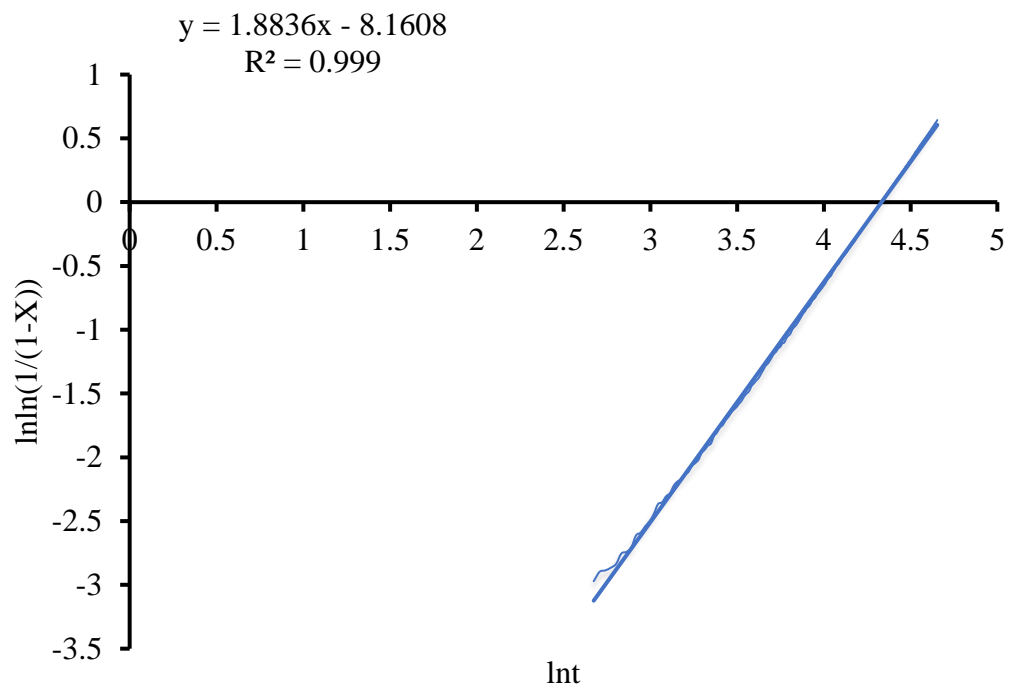
Figure 98 – Plot showing the evolution of Avrami exponent for hot deformed at 950°C Fe-30Ni-0.044%Nb to a strain of 0.2 (top figure) and 0.3 (bottom figure) with a starting modal grain size of 160 μm.

7.4   Comparison with empirical model

Using **Equation 2.3**, with D' equal to 1.1, D_o equal to 160µm and a strain of 0.3, the D_{rex} is calculated as 73.87µm and the modal grain size obtained by the CA model is 60µm and which is the same as the experimental data. The difference in the modal grain sizes maybe as result of the fitting parameter for the nickel based system.

The kinetics of austenite recrystallisation during hot deformation was also studied using the JMAK approach. A quantitative comparison of the simulated kinetics data from the improved CA-model with JMAK-kinetics data was performed for austinite recrystallisation. A random distribution of the nucleation sites was used, therefore the recrystallisation kinetics calculated by the CA model should be similar to the kinetics calculated from the JMAK equation.

Figure 99 shows the change in recrystallisation fraction with time as obtained from a CA-model simulation and from the JMAK-equation. It is seen that the agreement between the CA-model and the JMAK-kinetics is good, since in both models the same interface velocity is used. The morphological and impingement aspects of the microstructural evolution are well captured by the model.
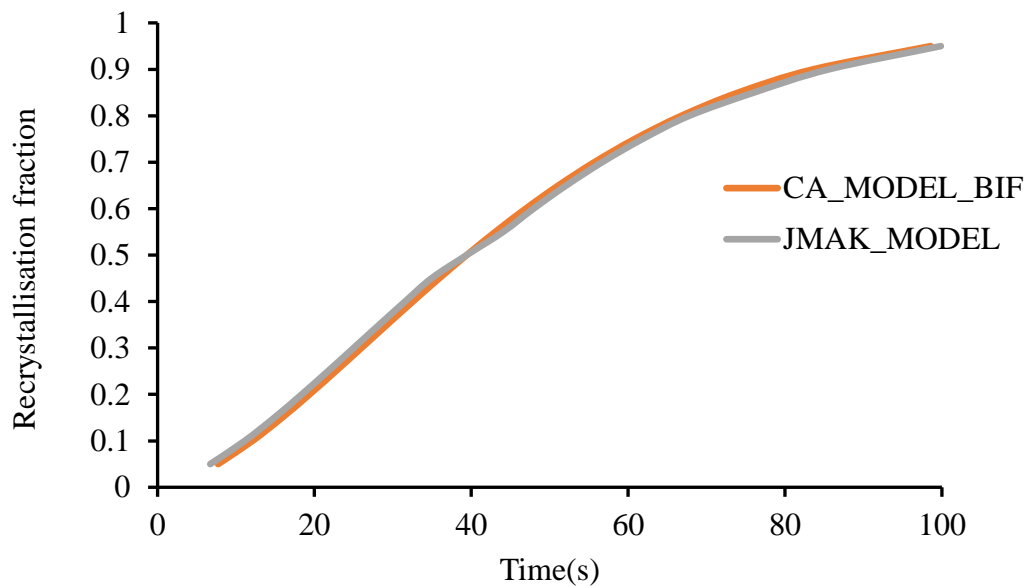
Figure 99-Shows the recrystallisation fraction with time obtained from the CA-model simulation and the JMAK-equation for hot deformed at 950°C Fe-30Ni-0.044%Nb to a strain of 0.3 with a starting modal grain size of 160 µm. .

8   Conclusion and future work

A cellular automata model, using a 3D grain size distribution as the input, developed to predict microstructure development during hot rolling and transformation on cooling has been assessed for its effectiveness in predicting recrystallisation kinetics and the full recrystallised grain size distributions. It has been found that:

1. The initial model showed some inaccuracies compared to expected trends for the recrystallised grain size predictions, with a temperature dependency and strain insensitivity being observed that does not match literature experimental observations.

2. From the sensitivity analysis, those parameters that affect the recrystallisation kinetics, and therefore the processing conditions, are the shear modulus (μ), pre-exponential mobility (M_o) and the sub-grain growth factor (K_{ad}). While the parameters that significantly impact the recrystallisation kinetics and the final microstructure are the Burgers vector (b), temperature (T), strain (ε), activation energy (Q) and the initial dislocation density (ρ_{init}). Using the correct values for these parameters is essential for accurate determination of the processing conditions and therefore the resulting mechanical properties of hot rolled steels.

3. Introducing a boundary intensity factor (BIF), to accurately reflect the experimentally observed inhomogeneous dislocation density with a higher dislocation density occurring close to the grain boundaries, results in changes in the nucleation and sub-grain growth to critical size. The resulting lower dislocation density in the grain bulk then changes the critical sub-grain growth.

4. The introduction of the BIF means that the dislocation density (stored energy) is related the individual grain size i.e. smaller grains have a higher dislocation density representative of the higher grain boundary area, which means they recrystallise earlier than larger grains, which is observed in the literature.

5. The critical radius is incredibly hard to measure (the point where a sub grain with low angle grain boundaries turns to a grain with high angle boundaries) and it is dependent on the dislocation density (i.e. strain and stored energy). The sub-grain growth is temperature and stored energy driven and the introduction of the boundary intensity factor (BIF) means that sub grain nucleation and growth to critical size is affected by the applied strain (giving

strain sensitivity) but is less dependent on temperature (temperature insensitivity).

6. The introduction of the boundary intensity factor accurately reflects the experimentally observed inhomogeneous dislocation density in deformed samples, where higher dislocation density at the grain boundaries occurs, which results in changes in the nucleation and sub-grain growth to critical size. The width of the 'boundary' has been determined based on the experimental observations and the value of the boundary intensity factor for the stored energy was determined by fitting to literature experimental data for a Fe-30Ni steel, with a starting average grain size of 160 µm at a strain of 0.3 considering deformation at 950°C.

7. The introduction of the boundary thickness has helped to introduce the inhomogeneity observed in experimental data by reducing the core dislocation density and driving the growth after nucleation and hence has significantly improved the recrystallisation starting time Rs, recrystallisation finishing time and the Avrami values to have a good agreement with the experimental data.

8.1 Future work

The cellular automata model, with the modifications introduced in this PhD work, is able to predict the recrystallisation kinetics and recrystallised grain size distribution in agreement with the experimental observations for hot deformed steel. The model can therefore form part of through process modelling capabilities that in the future will allow for an understanding of how upstream variability (as-cast segregation and reheated grain size variations) can impact downstream microstructures. However, there still exists some limitations/unknowns which are worth addressing in future versions. Some of the possible areas in which the model can be further refined are listed below:

1. It has been seen that the initial Voronoi microstructure created does not match well, in terms of the larger grain sizes in the distribution, with the experimental data. The 2D plane distributions from the 3D models do not fit the experimental shape - instead of the expected log normal distribution, a log log scale distribution is generated. One possible explanation may be because what we are getting from the CA is equivalent volume diameter instead of the equivalent area diameter. A potential solution may be to use the Voronoi software to give a weighted distance between initiation points - this is the Laguerre Voronoi approach with recent literature results showing that more accurate representation of experimentally determined grain size distributions being produced[152].

2. Changing the grid spacing during the simulation to accommodate issues with large differences between the critical nucleation event and grain size. This is likely to be necessary when simulating for different strains where the critical nuclei may be smaller than the current grid spacing being used. Ultimately it would be better to have a variable grid size in the simulation with finer spacing at the grain boundaries.

3. To investigate the effect of BIF on smaller grain sizes. The fitted BIF of 2.2 works well for the 100μm average initial austenite grain size to match the recrystallised grain size and kinetics. However as the grain size gets smaller

(e.g. close to and less than 50 µm) the BIF chosen and boundary width may be inappropriate and therefore it may be necessary for the BIF to be a function of grain size. Comparing predictions to experimental results for smaller starting average grain sizes is required to investigate this potential effect.

4. To keep the recrystallized fraction curve smooth, the CA model starts all nuclei at the size of a single cell. If the critical sub-grain size is larger than a single cell an enhanced growth rate is applied so a nucleus quickly grows to its critical size. Within the critical sub-grain size no other nuclei are allowed to be formed next to the nucleation cell. However, the grain boundary area is not reduced in the counting of the interface area.

5. The driving force for nucleation is the difference in dislocation density, $\Delta\rho$ across the grain boundary. For the model development the dislocation density at the boundary was made to be higher than the dislocation density at the grain core and this principle applied equally to all the grains. That implies that all the grains have the same dislocation density at the grain boundary and at the core. Another option to explore would be to assume a dislocation density distribution and possibly map the dislocation density distribution from EBSD into the model. Currently the dislocation density at the boundary and the grain interior is the same irrespective of the size of the grains within the grain size distribution even with the same BIF. Introducing a dislocation density map, would allow variation in the dislocation densities within the individual grains in the distribution.

6. Since the effect of precipitation on both recrystallisation and recovery kinetics has not been considered, the model should be modified in future to capture the effect of precipitation on recrystallisation and also on subsequent grain growth.

7. In order to further quantify the effect of BIF on grain size distributions and recrystallisation kinetics, the model can be compared to commercial packages assuming a homogeneous defect density.

189

References

[1]   "About Steel | Worldsteel." https://www.worldsteel.org/about-steel.html (accessed May 21, 2020).

[2]   X. Li, L. Shi, Y. Liu, K. Gan and C. Liu, "Achieving A Desirable Combination Of Mechanical Properties In HSLA Steel Through Step Quenching." *Mater. Sci. Eng. A*, vol. 772, pp. 138683, 2020.

[3]   A. J. Nathan and A. Scobell, "How China Sees America." *Foreign Aff.*, vol.91, no.5, pp.1, 2012, doi.1017/CB09781107415324.004.

[4]   M. Kashif and Ur Rehman, "Modelling The Microstructure Evolution During Hot Deformation." Ph.D thesis, Materials Science & Engineering, McMaster University, Ontario, 2014.

[5]   Q. Y. Sha, Z. Q. Sun and L. F. Li, "Refinement Of Coarse Grained Austenite In Nb–V–Ti Microalloyed Steel During Roughing Rolling." *Ironmak. Steelmak.*, vol. 42, no. 1, pp. 74–80, 2015, doi: 10.1179/1743281214Y.0000000205.

[6]   C. Roucoules, P. D. Hodgson, S. Yue and J. J. Jonas, "Softening And Microstructural Change Following The Dynamic Recrystallization Of Austenite." *Metall. Mater. Trans. A*, vol. 25, pp.389-400, 1994.

[7]   L. Blaz, E. Evangelista and M. Niewczas, "Precipitation Effects During Hot Deformation Of A Copper Alloy." *Metall. Mater. Trans. A,* vol. 25, no.2, pp.257-266, 1994.

[8]   Q. Yun Sha, D. Hang Li and G. Yan Li, "Dynamic And Static Recrystallization Behaviour Of Coarse-Grained Austenite In A Nb-V-Ti Microalloyed Steel." *J. Iron Steel Res. Int.*, vol. 21, no. 2, pp. 233–239, 2014, doi: 10.1016/S1006-706X(14)60036-4.

[9]   Y. Weng, "Ultra-Fine Grained Steels." Beijing: Metallurgical Industry Press; Berlin: Springer, 2009, pp.53-85.

[10]   H. E. Vatne, K. Marthinsen and E. Nes, "Modeling Recrystallization Kinetics, Grain Sizes, And Textures During Multipass Hot Rolling." *Metall. Mater. Trans. A*, vol. 27, no.2, pp.4133-4144, 1996.

[11]   T. Gladman, "The Physical Metallurgy Of Microalloyed Steels." The Institute of Materials. London: Maney Publishing, 1997, pp. 1-17.

[12]   E. Pereloma and D.V. Edmonds, "Phase Transformations In Steels: Diffusionless Transformations, High Strength Steels, Modelling And Advanced Analytical Techniques.", Burlington : Elsevier Science, 2012.

[13]   A. Rollett, F. Humphreys, S. Gregory and R. M. Hatherly, "Recrystallization And Related Annealing Phenomena." 2nd ed, Pergamon, 2004, pp. 658.

[14]   B. Dutta and C. M. Sellars, "Effect Of Composition And Process Variables On Nb(C, N) Precipitation In Niobium Microalloyed Austenite." *Mater. Sci. Technol.*, vol. 3, no.3, pp. 197–206, Feb. 2012.

[15]   F.J. Humphreys and M. Hatherly, "Recrystallization and related annealing phenomena." 2nd ed, Amsterdam; Boston: Elsevier, 2004 , pp. 628.

[16]   H. S. Zurob, C. R. Hutchinson, Y. Brechet, and G. Purdy, "Modeling Recrystallization Of Microalloyed Austenite: Effect Of Coupling Recovery, Precipitation And Recrystallization." *Acta Mater.*, vol. 50, no. 12, pp. 3077–3094, Jul. 2002, doi: 10.1016/S1359-6454(02)00097-6.

[17]   M. K. Rehman and H. S. Zurob, "A Novel Approach To Model Static Recrystallization Of Austenite During Hot Rolling Of Nb Microalloyed Steel. Part I: Precipitate-Free Case." *Metall. Mater. Trans. A Phys. Metall. Mater. Sci.,* vol. 44, no. 4, pp. 1862–1871, Apr. 2013, doi: 10.1007/s11661-012-1526-5.

[18]   A. Kundu, C. Davis and M. Strangwood, "Modeling Of Grain Size Distributions During Single Hit Deformation Of A Nb-Containing Steel." *Metall. Mater. Trans. A,* vol. 41, no. 4, pp. 994–1002, Apr. 2010, doi: 10.1007/s11661-009-0167-9.

[19]   A. Kundu, C. L. Davis and M. Strangwood "Grain Structure Development During Reheating And Deformation Of Niobium-Microalloyed Steels." *Mater. and Man. Proc.*, vol. 25, no.1-3, pp. 125-132, 2010.

[20]   M. K. M. Kaonda, "Prediction Of The Recrystallised Grain Size Distribution After Deformation For The Nb Free And Nb Model Steel," PhD thesis, Sch.Met. and Mat., Coll. of Eng and Phy. Sci.,Uni. of Birmingham, 2017.

[21] C. M. Sellars and G. J. Davies, "Hot Working And Forming Processes: Proceedings Of An International Conference On Hot Working And Forming Processes." Sheffield Metallurgical and Engineering Association, Department of Metallurgy and Metals Society, University of Sheffield., London: The Society, Series 264,1980.

[22] P. Yan and H. K. D. H. Bhadeshia, "Austenite–Ferrite Transformation In Enhanced Niobium, Low Carbon Steel. " *Mater. Sci. and Tech*., vol. 31, no.9, pp.1066-1076, 2015, doi: 10.1179/1743284714Y.0000000673.

[23] N. A. Razani, B. M. Dariani and M. Soltanpour, "Microstructure And Mechanical Property Improvement Of X70 In Asymmetrical Thermomechanical Rolling." *Int. J. Adv. Manuf. Technol.*, vol. 97, no. 9–12, pp. 3981–3997, Aug. 2018, doi: 10.1007/s00170-018-1823-2.

[24] Z. Fan, "A Microstnietural Approach To The Effective Transport Properties Of Multiphase Composites." *Philos. Mag. A*., vol. 73, no. 6, pp. 1663–1684, 1996.

[25] S. Falco, J. Jiang, F. De Cola and N. Petrinic, "Generation Of 3D Polycrystalline Microstructures With A Conditioned Laguerre-Voronoi Tessellation Technique." *Comput. Mater. Sci.*, vol. 136, pp. 20–28, 2017.

[26] Y. Wu, W. Zhou, B. Wang and F. Yang, "Modeling And Characterization Of Two-Phase Composites By Voronoi Diagram In The Laguerre Geometry Based On Random Close Packing Of Spheres." *Comput. Mater. Sci.*, vol. 47, no. 4, pp. 951–961, 2010, doi: 10.1016/j.commatsci.2009.11.028.

[27] S. Ghosh, Z. Nowak and K. Lee, "Tessellation-Based Computational Methods For The Characterization And Analysis Of Heterogeneous Microstructures." C*ompos. Sci. Technol.,* vol. 57, no. 9–10, pp. 1187–1210, 1997, doi: 10.1016/s0266-3538(97)00042-0.

[28] S. Falco, J. Jiang, F. De Cola and N. Petrinic, "Generation Of 3D Polycrystalline Microstructures With A Conditioned Laguerre-Voronoi Tessellation Technique." *Comput. Mater. Sci.,* vol. 136, pp. 20–28, 2017.

[29] R. Shi, Z. Nie, Q. Fan, F. Wang, Y. Zhou and X. Liu, "Correlation Between Dislocation-Density-Based Strain Hardening And Microstructural Evolution In Dual Phase TC6 Titanium Alloy." *Mater. Sci. Eng. A*, vol. 715, no.8, pp. 101–107, 2018, doi: 10.1016/j.msea.2017.12.098.

[30] J.-P. Tovee, "Microstructural Influence On The Effects Of Forward And Reverse Mechanical Deformation In HSLA X65 And X80 Linepipe Steels." *Materials Science,* p. 231, 2014.

[31] A. Laasraoui and J. J. Jonas, "Recrystallization Of Austenite After Deformation At High Temperatures And Strain Rates-Analysis And Modeling." *Metall. Trans. A*, vol. 22, no. 1, pp. 151-160, 1991, doi:10.1007/BF03350957.

[32] A. Gholinia, F. Humphreys and P. Prangnell, "Production Of Ultra-Fine Grain Microstructures In Al–Mg Alloys By Coventional Rolling." *Acta Mater.*, vol. 50, no. 18, pp. 4461–4476, Oct. 2002, doi: 10.1016/S1359-6454(02)00253-7.

[33] E. A. Simielli, "Deformation And Crystallisation Kinetics Of Microalloyed Steels In The Intercritical Region." Ph. D. thesis, McGill University, Montreal, Canada, 1990.

[34] T. Gladman, "The Physical Metallurgy Of Microalloyed Steels. " *London Institute of Materials,* pp. 351-363, 1997.

[35] N. Hansen, "Cold Deformation Microstructures." *Mater. Sci. Technol. (United Kingdom)*, vol. 6, no. 11, pp. 1039–1047, Sep. 1990.

[36] D. Hull and D. J. Bacon, "Introduction To Dislocations." Fifth Edition, Butterworth-Heinemann, 2011, pp. 21-41, doi.org/10.1016/B978-0-08-096672-4.00002-5.

[37] M. D. K. Rehman and H. S. Zurob, "A Novel Approach To Model Static Recrystallization Of Austenite During Hot Rolling Of Nb Microalloyed Steel. Part I: Precipitate-Free Case." *The Min., Metals & Mater. Soc. and ASM Int.*, vol. 44A, Apr. 2013, doi: 10.1007/s11661-012-1526-5.

[38] R. L. Gall and J. J. Jonas, "Solute Drag Effects During The Dynamic Recrystallisation Of Nickel." *Acta material*, vol. 47, pp. 4365-4374, 1999, doi: 10.1016/s1359-6454(99)00319-5.

[39]   M. Kazeminezhad, "On The Modeling Of The Static Recrystallisation Considering The Initial Grain Size Effects." *Mater. Sci. and Eng. A*, vol. 486, pp. 202-207, 2008.

[40]   R. O. Williams, "The Stored Energy Of Copper Deformed At 24C." *Acta Metallurgica,* vol. 13, pp. 163-168, 1965.

[41]   J. E. Bailey, "The Dislocation Density, Flow Stress And Stored Energy In Deformed Polycrystalline Copper." *Philos. Mag.*, vol. 8, no. 86, pp. 223–236, 1963, doi: 10.1080/14786436308211120.

[42]   R. D. Doherty, "Recrystallisation And Texture." *Progress in Mater. Sci.,* vol. 42, pp. 39-58, 1997, doi: 10.1016/0956-7151(93)90117-B.

[43]   M. F. Ashby, "The Deformation Of Plastically Non-Homogeneous Materials." *Philos. Mag.*, vol. 21, no. 170, pp. 399–424, 1970.

[44]   A. J. DeArdo, J. M. Gray and L. Meyer, "Fundamental Metallurgy Of Niobium In Steels." Proceeding of Niobium international symposium, University of Pittsburgh, Pittsburgh, 1984.

[45]   P. Cizek, J. A. Whiteman, W. M. Rainforth and J. H. Beynon, "EBSD And TEM Investigation Of The Hot Deformation Substructure Characteristics Of A Type 316L Austenitic Stainless Steel." *Journal of Microscopy*, vol. 213, no. 3, pp. 285–295, Mar. 2004, doi: 10.1111/j.0022-2720.2004.01305.x.

[46]   F. J. Humphreys and M. G. Ardakani, "The Deformation Of Particle-Containing Aluminium Single Crystals." *Acta Metall.*, vol. 42, no. 3, pp. 794-761, 1994.

[47]   M. H. Loretto and A. J. White, "The Influence Of Grain Size On The Energy Stored In Deformed Copper." *Acta Metallurgica*, vol. 9, pp. 512-513, 1961.

[48]   R. O. Willams, "The Stored Energy In Deformed Copper: The Effect Of Grain Size And Silver Content." *Acta Metallurgica*, vol. 9, pp. 949-957, 1961.

[49]   R. O. Williams, "The Stored Energy In Deformed Copper At 24C." *Acta Metallurgica,* vol. 13, pp. 163-168, 1965.

[50] I. Baker, L. Liu and D. Mandal, "The Effect Of Grain Size On The Stored Energy Of Cold Work As A Function Fo Strain For Polycrystalline Nickel. " *Scripta Metallurgica et Materiala,* vol. 32, pp. 167-171, 1995.

[51] M.F.Ashby and D.R.H. Jones, "Engineering Materials 1 : An Introduction To Properties, Applications And Design." 3rd ed. Parker: Elsevier Butterworth-Heinemann, 2005.

[52] F. J. Humpreys and M.Hatherly, "Recrystallisation And Related Annealing Phenomena." Elsevier Ltd, 2nd Edition, ISBN: 978-0-08-044164-1, 2004.

[53] D. G. Cram, H. S. Zurob, Y. J. M. Brechet and C. R. Hutchinson, "Modelling Discontinuous Dynamic Recrystallization Using A Physically Based Model For Nucleation." *Mater. Sci. Forum*, vol. 4, pp. 715-716, 2012.

[54] T. Sakai, A. Belyakov, R. Kaibyshev, H. Miura and J. J. Jonas, "Dynamic And Post-Dynamic Recrystallization Under Hot, Cold And Severe Plastic Deformation Conditions." *Progress in Mater. Sci.*, vol. 60, no.1, pp. 130–207, Mar. 01, 2014, doi: 10.1016/j.pmatsci.2013.09.002.

[55] H. Mecking and U.F. Kocks, "Kinetics Of Flow And Strain-Hardening." A*cta Metallurgica*, vol. 29, pp.1865-1875, 1981,doi:10.1016/0001-6160(81)90112-7.

[56] S. Vervynckt, K. Verbeken, B. Lopez and J. Jonas, "Modern HSLA Steels And Role Of Non-Recrystallisation Temperature." *Int. Mater. Reviews*, vol. 57, no.4, pp.187-207, 2012.

[57] X. Zhang, H. Roelofs, S. Lemgen, U. Urlau and S. V. Subramanian, "Application Of Thermodynamic Model For Inclusion Control In Steelmaking To Improve The Machinability Of Low Carbon Free Cutting Steels." *Steel Res. Int.*, vol. 75, no. 5, pp. 314–321, 2004, doi: 10.1002/srin.200405961.

[58] C.N. Homsher, "Determination Of The Non-Recrystallization Temperature (TNR) In Multiple Microalloyed Steels." M.S Thesis, Colorado School of Mines, 2013.

[59] H. McQueen and J. Jonas, "Plastic Deformation Of Materials." New York, Academic Press, Inc., 1975 ,pp. 393-493.

[60] F. Humphreys and M. Hatherly, "Recrystallization And Related Annealing Phenomena." Pergamon Press, Oxford, 1995, pp.8-235.

[61] R. Sandsttröm, "Subgrain Growth Occurring By Boundary Migration." *Acta Metall Mater.*, vol. 25, no.8, pp. 905-911, 1977.

[62] A. Rollett, F. Humphreys, G. Rohrer and M. Hatherly, "Recrystallization And Related Annealing Phenomena." 2nd edition, Elservier, 2004.

[63] A. Zadeh, "The Investigation Of Deformation, Recovery, Recrystsallisation And Precipitation In Austenitic HSLA Steel Analogue Alloys." Ph.D Thesis, University of Wollongong, 1996.

[64] S. Yamamoto, C. Ouchi and T. Osuka, "The Effect Of Microalloying Elements On The Recovery And Recrystallization In Deformed Austenite." *In Proceedings of the International Symposium on Thermomechanical Processing of Microalloyed Austenite*, Pittsburgh, PA, USA, 1981, pp. 613–639.

[65] J. J. Jonas and M.G. Akben, "Retardation Of Austenite Recrystallization By Solutes: A Critical Appraisal." *Metals Forum,* vol. 4, no.l&2, pp. 92-101, 1981.

[66] R. J. McElroy and Z. C. Szkopiak, "Dislocation-Substructure-Strengthening And Mechanical-Thermal Treatment Of Metals." *Int. Metall. Rev.*, vol. 17, no. 1, pp. 175–202, Jan. 1972, doi: 10.1179/imtlr.1972.17.1.175.

[67] A.F. Padilha, R. L. Plaut and P.R. Rios, "Annealing of Cold-worked Austenitic Stainless." *ISIJ Int.*, vol. 43, no. 2, pp. 135-143, 2003.

[68] E. Nes, "Analytical Modelling Of Grain Growth In Metals And Alloys In The Presence Of Growing And Dissolving Precipitates—II. Abnormal Grain Growth. " *Acta metallurgica et materialia*, vol. 43. no. 7, pp.2689-2700, 1995.

[69] J. Friedel, "Dislocations. " 1st English ed. International series of monographs on solid state physics, Oxford, New York, Pergamon Press; U.S.A., 1964.

[70] M. Militzer, E. B. Hawbolt and T. R. Meadowcroft, "Microstructural Model For Hot Strip Rolling Of High-Strength Low-Alloy Steels." *Metall. Mater. Trans. A Phys. Metall. Mater. Sci.*, vol. 31, no. 4, pp. 1247–1259, 2000.

[71] N. Maruyama, R. Uemori and M. Sugiyama, "The Role Of Niobium In The Retardation Of The Early Stage Of Austenite Recovery In Hot-Deformed Steels." *Mater. Sci. and Eng. A*, vol. 250, no. 1, pp.2-7, 1998.

[72] B. Babu, "Physically Based Model for Plasticity and Creep of Ti-6Al-4V" Licentiate Thesis, Division of Material Mechanics, Department of Applied Physics and Mechanical Engineering, Luleˆa University of Technology, Sweden, 2008.

[73] J. C. M. Li, "Dislocation Dynamics In Deformation And Recovery." *Can. J. Phys.*, vol. 45, no. 2, pp. 493–509, Feb. 1967, doi: 10.1139/p67-043.

[74] A. Serra and D. J. Bacon, E. Nes, "Computer Simulation Of Screw Dislocation Interactions With Twin Boundaries In H.C.P. Metals." A*cta metallurgica et materialia*, vol. 43, no.12, pp. 4465-4481, 1995.

[75] F. R. Castro-Fernáandez and C. M. Sellars, "Relationship Between Room-Temperature Proof Stress, Dislocation Density And Subgrain Size. " *Phil. Mag. A*, vol. 60, no. 4, pp.487-506,1989.

[76] M. Verdier, Y. Brechet and P. Guyot, "Recovery Of Almg Alloys: Flow Stress And Strain-Hardening Properties." *Acta Materialia*, vol. 47, no. 1, pp. 127-134, 1998, doi.org/10.1016/S1359-6454(98)00350-4.

[77] R. E . Cook, G. Gottstein and U. F Kocks, "Recovery In Deformed Copper And Nickel Single Crystals." *J Mater Sci.*,vol. 18, pp. 2650–2664 ,1983.

[78] V. Anderson, L. Arnberg, Z. Jinyuan, M. Lindenmo, S. Savage and A. Scholin, "High-Temperature Tensile Properties Of Rapidly Solidified Tin Precipitation Hardened 316l Stainless Steel." Swedish Inst. Metals Res., Stockholm, Rep. No. IM 1211, 1987.

[79] E. J. Palmiere, C. I. Garcia and A. J. De Ardo, "Compositional And Microstructural Changes Which Attend Reheating And Grain Coarsening In Steels Containing Niobium." *Metal. Mater. Trans. A*, vol. 25, pp. 277–286, 1994.

[80] A. Nishimoto, Y. Hosoya and K. Nakaoka, "Fundamentals Of Dual-Phase Steels." *Proceedings of A Symposium at the 110th AIME Annual Meeting*, R. A. Kot, B. L. Bramfitt Eds., Chicago, IL, USA, 1981.

[81] R.D. Doherty, "Recrystallisation And Texture." *Progress in Materials Science*, vol. 42, no. 1–4, pp. 39-58, 1997, doi:10.1016/S0079-6425(97)00007-8.

[82] A. Kreisler and R. D. Doherty, "Structure Of Well-Defined Deformation Bands And Formation Of Recrystallization Nuclei In Aluminium." *Met. Sci*., vol. 12, no. 12, pp. 551–560, Dec. 1978, doi: 10.1179/msc.1978.12.12.551.

[83] P. Faivre and R. D. Doherty, "Nucleation Of Recrystallization In Compressed Aluminium: Studies By Electron Microscopy And Kikuchi Diffraction." *J. Mater. Sci*., vol. 14, no. 4, pp. 897–919, Apr. 1979, doi: 10.1007/BF00550722.

[84] T. R. McNelley, D. L. Swisher, and M. T. Prez-Prado, "Deformation Bands And The Formation Of Grain Boundaries In A Superplastic Aluminum Alloy." *Metall. Mater. Trans. A Phys. Metall. Mater. Sci*., vol. 33, no. 2, pp. 279–290, 2002, doi: 10.1007/s11661-002-0089-2.

[85] H. Inagaki, "Rate Of Annealing Twins For Grain Refinement In Controlled Rolling Of Low Carbon Microalloyed Steel." *ISIJ int*., vol. 23, pp. 1059, 1983.

[86] E. Essadiqi and J. J. Jonas, "Effect Of Deformation On Ferrite Nucleation And Growth In A Plain Carbon And Two Microalloyed Steels." *Metall. Trans. A,* vol. 20, no. 6, pp. 987–998, Jun. 1989, doi: 10.1007/BF02650136.

[87] E. Essadiqi and J. J. Jonas, "Effect Of Deformation On The Austenite-To-Ferrite Transformation In A Plain Carbon And Two Microalloyed Steels." *Metall. Trans. A,* vol. 19, no. 3, pp. 417–426, Mar. 1988.

[88] T. Gladman, "Precipitation Hardening In Metals." *Mater. Sci. Technol*., vol. 15, no. 1, pp. 30–36, 1999, doi: 10.1179/026708399773002782.

[89] A. J. DeArdo, G.A. Ratz and P.J. Wray, "Thermomechanical Processing Of Microalloyed Austenite." Ed., AIME, Pittsburgh, 1982, pp. 613-639.

[90] P. J. Wray, "Tensile Failure Behavior Of Plain Carbon Steels At Elevated Temperatures." *Metall. Trans. A, Phys. Metall. Mater. Sci*., vol. 15 A, no. 11, pp. 2059–2073, 1984, doi: 10.1007/BF02646840.

[91] I. Baker, " Recovery, Recrystallization And Grain Growth In Ordered Alloys." *Intermetallics*, vol. 8, no. 9–11, pp. 1183-1196, 2000.

[92]   R. A. P. Djaic and J. J. Jonas, "Recrystallization Of High Carbon Steel Between Intervals Of High Temperature Deformation." *Metall. Trans.*, vol. 4, no. 2, pp. 621–624, Feb. 1973, doi: 10.1007/bf02648720.

[93]   A. J. DeArdo, G.A. Ratz and P.J. Wray, "Thermomechanical Processing Of Microalloyed Austenite." TMS- AIME, Warrendale, PA, 1982, pp. 129.

[94]   I .Kozasu, C. Ouchi, T. Sampei and T. Okita, "Microalloying' 75" ,*Proc. Int. Symp. HSLA Steels*, Union Carbide Corporation, N.Y., 1977, pp. 120.

[95]   Z. Q. Sun, W. Y. Yang and J.J. Qi, "Characteristics of Deformation-Enhanced Transformation in Plain Low Carbon Steel. " *Mater. Sci. Forum,* vol. 334, no.1-2, pp. 201, 2002.

[96]   J. J. Jonas, C. M. Sellars and W. J. M. G. Tegart, "Strength And Structure Under Hot-Working Conditions." *Metall. Rev.*, vol. 14, no. 1, pp. 1–24, 1969, doi: 10.1179/mtlr.1969.14.1.1.

[97]   H. Sekine and T. Maruyama, "The Microstructure and Design of Alloys." *Proceedings of the third international conference on the strength of metals and alloys*, Vol. 1, Cambridge, England, Aug, 1973.

[98]   A. Le Bon, J. Rofes-Vernis and C. Rossard, "Recrystallization And Precipitation During Hot Working Of A Nb-Bearing Hsla Steel," *Met. Sci.,* vol. 9, no. 1, pp. 36–40, Jan. 1975, doi: 10.1179/030634575790444919.

[99]   I. Weiss and J. J. Jonas, "Interaction Between Recrystallization And Precipitation During The High Temperature Deformation Of HSLA Steels." *Metall. Trans. A*, vol. 10, no. 7, pp. 831–840, Jul. 1979.

[100]   R. Kaspar and O. Pawelski, "Austenite Grain In The Process Of Thermomechanical Treatment." *Steel Res.*, vol. 57, no. 5, pp. 199–206, May 1986, doi: 10.1002/srin.198600754.

[101]   J. P. Sah, G. J. Richardson and C. M. Sellars, "Grain-Size Effects During Dynamic Recrystallization Of Nickel." *Met. Sci.*, vol. 8, no. 1, pp. 325–331, Jan. 1974, doi: 10.1179/msc.1974.8.1.325.

[102] J. H. Beynon and C. M. Sellars, "Modelling Microstructure And Its Effects During Multipass Hot Rolling." *ISIJ Int.*, vol. 32, no. 3, pp. 359–367, Mar. 1992, doi: 10.2355/isijinternational.32.359.

[103] H. Ahlborn, E. Hornbogen and U. Köster, "Recrystallisation Mechanism And Annealing Texture In Aluminium-Copper Alloys." *J. Mater. Sci.*, vol. 4, no. 11, pp. 944–950, Nov. 1969, doi: 10.1007/BF00555308.

[104] K. Holm and E. Hornbogen, "Annealing Of Supersaturated And Deformed Al-0.042 Wt % Fe Solid Solutions." *J. Mater. Sci.*, vol. 5, no. 8, pp. 655–662, Aug. 1970, doi: 10.1007/BF00549749.

[105] H. Jazaeri and F. J. Humphreys, "The Transition From Discontinuous To Continuous Recrystallization In Some Aluminium Alloys." *Acta Mater.*, vol. 52, no. 11, pp. 3251–3262, Jun. 2004, doi: 10.1016/j.actamat.2004.03.031.

[106] R. D. Doherty, D. A. Hughes, F.J. Humpreys, J. J. Jonas, J. Jensen, D. Kassner, M. E. King, W. E. McNelley, T. R. McQueen and A. D. Rollett, "Current Issues In Recrystallization: A Review." *Mater. Sci. and Eng.*, vol. A238, pp. 219 - 274, 1997.

[107] J. W. Martin, R. D. Doherty and B. Cantor, "Stability Of Microstructure In Metallic Systems." 2nd Edition, Cambridge University Press, 1997, pp. 147-257.

[108] P. R. Rios, F. Siciliano Jr, H. R. Sandim, R. L. Plaut and A. F. Padilha, "Nucleation And Growth During Recrystallisation." *Materials Research*, vol. 8, pp.225-238, 2005.

[109] R. D. Doherty, D. A. Hughes, F.J. Humphreys, J. J. Jonas, D.J. Jensen, M. E. Kassner, W. E. King, T. R. McNelley, H. J. McQueen and A. D. Rollett, "Current Issues In Recrystallization: A Review." *Mater. Sci. and Eng.: A - Structural Materials: Properties, Microstructure and Processing*, vol. 238, pp. 219-274, 1997.

[110] J. E. Burke, D. Turnbull, "Recrystallization And Grain Growth" *Progress in Metal Physics*, vol. 3, pp. 220-292, 1952.

[111] P. J. Hurley and F.J. Humphreys, "Modelling The Recrystallization Of Single-Phase Aluminium." *Acta Materialia*, vol. 51, no.13, pp. 3779-3793, 2003, doi.org/10.1016/S1359-6454(03)00192-7.

[112] H. S. Zurob, Y. Bréchet and J. Dunlop, "Quantitative Criterion For Recrystallization nucleation In Single-Phase Alloys: Prediction Of Critical Strains And Incubation Times." *Acta Materialia,* vol. 54, no. 15, pp. 3983-3990, 2006, doi:10.1016/j.actamat.2006.04.028.

[113] H. Izadi, R. Sandstrom and A. P. Gerlich, "Grain Growth Behavior And Hall–Petch Strengthening In Friction Stir Processed Al 5059." *Metall. Mater. Trans. A, Phys. Metall. Mater. Sci.,* vol. 45, no. 12, pp. 5635–5644, 2014, doi: 10.1007/s11661-014-2492-x.

[114] J. E. Bailey and P. B. Hirsch, "The Dislocation Distribution, Flow Stress, And Stored Energy In Cold-Worked Polycrystalline Silver." *Philos. Mag.*, vol. 5, no. 53, pp. 485–497, 1960, doi: 10.1080/14786436008238300.

[115] P. A. Beck and P. R. Sperry, "Strain Induced Grain Boundary Migration In High Purity Aluminum." *J. Appl. Phys.*, vol. 21, no. 2, pp. 150–152, 1950.

[116] C. J. L. Wilson, "The Prograde Microfabric In A Deformed Quartzite Sequence." *Mount Isa, Australia Tectonophysics*, vol. 19, no.1, pp. 39-81,1973, doi.org/10.1016/0040-1951(73)90142-X.

[117] F. J. Humphreys, "Nucleation In Recrystallization." Second Joint International Conference on Recrystallization and Grain Growth, ReX & GG2, SF2M, Switzerland: Trans Tech Publications, 2004.

[118] P. Bate and B. Hutchinson. CA Re-evaluation Of The Mechanism of SIBM." *Scripta Materialia*, vol. 36, no. 2, pp. 195-198, 1997.

[119] E. M. Lauridsen, H. F. Poulsen, S. F. Nielsen and D. Juul Jensen, "Recrystallization Kinetics Of Individual Bulk Grains In 90% Cold-Rolled Aluminium." *Acta Mater*, vol. 51 , pp. 4423-4435, 2003.

[120] S. K. Rhee, "Grain Growth In Alpha Brass And In Alpha Iron." *Mater. Sci. and Eng.*, vol. 9, pp. 246-248, 1972.

[121] M. Gómez, L. Rancel, B. J. Fernandez and S.F. Medina., "Evolution Of Austenite Static Recrystallization And Grain Size During Hot Rolling Of A V Microalloyed Steel." *Mater. Sci. and Eng. A*, vol. 501, no.1-2, pp. 188–196, 2009, doi: 10.1016/j.msea.2008.09.074.

[122] E. A. Holm, D. J. Srolovitz and J. W. Cahn, "Simulation of Microstructural Evolution in Two-Phase Polycrystals: Microstructures and Kinetics." *Act Met. & Mat.,* vol. 41, pp. 1119-1136, 1993.

[123] J. W. Cahn, "The Kinetics of Grain Boundary Nucleated Reactions. " *Acta Met.,* vol. 4, pp.449-459, 1956.

[124] K. Lucke and H. P. Stuwe, "Theory of Impurity Controlled Grain Boundary Migration." *Acta Metall Mate*r, vol. 19, pp. 1087-1099, 1971.

[125] S. Yamamoto, C. Ouchi and T. Osuka, "Effect Of Microalloying Elements On The Recovery And Recrystallization In Deformed Austenite." Metallurgical Society of AIME, Pittsburgh, PA, USA, 1982, pp.613-638.

[126] L. J. Cuddy, "The Effect of Microalloy Concentration on the Recrystallisation of Austenite during Hot Deformation",*Thermomechanical Processing of Microalloyed Austenite*, Warrendale, PA, 1982, pp.129-140

[127] J. G. Speer and S. S. Hansen, " Physical Metallurgy And Materials Science. " *Metall. Trans. A*, vol. 20A, pp. 25-94, 1989.

[128] T. R. Malow and C. C. Koch, " Grain Growth In Nanocrystalline Iron Prepared By Mechanical Attrition." *Acta Materialia*, vol. 45, no. 5, pp. 2177-2186, 1997.

[129] I. Kozasu, I. C. Ouchi, I. Sampei and T. Okita, " Microalloying 75." Union Carbide, *Proceedings of an International Symposium on High-strength, Low-alloy Steels*, 1975, pp. 120.

[130] J. W. C. Dunlop, Y. J. M. Bréchet, L. Legras and H. S. Zurob, "Modelling Isothermal And Non-Isothermal Recrystallisation Kinetics: Application To Zircaloy-4." *Journal of Nuclear Materials*, vol. 366 , no. 1-2, pp.178-186, 2007.

[131] C. W. Sinclair, J. D. Mithieux, J. H. Schmitt and Y. Bréchet, "Recrystallization Of Stabilized Ferritic Stainless Steel Sheet," *Metall. Mater. Trans. A Phys. Metall. Mater. Sci.*, vol. 36, no. 11, pp. 3205–3215, 2005.

[132] E.Nes,N. Ryum, and O. Hunderi, "On the Zener Drag." *Acta Metall Mater*, vol. 33, no.1, pp. 11-22, 1985, doi.org/10.1016/0001-6160(85)90214-7.

[133] G. S. Rohrer, "Introduction To Grains, Phases, And Interfaces-An Interpretation Of Microstructure." *Trans. AIME,* vol. 175, pp. 15-51, 1948.

[134] S. F. Medina and P. Fabregue, "Activation Energy in the Static Recrystallization of Austenite." *Journal of Material Science*, vol. 303A, pp.26-5427, 1991.

[135] A. Najafizadeh and J. J. Jonas, "Predicting The Critical Stress For Initiation Of Dynamic Recrystallization." *ISIJ Int.*, vol. 46, no. 11, pp. 1679–1684, 2006, doi: 10.2355/isijinternational.46.1679.

[136] S. H. Cho, K. B. Kang and J. J. Jonas, "The Dynamic, Static and Metadynamic Recrystallization of a Nb-microalloyed Steel." *ISIJ Int.,* vol. 41, no. 1, pp. 63-69, 2001.

[137] W. P. Sun and E .B. Hawbolt, "Comparison Between Static And Metadynamic Recrystallization-An Application To The Hot Rolling Of Steels." *ISIJ Int*, vol. 37, no. 10, pp. 1000-10009, 1997.

[138] F. J. Humphreys, "A Unified Theory Of Recovery, Recrystallization And Grain Growth, Based On The Stability And Growth Of Cellular Microstructures—I. The Basic Model." *Acta Mater.,* vol. 45, no. 10, pp. 4231–4240, Oct. 1997, doi: 10.1016/S1359-6454(97)00070-0.

[139] B. Pereda, J. M. Rodriguez-Ibabe and B. López, " Improved Model Of Kinetics Of Strain Induced Precipitation And Microstructure Evolution Of Nb Microalloyed Steels During Multipass Rolling." *ISIJ Int*., vol. 48, no. 10 ,pp. 1457-1466, 2008.

[140] B. Hutchinson, S. Jonsson and L. Ryde, "On the kinetics of recrystallisation in cold worked metals," *Scripta metallurgica*, vol. 23, pp. 671- 676, 1989.

[141] M. Ji, C. Davis, and M. Strangwood, "Effect Of Grain Size Distribution On Recrystallisation Kinetics In An Fe-30ni Model Alloy." *Metals*, vol. 9, pp. 369-380, 2019, https://doi.org/10.3390/met9030369.

[142] C. Bos, M. G. Mecozzi and J. Sietsma, "A Microstructure Model For Recrystallisation And Phase Transformation During The Dual-Phase Steel Annealing Cycle." *Comput. Mater. Sci.*, vol. 48, no. 3, pp. 692–699, 2010, doi: 10.1016/j.commatsci.2010.03.010.

[143] C. Bos, M. G. Mecozzi, D. N. Hanlon, M. P. Aarnts and J. Sietsma, "Application Of A Three-Dimensional Microstructure Evolution Model To Identify Key Process Settings For The Production Of Dual-Phase Steels." *Metall. Mater. Trans. A Phys. Metall. Mater. Sci.*, vol. 42, no. 12, pp. 3602–3610, 2011, doi: 10.1007/s11661-011-0696-x.

[144] D. Raabe, "Introduction Of A Scalable Three-Dimensional Cellular Automaton With A Probabilistic Switching Rule For The Discrete Mesoscale Simulation Of Recrystallization Phenomena." *Philos. Mag. A Phys. Condens. Matter, Struct. Defects Mech. Prop.*, vol. 79, no. 10, pp. 2339–2358, 1999, doi: 10.1080/01418619908214288.

[145] D. Raabe, "Cellular Automata In Materials Science With Particular Reference To Recrystallization Simulation." *Annual Review of Materials Science,* vol. 32. pp. 53–76, 2002, doi: 10.1146/annurev.matsci.32.090601.152855.

[146] D. Raabe and R. C. Becker, "Coupling Of A Crystal Plasticity Finite Element Model With A Probabilistic Cellular Automaton For Simulating Primary Static Recrystallization In Aluminum." In Microstructures, Mechanical Properties and Processes - Computer Simulation and Modelling, Wiley-VCH Verlag GmbH & Co. KGaA, 2005, pp. 1–8.

[147] M. Verdier,Y. Brechet and P. Guyot, "Recovery Of A1Mg Alloys: Flow Stress And Strain-Hardening Properties." *Acta Materialia*, vol. 47, no.1, pp.127-134, 1998.

[148] K. B. Kang, O. Kwon, W. B. Lee and C. G. Park. "Effect Of Precipitation On The Recrystallization Behavior Of A Nb Containing Steel." *Scripta Materialia*, vol. 36, no. 11 , pp. 1303-1308, 1997.

[149] O. Kwon and A.J. DeArdo,"Interactions Between Recrystallization And Precipitation In Hot-Deformed Microalloyed Steels." *Acta Metallurgica et Materialia*, vol. 39, no. 4, pp. 529-538, 1991.

[150] S. S. Hansen, J. B. V. Sande, and M. Cohen, "Niobium Carbonitride Precipitation And Austenite Recrystallization In Hot-Rolled Microalloyed Steels." *Metall. Trans. A,* vol. 11, no. 3, pp. 387–402, Mar. 1980.

[151] M. Winning, A. D. Rollett, G. Gottstein, D. J. Srolovitz, A. Lim and L.S. Shvindlerman, "Mobility Of Low-Angle Grain Boundaries In Pure Metals." *Phil. Mag.*, vol. 90, no. 22, pp. 3107-3128, 2010.

[152] D. G. Cram, H.S. Zurob, Y.J.M. Brechet, C.R. Hutchinson, "Modelling Discontinuous Dynamic Recrystallization Using A Physically Based Model For Nucleation. " *Acta Materialia*, vol. 57, no. 17, pp. 5218-5228, 2009.

[153] D. Raabe, F. Roters, F. Barlat, and L. Chen, "Continuum Scale Simulation of Engineering Materials Continuum Scale Simulation of Engineering Materials." Fundamentals - Microstructures - Process Applications. May 2004, Wiley-VCH, ISBN: 978-3527307609 2004.

[154] D.A. Hughes and N. Hansen, "Deformation Structures Developing On Fine Scales. " *Phil. Mag.*, vol. 83, no. 31-34, pp. 3871-3893, 2003.

[155] D. A. Hughes, D. C. Chrzan, Q. Liu, and N. Hansen, "Scaling of Misorientation Angle Distributions," *Phys. Rev. Lett.*, vol. 81, no. 21, pp. 4664–4667, Nov. 1998, doi: 10.1103/PhysRevLett.81.4664.

[156] A. Yoshie, M. Fujioka, Y. Watanabe, K. Nishioka, and H. Morikawa, "Modelling Of Microstructural Evolution And Mechanical Properties Of Steel Plates Produced By Thermo-Mechanical Control Process." *ISIJ Int*, vol. 32, pp. 395-404, 1992.

[157] T. Zhou, R. J. O'Malley and H. S. Zurob, "Study Of Grain-Growth Kinetics In Delta-Ferrite And Austenite With Application To Thin-Slab Cast Direct-Rolling Microalloyed Steels." *Metall Mater Trans A*, vol. 41, pp.2112-2120, 2010.

[158] C. W. Sinclair, C. R. Hutchinson and Y. Bréchet, "The Effect of Nb on the Recrystallization And Grain Growth Of Ultra-High-Purity α-Fe: A Combinatorial Approach. " *Metall. and Mat. Transactions A*, vol. 38, no. 4, pp. 821-830, 2007.

Appendix

Initial Voronoi microstructure creation:

User supplies number of cells in x direction: Nx

User supplies number of cells in x direction: Ny

User supplies number of cells in x direction: Nz

User supplies cell size (cells are cubic): d

User supplies a grain density: Nstar

Algorithm:

- Calculate number of grains in system, Ngrains, with Ngrains = Nstar*Nx*Ny*Nz*d*d*d
- Create list of Voronoi seeds points of length Ngrains with:
  - Repeat Ngrains times:
    - Generate random cell location (i,j,k)
    - if location not already occupied by another Voronoi seed point:
      - Add location to Voronoi seed list
    - If already occupied by another Voronoi seed points:
      - Repeat above
- The obtained list of Voronoi seeds is equal to the list of grains in the system (position in the list determines the grain id)

206

- Now assign a grain id to each cell in the system by:
  - Loop over all cells in x direction i → [0, Nx)
    - Loop over all cells in y direction j → [0, Ny)
      - Loop over all cells in z direction k → [0, Nz)
        - Assign grain id by loop over all Voronoi seeds in list
          - Calculate distance between current cell (i,j,k) and current Voronoi seed (take periodic boundaries into account!)
          - If distance shorter than current shortest distance store current Voronoi point as grain id of current cell and update current shortest distance

Deformation

The deformation algorithm assumes that the y-direction is the strip thickness direction and the x-direction the rolling direction (the z-direction is the strip width direction). The deformed structure is applied by reducing the number of cells in the y-direction and increasing the number of cells in the x-direction.

User supplies the deformation as a scale factor: SY

Algorithm:

- Calculate new number of cells in y-direction: Ny_new= SY * Ny
- Calculate new number of cells in x-direction: Nx_new= round((Nx * Ny)/ Ny_new)
- Set new number of cells in z-direction: Nz_new = Nz
- Calculate scale factor in x-direction: SX = Nx_new/Nx
- Setup a new system of cells with dimensions (Nx_new, Ny_new, Nz_new) by copying grain id, phase from the appropriate cell in the old (undeformed) system by:
  - Loop over all new cells in x direction i_new → [0, Nx_new)
    - Loop over all new cells in y direction j_new → [0, Ny_new)

207

- Loop over all new cells in z direction k_new → [0, Nz_new)
  - Calc new x coordinate x_new=(i_new+0.5)*d
  - Calc new y coordinate y_new=(j_new+0.5)*d
  - Calc new z coordinate z_new=(k_new+0.5)*d
  - Calc corresponding old x coordinate x_old=x_new/SX
  - Calc corresponding old x coordinate y_old=y_new/SY
  - Calc corresponding old x coordinate z_old=z_new
  - Calc old i index from (old) x coordinate i_old=floor(x_old/d)
  - Calc old j index from (old) y coordinate j_old=floor(y_old/d)
  - Calc old k index from (old) z coordinate k_old=floor(z_old/d)
  - Copy information from old cell (i_old,j_old,k_old) to new cell (i_new,j_new_k_new)

Assign dislocation density to deformed grains.

User supplies average dislocation density: rho_average

User supplies boundary intensity factor: BIF

User supplies boundary thickness: delta

Based on the grain boundary thickness, average dislocation density, boundary intensity factor, and the grain boundary area the grain interior, rho_core, and the boundary dislocation density, rho_gb as follows.

Algorithm:

- Calculate total grain boundary area: A_GB_tot = d*d*0.5*N_GB_tot (N_GB_tot is the total number of austenite-austenite grain boundary interface cells, the facto 0.5 appears as cells are counted on both sides of the interface)
- Calculate total boundary volume: V_GB_tot = A_GB_tot*delta
- Calculate total system volume: V_tot = Nx*Ny*Nz*d*d*d
- Calculate grain core volume: V_core_tot = V_tot-V_GB_tot
- Calculate boundary dislocation density: rho_boundary = BIF* rho_average
- Calculate core dislocation density: rho_core = ((V_tot-V_GB_tot*BIF) *rho_average)/V_core_tot
- Loop over all grains:
  - Assign rho_core and rho_boundary to grain

Recovery

The recovery model calculates the evolution of the dislocation densities (boundary and core) and of the average sub grain sizes (boundary and core). The calculation is the same for all grains and the same for the boundary and core (but of course with different values). To keep the description short the functions to calculate the Burgers vector, the shear modulus, elasticity modulus, the molar volume, iron self-diffusivity and the boundary energy as a function of temperature are not given.

User supplies sub grain growth parameter: Kad

User supplies recovery constants: C1 and C3

User supplies recovery activation energy: Qrec

User supplies recovery alpha parameter: alpha

User supplies Taylor factor: Taylor

User supplies Debye frequency: Debye

User supplies Nb concentration: XNb

Algorithm (current temperature is given by T and the timestep size by delta_t):

- For each grain
  - Set dislocation density to core dislocation density: rho = rho_core
  - If sub grain size not yet initialized calculate (initial) sub grain size as dsub = 10/sqrt(rho)

209

- Else set dsub to core average sub grain size: dsub = dsub_core
- Calculate auxiliary variable T1 as: T1= 128.0*ShearModulus(T)*Burgers(T)*Debye/ (9.0*alpha*ElasticityModulus(T)*TaylorFactor*Taylor)
- Calculate auxiliary variable T2 as: T2 = Taylor)*alpha*ShearModulus(T)*Burgers(T)/K_BOLTZMANN
- Calculate auxiliary variable sig as: sig = alpha* Taylor* ShearModulus(T)*Burgers(T)
- To calculate the evolution of rho and dsub over a time period delta_t an adaptive stepsize control Runge-Kutta adapted from ref [1] is used. The full algorithm will not be given here, instead only the integrand function (i.e. the function that gives the time derivatives of rho and dsub) is described:
- Integrand function (input: current values for dsub and rho):
  - Calculate Va_norm as: Va_norm= Burgers(T)*Burgers(T)/ (C1*sqrt(rho)+C3*XNb^(1/3)/ Burgers(T))
  - Calculate Va_def as Va_def = 35* Burgers(T)^3
  - Set Va to smallest value of Va_norm and Va_def: Va = min(Va_norm, Va_def)
  - Set time derivate of rho to drhodt = - T1*rho*sqrt(rho)*exp(Qrec/(RT))* sinh(T2*Va*sqrt(rho)/T)
  - If dsub larger than half times the grain size set the sub grain growth rate to zero
  - else
    - Calculate L as: L=1/(C1*sqrt(rho+C3*XNb^(1/3)/Burgers(T)))
    - Set sub grain growth rate ddsubdt to: ddsubdt = 2*(Diffusivity(T)/L)* sinh(sig*sqrt(rho)*Kad*Burgers(T)*Burgers(*T)*L/(K _BOLTZMANN*T)
- Set dislocation density to boundary dislocation density: rho = rho_boundary
- If sub grain size not yet initialized calculate (initial) sub grain size as dsub = 10/sqrt(rho)

- Else set dsub to boundary average sub grain size: dsub = dsub_boundary
- Repeat above with these values for rho and dsub

Note that the algorithm divides the timestep into smaller sub time steps if required for proper integration of the differential equations. Also note that in the given timestep delta_t the temperature is assumed to be constant.

Recrystallisation nucleation

To keep the description short the functions to calculate the Burgers vector, the shear modulus, elasticity modulus, the molar volume, iron self-diffusivity and the boundary energy as a function of temperature are not given.

Algorithm (current temperature is given variable T):

- loop over all grain boundary cells to count for each grain pair interface (i.e. face of a grain)   how many cells there are on the interface (only for deformed grains)
- Now we have for each deformed austenite grain a map which contains the number of cells on each grain face (with an austenite neighbour grain). Which means we can ask each grain to calculate the number of new nuclei on each face for the given time step size:
- Loop over all grains:
    - Loop over all faces of grain (with deformed neighbor):
        - Set delta_rho to: delta_rho = 0.5*rho_boundary (of grain)
        - Calculate critical sub grain diameter dcrit as:
          dcrit = (8* GB_energy(T)/(delta_rho*ShearModulus(T)
          *Burgers (T)^2))
        - Calculate ChiCrit as: ChiCrit = dcrit/dsub_boundary (of grain)
        - Calculate the chance that a critical sub grain is located on the current face (with nCellsOnFace interface cells on the face), pOnFace:
          pOnFace= 0.6*nCellsOnFace*d*d/(π*(0.5*dcrit)^2) /
          (Grain_volume/ average_boundary_sub_grain_volume)

[factor 0.6 accounts for average difference in real surface and surface based on number of cells (in 3d)]

- Check if grain face area larger than critical area, if not set nucleation rate to zero and continue with next face
- Calculate, ft, fraction of subgrains > critical size: ft = exp(-0.25*π*Chirit^2)
- Calculate, Nt, number of nuclei: Nt = Ft*pOnFace*(Grain_volume/ average_boundary_sub_grain_volume)
- If difference between Nt and the previous number of formed nuclei is larger than 1 add the newly formed nuclei to the list of seeds to be placed on this face (can't have fractional number of nuclei)

- Place seeds:
  - Loop over all interface cells in random order:
    - Check if current interface cell belongs to a face on which a new seed has to be placed, if not continue to next interface cell
    - Check if distance of current interface cell to (possible) earlier placed seeds on this face is larger than critical sub grain size diameter, if not continue to next interface cell
    - Set current interface cell as seed point of a new grain (i.e. a nucleus) with an initial volume of the current interface cell only

Recrystallisation growth

To keep the description brief the function for the temperature and Nb concentration dependent interface mobility, M_sol_drag, is not given.

Algorithm (current temperature is given variable T and timestep size by delta_t):

- For each interface cell on the recrystallisation front (i.e. interface cells with neighbours of both deformed and recrystallized grains) a growth radius, r, is stored and updated each timestep
- Loop over all interface cells:

- o Find the first neighbor cell of the interface cell that belongs to a deformed austenite grain and set rho to the dislocation density of that deformed grain
- o Set the interface velocity, v, to: v= M_sol_drag(T, XNb)* 0.5*ShearModulus(T)* Burgers(T)^2*rho*AusteniteMolarVolume(T)
- o If the current radius of the growing grain is smaller than the critical sub grain size multiply the interface velocity with a factor 10 (remember that each grain starts as a nucleus with the size of only one cell)
- o Calculate the new growth radius: r= r+delta_t*v
- o If r is larger than nearest/next-nearest or next-next-nearest neighbours transform those cells (if they belong to deformed austenite grains) and make them part of the grain of the current interface cell
- o If r larger than next-next-nearest neighbours stop being an interface cell